STUDIES ON CHEMICAL BATH DEPOSITED SEMICONDUCTING COPPER SELENIDE AND IRON SULFIDE THIN FILMS USEFUL FOR PHOTOVOLTAIC APPLICATIONS

Thesis submitted to

COCHIN UNIVERSITY OF SCIENCE AND TECHNOLOGY

for the award of the degree of

DOCTOR OF PHILOSOPHY

By

Lakshmi M.

Department of Physics

Cochin University of Science and Technology

Cochin – 682 022, India

2001

CERTIFICATE

Certified that the work presented in this thesis entitled *"Studies on chemical bath deposited semiconducting copper selenide and iron sulfide thin films useful for photovoltaic applications"* is based on the bonafied research work done by Smt. Lakshmi. M under my guidance, at the Department of Physics, Cochin University of Science and Technology and has not been included in any other thesis submitted previously for the award of any degree.
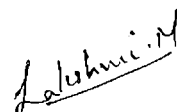
Kochi -22

May 5, 2001

Dr. C. Sudha Kartha

(Supervising Guide)

DECLARATION

I hereby declare that the work presented in this thesis entitled *"Studies on chemical bath deposited copper selenide and iron sulfide thin films useful for photovoltaic applications"* is based on the original research work carried out by me under the guidance and supervision of Dr. C. Sudha Kartha, Sr. Lecturer, Department of Physics, Cochin University of Science & Technology, Kochi and has not been included in any other thesis submitted previously for the award of any degree.

Cochin – 22

11-06-2001

Lakshmi.M

Acknowledgement

Words are insufficient to express my gratitude to my colleagues, Mr. Ramkumar. S, Mrs. Syamala. S. B, Ms. Bindu. K, Mrs. Bini Satheesh, Mrs. Shiji Joemon, Mr. Shaji. S, Mr. Paulraj M, Ms. Roopa R. Pai, Mr. Harish. P and Ms. Teny Theresa John for their support throughout my research career. I am also thankful to my seniors Dr. P. K. Vidyadharan Pillai, Dr. K. P. Varkey and Dr. N. A. Zeenath for their moral support.

I express my sincere appreciation for the patience, understanding and encouragement expressed by my family. A special thanks to my husband Mr. Sethumadhavan. N, whose support helped me endure the pains of completing this work.

Last but not least, I thank all my well wishers and to them I dedicate this thesis.

CONTENTS

CHAPTER - 4

Interphase conversion of $Cu_{2-x}Se$ and Cu_3Se_2 thin films

CHAPTER - 5

Iron pyrite thin films

CHAPTER – 6

Conclusion

Preface

Photovoltaic is the cleanest and the most efficient mode of conversion of solar energy to electrical power. Today silicon is the most popular material in this field. In the US, the current voltaic system based on crystalline silicon wafers has an estimated cost between $ 0.25 and $ 0.6 / kWh. This increased cost of Si cells is mainly due to the high manufacturing cost, in spite of reasonably high efficiency. It is estimated that 50% of the cost of a module is due to the cost of processed silicon wafer. It is surprising to note that in spite of this high cost and complicated manufacturing process, crystalline silicon still dominates the market. The best laboratory efficiency for single crystal silicon is today 24.5%. But this efficiency can only be realised with very elaborate technology. The best commercial cells now have an efficiency of only 15 -16 %.

Moreover, when we think of future, the big question mark before us is the source of highly purified silicon for this purpose. For 1 GW photovoltaic instillation, the required quantity of high quality silicon is estimated as 8000 tons. In such a scenario, if photovoltaics have to supplement or at least complement the conventional energy system of today, it is necessary to develop other cost effective materials. It can be argued that efficiency can be sacrificed to some extent, provided the cell is cheap and eco friendly.

In such a context, success of photovoltaics largely depends on the deposition of semiconductors in large areas. Hence the PV technology is undergoing a transition to a new generation based on thin films. The main attractions of thin film technology are the possibility of large area deposition in any predetermined shape, with large variety of available deposition processes with minimum material input and the possibility of controlling the doping profile as required. Though much has been talked about the copper ternary compounds like $CuInSe_2$ and $CuInS_2$ in this field, today the attraction is slowly shifting towards new promising materials that can be prepared easily and are environment friendly. The present work concentrates on preparation and characterization of few of such materials viz., different phases of copper selenide thin films and Iron sulfide thin films.

The thesis is organized in six chapters. Each chapter has separate conclusion and reference section. The chapter wise description of the contents of this thesis is given below.

First chapter of the thesis includes a detailed review on the technique of Chemical Bath Deposition for the preparation of compound semiconductor thin films. This technique involves controlled precipitation of a compound from a solution on a suitable substrate. Significance of this simple technique is duly highlighted, while references are made to a wide range of chalcogenides (eg. CdS, CuSe, ZnS, CdSe, Bi_2Se_3, Sb_2S_3, etc.) and chalcopyrite materials (eg. $CuInSe_2$, $CuInS_2$) which can be prepared using CBD.

Second chapter refers to the material, copper selenide. Various techniques of preparation of this material are touched upon, with due emphasis on preparation of $Cu_{2-x}Se$ and Cu_3Se_2 thin films using CBD technique. In the present work cubic $Cu_{2-x}Se$ and tetragonal Cu_3Se_2 thin films could be prepared by the above technique by varying the ratio of Cu:Se in the reaction mixture and it is observed that pH of the reacting mixture is the main factor that determines the composition of the film. Hence these phases could also be prepared from a similar reaction mixture containing same Cu:Se ratio but differing in pH.

Analysing thin film with precession is a challenging job. Third chapter gives a detailed description of characterization of these two phases. Morphology of the film was studied using SEM. Electrical studies include resistivity measurements and Hall measurements, while optical band gap is calculated from the absorption spectrum. XRD confirms the phase identification. Stoichiometry is confirmed using XPS and ICP techniques. XPS depth profile revealed a uniform composition through out the depth.

Inter phase conversion of $Cu_{2-x}Se$ <-> Cu_3Se_2 is dealt in detail in chapter four. Reddish brown colour of $Cu_{2-x}Se$ thin film slowly changes to bluish green (typical of Cu_3Se_2 phase) on exposure to ambient conditions. ie. as an effect of aging the $Cu_{2-x}Se$ phase gets converted to the Cu_3Se_2 phase along with the formation of copper oxide impurity. It is also found that the Cu_3Se_2 phase reverts to $Cu_{2-x}Se$ phase when heated above 140 ^{0} C. This inter phase conversion was confirmed using different analytical techniques and is described in detail in this chapter. The cyclic nature of this

conversion and the possible theory behind the process is mentioned along with measures to prevent the phase conversion.

Chapter five highlights the advantages of the material Iron pyrite as a promising photovoltaic material. Various preparation techniques of the material are summarized in the form of a table. Later part of this chapter deals with the report on preparation of pyrite using Chemical Bath Deposition. Instability of the as-prepared films was investigated and is accounted as mainly due to deviation from stoichiometry and the formation of iron oxide impurity. A detailed account of the trials carried out to improve the stoichiometry by annealing the film in sulfur atmosphere is also included in this chapter. A sulfur-annealing chamber for this work was designed and fabricated. These samples were also analysed using optical absorption technique, XPS and XRD. The pyrite films obtained by CBD technique showed amorphous nature and the electrical studies carried out showed the films to be of high resistive nature.

Chapter six summarises the results pertaining to the preparation of copper selenide and iron sulfide thin film by Chemical Bath Deposition process and also the inter phase conversion of copper selenide thin films.

List of Publications

1. Reversible $Cu_{2-x} \leftrightarrow Cu_3Se_2$ phase transformation in Copper Selenide thin films prepared by chemical bath deposition

   M.Lakshmi, K.Bindu, Bini.S, Sudha Kartha.C, K.P.Vijayakumar, Abe.T and Kashiwaba.Y

   Thin Solid films ,Vol. 386, p. 127 (2001).

2. Chemical bath deposition of different phases of Copper Selenide thin films by controlling bath parameters

   M.Lakshmi, K.Bindu, Bini.S, Sudha Kartha.C, K.P.Vijayakumar, Abe.T and Kashiwaba.Y

   Thin Solid Films ,Vol. 370, p. 89 (2000).

3. Sulfurisation – a technique to improve stoichiometry of Iron Pyrite thin film

   Lakshmi. M, Bindu. K, Bini. S, Sudha Kartha. C, Vijayakumar. K.P, Abe.T and Kashiwaba.Y

   National seminar on Current trends in Materials Science, March 23-24, 2001, School of pure and applied Physics, Mahatma Gandhi University, Kottayam, Kerala.

4. Preparation of Pyrite thin films using Chemical Bath Deposition technique: An attempt

   M. Lakshmi, K. Bindu, C. Sudha Kartha and K.P.Vijayakumar.

   Renewable Energy 1999, ANERT National conference, 1999, Thiruvananthapuram.

5. Preparation of different phases of copper selenide using CBD technique

   M.Lakshmi, K.Bindu, Bini.S, Sudha Kartha.C, K.P.Vijayakumar, Abe.T and Kashiwaba.Y

   The 53rd meeting of the Tohoku branch of **The Japan Society of Applied Physics,** 1999, Tohoku University.

6. Structural and optical absorption changes of chemically prepared $Cu_{2-x}Se$ due to indium diffusion

   K.Bindu, M.Lakshmi, C. Sudha Kartha, K.P.Vijayakumar,

   DAE Solid State Symposium, 1999, IGCAR, Kalpakkam

Papers related to collaborative work:

7. Preparation of $CuInS_2$ thin films using CBD Cu_xS films.
   S.Bini, K.Bindu, M.Lakshmi, C.Sudha Kartha, K.P.Vijayakumar,
   Y.Kashiwaba and T.Abe
   Renewable Energy, Vol.20, No.(4), p.405 (2000)

8. Study of trap levels by electrical techniques in p-type CuInSe2 thin films prepared using chemical bath deposition
   N.A.Zeenath, P.K.V.Pillai, K.Bindu, M.Lakshmi, & K.P.Vijayakumar
   Journal of Material Science 35 (2000) 1-6.

9. Amorphous Selenium thin films prepared using CBD: Optimization of the deposition process and Characterization
   Bindu. K, Lakshmi. M, Bini. S, Sudha Kartha. C, Vijayakumar. K.P, Abe. T and Kashiwaba.Y
   (Accepted for publication in **Thin Solid Films**)

10. Deposition of $CuInS_2$ films using a new technique
    S.Bini,K.Bindu, M.Lakshmi, C.Sudha Kartha, K.P.Vijayakumar, T. Abe, and Y.Kashiwaba.
    The 53rd meeting of the Tohoku branch of **The Japan Society of Applied Physics, 1999,** Tohoku University.

11. Studies on different trap levels present in $CuInSe_2$ thin films prepared using CBD
    N.A.Zeenath, M.Lakshmi, K. Bindu, and K.P.Vijayakumar.
    Symposium on Current status of Solar Energy Materials, 1997,
    Anna University, Madras.

12. TSC Measurements on Chemically Deposited $CuInSe_2$ Thin film
    N.A.Zeenath, M.Lakshmi, K. Bindu, and K.P.Vijayakumar.
    DAE- Solid State Symposium, 1997, CUSAT, Kochi.

13. CBD - A technique to prepare different phases of Copper Selenide
    K.Bindu, M Lakshmi, C. Sudha Kartha and K.P.Vijayakumar.
    DAE- Solid State Symposium, 1998, Kurukshetra, Haryana

CHAPTER 1

CBD technique in the preparation of semiconductor thin films for photovoltaic applications – A review

1.1   Chemical Bath Deposition (CBD)

1.2   Various semi-conducting thin films prepared by CBD technique for use in photovoltaic applications.

1.3   Conclusion

Reference

1.1 Chemical Bath Deposition (CBD)

As David Smyth-Boyle's homepage[†] puts it, CBD refers to '..... a typical synthesis employing mild conditions.' The technique of Chemical Bath Deposition involves the controlled precipitation of a compound from a solution on a suitable substrate. This technique offers many advantages over the more established vapour phase routes to semiconducting thin films, such as CVD, MBE and spray pyrolysis. In this preparation technique it is possible to control the film thickness and composition by varying the solution pH, temperature and reagent concentration. The ability of CBD to coat large areas in a reproducible and low cost process is one added attraction of this method. The first report of CBD was in 1884 [1] for the preparation of PbS. Today a wide range of chalcogenides (eg. CdS, ZnSe, MnS) and chalcopyrite materials (e.g. $CuInS_2$ and $CuInSe_2$) have been prepared using this method.

The pioneers in this field include Bode *et al.* at Santa Barbara Research Center, G.A Kitaev *et al.* at Ural Polytechnic, USSR, Chopra *et al.* at Indian Institute of Technology, Delhi, and P.K. Nair *et al.* at Centro de investigation en Energia , Mexico.

1.1.1 Applications of CBD

The use of PbS and PbSe as photodetectors form the first recorded application of chemically deposited semiconductor thin films [2]. This was followed by CdSe photodetectors [3]. Around 1980, the focus of CBD films slowly turned towards solar energy applications. One of the earlier developments towards this was in solar absorber coatings [4]. Application in the field of solar control coating was suggested in 1989 [5]. It has been found that chemical bath deposited PbS and Cu_xS thin films offer comparable or superior solar control characteristic as against commercial solar control coatings deposited by much expensive vacuum coating techniques.

[†] http://www.ch.ic.ac.uk/obrien/barton/dsb/dsbcbd.html

CdS and CdSe turned out as probable candidates in the field of photo electrochemical solar cells [6-9]. Recently, work on chemically deposited CdSe and Sb_2S_3 films with incorporation of WO_3 has shown appreciable conversion efficiency and stability in photo electrochemical solar cell configuration [10].

It is only 10 years since chemically deposited thin films have found their active role in thin film solar cells. In 1990, a thin layer of CBD CdS thin film was integrated into a structure $Mo/CuInSe_2/CdS/ZnO$ producing approximately 11% conversion efficiency [11]. Later improved cell design resulted in record efficiencies greater than 17% [1-18]. Theoretical calculations have shown that the thickness of CdS film should be as small as possible for better cell efficiency. This could be attained easily by CBD technique. The fabrication of heterojunction solar cells using chemically deposited Sb_2S_3 thin films on p(Si)/p(Ge)/p(InP) wafers has been reported recently [13,14].

P. K. Nair and group have many publications on this simple technique of CBD [15-18]. Lokhande *et al.* [19] in his review article has mentioned about more than 35 compounds prepared using this technique. All these hint that the number of materials that are deposited by CBD will increase significantly in the coming years.

In the field of CBD, the Photovoltaic laboratory at University of Science and Technology has also contributed significantly. The first CIS/CdS trial thin film solar cell in which both the n- and p- type materials were prepared using CBD technique comes to the credit of the same group (section 1.2.1.h). We have also succeeded in depositing elemental selenium thin films from an acidified bath of sodium selenosulfate. This work is to be published in the forthcoming issue of Thin Solid Film [20]. Moreover, work in the direction of preparation of ternary chalcogenides of $CuInSe_2$ and $CuInS_2$ by diffusing In into the chemically deposited thin film of Cu_2Se and Cu_xS are in progress.

So to conclude the history of CBD technique- The scope of this technique in the field of photovoltaics is immense. This can form the most ideal technique for the production of large area thin films required for solar energy applications.

1.1.2 Principle of CBD technique

In chemical bath deposition process, precipitation of the solid phase occurs due to the super saturation in the reaction bath. At a given temperature when ionic

product of reactants exceeds the solubility product, precipitation occurs. Where as if the ionic product is less than the solubility product, then the solid phase produced will dissolve back to the solution resulting in no net precipitation. This forms the basic principle behind any chemical deposition process. Or in other words, the principle of CBD technique is to control the chemical reaction so as to effect the deposition of a thin film by precipitation.

This deposition technique is mostly used for preparation of metal chalcogenide thin films. In a typical CBD procedure, substrates are immersed in a solution containing the chalcogenide source, the metal ion and an added base. A complexing agent is added to control the hydrolysis of the metal ion. The process depends on the slow release of chalcogenide ions into an alkaline solution in which the free metal ion is buffered at a low concentration. The free metal ion concentration is controlled by the formation of complex species according to the general reaction,

$$M(A)^{2+} \leftrightarrow M^{2+} + A.$$
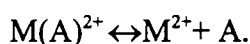
Here concentration of the free metal ions at a particular temperature is represented by the relation $\dfrac{[M^{2+}][A]}{[M(A)^{2+}]} = K_i$ (K_i being the instability constant of the complex ion). The instability constant is different for different complexing agents. As the instability constant increases, more number of ions will be released. The stability of the complex also depends on temperature and pH of the reaction bath. Increase in temperature of the solution will make the complex less stable, where as an increase in pH generally makes it more stable. Thus the concentration of metal ions can be controlled by the concentration of an appropriate complexing agent and the temperature of the reaction bath. The common complexing agents needed for certain ions are given in Table (1.1).

If high concentration of S^{2-} or Se^{2-} ions exists locally such that the solubility product is exceeded, localized spontaneous precipitation of a sulfide or selenide may occur as the case may be. This situation can be avoided by generating chalcogen ions slowly and uniformly throughout the volume of the solution. For example, this is achieved in the case of sulfur by having thiourea in alkaline aqueous solution, so that the reaction given below proceeds slowly.

$$(NH_2)_2 CS + OH^- \rightarrow CH_2N_2 + N_2 + H_2O + HS^-$$

$$HS^- + OH^- \rightarrow H_2O + S^{2-}$$
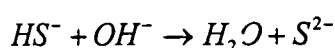
Selenide films are obtained by replacing thiourea by selenourea or other derivatives. Selenium ions are generated by dissolving inorganic sodium selenosulphate in an alkaline solution as given by the reaction

$$Na_2SeSO_3 + OH^- \rightarrow Na_2SO_4 + H_2O + Se^{2-}$$
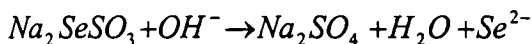
Elements	Complexing agent
Ag	CN^-, NH_3, Cl^-
Cd	CN^-, NH_3, Cl^-, $C_6H_5O_7^{3-}$, $C_4H_4O_6^{2-}$, EDTA
Co	CN^-, NH_3, SCN^-, $C_6H_5O_7^{3-}$, $C_4H_4O_6^{2-}$
Cu	CN^-, NH_3, Cl^-, EDTA
Hg	CN^-, NH_3, Cl^-, EDTA
Mn	$C_2O_4^{2-}$, $C_6H_5O_7^{3-}$, $C_4H_4O_6^{2-}$, EDTA, CN^-
Ni	CN^-, NH_3, SCN^-, EDTA
Pb	EDTA, $C_6H_5O_7^{3-}$, $C_4H_4O_6^{2-}$, OH^-
Sn	$C_6H_5O_7^{3-}$, $C_4H_4O_6^{2-}$, OH^-, $C_2O_4^{2-}$
Zn	CN^-, NH_3, $C_6H_5O_7^{3-}$, $C_4H_4O_6^{2-}$, EDTA

Table (1.1) Ions and their common complexing agents

1.1.3 Process of thin film deposition

There are three different possibilities for the process of thin film deposition in CBD technique. They are schematically shown in Fig.(1.1). First possibility is the ion-by-ion process in which the ions condense at the reacting surface to form the film. The second is the cluster-by-cluster process in which colloidal particles that are formed in the solution as a result of homogenous reaction gets adsorbed at the substrate surface to form thin layers. Usually both these processes may occur or may interact each other, leading to films in which colloidal material is included in the growing films. The predominance of one mechanism over the other is governed by the extent of heterogeneous and homogeneous nucleation. Heterogeneous nucleation is a result of reaction occurring at the surface of the substrate while homogeneous nucleation is a result of reaction occurring within the bulk of the solution.

1.1.4 Factors influencing the deposition process

The various factors that influence the deposition process in CBD technique are (1) nature and concentration of reactants and complexing agent, (2) temperature, pH and duration of the reaction and (3) nature and spacing of the substrates.

1.(a) Nature of the reactants

Nature of the reactants influences the composition of the products. In the preparation of copper selenide it is observed that when sodium selenosulfate is used as the selenium source, the final phase is usually Cu_2Se, while the use of dimethyl selenourea results is CuSe phase [21-23]. The growth kinetics also depends on the nature of reactants. For example, when metal sulfate is employed to deposit metal selenide films using sodium selenosulfate, the rate of deposition decreases and the terminal thickness increases. Here the SO_4^{2-} ions obtained from the metal sulfate reduce the concentration of Se^{2-} ions.

1.(b) Concentration of reactants

The deposition rate and terminal thickness initially increases with an increase in the ionic concentration of the reactants. However, at high concentration the precipitation becomes very fast, leading to decrease in film thickness on the substrate.

1.(c) Nature of complexing agent

Nature of complexing agents may influence the final products. For example, when ammonia is used as a complexing agent for the preparation of ZnS thin film, it is found to result in $ZnO/Zn(OH)_2$ phase rather than ZnS. However when two complexants ammonia and hydrazine are used, the oxide and hydroxide phases could be avoided to a great extend [24].

1.(d) Concentration of complexing agent

In a general reaction the metal ion concentration decreases with increasing concentration of the complexing ions. Consequently the rate of reaction and hence precipitation are reduced leading to a larger terminal thickness of the film. Such behaviour has been observed for CdSe, CdS, PbSe and ZnS films.

2.(a) Reaction temperature

Temperature of deposition is another factor that influence the rate of reaction. As temperature increases dissociation of the complex increases. The kinetic energy of

the molecules also increases leading to greater interaction between ions. This will result in increase or decrease of terminal thickness, depending on the extent of super saturation of the solution.

2.(b) Reaction pH

When the pH value of the reaction bath increases, the metal complex usually becomes more stable, reducing the availability of free metal ions. This will decrease the reaction rate resulting in higher terminal thickness.

Recently there was a report by Paul O' Brien [25], on a novel approach to the deposition of CdS by CBD. He succeeded in depositing CdS from an acidic bath for the first time. It was observed that the film properties were very much different in the case of such films when compared with that of films deposited from alkaline bath.

2.(c) Duration of reaction

The dependence of film thickness on the duration of deposition (all the other factors remaining the same) has been studied in detail for different semiconductor thin films obtained by CBD technique [15]. The results are summarised in Fig.[1.2]. In general, the growth of good quality semiconductor thin films proceeds at a slow rate. This technique of CBD is ideally suited for producing uniform films with thickness in the 0.05-0.3 µm range in most cases and rarely to an extend of few microns.

3.(a) Nature of substrates

This factor plays a major role in the reaction kinetics and in the adhesion of the deposited film. Hence cleaning of substrate surface form the first important step in the thin film deposition procedure.

Higher deposition rates and terminal thickness are observed for those substrates whose lattices and lattice parameters match well with those of the deposited material. During deposition of PbSe thin films under similar conditions, higher rates and thickness have been observed on Ge rather than on Si because of better matching of the lattice parameters of PbSe with those of Ge [26].

On a presensitised substrate surface, no incubation period for nucleation is observed since nucleation centers already exist on the substrate. Also when the substrates are suspended in the container before forming the complex in the solution, film thickness increases in a manner similar to that of the sensitised surface, there by
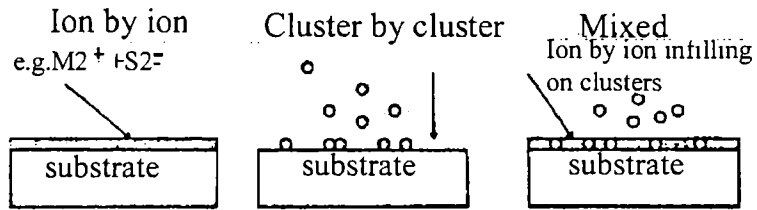
Fig.(1.1) Representation of various processes of thin film deposition in CBD technique
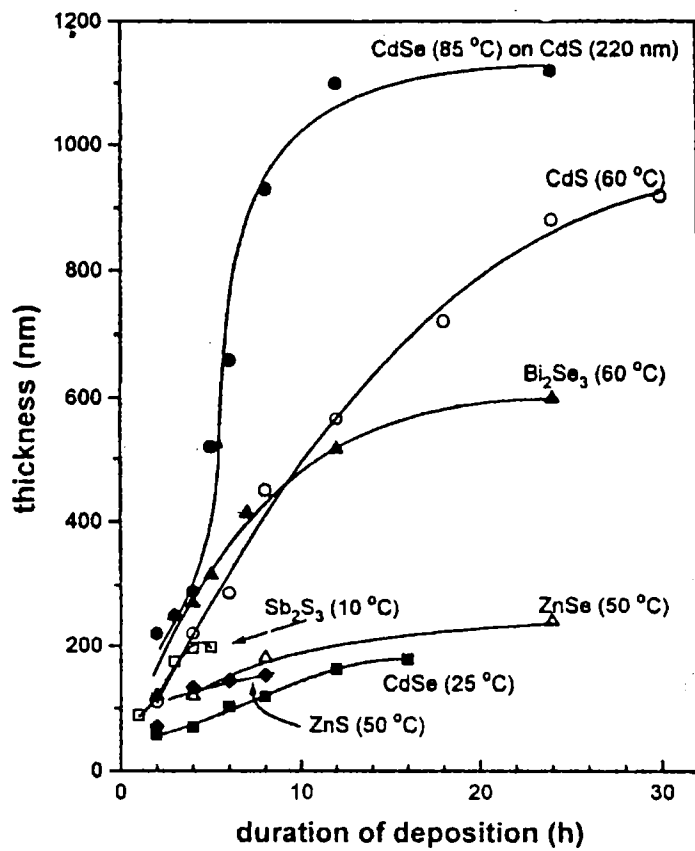
Fig.(1.2) Dependence of film thickness on duration of deposition

showing that the nuclei for the formation of the film are provided by the solution itself.

3.(b) Spacing of substrates

Recently Arias- Carbajal *et al.* [27] have studied the film thickness as a function of separation between substrates in batch production. It was observed that film thickness reach an asymptotic maximum with increase in substrate separation. This behaviour is explained on the basis of the existence of a critical layer of solution near the substrate, within which the relevant ionic species have a higher probability of interacting with the thin film layer that contribute to precipitate formation. The critical layer depends on the solution composition, the temperature of the bath, as well as the duration of deposition. In the case of CdS thin film, this critical layer is found to extend from 0.5 to 2.5 mm from the substrate surface, depending on the deposition conditions.

The above mentioned influencing factors do not actually affect the chemical reaction individually, but the final result is due to the cumulative effect of interdependence of all these factors. K. L. Chopra and S. R Das in 'Thin Film Solar Cells' have represented the influence of few of the above parameters on the thickness of the deposited film as experimental graphs. [26].

1.1.5 Mathematical model for CBD growth

P. K. Nair *et al.* has worked out a mathematical model simulating the growth of compound semiconductor thin films via. chemical bath deposition [28]. This model can be used to simulate the growth curve of the CBD thin films for large area coatings as a function of the initial concentration, temperature and duration of deposition. Development of this model was based on the experimental growth curve of thin films of different materials grown in this method. The general characteristics of the different stages in CBD growth process were classified as:

1 The existence of an induction period called the nucleation or incubation period, during which the various chemical equilibria are established in the bath and an initial monolayer of the metal chalcogenide is formed on the substrate.

2 The initial monolayer of the metal chalcogenide formed on the substrate acts as a catalytic surface for the condensation of the metal ions and chalcogenide ions resulting in the film growth. This is called the growth phase.

3 Film growth assumes a maximum rate at a certain time, depending on the bath parameters and finally reaches a terminal phase at which the film ceases to grow.

4 A decrease in the duration of the induction period with increase in the temperature as well as with the concentration of ions in the bath.

5 An optimum temperature-concentration combination to obtain maximum film thickness for a given duration of deposition.

In this technique, the metal ions are complexed with ligands and depending on their instability constant they will slowly dissociate releasing free metal ions. This forms the main rate determining step. Hence first order reaction rate kinetics is applied to the dynamics involved in CBD process.

$$\frac{dC(t)}{dt} = -kC(t)$$ where C(t) is the unreacted metal ion concentration at time t resulting from an initial concentration Ci.

C(t) = Ci exp (-kt) where k = A exp(-E_a/RT)

(A is the Arrhenius constant, E_a the activation energy, R the universal gas constant and T the temperature). The used up concentration C_u(t) of the metal ions can be expressed in the form of Avrami equation

C_u (t) = C_i [1- exp (-kt)]

Based on the theory developed with this idea and the concepts of geometric factor and induction factor, the growth curve for CdS thin film was simulated. This was found to be in good agreement with the experimental curve.

The other important experimental observations that were reaffirmed through this modal include,

(i) It is necessary to combine a relatively high initial metal ion concentration with a relatively low temperature of deposition for getting films of thickness greater than 0.5 µm by single dip.

(ii) If the objective is to deposit a very thin film of typically 0.05 µm, a very dilute bath and a relatively high deposition temperature is appropriate.

1.1.6 Quantum confinement effect

Thin films of several materials deposited using chemical bath possess a nanocrystalline structure [29]. Small crystal size leads to quantum size effect and a blue shift is observed in the optical spectra. In the case of CdSe, it is observed that there is a certain critical ratio between the complexing agent and Cd concentration in the bath used for preparation of the film, below which there is a pronounced blue shift [30]. This observation was correlated with decrease in crystal size.

In the case of a polycrystalline semiconductor with crystalline grain width L, the enhancement of band gap $(Eg)_{pc}$, as compared to that of a bulk semiconductor crystal, can be represented as [31].

$$(Eg)_{pc} = (Eg)_{bulk} + \frac{1}{2}\left(\frac{h}{2\pi}\right)^2 \pi^2 \frac{\left(m_e^{-1} + m_h^{-1}\right)}{L^2} - \frac{1.8}{\xi L}$$

where m_h and m_e are the effective masses for hole and electron respectively. The last term represents 'screening term' in a medium of permittivity ξ. $(Eg)_{pc}$ generally approaches $(Eg)_{bulk}$ for L > 50 nm, but takes values considerably higher than the bulk value for L < 5 nm. For example, in the case of CBD-CdSe films, with grain sizes < 5 nm, optical band gap goes up by ~0.7 eV above the bulk value (1.74 eV) [29]. Annealing of as-prepared films improves the crystallinity and hence the discrepancy in band gap will be reduced [32].

1.1.7 Photoresponse of CBD films

A comparative study on photocurrent response of a number of chemically deposited thin films has been reported, Fig (1.3) [15]. Except for CdS, the films do not exhibit large photocurrent. Most of the films were highly resistive in the dark and their electrical conductivities in dark varied in the range 10^{-8} to 10^{-6} $\Omega^{-1}cm^{-1}$. Exceptions were CuS and $Cu_{2-x}Se$ thin films, where conductivities were in the range 10^4 -10^3 $\Omega^{-1}cm^{-1}$. Such high conductivities were reported to arise from copper deficiency in these films, which make them p-type [33]. This is also responsible for the large free carrier absorption in these films in the IR region.

Air annealing is found to have significant influence in the photoresponse of some of the chemically deposited semiconductor films. It is reported that though the CdSe thin films possess very poor photosensitivity, annealing in air makes the film highly photoconductive. This is due to the combined effect of grain size growth and

chemisorption of oxygen [34,35]. Fig.(1.4) represents this effect figuratively, where photosensitivity S is defined as $S = (I_{ph}-I_d) / I_d$ (I_{ph} and I_d are the photocurrent and dark current respectively)

On the other hand photoconductivity of CdS is found to degrade under the same annealing process, [Fig.1.5]. The photosensitivity of the as-prepared films gets lowered by 4 to 5 orders due to annealing at 300-400^{0}C. Annealing at high temperatures improves the dark conductivity drastically [36]. This is due to the formation of a top layer of CdO [37].

1.1.8 Advantages and disadvantages of CBD technique

Advantages

1) CBD is a simple and low cost technique:

Of all the thin film deposition techniques, CBD is the simplest as no elaborate arrangement is required. It can be as simple as given in Fig.[1.6], with a beaker containing the reaction bath and glass slides dipped in it. It is to be specifically noted that the deposition is usually carried out at atmospheric pressure and at relatively low temperature.

The above mentioned reasons along with the fact that high purity chemicals is not an essential requirement, makes this a low cost technique. In this method there is very little chance of incorporation of impurities from the reaction bath on to the deposited thin films. Only if the impurities present in the bath are capable of forming insoluble compounds under the existing conditions of deposition, there is chance of incorporation into the film. This will happen only if the ionic product of the impurity species is greater than its solubility product. However chances of this are rare, as the impurity concentrations will be usually less than 2%.

2) Multicomponent films can be prepared

With CBD technique it is possible to deposit multicomponent chalcogenide thin films over a wide range of stoichiometry. Some of the ternary alloys prepared using this method are given in Table (1.2) [26].

Alloys of chalcogenide films are prepared by reacting sodium selenosulfate or thiourea with a mixture of different complexed metal ions. If two non-interfering and independent complexing agents (say A and B) are used for complexing two
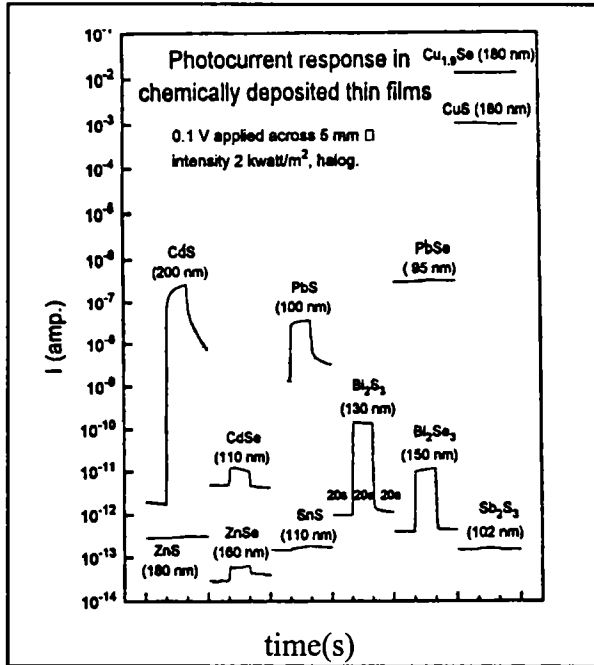
Fig.(1.3)   Photocurrent response of various semiconductor thin films
prepared by chemical bath deposition technique.
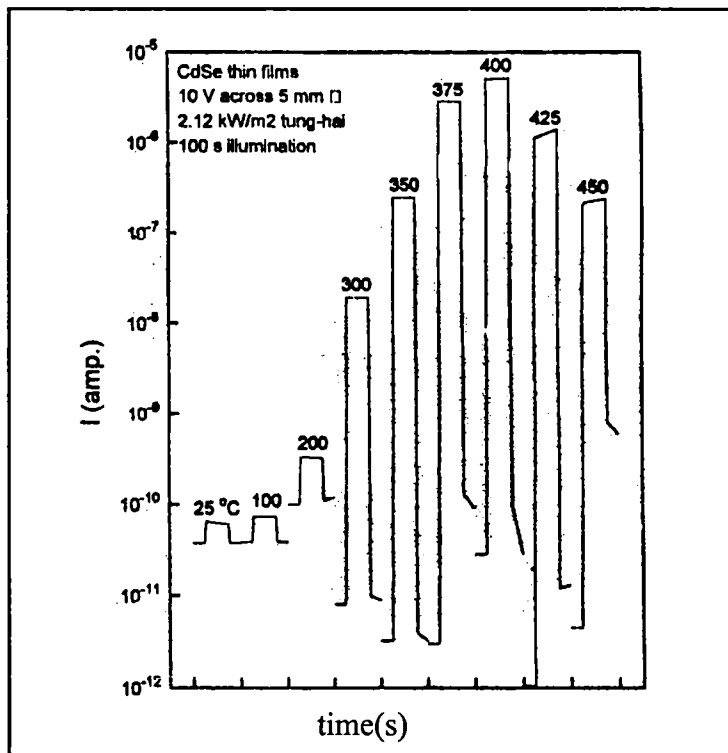
Fig.(1.4)   Variation in the photosensitivity of the films produced by annealing
of a CdSe film (~150nm) in air for 1 h each at different temperature.
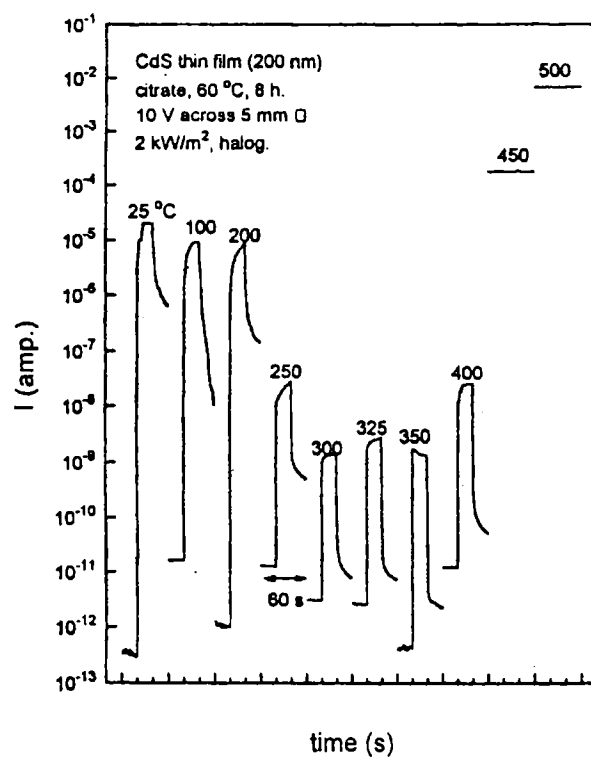
Fig.(1.5)   Variation of photosensitivity of CdS film with annealing in air
at different temperatures for 1hr
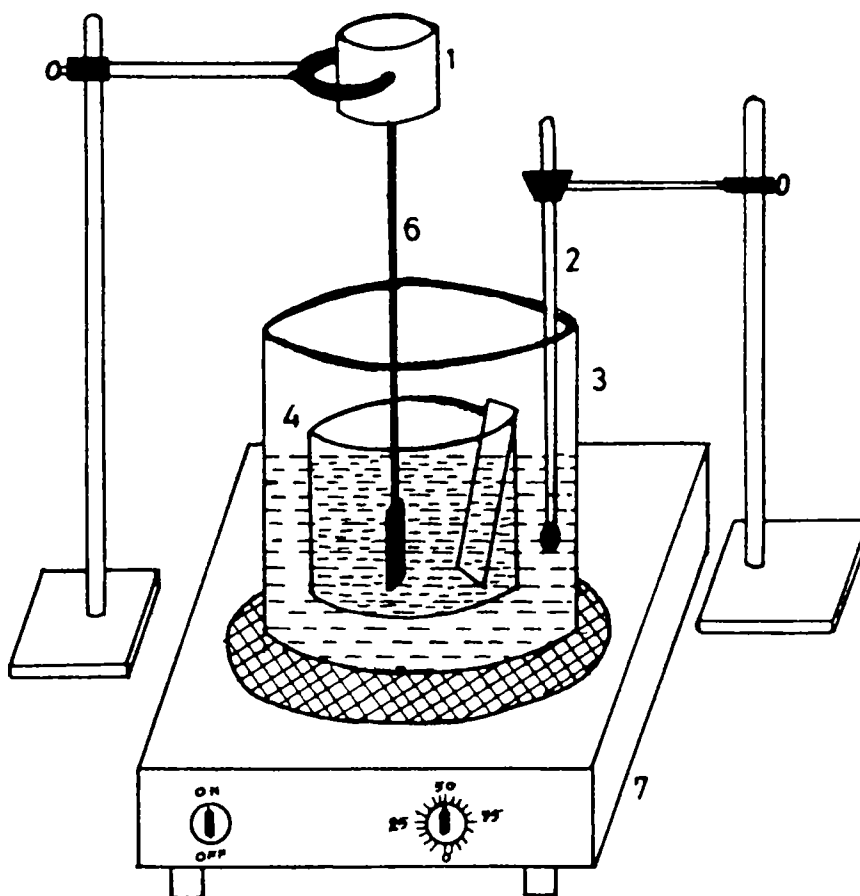
1. Motor   2. Thermometer
3. Water bath   4. Glass beaker
5. Glass slide   6. Stirrer
7. Heater

Fig.(1.6) Set up for chemical bath deposition of thin films

cations (say M and M^1), then the ions dissociate in an aqueous solution to give free metal ions according to the reactions

$$M(A)_n^{2+} \leftrightarrow M^{2+} + nA$$

$$and \quad M^1(B)_m^{2+} \leftrightarrow M^{1\,2+} + mB$$
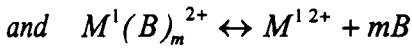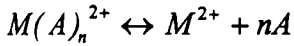
The stoichiometry of the as-deposited film depends on the initial salt concentration, complexing salt concentration and temperature of the bath. An alternative technique to vary the composition is to change the concentration of the complexing agents without altering the ratio of the salt concentrations. For example, the composition of $Cd_{1-x}Pb_xSe$ films could be varied by adding different amounts of NH_4Cl solution to the reaction mixture [26].

Alloy	Composition
$Pb_{1-x}Hg_xS$	$0 \leq x \leq 0.33$
$Pb_{1-x}Hg_xSe$	$0 \leq x \leq 0.35$
$Cd_{1-x}Hg_xS$	$0 \leq x \leq 1.30$
$Cd_{1-x}Hg_xSe$	$0 \leq x \leq 0.15$
$Cd_{1-x}Zn_xS$	$0 \leq x \leq 1$
$Cd_{1-x}Pb_xSe$	$0 \leq x \leq 1$
$CdSe_{1-x}S_x$	$0 \leq x \leq 1$
$PbSe_{1-x}S_x$	$0 \leq x \leq 1$

Table (1.2)   Few alloys prepared using CBD technique

3) Intertype conversion possible by easy methods

Many of the chemical bath deposited intrinsic semiconductors can be converted to n-type or p-type by easy and simple methods. For example, immersion of intrinsic CBD-CdS thin film in a dilute solution (0.05 M) of $HgCl_2$ for a few minutes and annealing in air at 200°C, produces n-type conductivity of ~ 1 $\Omega^{-1}cm^{-1}$ [36]. Similar results are reported for CdSe also [38]. This result is attributed to chlorine incorporation in the film. The main drawback of this conversion is loss of conductivity at high annealing temperatures. Recently another method was suggested for the conversion of CdS and CdSe to n-type [39-41]. This was based on evaporation

of a 20 nm thick indium layer on to the film surface and annealing at 300-350⁰C. This resulted in n type films of low resistance and high stability.

The conversion of CBD-CdS thin films to p-type by topoaxial reaction in copper chloride solution is well known. The incorporation of copper ions in CBD-CdSe thin films by immersion in a dilute solution of $CuCl_2$ (0.005 M) result in p-type conductivity with the reduction in sheet resistance from 10^{12} Ω/ □to 10^5 Ω/ □[15]. A similar case with ZnSe is also reported [42]. In ZnS-CuS or PbS-CuS multilayers, thermally stable p-type films of low sheet resistance can be prepared by interfacial diffusion of metal ions [16].

4) It is a safe procedure with minimum environmental hazards

Safety of this technique arises from two angles: 1) Due to the simplicity of the procedure which avoids sophisticated setup or high temperature and pressure. 2) It does not involve reactants in the vapour phase. For example, while the usual selenisation process involves H_2Se or Se vapour, they can be avoided in CBD processes. It is well known that toxicity hazards associated with lead, cadmium, mercury, selenium, etc. are severe when inhaled. An analysis on the toxicity hazards in the production of chemically deposited PbS thin films is given in Ref.[43] ,where it was established that the chemical bath technique does not entail the usual health hazards associated with lead pollution.

5) Suitable for large area deposition

Large area deposition is necessary for commercial purpose. This is possible with in this technique by carefully laying down the substrate on a shallow tray containing the deposition bath. The substrate surface should be kept at a height of 5 mm from the bottom of the tray with the help of spacers. In such an arrangement the film deposited at the bottom surface is found to be of better quality. Coatings on glass sheets of 60x60 cm^2 are usually prepared from 2000 ml of solution using the above arrangement [15]. This technique can be used for uniform film coating on substrates of any desired shape and form by suitably choosing the bath container.

6) Reproducibility is high

Once all the bath parameters that influence the deposition of thin film are standardised, this technique can give good reproducibility especially in the case of binary compounds.

7) Wastage can be minimized

Precipitates are unavoidable in CBD technique. However, in large-scale deposition, precipitate can be filtered out and reacted with acids or other suitable reagents to retrieve the starting materials for deposition. In many cases the precipitate may be rinsed well, dried and stored to serve as precursor for other deposition techniques.

For example, some precipitates can be used for screen-printing or production of composite coatings. Screen-printing has been successfully used in the production of CdSe-CdTe solar cells [44]. This process involves the precipitation of a paste containing the semiconductor pigment, a flux material that will fuse at a temperature much below the melting point of the pigment and a binder usually ethylene glycol or propylene glycol. This paste is printed on suitable substrate using a silk screen or polyester screen, dried for a few hours at 50-80°C and then sintered at a temperature higher than the melting point of the flux.

The precipitate produced in the chemical deposition bath is usually stoichiometric. The purity of such precipitate will be superior to that of the starting chemicals in the bath as the chances of incorporation of impurity is very less in this deposition technique. Thus the precipitate can serve as a relatively pure source of semiconductor material for vapour phase deposition [45].

Disadvantages

1. It is not easy to dope the intrinsic semiconductor thin films with external dopants at the time of film formation. This is due to the fact that slight concentrations of dopants included in the reaction bath will not be incorporated to the film unless the condition for precipitation (i.e. ionic product > solubility product) for that particular dopant is satisfied.

2. When used for the deposition of ternary and other multicomponent compounds, the control of stoichiometry will be difficult. In order to ensure the reproducibility of the process a precise knowledge of the effect of various parameters on the growth medium should be thoroughly understood.

3. Selection of substrate is restricted in CBD as there is possibility of reaction of substrate with the reaction mixture. Hence inert materials such as glass or SnO_2/ITO coated glass or inert metal surfaces are required.

4. Deposition of multilayers by CBD technique has to be done carefully. Or in other words, order of deposition of multilayers is to be selected. This is due to the possibility of reaction of the initially deposited layer with the solution bath meant for depositing the second layer. For example, $CuInSe_2$ cannot be deposited over CdS to form a multiplayer since CdS when dipped in a copper containing solution gets partially converted to Cu_xS.

5. This technique cannot be used to deposit very thick layer of materials. The maximum thickness attainable in a single dip is more or less fixed. Hence repeated dipping cannot lead to thickness greater than few microns. Moreover, in repeated dipping the chances of pealing off the film is high.

1.2 Various semiconducting thin films prepared by CBD technique for use in photovoltaic applications

The number of semiconducting materials that are deposited by this simple technique of CBD is increasing at a rapid rate. In this review a list of materials that finds application in the field of photovoltaics are included. Neither the list nor the cited references is complete or exhaustive. In the following section an attempt is made to introduce a few of these materials, with special emphasis on CdS and $CuInSe_2$.

1.2.1 Cadmium sulfide (CdS)

As far as photovoltaic is considered, CdS is the most successful material prepared using CBD technique. This is an extensively studied material with its direct band gap, high absorption coefficient, good electronic affinity and effective ohmic contact [46]. Growth of CdS is usually columar and perpendicular to the substrate surface [47]. This means that grain boundaries parallel to the junction that impedes the flow of photogenerated carriers are few. This material with its high conversion efficiency and stability has proved to be a good window material in solar cells [48]. Though various deposition techniques such as sputtering [49], spray pyrolysis [50],

vacuum evaporation [51] electrodeposition [52], screen printing [53] and molecular beam epitaxy [54] have been reported for the preparation of CdS, CBD technique has attracted much attention as a simple and promising one to obtain device quality films [55-57].

Even within the field of CBD-CdS, a comparative study of properties is impossible as no two preparation conditions coincide. For example, in the list of preparations given below, the cadmium salt can be seen to vary from sulfate, chloride, acetate, iodide and so on, leave alone the variations in deposition conditions like temperature, pH, duration of deposition, etc. Here an attempt is made to mention some of the gradual progresses on CBD films of this material, with more emphasis on recent works.

a) Photoconductive CdS by CBD process

In 1977 N. R. Pavaskar *et al.* [36] reported a detailed study on photoconductivity in CBD CdS films. He standardised the conditions under which these films could be produced with a high degree of reproducibility with respect to thickness, structure and electrical behaviour. The preparation procedure was as follows: 10 ml of 1 M cadmium sulfate solution and 50 ml of 2 M ammonia solution were mixed to form a complexed compound. To this solution, 10 ml of 1 M thiourea was added. The reaction bath was heated to 80-90^{0}C for 30 min. A pre-cleaned pair of substrate was kept rotating approximately 2.5 cm below the surface of the solution. The films formed were washed in distilled water and preserved in dark desiccator.

b) Growth kinetics

K. L. Chopra *et al.* [58] revealed the growth kinetics of chemical deposition of CdS film from alkaline solution of cadmium acetate, in the year 1980. The kinetics was studied with respect to temperature of deposition and the relative concentrations of the various reactants in the solution. It was established that the growth of the film takes place either by ion-by-ion condensation of Cd^{+2} and S^{-2} ions or by adsorption of colloidal particles of CdS formed in the solution, depending on the various deposition parameters and the method of preparation. The former process of growth result in thin, hard, adherent and highly reflecting films. The same group also proposed a model for growth mechanism.

c) Preparation of device quality CdS films

T. L. Chu *et al.* in the year 1992, deposited device quality CdS film on glass and on SnO_2:F/glass substrates from an aqueous solution containing cadmium acetate, ammonia, ammonium acetate and thiourea [59]. Well cleaned S_nO_2:F/glass substrates were vertically suspended in an aqueous mixture of $CdAc_2$ (10^{-3} M), NH_4Ac (0.02 M), NH_4OH (0.4 M) and $(NH_2)_2CS$ (5×10^{-3} M) at 85^0C under constant stirring. This solution had a pH around 9.1. The reaction started within 10-15 min and was complete in about an hour. The average deposition rate of CdS on SnO_2/glass substrate was 20-30 A^0/min.

The expected reactions were as follows

$$NH_3 + H_2O \leftrightarrow NH_4^+ + OH^-$$
$$Cd^{2+} + 2\,OH^- \leftrightarrow Cd\,(OH)_2$$
$$Cd^{2+} + 4\,NH_3 \leftrightarrow Cd\,(NH_3)_4^{2+}$$
$$(NH_2)_2\,CS + 2\,OH^- \leftrightarrow S^{2-} + 2\,H_2O + H_2CN_2$$
$$Cd^{2+} + S^{2-} \leftrightarrow CdS$$
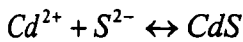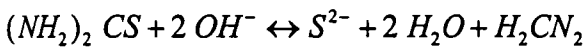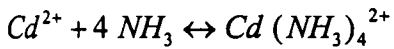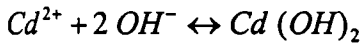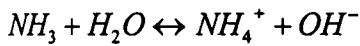
d) Conversion to n-type by boron doping

Boron doping was tried by adding Boric acid to the above mentioned reaction mixture [59]. Boron atoms were expected to occupy Cd sites in CdS to serve as donors. Studies were done by varying the molar ratio of BO_3^{2-}/Cd^{2+} in the solution in the range 10^{-5} to 10^{-2}. This doping made CdS n-type and it was found to have a pronounced effect on the dark conductivity. A minimum in dark resistivity was observed at a BO_3^{2-}/Cd^{2+} ratio of 0.001. With further increase in boron concentration, the dark resistivity was found to increase and it finally approached the value for undoped film (around 2×10^4 Ωcm). However, the illuminated resistivity of boron doped CdS films deposited at large BO_3^{2-}/Cd^{2+} ratios was found to be independent of the boron concentration. From the photoconductivity study of these films it was observed that the incorporation of boron into CdS films increases the time constant appreciably indicating the formation of slow states in the band gap.

e) Conversion to n-type by indium diffusion

Boron doping in CBD-CdS reduced the optical band gap of the as-prepared film. Hence in 1996, P. J. George *et al.* suggested a successful method of indium

diffusion to make CdS n-type and that too without tempering the large band gap of the material [60]. As-prepared CdS thin films were deposited at 80^{0}C for 4 hrs from a chemical bath containing citratocadmium ions and thiourea. An indium layer of 10-40 nm thickness was evaporated on to the CdS film surface that was thermally diffused by heating the sample in air at 250^0- 350^{0}C for 1-4 hrs. XPS analysis revealed the diffusion of indium into the CdS film leading to the conversion of chemically deposited intrinsic CdS thin film into n-type with conductivity upto 50 Ω^{-1}cm^{-1}. Optical transmittance spectra of these films indicated that the band gap was still > 2.5 eV. This has opened up the scope for using such n-type CdS films directly as a window layer in heterojunction solar cells.

f) CdS deposition from acidic bath

CdS deposition is always associated with baths that are alkaline [61]. However, Paul O' Brien et al. have very recently (1999) reported for the first time that CdS can be deposited from acidic bath containing thioacetamide [62]. CdS thin film was grown on pre-cleaned tin oxide glass substrates from solution containing cadmium salt (chloride 0.02 mol/dm^3), urea (0.5 mol/dm^3) and thioacetamide (0.2-0.02 mol/dm^3), to obtain a solution (100 cm^3) of final pH 5.5-4.9. The temperature of deposition was around 75^{0}C and occasional stirring was given.

The adherence of the film was good, but they did not resemble in morphology or properties to the alkaline bath CdS. Air annealing improved the crystallinity of this hexagonal phase and it also induced the migration of chloride ions to the surface region. No evidence of oxidation was observed on air annealing. These results have opened up the possibility of developing ternary films of (CdZn)S under acidic conditions.

g) Modification of CBD apparatus

In the year 2000, G. Sasikala et al. [63] has suggested a modified set up for CBD deposition of CdS. This modification is in order to obtain a precise control over the pH of the reaction mixture. The vital role of pH on the quality of the CBD–CdS films were also revealed with this modified apparatus, Fig.[1.7]. Here the substrate suspended from the sample holder can be rotated at a constant speed so as to ensure homogenous heat transfer to the substrate from the hot reaction bath. A reservoir

arrangement was made for simultaneous addition of thiourea into the bath during the growth process. A pinch cork was provided to adjust the rate of flow. The other reactant was cadmium chloride complexed with ammonia. Temperature of deposition was maintained at (0^0C) with the help of oil bath. pH of the reaction bath will decrease slowly due to evaporation of NH_3 gas. In order to avoid this, the vessel was provided with mercury liquid seal for the stirrer. Main upper portion of the vessel was arranged to be exposed to atmosphere in order to help ammonia vapour to condense and fall back to the deposition solution. To take care of high pressure, a safety valve was also provided.

h) CBD –CdS based solar cells

CdS/CdTe cell: (1992)

T. L. Chu *et al.* reported an n-CdS/p-CdTe solar cell where the CdS layer was prepared using chemical deposition [59]. On $SnO_2.F$/glass substrate device quality CdS films of thickness 600-1000A^0 was deposited as mentioned earlier in section (c). It was converted to n-type through boron doping (as mentioned in section (d)). On to such a layer, p-CdTe film was deposited using close-spaced sublimation (CSS) technique. Substrate (CdS/SnO_2:F/glass) and the polycrystalline CdTe source were separated by about 0.2 cm. Source materials and substrate were maintained at about 700^0C and 600^0C respectively. The deposited film was 4 to 5 µm thick. Devices of about 1cm^2 area were isolated. The study conducted at NREL revealed that such solar cells could give efficiency higher than 14.5% under global AM 1.5 conditions.

CdS/CIS cell: (1996)

Hai-Ning Cui and Shi-Quan Xi in 1996 reported the test trial of ITO/dip-CdS/CIS/Mo/glass structured cell. This cell with chemically deposited CdS acting as widow layer and CIS ($CuInSe_2$) acting as absorber layer showed considerably high efficiency [64]. Here chemically deposited CdS was prepared as follows

Solution 1: $CdCl_2$ (0.01 M), NH_4Cl (0.039 M), NH_4OH (0.76 M)

Solution 2: Thiourea (0.17 M); NH_4Cl (0.039 M); NH_4OH (0.76 M)

Equal volumes of solutions 1 and 2 were mixed at 50^0C and placed in the deposition beaker in which cleaned glass slides were kept vertically. This beaker was placed in a water bath held at 73^0C. pH value of combined solution was approximately 11.

During cell construction, in order to increase the optical transmission range of the window material, only a very thin resistive layer of the CdS was used. On this a transparent conducting layer of ITO was deposited using rf sputtering. This double layer formed a good window region for the solar cell.

Recently, a CBD-CdS/CBD-CIS cell was reported and the details of this are included under the following section 'All-CBD cell'.

CdS/CIGS cells: (1998)

Y. Hashimoto *et al.* [65] fabricated a solar cell with an active area of 0.48 cm^2, with a structure MgF$_2$/ITO/ZnO/CdS/CIGS/Mo/glass. The high quality CIGS (copper indium gallium selenide) film was deposited on Mo coated soda lime glass by applying the composition monitoring system to the 3-stage process. Stoichiometric CdS layer of thickness 100A^0 was deposited on the CIGS layer by CBD technique. The chemicals used for this include equal amount of 0.0014 M CdI$_2$, NH$_3$ and 0.14 M CdI$_2$, NH$_3$ and 0.14 M thiourea solution. The deposition was carried out in a solution of pH 11.8, at a temperature of 70^{0}C and the duration of deposition was 20 min. The ZnO layer with thickness of 0.2 μm and the ITO layer with thickness of 0.1 μm were deposited by RF magnetron sputtering. The MgF$_2$ antireflection layer with thickness of 0.12 μm was deposited by electron beam evaporation. The device had a high conversion efficiency of 17% (V_{oc} = 0.65 V, J_{sc}=35.1 mA/cm^2, FF = 0.747). This result indicates that the performance of the solar cell becomes appreciable on improving the stoichiometry of the CdS layer by CBD technique.

All – CBD Cell:

The first report of 'All-CBD cell' i.e. CBD-CdS/CBD-CIS cell was from the Photovoltaic laboratory, Dept. of Physics, Cochin University of Science and Technology [66]. The details of cell fabrication is as given below:

A SnO$_2$:F/glass substrate was dipped in a reaction mixture containing aqueous solutions of copper citrate (7.5 ml, 0.2 M), indium citrate (25 ml, 0.2 M) and sodium selenosulphate (20 ml, 0.1 M). Deposition was carried out at room temperature at a pH of 6.5, under stirring. For a deposition time of 1hr, a thickness ~ 120 nm was obtained. For higher film thickness, repeated deposition was done.

As a next step CdS was deposited on this by CBD technique itself. A reaction bath containing cadmium chloride ($CdCl_2$), triethanol amine, thiourea and ammonium hydroxide was used. The temperature was kept controlled at $90^{\circ}C$ and pH at ~10.5. Film of thickness ~ 600 nm was obtained in 30 min time.

These samples were then annealed in air at $200^{\circ}C$ for 7 hrs to improve and stabilise the characteristics. Then the top CdS layer was given a chemical treatment by dipping the sample in hot ($50^{\circ}C$) stannic chloride solution (0.5 M) for few seconds and drying at $100^{\circ}C$ for 5 min. This was done to reduce the series resistance of the cell. The device fabrication was completed with deposition of a top electrode. The electrode was vacuum evaporated indium in the form of a grid. Then the sample was annealed in a low vacuum of 10^{-1} Torr at a temperature of $150^{\circ}C$ for 1 hr. The total area of the film deposited was 5x1.25 cm^2. It was divided into small cells of area 0.1cm^2. Each cell was then tested for its photovoltaic activity.

The schematic diagram of CBD-CuInSe$_2$/CBD-CdS thin film solar cell is shown in Fig.[1.8] [67]. The cell parameters obtained for the best cell were, V_{oc} = 365 mV, J_{sc}= 12 mA/cm^2, FF= 61% and η=3.1% under an illumination of 85 mW/cm^2 on cell of active area 0.1 cm^2. The J-V and C-V characteristics and the spectral response were also studied.

1.2.2 Cadmium selenide (CdSe)

CdSe thin films with a direct band gap of 1.7 eV and n-type conduction are of great relevance in photovoltaic systems [68]. A recent report of p-type conduction in this material prepared by molecular beam epitaxy (MBE) technique has enhanced its scope [69]. Highly stoichiometric CdSe films are prepared by hot-wall epitaxy, vacuum evaporation and MBE [70,71]. Chemical techniques like spray pyrolysis, screen-printing, electrodeposition and evaporation of the residual precipitate from chemical bath deposition [72-75] are also reported. But a major problem with this polycrystalline film is the considerable reduction in photo response due to the grain boundary defects. A report that appeared this year on the success of laser annealing has given rays of hope for betterment [76].

Based on chemical kinetics it has been found that initiation of CdSe film formation will be possible by CBD technique only in the region of existence of hydroxide [77]. Nair and Nair has suggested the following preparation procedure
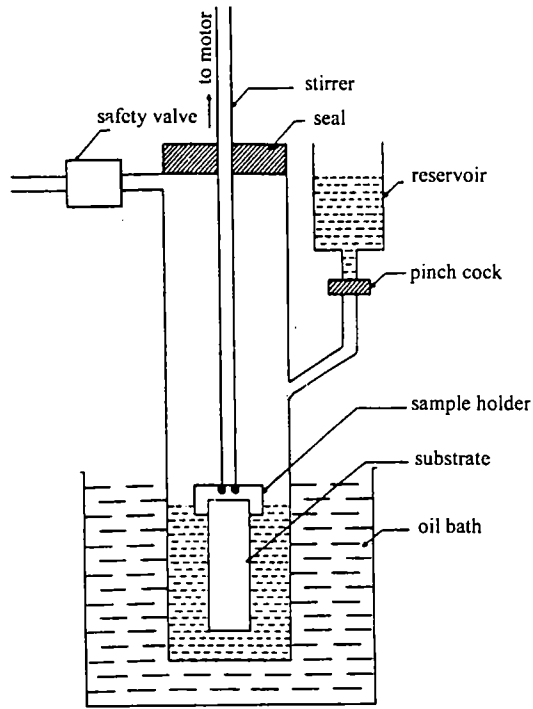
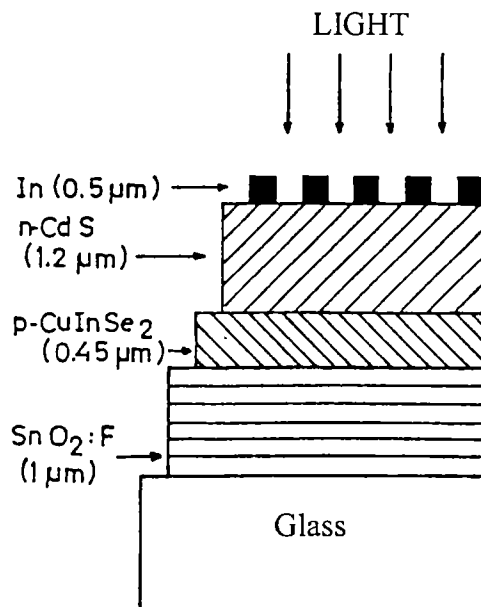Fig.(1.7)   Modified chemical bath deposition set up

Fig.(1.8)   Schematic diagram of the CuInSe$_2$/ CdS 'All-CBD'

solar cell structure

[34,35], 30 ml of 0.1 M $Cd(NO_3)_2$ $4H_2O$, 12 ml of 1 M sodium citrate, 1.2 ml of 30% (~ 15M) NH_4OH and 0.4 g of N,N-dimethyl selenourea dissolved in 30 ml of freshly prepared 0.01 M Na_2SO_3 is mixed and the volume is made upto 100 ml by addition of water. Thin film deposited from this reaction bath at room temperature after a duration of 24 hrs, is found to be smooth and uniform.

1.2.3 Copper sulfide (Cu$_x$S)

Ever since the discovery of photovoltaic effect in CdS/Cu$_x$S structure in mid fifties, there has been wide spread interest in Cu$_x$S thin films. Various methods such as evaporation, reactive sputtering and improved topoaxial reaction has been tried to obtain Cu$_x$S films with x~1.997 as required for solar cell applications [18]. In recent years this material is pursued for its solar control application also [5,8].

Many researchers have reported on chemical bath deposition of Cu$_x$S. Fatas *et al.* [78] mixed 1 M $CuSO_4$, 1 M sodium acetate and 7.4 M TEA solution and then added 1 M thiourea in alkaline medium. They reported an optical band gap of 2.58 eV and resistivity of the order of $3x10^{-3}\Omega cm$. A. J. Varkey [79] has reported Cu$_x$S deposition using EDTA as a complexing agent in a bath comprising of CuCl, NaCl and hydroxylamine hydrochloride solutions. In 1993, Gadave *et al.* [80] did this in a different way. An aqueous solution of 15 ml 0.1 M $CuSO_4$ and 15 ml 1 M sodium thiosulfate was mixed and clean glass slides were introduced in this reaction bath of pH 0.5 for ~ 40 min. The temperature of deposition was 60^0C. This resulted in Cu$_x$S films of band gap 2.4 eV and electrical resistivity of the order of $10^{-4}\Omega cm$.

1.2.4 Antimony sulfide (Sb$_2$S$_3$)

Sb_2S_3 thin films have been successfully used in schottky barrier solar cells (Pt-Sb_2S_3) [81] and in hetero junction solar cells (n-Sb_2S_3/p-Ge) [14] with conversion efficiencies of 5.5% and 7.3% respectively. This material is usually prepared by vacuum evaporation technique [82] and chemical bath deposition technique [14,83,81]. Depending on the deposition process the films may show n or p type conduction [84,85].

For the deposition of antimony sulfide thin films by chemical bath method, Mandal and Mondal [83] used a solution containing potassium antimony tartarate, triethanol amine, aqueous ammonia and thioacetamide. Later, Savadogo and Mandal

[86] showed that addition of a small quantity of silicotungstic acid in the bath yields films with enhanced photoconductivity with WO_3 incorporated in them. Grozdanov [87] reported deposition of Sb_2S_3 films from a bath consisting a solution of $SbCl_3$ (3.5 to 4 g) dissolved in glacial acetic acid (7 ml), 1 M sodium thiosulfate (100 ml) and cold (10-15°C) distilled water (400 to 500 ml). Thin films of thickness up to 1.3 μm were obtained from this bath after 24 hrs of deposition. In 1998, Nair *et al.* [85] did this in a slightly different way. In a 100 ml beaker, 650 mg of Sb_2S_3 was dissolved in 2.5 ml of acetone. 25 ml of 1 M sodium thiosulfate at 10°C was added to this and it was followed by the addition of 70 ml deionised cold water. The deposition was carried out at 10°C. Annealing of these as–prepared films at 250°C in nitrogen atmosphere improved the crystallinity, decreased the band gap from 2 eV to 1.7 eV and increased the photosensitivity.

1.2.5 Zinc oxide (ZnO)

Zinc oxide can be used as a transparent electrode material in photovoltaic cells because of its good material properties [88]. Recently this material has evolved as a suitable buffer layer on p-$CuInS_2$, so as to replace the CdS layer. ZnO layer with its band gap of 3.3 eV is found to improve the light transmission in the blue wavelength region. It can be a substitute for CdS layer, thus avoiding the toxic cadmium. There are various deposition techniques for this material [89].

Paul O'Brien [89] deposited ZnO films by CBD. The reaction bath consisted of 0.0188 M Zn and 0.042 M ethylenediamine. The starting pH was made upto 10.5-11 by addition of NaOH. The film grown on clean glass substrates dipped in this reaction bath was uniform and adherent.

Recently, Ennaoui *et al.* [90] deposited CBD–ZnO by two other procedures. In the first method the substrates were immersed in the beaker containing reaction mixture of dilute tetraamine zinc at 65°C. The second method was SILAR (Successive Ionic Layer Adsorption and Reaction) which consisted of there main steps: (i) specific adsorption of zinc amine solution by substrate immersion in a solution containing $Zn(NH_3)_4{}^{2+}$ at room temperature (ii) introduction of the substrate in hot water at 95°C (iii) water rinsing in order to remove loose ZnO particles before starting a second cycle. A ZnO/$CuInS_2$ junction was fabricated with this CBD-ZnO layer.

In order to compare the performance of this $ZnO/CuInS_2$ junction with that of the standard $CdS/CuInS_2$ solar cell, both junction were prepared and the device properties were measured under AM 1.5 solar spectrum. The output characteristics of the cells and corresponding spectral quantum efficiencies are shown in Fig.[1.9-a,b]. Due to the higher band gap of the ZnO layer, an enhanced response in the short wavelength of the spectrum was observed. However this cell had only a low efficiency of around 4%, while the CdS cell prepared under the same conditions had efficiency of 9%. Fill factor and photocurrent values were comparable. Anyway this has opened up the scope for Cd free cells.

1.2.6 ZnS, $Cd_xZn_{1-x}S$ and ZnSe

These are few other materials that could be prepared by CBD technique, which finds applications in photovoltaic devices [24]. It is expected that in CdS based solar cells the use of wider band gap materials such as ZnS or $Cd_xZn_{1-x}S$ can lead to decrease in window absorption losses and improvement in the short circuit current of the cell.

Reports have shown that it is not easy to prepare high quality ZnS by CBD, though Paul O' Brien has suggested strategies for the same [24]. Nair and Nair [91] have given the recipe as, 5 ml of 1 M zinc sulfate, 4.4 ml of NH_3/NH_4Cl (pH 10), 54 ml of 50% TEA, 2 ml of 1 M thioacetamide and the rest deionised water to make up to 100 ml by volume. Deposition of ZnS films of 0.2 μm thickness could be obtained at 50^0C by about 6 hrs or at room temperature by about 20 hrs.

$Cd_xZn_{1-x}S$ is a more promising material for photovoltaic cells due to the possibility of tailing its semiconductor properties between the values corresponding to the pure binaries. This fact allows to adjust the material properties as per the device requirements. The techniques adopted for preparation of $Cd_xZn_{1-x}S$ include evaporation, CVD, spray, electrodeposition, SILAR and CBD. Dona et al. [92] has prepared this phase by CBD using 1.4 M 5% ammonia, 2.25 M 80% hydrazine, 0.14 M thiourea and $CdSO_4$ and $ZnSO_4$ concentration between 0 and 0.1 M, i.e. $[ZnSO_4]$ + $[CdSO_4]$ = 0.1 M. $CdSO_4$ and $ZnSO_4$ were added first to the NH_3/NH_2-NH_2 solution under stirring followed by the addition of thiourea solution. The temperature of deposition was 70^0C.
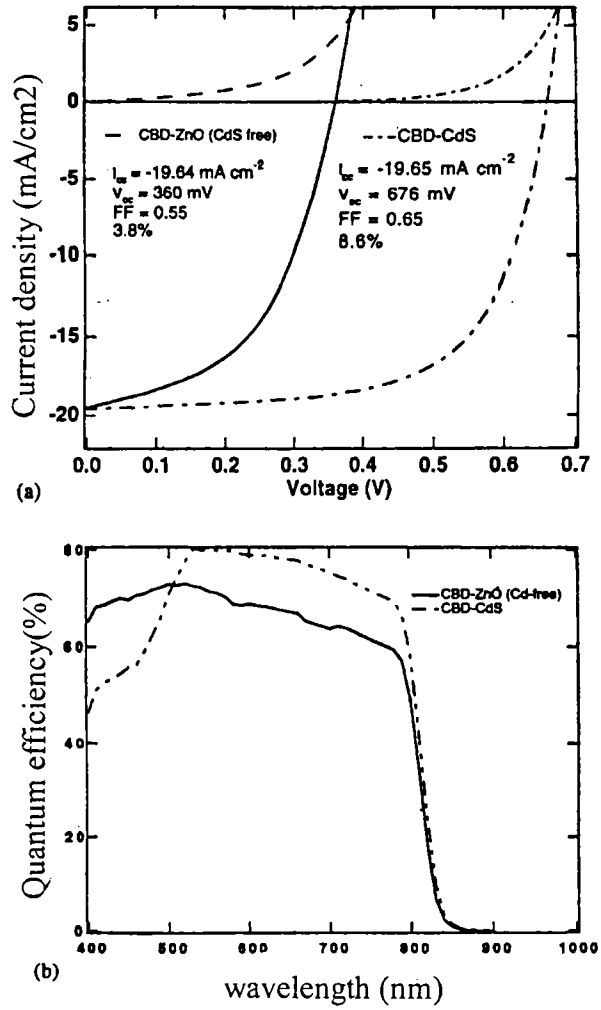
Fig.(1.9) (a) Output characteristics of thin film CuInS$_2$ solar cells with
CdS and ZnO buffer layers

(b) Spectral quantum efficiencies of thin film CuInS$_2$
solar cells with CdS and ZnO buffer layers

P.K. Nair *et al.* [15] has found ZnSe to be more photosensitive than ZnS. The preparation suggested was, 35 ml of 0.1 M zinc acetate, 16 ml of 0.8 M sodium citrate, 5 ml of 7.4 M ammonium hydroxide mixed with 20 ml of 0.07 M N, N dimethyl selenourea and the volume made up to 100 ml with deionised water. Depositions could be made at room temperature or at 60°C.

1.2.7 Bi_2S_3 and Bi_2Se_3

Sulfides and selenides of bismuth are also finding their place in the field of photovoltaics. P. K. Nair *et al.* [45,93] prepared Bi_2S_3 from a bath of 10 ml of ~0.5 M $Bi(NO_3)_3$. 5 H_2O solution, 8 ml of 50% triethanol amine and 4 ml of 1 M thioacetamide made upto 100 ml. The duration of deposition was 24 hrs.

Similarly, the same group has reported the deposition of $Bi_2 Se_3$ thin films from a bath consisting of 7 ml of 0.5 M $Bi(NO_3)_3$ solution, 7 ml of 50% triethanolamine an 20 ml of 0.07 M N,N-dimethyl selenourea solution finally made up to 100 ml. Films of 0.2 μm thickness could be deposited in about 9 hrs at 40°C or in about 60 hrs at room temperature [94].

1.2.8 Indium hydroxy sulfide

Most recent trend in R&D activities in solar cell include the idea of fabricating chalcopyrite based devices replacing the CdS buffer layer by other CBD compounds with similar or even better properties [95]. One promising candidate to achieve this goal is the CBD-prepared indium hydroxy sulfide. $In(OH)_xS_4$ when used as buffer layer in solar cells gave good 1-V characteristics [96,97]. Some of the thin film properties of this material are mentioned in Ref. [98].

Conditions of chemical bath deposition that lead to good quality indium hydroxy sulfide thin films with high growth rate were [99]- [In Cl_3] = 0.025 M, [thioacetamide] = 0.1 M and [acetic acid] = 0.1 M at 70°C and at acidic pH. A terminal thickness of 1800A° was obtained after 45 min of deposition. XPS analysis showed the as-prepared samples to be consisting of more than 80% indium hydroxy sulfide and some quantities of indium oxide and indium sulfate. The molecular formula suggested for this phase was close to InOHS with slight variation in the OH:S proportion.

1.2.9 Copper indium diselenide (CIS) (CuInSe₂)

In the field of heterojunction solar cells, $CuInSe_2$ has a potential scope with its attractive properties of direct band gap (~1 eV), high optical absorption coefficient (α ~ 10^5 cm⁻¹), good lattice match and electron affinity with other binary semiconductors such as CdS. In recent times, $CuInSe_2$ thin film based single junction solar cells have shown efficiencies as high as 18.8% [100].

There are various preparation techniques reported for this material [101]. However all these techniques involve sophisticated and expensive set up. Moreover, handling of poisonous gases like H_2Se or selenium vapour is a major problem in many of these processes. It is in this context that the significance of chemical bath deposited CIS arise.

The first report on CBD-CIS came in the year 1987 [102]. The preparation procedure was as follows: 10 ml of 0.5 M copper chloride solution was mixed with 6 ml of 7.4 M triethanolamine and 20 ml of 13.4 M ammonia solution. To this mixture 18 ml of 0.5 M freshly prepared sodium selenosulfate solution was added to get a resulting pH of 10. The deposition mixture was magnetically stirred during the growth process and the duration of depositions was standardized at 30 min. It was observed that at low temperatures of deposition (~50⁰C), Cu reacts much faster with selenium than In does. This resulted in the incorporation of CuSe phase. The stoichiometry of the as-prepared films deposited at 50⁰C and 90⁰C were evaluated as $Cu_{1.09}In_1Se_{2.02}$ and $Cu_{0.01}In_1Se_{1.85}$ respectively, from EDS analysis.

In the next year (1988) there was a report on fabrication of a junction on a trial basis [103]. $CuInSe_2$ preparation was reported as: Cu^{2+} ions were complexed with ammonia solution and mixed with Na_2SeSO_3 solution. To this mixture, solution containing a complex ion of indium and citrate was added. The reaction was carried out at 40⁰C for 14 hrs to obtain uniform films of $CuInSe_2$ on glass and quartz substrates. The XRD analysis showed a chalcopyrite structure. While EPMA analysis revealed the composition to be nearly stoichiometric, Hall measurements showed that the films were p-type with a carrier concentration of about 10^8cm⁻³, μ_H ~1cm²V⁻¹s⁻¹ and conductivity of about $10^{-3}\Omega^{-1}$cm⁻¹. The photosensitivity of the film was found to be maximum when annealed at temperature greater than 450⁰C.

A p-$CuInSe_2$/n-Si hetero junction was tried by depositing this CIS layer of 2 μm thickness on a Si wafer of 1 Ωcm resistivity. This cell suffered from large series

resistance that lead to deterioration of short circuit current and fill factor. After a heat treatment of the device at 520^0C in air for 30 min, the open circuit voltage was 300 mV. However in general the junction performance was not appreciable.

In the year 2000, there was a report on CBD-CIS [101]. The deposition bath consisted of $CuCl_2$, $InCl_3$, H_2SeO_3 and LiCl dissolved in deionised water. The pH of the bath was adjusted to 2.2 by adding dil. HCl. EDAX analysis showed the composition of the surface layer of the film to be close to the required stoichiometry. However the composition determined by ICP analysis deviated much from the EDAX results. Hence it was inferred that an indium rich region is formed near the surface and a Cu rich region is formed towards the bottom. For the same reason, the as-prepared films could only be considered as a good precursor for CIS films. The film property was found to improve with annealing in Se atmosphere.

The first report on device level $CuInSe_2$ thin film by chemical deposition is from the Photovoltaic lab of Cochin University of Science and Technology [104]. The details are already included in section (1.2.1.h) under the heading 'All-CBD cell'.

1.2.10 Copper indium disulfide (CuInS₂)

The ternary compound semiconductor of $CuInS_2$ is an attractive material for solar energy conversion as its band gap is 1.55 eV. A number of deposition techniques are used for the synthesis of this material. This includes single, dual and three source evaporation, spray pyrolysis, RF sputtering, electrodeposition and sulfurisation. The highest conversion efficiency attained with this material was 7.3% [105].

G.K. Padam *et al.* has reported the preparation of this material by CBD [106]. The deposition mixture consisted of 10 ml $CuCl_2.2H_2O$ (0.5 M), 5.5 ml $InCl_3$ (0.5 M), 40 ml thiourea (0.5 M), 6 ml triethanolamine (0.5 M) and 20 ml ammonia (13.4 M). The deposition was carried out at 80^0C and the duration of deposition was 45 min. Films obtained were found to be extremely adherent to the glass substrate and homogenous in appearance when stirring was given to the mixture, where as unstirred films gave powdery appearance. X-ray analysis proved this material to be crystalline but with slight deviation from the standard d-values of $CuInS_2$. Both the EDS and the spectrochemical methods showed that the Cu to In ratio is 1.08 instead of 1.

1.2.11 Copper selenide

Cu_2Se is a cuprous chalcogenide film that always show p-type conduction due to copper vacancies. This material has an indirect band gap 1.1-1.27 eV [107], which makes it an absorber material and a direct band gap > 2eV [108], which makes it a window material in solar cells. Photovoltaic junctions Cu_2Se/Si, $Cu_{2-x}Se/CdS$, $Cu_{2-x}Se/CdSe$ and Cu_2Se/InP are reported. Prospects for this material also lies in the feasibility of producing the ternary compound $CuInSe_2$, starting with $Cu_{2-x}Se$ precursor. Though there are various deposition techniques for this material, CBD is the simplest. Chapter 2 elaborates the preparation technique and applications of this material in photovoltaics.

1.3 Conclusion

The principle behind chemical bath deposition technique is the controlled precipitation of a compound from a reaction bath. Nature of reactants and substrates and the temperature and pH of the reaction are few of the factors that influence the deposition process.

Semiconducting thin films prepared using CBD find applications as photo detectors, solar control coatings and solar cells. In the field of solar cells, apart from the direct use of CBD films of binary compounds, there is also scope for use of films like Cu_xS and Cu_2Se as a precursor for preparing the leading materials such as $CuInS_2$ and $CuInSe_2$. Efforts in this direction by diffusing indium into these binary CBD films have been reported from Photovoltaic laboratory, Dept. of Physics, Cochin University of Science and Technology [109].

Theoretical modeling of thin film deposition by this technique has been an area of constant interest among researchers [110]. The advantages of CBD include simplicity and low cost of the procedure, minimum wastage of chemicals and possibility of deposition on large areas. In this chapter the disadvantages of this technique are also described in detail. Few CBD based cells are highlighted along with the reported cell efficiencies. The preparation procedures of various thin films by this chemical method, that finds application in photovoltaics are also briefly mentioned.

The Photovoltaic division of Cochin University of Science & Technology has been working in this field of CBD thin films for the past few years. PbS, CdS, Cu_xS, $CuInSe_2$ etc. has been our material of constant interest. An 'All-CBD cell' with $CdS/CuInSe_2$ junction was fabricated in this lab [66]. Though the efficiency was only around 3%, it has opened the avenue for large area-low cost thin film solar cells. Recently our interest has been slowly shifting towards relatively new materials that may turn out as successful candidates of tomorrow. This thesis work forms a part our sincere endeavor in this direction.

Reference

[1]   J. E. Reynolds, *J. Chem. Soc.*, 45 (1884) 162.

[2]   D. E. Bode, in: G. Hass and R. E. Thun (Eds.), *Physics of Thin Films*, Academic Press, New York, 3 (1966) 275.

[3]   S.V. Svechnikov and E. B. Kaganovich, *Thin Solid Films*, 66 (1980) 41.

[4]   G. B. Reddy, V. Dutta, D. K. Pandya and K. L. Chopra, *Sol. Energy Mater.*, 15 (1987) 383.

[5]   P. K. Nair, M. T. S. Nair, A Fernandez and M. Ocampo, *J. Phys. D*, 22 (1989) 829.

[6]   K. L. Chopra, R. C. Kainthla, D. K. Pandya, A. P. Thakoor, in: G. Hass, M. H. Francombe and J. L. Vossen (Eds.), *Physics of Thin Films*, Academic Press, New York, 12 (1982) 201.

[7]   R. A. Boudreau and R. D. Rauh, *J. Electrochem. Soc.*, 130 (1983) 513.

[8]   M.E. Rincon, M. Sanchez, A. Olea, I. Ayala and P. K. Nair, *Sol. Energy Mater. Sol. Cells*, 52 (1998) 399.

[9]   C. D. Lokhande and S. H. Pawar, *Sol. Energy Mater.*, 7 (1982) 313.

[10]   O. Savadogo, Chemically and Electrochemically deposited thin films for solar energy materials, *Sol. Energy Mater. Solar Cells*(1997) proceedings.

[11]   B. Bluent and K. Vijay, *IEEE Trans. Electron Dev.*, 37 (1990) 418.

[12]   T. R. Tuttle, M. A. Contrevas, J. S. Ward, A. L. Tennant, K. R. Ramanathan, J. Keane, R. Noufi in: C. M. Lampert et al. (Ed.), *Proc. SPIE, Bellingham*, 2531 (1995) 194.

[13]   O. Savadogo and K. C. Mandal, *Appl. Phys. Lett.*, 63 (1993) 12.

[14]   O. Savodogo and K. C. Mandal, *J. Phys. D*, 27 (1994) 1070.

[15]   P. K. Nair, M. T. S. Nair, V. M. Garcia, O. L. Arenas, Y. Pena, A. Castillo, I. T. Ayala, O. Gomezdaza, A. Sanchez, J. Campos, H. Hu, R. Suarez and M. E. Rincon, *Sol. Energy Mater. Sol. Cells*, 52 (1998) 313.

[16]   L. Huang, P. K. Nair, M. T. S. Nair, R. A. Zingaro and E. A. Meyers, *J. Electrochem. Soc.*, 141 (1994) 2536.

[17]   C. A. Estrada Gasca, G. Alvarez – Garcia, R. E. Cabanilals and P. K. Nair, *Renewable Energy*, 2 (1992) 477.

[18] P. K. Nair, V. M. Garcia, A. B. Hernandez and M. T. S. Nair, *J. Phys. D*, 24 (1991) 1466.

[19] C. D. Lokhande, *Mater. Chem. Phys.*, 27 (1991) 1443.

[20] K. Bindu, M. Lakshmi, C. Sudhakartha, K. P. Vijayakumar, T. Abe and Y. Kashiwaba (Accepted for publication in Thin solid Films).

[21] C. A. Estrada, P. K. Nair, M. T. S. Nair, Ralph A. Zingaro and E. A. Meyers, *J. Electrochem. Soc.*, 141 (1994) 802.

[22] I. Grozdanov, *Synthetic Metals*, 63 (1994) 213.

[23] V. M. Garcia, P. K. Nair and M. T. S. Nair, *J. Crystal Growth*, 203 (1999) 113.

[24] P. O'Brien and J. McAleese, *J. Mater. Chem.*, 8 (1998) 2309.

[25] D. S. Boyl, P. O'Brien, J. Otway and O. Robbe, *J. Mater. Chem.*, 9 (1999) 725.

[26] K. L. Chopra and S. R. Das, *Thin film Solar Cells*, Plenum Press, New York, (1983).

[27] A. A. C. Readigos, V. M. Garcia, O. Gomezdaza, J. Campos, M. T. S. Nair and P. K. Nair, *Semicond. Sci. Technol.*, 15 (2000) 1022.

[28] P. K. Nair, P. Parmananda and M. T. S. Nair, *J. Crystal Growth*, 206 (1999) 68.

[29] G. Hodes, A. A. Yaron, F. Decker and P. Motisuke, *Phys. Rev. B*, 36 (1987) 4215.

[30] S. Gorer and G. Hodes, *J. Phys. Chem.*, 98 (1994) 5338.

[31] L. Brus, *J. Chem. Phys.* 90 (1986) 2555.

[32] B. K. Rai, H. D. Bist, R. S. Katiyar, M. T. S. Nair and P. K. Nair, *J. Appl. Phys.*, 82 (1997) 1310.

[33] J. J. Loferski, J. Schewchun, S. D. Mittleman and G. Chapman, *Sol. Energy Mater.*, 1 (1979) 157.

[34] M. T. S. Nair, P. K. Nair, H. M. K. K . Pathirana, R. A. Zingaro and E. A. Meyers, *J. Electrochem. Soc.*, 140 (1993) 2987.

[35] V. M. Garcia, M. T. S. Nair, P. K. Nair and R. A. Zingaro, *Semicond. Sci. Technol.*, 11 (1996) 427.

[36] N. R. Pavaskar, C. A. Menezes and A. B. P. Sinha, *J. Electrochem. Soc.*, 124 (1977) 743.

[37] K. L. Narayanan, K. P. Vijayakumar, K. G. M. Nair and G. V. N. Rao, *Bull. Mater. Sci.*, 20 (1997) 287.

[38] M. T. S. Nair, P. K. Nair, H. M. K. K. Pathirana, R. A. Zingaro and E. A. Meyers, *J. Electrochem. Soc.*, 140 (1993) 2987.

[39] P. J. George, A. Sanchez, P. K. Nair and M. T. S. Nair, *Appl. Phys. Lett.*, 66 (1995) 3624.

[40] P. J. George, A. Sanchez – Juarez and P. K. Nair, *Semicond, Sci. Technol.*, 11 (1996) 1090.

[41] V. M. Garcia, P. J. George, M. T. S. Nair and P. K. Nair, *J. Electrochem Soc.*, 143 (1996) 2892.

[42] C. A. Estrada, R. A. Zingaro, E. A. Meyers, P. K. Nair and M. T. S. Nair, *Thin Solid Films*, 247 (1994) 208.

[43] P. K. Nair and M. T. S. Nair, *J. Phy. D*, 23 (1990) 150.

[44] H. Matsumoto, K. Kuribayashi, H. Uda, Y. Komatsu and A. Nakamoto, *Sol. Cells*, 11 (1984) 367.

[45] M. T. S. Nair and P. K. Nair, *Semicond. Sci. Technol.*, 5 (1990) 1225.

[46] A. Palafox, G. Romero-Paredes, A. Maldonado, R. Asomoza and D. R. Acosta, J. Palacios-Gomez, *Sol. Energy. Mater. Sol. Cells*, 55 (1998) 31.

[47] T. J. Coutts, *Thin Solid Films*, 90 (1982) 451.

[48] G. Morris, *Proceedings of the workshop on Low Cost Electronic Materials and Solar Cells*, Srilanka, 1997, P.35.

[49] I. Martil, N. deDiego, C. Hidalgo, *Phys. Stat. Sol. A*, 94 (1986) 587.

[50] K. P. Varkey, Fabrication and Characterisation of spray pyrolysed cadmium sulfide homojunction solar cell, *Ph. D Thesis*, Cochin University of Science and Technology, (1999).

[51] N. Romeo, G. Sberreglievi and L. Tarricone, *Thin Solid Films*, 43 (1977) L 15.

[52] A. S. Baranski, W. R. Faweett, A. C. McDonald, *J. Electrochem. Soc.*, 160 (1984) 271.

[53] I. Clemminck, M. Burgelman, M. Casteleyn, B.Depuydt, *Int. J. Solar Energy*, 12 (1992) 67.

[54] D. C. Cameron, W. Duncan and W. M. Tsang, *Thin Solid Films*, 58 (1979) 61.

[55] K. L. Narayanan, K. P. Vijayakumar, K. G. M. Nair and G. V. N. Roa, *Bull. Mater. Sci.*, 20 (1997) 287.

[56] O. Zelaya-Angel, J. J. Alvarado-Gil, R. Lozada-Morales, H. Varga, A. Ferreira da Silva, *Appl. Phys. Lett.*, 64 (1994) 291.

[57] S. Kuranouchi, T. Nakazawa, A. Ashida, N. Yamamoto, *Sol. Energy Sol. Cells,* 35 (1994) 185

[58] I. Kaur, D. K. Pandya and K. L. Chopra, *J. Electrochem. Soc.,* 127 (1980) 943.

[59] T. L. Chu, S. Shirley Chu, N. Schultz, C. Wang and C. Q. Wu, *J. Electrochem. Soc.,* 139 (1992) 2443.

[60] P. J. George, A. Sanchez, P. K. Nair and L. Huang, *J. Crystal Growth,* 158 (1996) 53.

[61] P. O. Brien and T. Saeed, *J. Crystal Growth,* 158 (1996) 497.

[62] D. S. Boyle, P. O'Brien, D. J. Otway and O. Robbe, *J. Mater. Chem.,* 9 (1999) 725.

[63] G. Sasikala, P. Thilakan and C. Subramanian, *Sol. Energy Mater. Sol. Cells,* 62 (2000) 275.

[64] Mai-Ning Cui, Shi-Quan Xi, *Thin Solid Films* 288 (1996) 325.

[65] Y. Hashimoto, N. Kohara, T. Negami, N. Nishitani, T. Wada, *Sol. Energy Mater. Sol. Cells,* 50 (1998) 71.

[66] P.K. Vidyadharan Pillai, Fabrication of $CuInSe_2$/CdS thin film solar cells by chemical bath deposition technique and characterisation, *Ph. D thesis* (1997).

[67] P. K. Vidyadharan Pillai and K. P. Vijayakumar, *Sol. Energy Mater. Sol. Cell,* 51 (1998) 47.

[68] T. Gruszecki and B. Holmstrom, *Sol. Energy Mater. Solar Cells,* 31 (1993) 227.

[69] T. Ohtsuka, J. Kawamata, Z. Zhu and T. Yao, *Appl. Phys. Lett,* 65 (1994) 466.

[70] J. Reichman and M. A. Russak, *J. Electrochem Soc.,* 128 (1981) 2025.

[71] M. Hyugaji and T. Miuva, *Jpn. J. Appl. Phys.,* 24 (1985) 1575.

[72] S. Weng and M. Cocivera, *J.Electrochem. Soc.,* 139 (1992) 3220.

[73] X. Xiao and H. J. Tien, *J. Electrochem. Soc,* 130 (1983) 55.

[74] A. C. Rastogi, K. S. Balakrishnan and K. Jain, *Mater. Res. Bull.,* 34 (1999) 1319.

[75] H. P. Sharma, V. Subramanian, N. Rangarajan and K. R. Murali, *Bull. Mater. Sci.,* 18 (1995) 874.

[76] U. Pal, S. Munoz-Avila, L. Prado-Gouzalez, R-Silva-Gonzalez and J. M. Gracia-Jimenez, *Thin Solid Films,* 381 (2001) 155.

[77] G. A. Kitaev and T. S. Terekhova, *Russian J. Inorg. Chem.,* 15 (1970) 25.

[78] E. Fatas, T Garcia, C. Ontemoyer, A. Media, E. G. Camerevo and F. Arjona, *Mater. Chem. Phys.* 12 (1985) 121.

[79] A. J. Varkey, *Solar Energy Mater.*, 19 (1989) 415.

[80] M. Gadave and C. D. Lokhande, *Thin Solid Films*, 229 (1993) 1.

[81] O. Savadogo and K. C. Mandal, *J. Electrochem. Soc*, 141 (1994) 2871.

[82] K. H. A. Mady, M. M. El-Nahas, A. M. Farid and H. S. Soliman, *J.Mater. Sci*, 23 (1988) 3636.

[83] K. C. Mandal and A. Mondal, *J. Phys. Chem. Solids*, 51 (1990) 1339.

[84] J. George and M. K. Radhakrishnan, *Solid State Commun.*, 33 (1980) 987.

[85] M. T. S. Nair, Y. Pena, J. Campos, V. M. Garcia and P. K. Nair, *J. Electrochem. Soc.*, 145 (1998) 2113.

[86] O. Savadogo and K. C. Mandal, *Sol. Energy Mater. Sol. Cells*, 26 (1992) 117.

[87] I. Grozdanov, *Semicond. Sci. Technol.*, 9 (1994) 1234.

[88] C. Eberspachev, A. L. Fahrenbruch and R. H. Bube, *Thin Solid Films*, 136 (1986)1.

[89] T. Saeed and P. O'Brien, *Thin Solid Films*, 271 (1995) 35.

[90] A. Ennaoui, M. Weber, R. Scheer and H. J. Lewerenz, *Sol. Energy Mater. Sol. Cells,* 54 (1998) 277.

[91] P. K. Nair and M. T. S. Nair, *Semicond. Sci. Technol.*, 7 (1991) 239.

[92] J. M. Dona and J. Herrero, *Thin Solid Films*, 268 (1995) 5.

[93] P. K. Nair, J. Campos, A. Sanchez, L. Banos and M. T. S. Nair, *Semicond. Sci. Technol.*, 6 (1991) 393.

[94] V. M. Garcia, M. T. S. Nair, P. K. Nair and R. A. Zingaro, *Semicond. Sci. Technol.*, 12 (1997) .

[95] H. W. Schock, *Sol. Energy Mater. Solar Cells*, 34 (1994) 19.

[96] D. Braunger, D. Harskos, T. Walter and H. W. Schock, *Sol. Energy Mater. Sol. Cells*, 40 (1996) 97.

[97] D. Hariskos, M. Ruckh, U. Ruhle, T. Walter, H. W. Schock, J. Hedstrom and L. Stolt, *Sol. Energy Mater. Sol. Cells*, 41 (1996) 345.

[98] R. Bayon, C. Guillen, M. A. Martinez, M. T. Cutierrez and J. Herrero, *J. Electrochem. Soc.,* 145 (1998) 2775.

[99] R. Bayon, C. Maffiotte and J. Herrero, *Thin Solid Films*, 353 (1999) 100.

[100] A. Goetzberger and C. Hebling, *Sol. Energy Mater. Sol. Cells*, 62 (2000) 1.

[101] M. Pattabi, P. J. Sebastian, X. Mathew and R. N. Bhattacharya, *Sol. Energy Mater. Sol. Cells*, 63 (2000) 315.

[102] G. K. Padam, *Mater. Res. Bull.*, 22 (1987) 789.

[103] J. C. Garg, R. P. Sharma and K. C. Sharma, *Thin Solid Films*, 164 (1988) 269.

[104] P. K. Vidyadharan Pillai, K. P. Vijayakumar and P. S. Mukherjee, *J. Mater. Sci. Lett.*, 13 (1994) 1725.

[105] T. Walter, A. Content, K. O. Velthaus and H. W. Schock, *Sol. Energy Mater. Sol. Cells*, 26 (1992) 357.

[106] G. K. Padam and S. U. M. Rao, *Sol. Energy Mater.*, 13 (1986) 297.

[107] G. P. Sorokin, Hu. M. Papshev and P. T. Oush, *Sov. Phys. Solid State*, 1 (1996) 1810.

[108] H. Okimura, T. Matsumae and R. Makabe, *Thin Solid Films*, 71 (1980) 53.

[109] S, Bini, K. Bindu, M. Lakshmi, C. Sudha Kartha, K. P. Vijayakumar, Y. Kashiwaba and T. Abe, *Renewable Energy*, 20 (2000) 405.

[110] M. Kostoglou, N. Andritsos and A. J. Karabelas, *Thin Solid Films*, 387 (2001) 115.

CHAPTER-2

Preparation of copper selenide thin films using CBD

2.1 Review on copper selenide

    2.1.1 Introduction

    2.1.2 $Cu_{2-x}Se$ phase

        2.1.2.1 Preparation techniques of $Cu_{2-x}Se$

            a. Vacuum evaporation

            b. Direct reaction

            c. Electrodeposition

            d. Chemical bath deposition

            e. Solid - solid reaction

            f. Epitaxial growth

            g. Hydrothermal deposition

            h. Reaction of Cu plate with selenous acid

            i. Flash Evaporation

        2.1.2.2 Applications of $Cu_{2-x}Se$ phase

            a. Photodiode

            b. Cu_xSe/InP solar cell

            c. $Cu_{2-x}Se$/CdS solar cell

            d. $Cu_{2-x}Se$/Si solar cell

            e. $Cu_{2-x}Se$ as a precursor for $CuInSe_2$ phase

            f. Cu_2Se as an electroconductive coating on polymers

    2.1.3 CuSe phase

    2.1.4 Cu_3Se_2 phase

2.2 Preparation of thin film samples of copper selenide using CBD technique

    2.2.1 Cleaning of substrate

    2.2.2 Preparation of SnO_2 substrate

    2.2.3 Preparation of $Cu_{2-x}Se$ phase

        2.2.3.1 Preparation of sodium selenosulphate solution

        2.2.3.2 Optimisation of concentration of reactants

        2.2.3.3 Optimisation of deposition temperature

2.1 Review on copper selenide

2.1.1 Introduction

Recent years have witnessed intensive research in the field of preparation and characterisation of thin film metal chalcogenides. These compound semiconductors find numerous applications in electronic and electro-optical devices. In the present century, thin film heterojunction solar cells are going to play an important role as low cost, large area and high efficiency devices in solar energy conversion. Today there are well established n-type semiconducting films such as SnO_2 [1], In_2O_3 [2], indium tin oxide [3] and CdS [4] which act as window material when deposited on p-type semiconductors, giving rise to various type of heterojunctions. On the contrary, there are only few thin films showing p-type conduction. Cuprous chalcogenide binary films such as Cu_2S, Cu_2Se and Cu_2Te are typically p-type and highly conductive.

Among these, copper selenide is an interesting metal chalcogenide semiconductor with a wide range of stoichiometric compositions and also with various crystallographic forms for each of these compositions. The well-known forms of this compound include Cu_2Se, $CuSe$ and Cu_3Se_2, though other compositions such as $CuSe_2$, Cu_3Se etc. are also reported [5,6]. Phase diagram of copper-selenium system [Fig.(2.1)] as reported by R. D. Heyding [7] shows that thermal stability of these compounds varies depending on the stoichiometry.

2.1.2 $Cu_{2-x}Se$ phase

Copper (I) Selenide in the Cu_2Se form (more precisely in the $Cu_{2-x}Se$ form) is a p-type semiconductor. It exists in widely differing crystallographic modifications even at room temperature. This includes orthorhombic [8,9], monoclinic [5,10] and cubic [11-15] forms depending on the method of preparation.

This material has an indirect energy gap of 1.1-1.29 eV [16] which is near the optimum value for solar cell applications. Apart from this, it has a direct band gap >2 eV [11] that makes it a suitable window material. In vacuum evaporated thin films of $Cu_{2-x}Se$, for the value of non-stoichiometric index (x) between 0.1 and 0.3, hole mobility of the order of 10 $cm^2V^{-1}s^{-1}$ and carrier concentration in the range of 10^{18}-10^{21} cm^{-3} are reported [17]. This material with its advantageous property of high

electrical conductivity, also finds application as an electroconducting layer on transparent polyester sheets [18]. Moreover, $Cu_{2-x}Se$ is a well-accepted superionic conductor in its high temperature phase [14].

$Cu_{2-x}Se$ has been used in several heterojunction systems: $Cu_{2-x}Se/ZnSe$ for injection electroluminescence [19], $Cu_2Se/AgInSe_2$ [20] and Cu_2Se/Si [21] for photodiodes, $Cu_{2-x}Se/CdS$ [20], $Cu_{2-x}Se/CdSe$, Cu_xSe/InP [11] and $Cu_{2-x}Se/Si$ [9] for solar cells. $Cu_{2-x}Se/InP$ cell has a reported efficiency of 1.7% [13], while $Cu_{2-x}Se/CdSe$ cell has 4% [22], $Cu_{2-x}Se/CdS$ cell has 5.3% [22] and $Cu_{2-x}Se/Si$ cell has 8.8% of efficiency [11]. Attraction of these cells lies not only on the gradual improvement in efficiency, but also on the simplicity of preparation procedure of $Cu_{2-x}Se$.

Better prospects for this material lies in the feasibility of producing the ternary compound $CuInSe_2$, which is one of the most attractive photovoltaic materials [23-25]. This is achieved by incorporating indium into this binary compound. In 1994, first heterojunction between p-$CuInSe_2$ (Cu_2Se being the precursor) and n-CdS was reported [26].

2.1.2.1 Preparation techniques of $Cu_{2-x}Se$ phase

a) Vacuum evaporation [11,13,22,27]

Vacuum evaporation is the frequently used technique for the preparation of $Cu_{2-x}Se$ phase when it is used for solar cell applications. A schematic representation of vacuum deposition system as adopted by Chen et al. [22] is shown in Fig.(2.2). Cu and Se were evaporated onto heated glass substrates at various temperatures $160 - 250^0C$. The Cu boat and Se ring source were concentrically mounted to prevent material compositional gradients across the substrate. Individual elemental evaporation rates were controlled using quartz crystal microbalances. By adjusting the individual rates, $Cu_{2-x}Se$ films of various compositions could be deposited. This technique was used to study the composition dependent properties such as resistivity, carrier density and carrier mobility in detail.

b) Direct reaction [15, 28- 30]

Kashida et al. prepared Cu_2Se samples by a direct reaction of stoichiometric amounts of copper (purity 99.99%) and selenium (purity 99.999%) sealed in
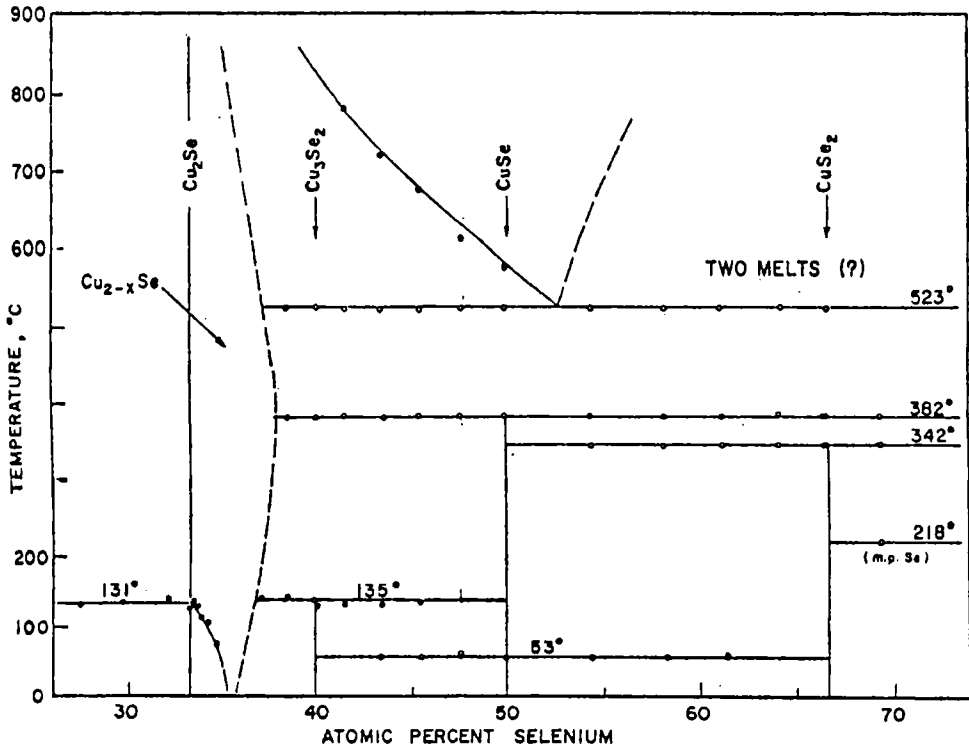
Fig. (2.1)   Phase diagram of copper / selenium system
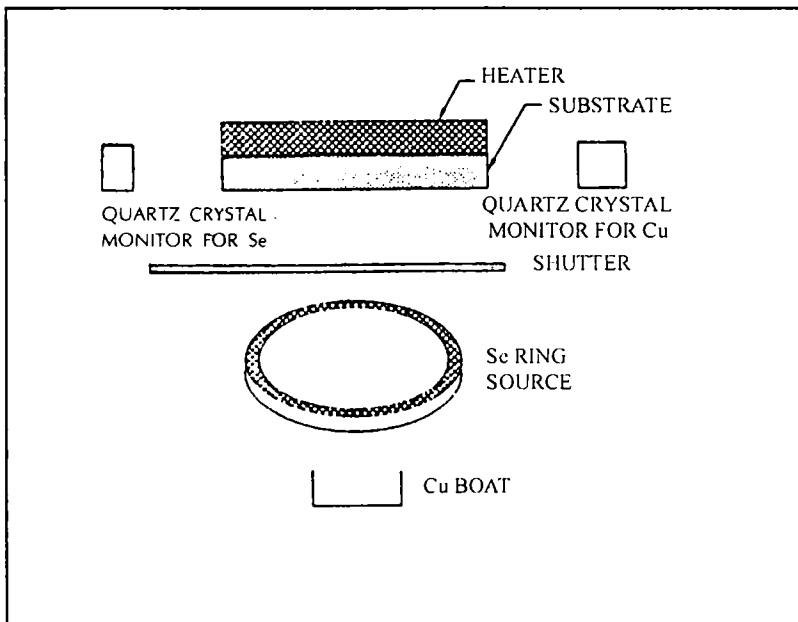

Fig. (2.2)   Schematic representation of vacuum deposition
apparatus for $Cu_{2-x}Se$ thin film

evacuated silica tubes [28]. The mixture of the components was kept at 1000^0C for about 1 week and then cooled gradually to room temperature. In another report making use of the same technique [14], powdered copper and selenium (99.999% pure) were mixed thoroughly in the atomic ratio of (2-x):1 before being sealed under vacuum in a Pyrex capsule. The mixture was heated at about 200^0C for 48 hrs. and after pressing into a pellet, it was heated again at 400^0C for 48 hrs.

c) Electrodeposition [31-33]

Thouin *et al.* used copper sulfate, selenous acid and citric acid for electro deposition [33]. The concentrations of $CuSO_4$, citric acid and H_2SeO_3 were 10^{-3}M, 0.4 M and 1.4×10^{-3}M respectively. Oxygen in the solution was removed using an argon flux and the pH was maintained at 1.8. Substrates were glass sheets covered with conductive and transparent tin oxide. Voltammograms were obtained using a three electrode cell and a potentiostat driven by a microcomputer. The potential was monitored with respect to a standard mercurous sulfate reference electrode (mse).

It was seen that at potentials less negative than an edge value, composition of the deposit was determined by the diffusion fluxes of the solutes. In a 200 mV wide potential range, the composition of the deposit was controlled by the composition of the solution, which is the only parameter acting on the fluxes of the species arriving at the electrode surface. According to various solution compositions, copper selenides such as Cu_2Se, Cu_3Se_2 and CuSe and their mixtures were obtained. For potentials more negative than $^-$0.8 vs. mse, cuprous selenide was formed. Here Se^{4+} arriving at the electrode was directly reduced to Se^{2-} state, due to the instability of cupric selenides at these potentials.

d) Chemical Bath Deposition (CBD) [18, 34-38]

CBD technique is the most frequently used method for depositing $Cu_{2-x}Se$ thin films. It is well accepted as the most convenient and simplest technique. In this technique, there are many variable parameters such as nature of reactants and complexing agents, concentration of reactants, pH, temperature and time of deposition and the nature of the substrate, that influence final composition and

properties of the products. This interesting fact makes each report on CBD different from the other and unique by itself. Few of the main reports are summarised here.

P. K. Nair *et al.* in 1999 have reported the cubic phase of $Cu_{2-x}Se$ from two similar reaction baths making use of sodium selenosulphate [35]. *Bath S1*: 10 ml of 0.5 M $CuSO_4.5H_2O$, 1.5 ml of 30% NH_3 (aq) (~ 15 M), 30 ml of freshly prepared solution of ~ 0.18 M Na_2SeSO_3 and the rest distilled water to make the volume to 100 ml. *Bath S2*: 10 ml of 0.5 M $CuSO_4.5 H_2O$, 1.5 ml of 30% NH_3 (aq) (~15 M), 12 ml of freshly prepared ~ 0.4 M Na_2SeSO_3 solution and the rest distilled water to make up to 100 ml. Substrates were placed vertically immersed in the deposition baths against the wall of the beaker. Deposition was allowed to proceed at room temperature ~ 25^0C for different durations, 2 to 25 hr.

Clement *et al.* prepared $Cu_{2-x}Se$ film on inert Pt substrate from a bath containing selenosulphate, at 75^0C [38]. The reaction bath was prepared by mixing 25 ml of a solution mixture (prepared by mixing 30 ml of 3 M copper acetate, 9 ml of 98% TEA, 7 ml of 25% ammonia and 45 ml distilled water), with 25 ml of another solution mixture (prepared by reacting 5 g of Se with 95% Na_2SO_3 in 25 ml distilled water).

In another report [33], for a total volume of 100 ml, 8 - 10 ml 0.5 M aqueous solution of $CuSO_4$ was introduced in a 100 ml beaker and 1: 3 aqueous solution of ammonia was added until a clear, deep-blue coloured solution was obtained. pH of the bath was in the range 9-11. Then 4-5 ml 1 M aqueous solution of sodium selenosulphate was added and the solution turned yellowish. Substrates were then vertically mounted in the bath and kept at 40-45^{0}C. Within a few minutes, transparent yellow to reddish films were deposited into the substrate. 25-40 minutes later the films were taken out, washed with distilled water and dried in air.

G. K. Padam [37] prepared $Cu_{2-x}Se$ (x = 0.1) films on glass substrates using a deposition mixture containing an aqueous solution of $CuCl_2.2H_2O$ (0.5 M, 24.6 ml) sodium selenosulfate (0.5 M,18 ml), triethanolamine (7.4 M, 6 ml) and ammonia solution (13.4 M, 20 ml). The pH of the resulting mixture was of the order of 10. The temperature of deposition was around 90-95^{0}C while the time of deposition was 30 minutes.

e) Solid-solid reaction [39, 40]

Preparation of copper selenide phases by solid-solid reaction was carried out in different ways. Experimental set up of evaporation sources of Kaito *et al.* [39] is shown schematically in Fig.(2.3). Two Cu films, one a polycrystalline Cu film and the other an epitaxially grown Cu film were produced by evaporating Cu from a tungsten boat A on a KCl substrate heated at 200^0C, at a pressure of 10^{-3} Pa. Se particles were also produced by two evaporation methods in Argon gas after the vacuum evaporation of Cu. One is the direct heating of Se ribbons from molybdenum boat B without boat C, which results in large Se particles with size of μm order. In order to produce Se particles less than 100 nm in size, two tungsten boats B and C were set. When boat B was heated to 1400^0C, boat C attained 300^0C and there by Se ribbons in boat C melted and evaporated.

With this experimental set up, Se particles of various sizes were put onto Cu film and the morphological image of the Se particles was elucidated based on the formation of selenides. The different reactions according to the particle size are summarised schematically in Fig.(2.4). Solid-solid reactions were clearly affected by the particle sizes. Se particles around 100 nm size resulted in Cu_2Se phase.

In another work [40] amorphous Se films of thickness 20-30 nm were vacuum deposited on glass substrates cooled to liquid nitrogen temperature. Copper films of micrometer thickness were prepared using vacuum deposition on cellulose acetobutyrate films. Se film was wet-stripped from the substrate and mounted on the copper film. CuSe crystals resulted immediately after specimen preparation while Cu_3Se_2 and $Cu_{2-x}Se$ crystals were formed after 20 and 50 days respectively.

f) Epitaxial growth [41, 42]

Shafizade *et al.* [42] have grown epitaxial films of Cu_2Se. It was prepared by depositing synthesised material of Cu_2Se composition onto single crystals of NaCl in the temperature range 200^0C and 400^0C with subsequent slow cooling to room temperature. For substrate temperature below 400^0C the films formed were textured. Monocrystalline films were obtained by deposition onto substrate at 400^0C.
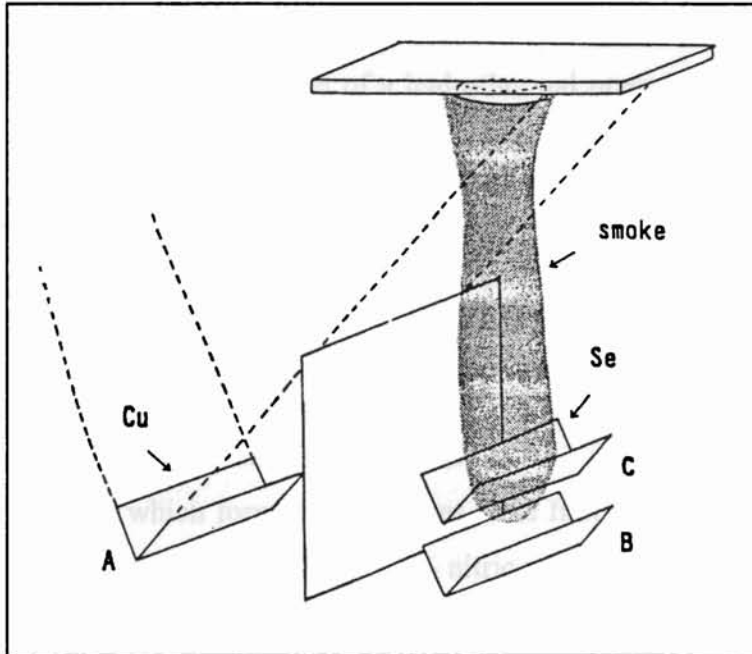
Fig. (2.3)   Schematic view of the process of depositing Se particles on
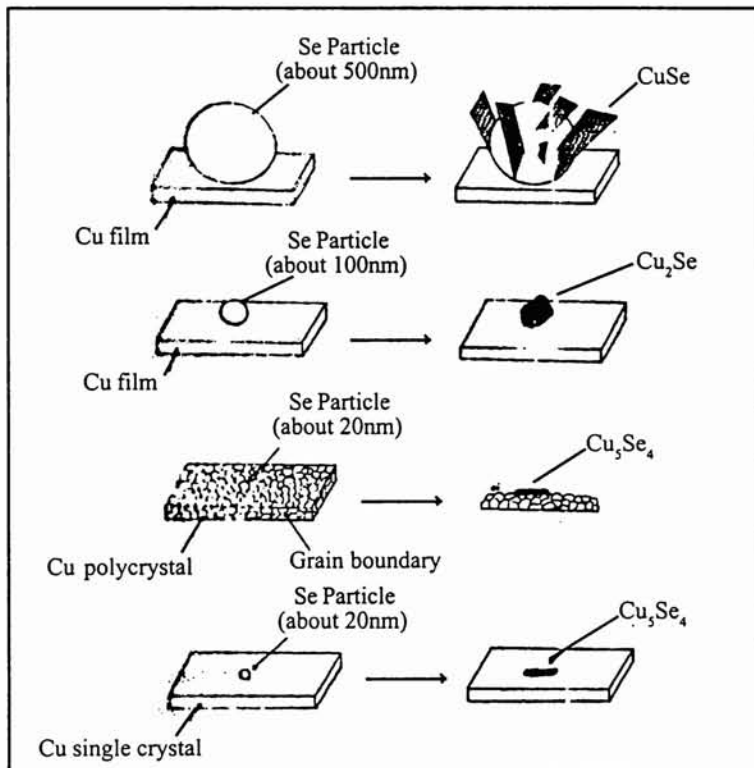Cu film by successive preparation of films and Se particles.

Fig (2.4)   Schematic representation of the reaction process
according to Se particle size.

g) Hydrothermal deposition [43, 44]

In one of the reports [43] Cu_2Se was produced as a byproduct of reaction between H_2SeO_4 and the copper gasket of a hydrothermal pressure vessel, during the production of α-quartz crystals. The growth took place in the presence of 0.5 N RdOH solvent at temperature of $(440 \pm 5)^0C$ and pressure of 1275 ± 35 M Pa. Crystals grown under these conditions were found to be $Cu_{2-x}Se$, rather than in stoichiometric form.

h) Reaction of Cu plate with selenous acid [8,9]

Here Cu plates which form the substrates were first polished to mirror finish. These were then etched with a solution of 10 % nitric acid in ethanol and later washed in distilled water [9]. Deposition was carried out by placing copper plates vertically in the plating solution for typically half an hour. Plating bath composed of selenous acid in 0.3 % sulfuric acid at a pH of about 1. After the film formation samples were immediately rinsed with Ar saturated distilled water and dried in a vacuum desiccator. In some cases, Ar gas was bubbled through the solution before and during film growth to avoid copper oxide formation. Reaction leading to the electroless synthesis of copper (I) selenide is given below.

$$4\,Cu + H_2SeO_3 + 4\,H^+ \rightarrow 2\,Cu^{2+} + Cu_2Se + 3H_2O$$
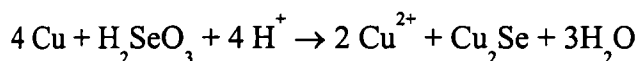
Films thus prepared were found to be orthorhombic $Cu_{2-x}Se$.

i) Flash evaporation [20,45]

Resistivity of copper selenide deposited using conventional vacuum evaporation was not reproducible. It was expected that excess of Cu was entering the deposit. In most cases a composite film of cuprous selenide and cuprous oxide was formed.

For these reasons, S. G. Ellis [45] tried flash evaporation for the first time to prepare Cu_2Se phase. For a given source temperature and rate of particle feed, reproducible results could be obtained with this technique. The other observations were, at slow rate of particle feed, resistivity of the film became higher and as the

film grew in thickness, resistance fluctuated considerably. However, proper rate of particle flow (which means that the time for a particle to evaporate is longer than the interval between the arrival of particles at the substrate) leads to good films with the same composition as the charge.

2.1.2.2 Applications of $Cu_{2-x}Se$ phase

a) Photodiode [20,21]

Tell et al. constructed a heterojunction of p-type Cu_2Se on n-type $AgInSe_2$ substrate [20]. 1 μm thick Cu_2Se layer was flash evaporated on $AgInSe_2$ substrate which was heated to 200-250^{0}C. Later this structure was annealed in Se atmosphere at 250^{0}C. In order to improve the characteristics of the junction, a thin layer of resistive Se was also tried on $AgInSe_2$ surface by sequential evaporation prior to Cu_2Se evaporation [46,47]. This junction appeared to operate as a switch, which is activated by light. This light detection mechanism is interpreted as a combination of photovoltaic and photoconductive effects. The rectifying barrier is between the Cu_2Se and an interfacial photoconductive layer in $AgInSe_2$. In dark, the structure exhibits reasonable diode characteristics. Under illumination, the diode characteristics deteriorate resulting in a dramatic increase in reverse current. Hence this could be better used as a highly sensitive detector or switch near $\lambda = 1.05$ μm.

In another work, design and fabrication of high-speed photodiodes with semi-transparent Cu_2Se film on silicon is reported [19]. Optimised width of the depletion layer of the photodiode was calculated for a selected cut-off frequency.

b) Cu_xSe/InP solar cell [13]

Tadashi Saitoh et al. reported a poly crystalline Cu_xSe/InP thin film solar cell [13]. Polycrystalline InP films were first chemically deposited on thick Mo sheets using an $In-PCl_3-H_2$ reaction system [48]. Later cuprous selenide film with a thickness of around 4000 Å was prepared in vacuum on this undoped 20 μm thick InP films. Gold grid patterns with 50 μm line width and 1 mm spacing were formed in vacuum on the Cu_xSe films. Then InP deposited on the Mo back surface and periphery of the cells was etched off to reduce the series resistance and the leakage current

respectively. Finally, a lead wire was attached to the gold grid with a silver epoxy resin and a SiO anti reflecting film was applied. The resulting configuration of Cu_xSe/ InP cell is schematically shown in Fig.(2.5).

As the Cu_xSe film is a degenerate semiconductor, the space charge layer in the InP side plays an important role in current injection. Fig.(2.6) shows the fill factor, short circuit current density and open circuit voltage to be 0.47, 11 mA/cm^2 and 0.34 V respectively for a cell of efficiency 1.7%. The highest collection efficiency obtained for this cell was 40 % at the 0.65 μm wavelength.

c) $Cu_{2-x}Se$/ CdS solar cell [6]

A cross section of the back wall 'all thin film' $Cu_{2-x}Se$/CdS cell is shown schematically in Fig.(7). As the first step, a Mo/Au grid was formed by a combination of sputtering and etching techniques, on glass substrate in order to reduce the cell series resistance. An indium tin oxide film of 1000 Å thickness and sheet resistivity of 7 Ω/ $\square$was rf sputtered over the Mo/Au grid to provide ohmic contact to the CdS. A CdS film of thickness 12-25 μm was vacuum evaporated using a graphite source onto the substrate heated to a temperature of 200-220^{0}C. CdS was then etched in 20% HCl for 30 s at room temperature. The $Cu_{2-x}Se$ film was deposited (vacuum evaporated) onto the etched CdS surface at a temperature of 200^{0}C. Finally, a gold electrode was vacuum evaporated on to the top layer.

Fig.(2.8) shows the photovoltaic characteristics of such a cell. The cell is reported to have an efficiency of 5.38 % under AM 1 illumination. The cell area was 1 cm^2 and there was no antireflection coating. V_{oc} was 457 mV, I_{sc} was 18.7 mA and fill factor was 0.63. It is reported that better output is possible by optimising the $Cu_{2-x}Se$ deposition, so as to eliminate Cu nodules for small values of 'x'. Theoretically they expected cells with 10 % efficiency, by minimising the reflection loss through anti-reflecting coatings and by redesigning the grid structure to reduce the shadowing loss.

d) $Cu_{2-x}Se$/ Si solar cell [11]

Cu_2Se powder (99.99% pure) was evaporated and deposited onto the (111) face of n-type silicon substrates. The source temperature was maintained around 1100^{0}C during evaporation. Each sample consisted of a small circular dot of $Cu_{2-x}Se$
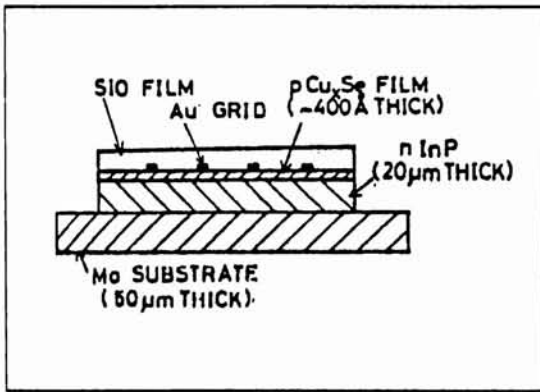
Fig.(2.5) Schematic representation of
p-type Cu$_x$Se on n-type
InP heterojunction solar cell.

Fig.(2.6) Current voltage characteristics
of Cu$_x$Se/InP solar cell meas
ured under AM 1 simulated
solar irradiation.
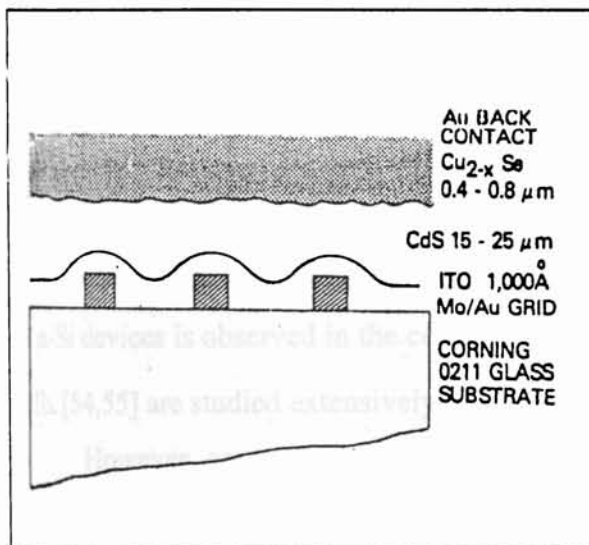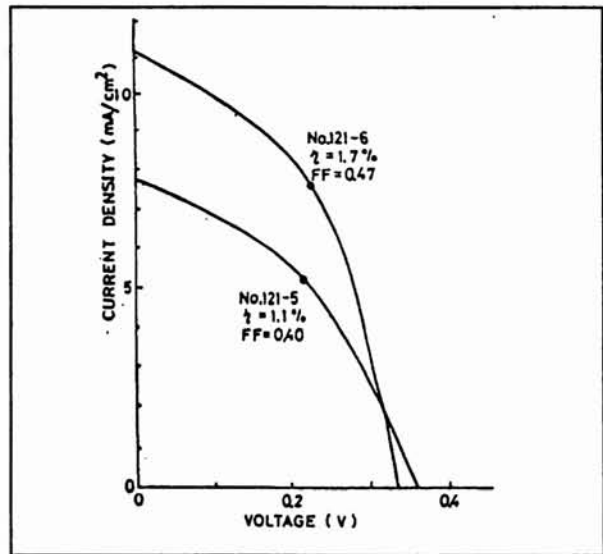

Fig.(2.7) Back wall structure of
Cu$_{2-x}$Se/CdS solar cell.

of diameter 1-3 mm, on an n-type silicon substrate with a standard dimension of 4x4 mm^2.

The junctions prepared on cold substrates showed better rectifying properties than those prepared on heated substrates. Junction capacitance C of the cell was investigated [49]. The junctions were assumed to be abrupt because of the high carrier density in the $Cu_{2-x}Se$ layers. C^{-2} was found to vary linearly with the applied voltage. The impurity concentration of the cell, obtained from the slope of C^{-2}–V plots, almost coincided with the carrier concentration of the n-type silicon substrate.

Here semitransparent and highly conductive $Cu_{2-x}Se$ films act advantageously as a window material to permit solar radiation to the junction. According to the electrical properties of this junction, the depletion layer is in the bulk material so that the substrate material mainly determines the photovoltaic properties of the cell.

The maximum values of the open-circuit photovoltage and the closed circuit photo current at room temperature for such a cell were 0.45 V and 2 mA/cm^2 respectively. The current-voltage-load characteristics of the cell without antireflection coatings are shown in Fig.(2.9). Under sunlight intensity of 75 mW cm^{-2}, at air mass 1.3-1.6, the maximum solar conversion efficiencies for a suitable load resistance were 8.3% for a $Cu_{2-x}Se$ layer of 3 mm in diameter and 8.8% for a $Cu_{2-x}Se$ layer of 2 mm diameter. Fill factor of these cells was in the range 0.62-0.65. Optimum thickness of $Cu_{2-x}Se$ films to obtain a good photovoltaic effect was in the range 300-400 Å. The lower conversion efficiency for the large area cells was assumed to be due to non-uniformity and pinholes in the $Cu_{2-x}Se$ layer.

e) Cu_2Se as a precursor for $CuInSe_2$ phase [25 - 26, 50]

$CuInSe_2$ (CIS) is a ternary compound semiconductor of the group $I-III-VI_2$ and has chalcopyrite structure with direct bandgap. Properties of this compound which make it suitable for solar cells are high absorption coefficient and desirable bandgap of 1.04 eV [52,53]. No evidence of long or short-term device degradation, as reported in a-Si devices is observed in the cells of $CuInSe_2$. $CuInSe_2$ based heterojunction solar cells [54,55] are studied extensively and they are one of the most promising devices.

However, control of elemental ratio of CIS thin film is very important as the character of these films change significantly with composition and method of preparation. Usual preparation methods of $CuInSe_2$ thin films are sputtering [56],
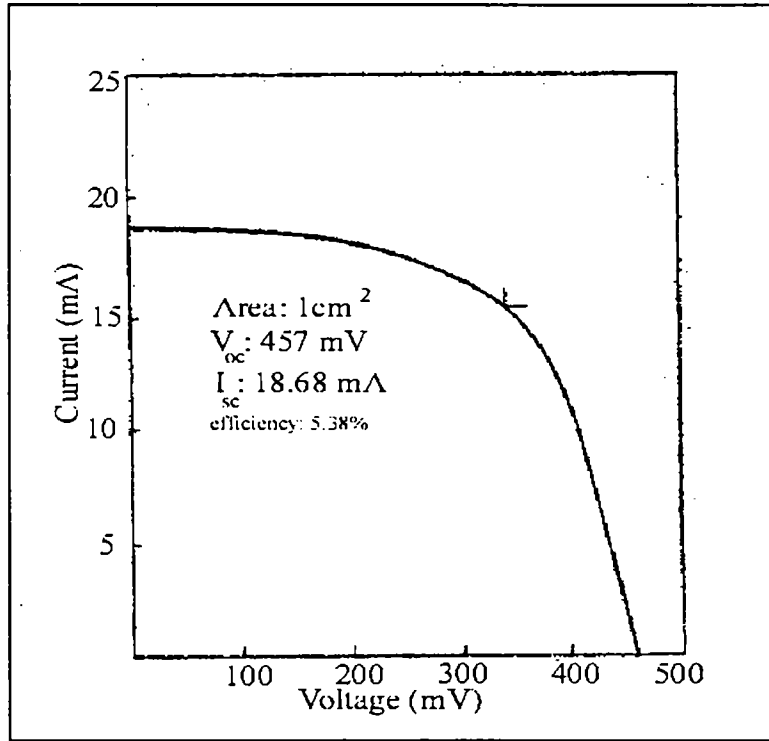
Fig (2.8)   Photovoltaic characteristics of $Cu_{2-x}Se/CdS$ solar cell.
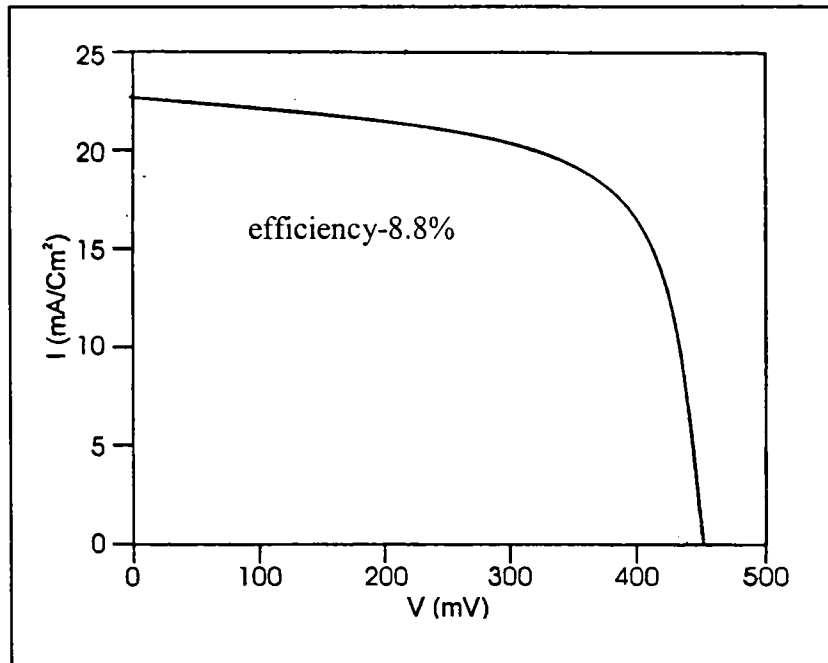

Fig.(2.9)   Current -voltage characteristics for $Cu_{2-x}Se/Si$ junction under sunlight of intensity 75mWcm^{-2}, for a junction of diameter 2mm.

molecular beam deposition [57], co-evaporation [58,59], selenisation [60] and so forth, but most of these methods require very complex set up for handling poisonous gases. In another method, selenisation of copper indium metallic films was carried out in H_2Se atmosphere [61,62]. Of all the methods, simple methods like chemical bath deposition [63,64] and evaporation of two binary compounds (Cu_2Se and In_2Se_3) [25,26] are gaining interest today.

Recently there was a detailed report on the $CuInSe_2$ phase formation during Cu_2Se/ In_2Se_3 inter diffusion reaction [65]. Cu_2Se and In_2Se_3 ingots were prepared and sectioned to slices of 3 mm thickness. These pieces were coupled with clamps made of invar to minimise thermal expansion during isothermal heat treatment. When this diffusion couple was annealed at 550^0C for 90 minutes, various binary phases along with $CuInSe_2$ developed. CIS phase precipitated with dentritic morphology and was produced within the Cu_2Se side, far from the initial interface, indicating that In was the fast component during inter diffusion. It was concluded that, orientation relationship and similar structure between these two phases, as well as their relative diffusion and nucleation behaviour, account for the development of CIS dentritic morphology within the Cu_2Se matrix.

Figure (2.10) shows schematic representation of the system to prepare $CuInSe_2$ thin films by using two-source vacuum evaporation method with rf plasma [26]. Binary compounds, Cu_2Se and In_2Se_3 powders were used as evaporation sources, as they are among the most stable selenide compounds of Cu and In. Temperature of the source was increased very quickly with large electric current, so that the source compounds would evaporate instantaneously and hardly decompose in vapour phase. It was found that by using rf plasma, the Cu_2Se phase completely disappears and only CIS phase results. At an rf power of 200 W the (112) oriented film contains other orientations also, where as at powers of 400 W or 600 W, a highly oriented film along (112) plane was obtained. With this arrangement p-$CuInSe_2$ thin films were prepared by shifting the source element ratio as required.

Such p-CIS was deposited on vacuum evaporated n-CdS thin films. Fig.(2.11) shows the current-voltage characteristics of the CIS/CdS/Glass film. Shape of the I-V curve suggested that CIS thin films prepared by this method could be used for fabricating good junction devices.
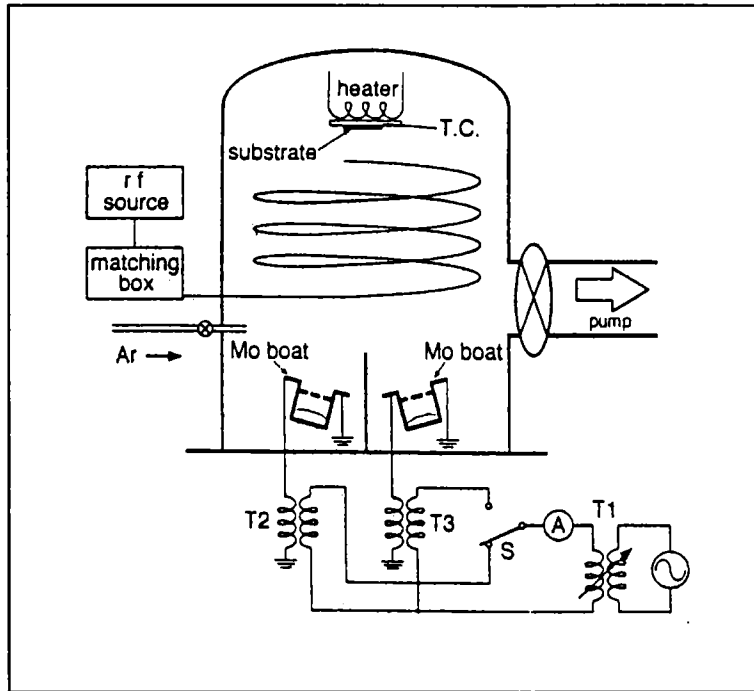
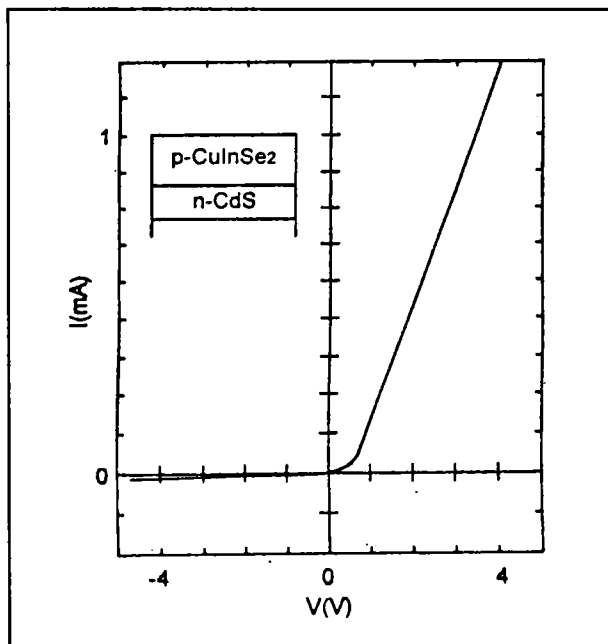Fig.(2.10) Schematic representation of the system for the preparation of CulnSe$_2$ thin films.

Fig.(2.11) Current - voltage characteristics of CulnSe$_2$/CdS junction.

Park *et al.* [25] deposited $CuInSe_2$ films by sequential evaporation of In_2Se_3 and Cu_2Se compounds through three-stage process on corning glass. The three stages were- i) the evaporation of In_2Se_3 films on glass substrate at 400^0C ii) the formation of Cu excess $CuInSe_2$ films by evaporation of Cu_2Se at $600-700^0C$ and iii) the removal of secondary Cu_2Se by further evaporation of In_2Se_3 on the $CuInSe_2$ film. CIS film prepared by this method was found to be Cu rich and hence electrical resistivity and composition were controlled by post annealing in hydrogen.

In 1992, R. N. O Brien and K. S. V Santhanam reported a novel method for incorporating In into copper selenide [24]. They prepared copper selenide by electroless deposition from a selenic acid bath containing copper sulfate and indium sulfate. Indium was incorporated into the film by a galvanostatic cathodic polarisation in an indium salt solution using a Ti anode i.e., when 8 mM $CuSO_4$, 8 mM H_2SeO_3 and 0.1M $In_2(SO_4)_3$ were electrolysed in a cell with Cu cathode and Ti anode, a black deposit of copper indium selenide was obtained. Though the resulting phase was non stoichiometric, it behaved well as a photo-anode in a photovoltaic cell. This was reported as one of the easiest methods of producing CIS.

f) Cu_2Se as an electro-conductive coating on polymers [18]

Electro conductive coating on non-conductive organic polymers has recently received considerable attention [66 - 69]. Such conductive coatings deposited on flexible substrates have numerous technological applications in opto-electronic devices [70], display devices [71] or active electrode material for energy storage [72]. Limitation in this direction arises due to the fact that organic polymers are usually inconvenient substrates for the most frequently used deposition techniques such as eletrodeposition and vacuum deposition. Also, the difficulty in achieving good adherence of the inorganic layer onto the polymer surface is an additional discouragement.

Recently, electroconductive thin films of copper selenide (Cu_2Se) were deposited on transparent polyester sheets by a simple electroless deposition technique based on hydrolic decomposition of selenosulfate in alkaline aqueous solution [18]. Surface resistivities of such films varied from 50 to 500 Ω/ $\square$These films were fairly transparent in the visible region, while the transmittance dropped substantially in the

near-infrared region. This also suggested the use of such films as microwave/infrared shielding coatings.

2.1.3 CuSe phase

Cupric selenide (CuSe) is a compound in which rectifying effect was observed during the early stages of semiconductor research. When CuSe was brought in contact with a proper metal, an asymmetrical resistance or rectification appeared [73]. Solid-state physics treat CuSe as a semiconductor, probably owing to this rectifying effect. But whether the rectification has to be ascribed to a possible semiconductivity of CuSe, or to some barrier formed on its surface is a question yet to be answered satisfactorily. Ogorelec et al. [74] feels that this rectifying effect cannot be ascribed to the bulk semiconductivity properties of this material, for cupric selenide behaves more or less like a typical metal. They also accept the fact that the signs of thermoelectric power and the Hall constant indicate that the charge carriers may be holes.

α CuSe (Klockmannite) is often reported as hexagonal with a = 3.934 Å c = 17.217 Å at 298 K [5,7]. It transforms to β CuSe at 323 K under atmospheric pressure with an enthalpy change of 0.84 ± 5 KJ/mol. This modification is orthorhombic with a = 3.948 Å, b = 6.958 Å , c = 17.239 Å at 324 K. With increasing temperature, the orthorhombic a/b ratio increases rapidly, until at 393 K the transition to γ CuSe is complete. This modification is hexagonal with a = 3.934 Å , c = 17.288 Å at 430 K. CuSe is unstable above 5 K bar at 298 K and it decomposes forming Cu_3Se_2 and CuSe.

The major preparation techniques of this material are summerised here.

i) Direct synthesis [74]: Cupric selenide was prepared by direct synthesis of pure and precisely weighed components in an evacuated and sealed quartz tube at 600^0 C. When the synthesis was completed after 8 hrs., the tube was cooled to room temperature over a period of 24 hrs. to get the gray-black ingots of CuSe. Single crystals of CuSe are not obtainable because of the phase transition at 53^0 C from α to β phase as mentioned earlier.

ii) Vacuum evaporation [75]: CuSe thin films of thickness 350 - 400 Å were prepared by vacuum evaporation of synthesised material onto NaCl single crystals at room

temperature. When the substrate temperature was maintained at 400^0C, monocrystalline specimens were obtained. The lattice parameters for CuSe samples at room temperature were found to be a = 3.96 A^0 and c = 17.26 A^0.

iii) Solid-solid reaction [39,40] : As explained in section 2.1.2.1.e, depending on the particle size of Se, CuSe phase can be prepared by solid-solid reaction of Cu and Se [39]. In reference [40] it was observed that CuSe crystals appear immediately after the mutual contact of Cu with Se.

iv) Chemical bath deposition [35,76-78]: The procedure of CBD technique, as reported by Nair *et al.* [76] is as follows- 35 ml of 0.05 M $CuCl_2$ and 20 ml of sodium tartrate were mixed in a 100 ml beaker. A freshly prepared solution of 0.2 g N, N-dimethylselenourea in 20 ml of 0.01 M sodium sulfite was added and the final volume was made to 100 ml with distilled water. The deposition was carried out at 50^0C. The obtained film was uniform and brownish black in colour, with a thickness of 0.25 μm for a deposition time of 5.5 hrs.

In another report [77], 5 ml of 0.5 M cupric sulfate solution was taken in a 50 ml beaker, to which about 8 ml of 9.8 % triethanolamine was added. About 6 ml of 0.25 % ammonia and 5 ml of 0.45 M sodium selenosulfate solutions were then added in succession to the reaction mixture. Volume of the resulting solution was made up to 50 ml with distilled water. Glass substrates were dipped in this mixture for 4 hrs. with continuous stirring. Then CuSe film was deposited on both sides of the substrates.

2.1.4 Cu_3Se_2 phase

Cu_3Se_2 phase (Umangite) is one of the least explored phases of copper selenide. Often this phase is reported as an impurity phase which grows accidentally along with copper (I) selenide [38,75]. There are reports of dentritic growth [79] as well as non-dentritic growth [80] for this material. These are only few techniques reported for preparing pure Cu_3Se_2 phase. For the same reason, properties and applications of this material are yet to be studied in detail. In the present work deposition of Cu_3Se_2 using CBD technique and its characterisation are reported.

Symmetry of this material is tetragonal with space group $P42_1m$ (a = 6.406 Å and c = 4.279 Å) [81]. Here Se atoms are arranged as a face centered tetragonal cell.

Each Cu (I) is surrounded by four Se at 2.49 Å and four Cu (II) at 2.63 Å; and each Cu (II) by four Se at 2.43 Å and 2.37 Å, two Cu (I) at 2.63 Å and by one Cu (II) at 2.66 Å. Each Se is surrounded by the two Cu (I) at 2.49 Å and by four Cu (II) at 2.43 Å and 2.37 Å.

Planar defects of Cu_3Se_2 crystals produced by solid-solid reaction were studied by Hiroshi Morikawa [82]. He expected narrow crystals precipitates on both (111) and (021) defect planes of Cu_3Se_2. These crystals may have a lattice similar to the Cu_3Se_2 crystals. Since selenium atoms of Cu_3Se_2 crystal frame up a face centered tetragonal lattice and are much larger than copper atoms, Cu_3Se_2 crystals may behave nearly as a simple face centered crystal composed of selenium atoms inspite of the defects that appear on (111) planes of the Cu_3Se_2 crystal. It was expected that the narrow crystals might have non-stoichiometric composition near to Cu_3Se_2.

The fact that at atmospheric pressure Cu_3Se_2 disproportionates to $Cu_{2-x}Se$ and β CuSe at 386 K has lead to many trials to prepare Cu_3Se_2 from reaction of $Cu_{2-x}Se$ with CuSe below 385 K. However this reaction was found to be very slow and remained incomplete even after several years at room temperature. This transformation is enhanced by pressure and shear and may be brought to completion by grinding for extended period with a mortar and pestle [5].

When $Cu_{2-x}Se$ and CuSe mixture was quenched from 633 K, it resulted in Cu_3Se_2 as the major phase [7]. It is uncommon for a phase to appear on quenching from well above its stability field, when the rate of transformation just below the transformation temperature is very slow. This can be explained on the assumption that selenium-rich limit of the $Cu_{2-x}Se$ phase moves to higher selenium concentration with increase in temperature, as indicated by the dotted line in Fig.(2.1). On quenching from the $Cu_{2-x}Se/ \beta$ CuSe field, Cu_3Se_2 may be formed by a precipitation mechanism imposed by the decreasing number of Cu vacancies in the $Cu_{2-x}Se$ solid solution. It was also found that when mechanical mixtures of $Cu_{2-x}Se$ and $CuSe_2$ in stoichiometric proportion were ground lightly with mortar and pestle, the conversion to Cu_3Se_2 was complete in less than 1 min [5].

In another report [81] copper and selenium in the ratio 2.9 to 2.0 were enclosed in an evacuated silica tube and kept at 500^0 C for 2 days. The product was

ground to fine powder, resealed in a new evacuated silica tube, kept first at 500^0C for a week and then at 80^0C for a month. After the run, the final product was covered with small crystals of Cu_3Se_2. However the inner portion had a mixture of $Cu_{1.8}Se$ and CuSe.

There are few reports on solid-solid reaction of Cu and Se leading to Cu_3Se_2 [40,82]. In one of the reports [82], selenium (99.999 % pure) was vacuum deposited from a tungsten filament onto a glass plate at room temperature. The deposited film was amorphous and it was wet-stripped from the substrates and mounted directly on copper grids. Copper selenide crystals in the Cu_3Se_2 form along with Cu_2Se and CuSe were formed by the reaction of copper with selenium films at room temperature.

Cu_3Se_2 could also be prepared by electrodeposition techniques by controlling the diffusion fluxes of the solutes. Details of this technique are already included in section 2.1.2.1. c.

2.2 Preparation of thin film samples of copper selenide using CBD technique.

As mentioned in the first chapter, CBD technique has many advantages such as simplicity and cost effectiveness, but repeatability forms the major limiting criteria. Parameters like concentration of reactants, temperature of deposition, pH of reacting mixture, and time of deposition decide repeatability to a great extent. Apart from these, various other factors such as nature of substrate and cleaning procedure and spacing between substrate, which appear to be insignificant at first sight, also play a major role in the reproducibility of samples. Hence each of these factors can form a field of research by its own [83].

2.2.1 Cleaning of substrate

The substrate material and its surface texture has a major role on the adhesion of thin films. Generally adhesion is better on rough surface rather than on perfectly smooth surface. In the present work, Cu_3Se_2 phase had good adhesion on rough surfaces like ground glass or spray pyrolysed SnO_2 substrate, while $Cu_{2-x}Se$ phase showed fairly good adhesion even on smooth glass substrates.

Procedure of cleaning of substrate is important, as it is one of the factors determining the composition and grain size of the film. One can opt for various cleaning methods depending on the nature of the substrate, type of contaminants and the extent of cleanliness required for thin film deposition. Surface of the substrate will be usually contaminated with fingerprints, oil, lint and dust. So the procedure can involve a 'solvent cleaning' at first stage and an ion beam bombardment cleaning as a secondary stage for extra cleanliness. But in CBD ion beam cleaning does not have much significance, as substrate is not maintained in vacuum after cleaning.

In this work, ordinary micro slides of soda lime glass of dimension 26 x 76 x 2 mm^3 were used as substrates. The 'solvent cleaning method' was as follows - Glass slides were first dipped is freshly prepared chromic acid heated to 60^0C. Nascent oxygen liberated from the chromic acid cleans the substrate surface. Slides were removed from acid and washed in flowing water. Then they were dipped in alkaline soap solution (Merck) for 10 minutes and after this, washing in running water was repeated. This point is of great significance as neutral or acidic soap solution is found to have undesirable effects on the deposited films. By keeping in alkaline soap solution traces of acid present on the surface can be removed. The slides were again washed in double distilled water. The next stage included ultrasonic cleaning in distilled water. This gives a scrubbing effect on the substrate and removes dust particles that still adhere to the surface. Finally the slides were dried in hot air oven.

2.2.2 Preparation of SnO$_2$ substrate

Fig.(2.12) shows the experimental set up used for preparation of SnO$_2$ thin film. Spray head and the substrate along with heater are kept inside a closed chamber provided with an exhaust fan for removing gaseous by-products. Size distribution of droplets and spray rate are mainly determined by geometry of the nozzles for carrier gas and sprayed solution. These parameters in turn determine the quality of the films prepared using this technique. A fine capillary tube is used for carrying the solution and another tube with comparatively larger diameter is used for carrying the carrier gas (air in the present case). Best results are obtained when both the tubes intercept at an angle of 80^0 [84].

Cleaned glass slides are placed on a hot plate made of thick iron block that can be heated to the required temperature with a controlled heater. Temperature of the

substrate holder was measured using a digital thermometer. During spraying the temperature of the substrate was kept constant. Crystallinity of the SnO_2 film does matter significantly, when the samples deposited on this layer are analysed for crystal structure using XRD. As the XRD peaks of the substrate should not interfere in the analysis and interpretations of the XRD spectrum of the sample, it becomes necessary that the SnO_2 film should have definite and well-defined XRD peaks having good reproducibility. Structural quality of SnO_2 largely depends on the temperature of the glass slides during spray pyrolysis. Moreover, when samples deposited on these substrates are analysed for optical studies like absorption or transmittance, it is a must that the substrate should have very low absorption of its own, so as to have least interference with the analysis of material under study. With these ideas in mind, the temperature of glass slides on which SnO_2 film is to be prepared was standardised. It was observed that the best quality SnO_2 films were obtained when substrate temperature was maintained at 400^0C. The temperature of substrate was kept constant with an accuracy of $\pm 5^0C$ during spraying.

In order to get good adhesion and the above-mentioned qualities, the spray solution was also standardised. Optimum composition of the solution was, 33 ml of hydrated stannic chloride ($SnCl_4.5\ H_2O$) dissolved in 33 ml of water and 33 ml of ethanol. About 15 ml of this mixture was sprayed for 90 seconds at a uniform rate. XRD spectrum of the standardised SnO_2 coated substrate is shown in Fig.(2.13).

2.2.3 Preparation of Cu$_{2-x}$Se phase

Preparation of $Cu_{2-x}Se$ phase using CBD involves reaction of Cu^{2+} ions with Se^{2-} ions in a controlled manner in the bath. Copper salt used for the preparation was LR grade of copper sulfate ($CuSO_4.5\ H_2O$). Initially, different sources of selenium were tried along with this. It is well accepted that the use of N, N-dimethylselenourea as the selenising reagent in the chemical deposition of metal selenides has several advantages over other reagents [76]. Though it is easy to prepare this reagent by dissolving N, N- dimethylselenourea in sodium sulfite solution, it has the disadvantage of instability on storing. It has to be carefully stored in a dry nitrogen atmosphere in a dark container. Moreover it is very costly and hence selenium dioxide
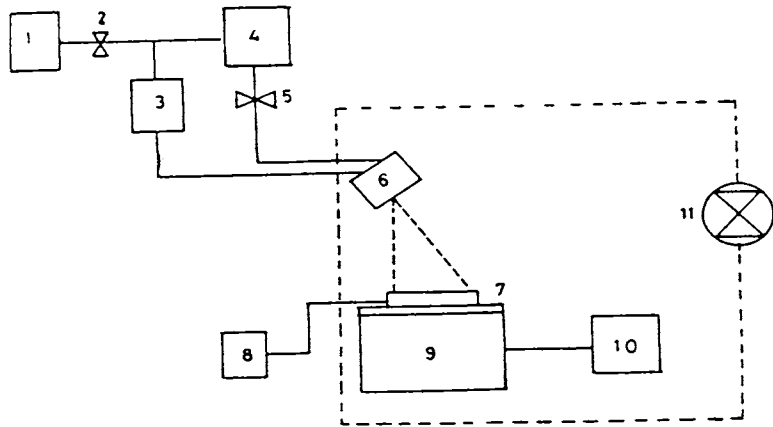
1. Air compressor   2. Gas flow control valve
3. Manometer   4. Solution reservoir
5. Solution flow control valve   6. Spray head
7. Substrate   8. Thermometer
9. Substrate heater   10. Heater control
11 Exhaust fan.

Fig.(2.12) Schematic diagram of experimental setup for spray pyrolysis of SnO_2
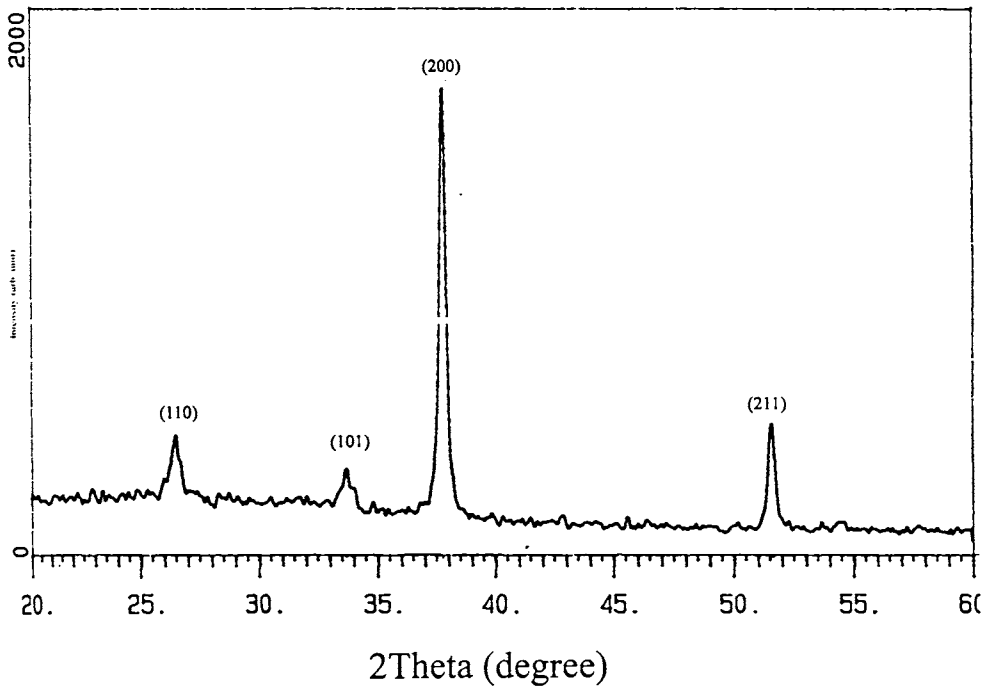

2Theta (degree)

Fig (2.13)   XRD spectrum of SnO_2 film on glass substrate

was tried. However in this case, the reaction speed could not be easily controlled. Finally sodium selenosulfate (Na_2SeSO_3) prepared in our lab, was opted.

2.2.3.1 Preparation of sodium selenosulfate solution

The procedure of preparation is as follows- Selenium granules of 99.99 % purity were ground to fine powder. Sodium sulfite was dissolved in water and heated to 90^0C. Selenium powder was then added to the sodium sulfite solution and vigorously stirred using a magnetic stirrer until all the Se powder dissolved in the solution. Sodium sulfite has to be added in excess for the complete conversion of Se into Na_2SeSO_3. For preparing 200 ml (0.2 M) solution, 15 gm of sodium sulfite was dissolved in 200 ml water. If excess Se is present, then it precipitates out on cooling. The final solution was filtered and stored for later use.

Direct reaction of copper sulfate solution and sodium selenosulfate solution did not yield any film deposition due to sudden precipitation. So the Cu^{2+} ions had to be complexed using a suitable complexing agent to ensure slow release. After many trials with complexing agents such as ammonium hydroxide, ethylene diamine tetraacetic acid (EDTA) and trisodium citrate (TSC), TSC was found to be the most suitable one.

2.2.3.2. Optimisation of concentration of reactants

Concentration of Na_2SeSO_3 was fixed at 0.2 M. Concentration higher than this was found to result in sudden precipitation of selenium. Concentration of copper sulfate solution was varied from 0.1 M to 1 M. 0.2 molarity was found to be the optimum concentration for $CuSO_4$ solution, so that the reaction rate was under control. Molarity of the complexing agent was always chosen to be slightly greater than the copper ion concentration.

2.2.3.3 Optimisation of deposition temperature

Temperature of the bath was varied from 5^0C to 70^0C and this influenced the rate of reaction. Finally for convenience, deposition at room temperature was opted.

2.2.3.4 Effect of stirring

Deposition was possible with or without stirring. For deposition with stirring, a 2V DC motor and a variable resistance to control the speed was used. The glass slides were arranged vertically along the inner wall of the beaker and stirring was given at the center. As deposition could be obtained without stirring also, most of the deposition was done without stirring. In the absence of stirring, the deposition arrangement could be modified so as to increase the area of deposition. This involves introducing a small clean beaker at the center of the main container, so as to increase the effective solution level in it. For example, 10 ml of each reagent (total 30 ml) taken in a 100 ml container, with a 25 ml beaker kept at the center, would give a total thin film area of 112.5 cm^2 (i.e., an area of 11.25 cm^2 on both sides of 5 glass slides kept vertically in between the main container and the 25 ml beaker). This arrangement minimises wastage of chemicals.

2.2.3.5 Optimisation of pH

Apart from variable parameters such as concentration of the reactants and temperature of deposition, pH of the reacting mixture also plays a major role in determining the composition and quality of the deposited thin film. From the preparation procedure given below, it can be inferred that pH of the final reaction mixture is the main factor that determines the phase of copper selenide thin films. pH values of some standard concentration of the various reagents used in the present study are given in Table(2.1). Digital pH meter (pH scan 2 of Merck) was used for measuring pH of the solution.

Variable parameters involved in this deposition process were concentration, temperature and pH. Depending on various permutations and combinations of these parameters, the preparation conditions are labeled as Bath 1:1, Bath 2:1, Bath 3:1, Bath 5:1, Bath 1:2 and Bath 1:1 Na.

CuSO$_4$		TSC		Na$_2$SeSO$_3$	
Molarity	PH	Molarity	pH	Molarity	pH
0.1 M	4.1	0.2 M	8.5	0.2 M	10.1
0.2 M	3.7	0.3 M	8.8		
0.4 M	3.5	0.5 M	8.9		
0.6 M	3.3	0.7 M	9.3		
1.0 M	3.1	1 M	9.5		

Table (2.1)   pH values of some standard concentrations of the various Reagents

Bath 1:1

Here Cu:Se ratio in the reacting mixture is taken as 1:1. 0.2 M (10 ml) CuSO$_4$ solution is mixed with 0.3 M (10 ml) TSC and 0.2 M (10 ml) sodium selenosulfate solution is added to this with constant stirring. 0.2 M CuSO$_4$ solution has a pH of 3.7, which on addition of 0.3 M TSC (pH 8.8) will lead to a resulting mixture of pH ~ 4.8. This mixture has blue colour of CuSO$_4$ solution. But when 0.2 M Na$_2$SeSO$_3$ solution (pH 10.1) is added to this mixture, the pH suddenly increases to a stable value around 7. At the same time, colour of the solution changes from blue to green. As the reaction slowly proceeds, the pH also increases slightly to around 7.7. Deposition is carried out at room temperature (27^{0}C) on glass substrates. It is observed that the film growth starts only after an initial nucleation period of about 30 minutes. Optimum deposition time is around 70 minutes, during which the terminal thickness (90% of the maximum film thickness) is attained. If kept for a longer time, the solution becomes transparent, with all the residual precipitates settled at the bottom of the beaker. When these samples are left for few hours in this residual bath, the deposited film either peals off or develops wrinkles on the surface. Hence, after reaching the terminal thickness the slides are taken out, washed with distilled water and then dried in flowing air. These samples are here after referred to as *sample No. 1* for convenience.

In order to increase the thickness of the film, double dipping can be given. Deposition time is to be modified in this case. Maximum time for double dip was

optimised as 90 minutes. Second dip solution should be prepared and kept ready for 30 minutes before finishing the first dip.

Bath 1:1 LT (Low temperature)

In order to rule out the dependence of composition of the film on temperature, deposition is carried out under the same bath conditions, but at a lower temperature of 5^0C. This is achieved by placing the beaker containing the solution mixture in a water bath, maintained at ice-cold temperature by continuous addition of ice cubes. Nucleation period for film formation depends on the extent of cooling. Here time of deposition prolongs for 3 to 4 hours and deposited copper selenide film is thick and uniform. A comparative study of this low temperature film with the Bath 1:1 film is done by different characterisation techniques and is detailed in the next chapter.

Bath 2:1

Here Cu:Se ratio is taken as 2:1 in the reaction mixture. The details are the same as that of Bath 1:1 except that the $CuSO_4$ solution is 0.4 M and TSC is 0.5 M, while concentration of Na_2SeSO_3 is maintained at 0.2 M. When 0.5 M TSC of pH 8.9 is added to 0.4 M $CuSO_4$ solution (pH 3.5), the resulting mixture has a pH of 4.3. When 0.2 M Na_2SeSO_3 solution is added to this, the pH increases to a stable value around 6.4. At the final stage of deposition pH remains around 6.7. The time of deposition is around 40 min.

Bath 3:1

Here Cu:Se ratio is taken as 3:1 in the reaction mixture. The details are the same as that of Bath 1:1 except that the $CuSO_4$ solution is 0.6 M and TSC is 0.7 M, while the concentration of Na_2SeSO_3 is maintained at 0.2 M. When 0.7 M TSC of pH 9.3 is added to 0.6 M $CuSO_4$ solution (pH 3.3), the resulting mixture has a pH of 4.2. When 0.2 M Na_2SeSO_3 solution is added to this, the pH increases to a stable value around 5.8. The duration of deposition is around 30 minutes.

Bath 5:1

Here Cu:Se ratio is taken as 5:1 in the reaction mixture. $CuSO_4$ solution is 1 M and TSC is 1 M, while the concentration of Na_2SeSO_3 is maintained at 0.2 M. When 1 M

TSC of pH 9.5 is added to 0.4 M $CuSO_4$ solution (pH 3.1), the resulting mixture has a pH of 3.9. When 0.2 M Na_2SeSO_3 solution is added to this, the pH increases to a stable value around 4.6. The duration of deposition is around 20 minutes.

2.2.4 Preparation of Cu_3Se_2 phase

While preparing Cu_3Se_2 phase, the initial arrangements and the chemicals used are similar to that of $Cu_{2-x}Se$ phase, except otherwise mentioned. The main difference in the deposition procedure of this phase, from that of the earlier phase, is in the pH of the reacting mixture. However altering of pH to a more alkaline value increases the rate of reaction, making film deposition impossible at room temperature. Hence this deposition is carried out at low temperatures below 10^0C. The procedure adopted for deposition at 5^0C has already been described in the previous section. In this case, the Na_2SeSO_3 solution and the mixture to which it is to be added, are taken in separate beakers and pre-cooled by keeping in cold-water bath. This reduces the chance of immediate precipitation when mixed with each other.

Cu_3Se_2 phase has little adhesion on glass substrate. Hence, SnO_2 coated glass (the preparation of which has already been explained in section (2.2.2)) is used as substrate. In this case, stirring is found to increase the film thickness considerably. Speed of the stirrer is adjusted to a moderate level using a potentiometer.

Bath 1:2

Here Cu: Se ratio is taken as 1:2 in the reaction mixture. For this, the copper sulfate concentration is reduced to half, i.e. 0.1 M $CuSO_4$ (10 ml) solution is mixed with 0.3 M (10 ml) of TSC. Addition of 0.3 M TSC of pH 8.8 to 0.1 M $CuSO_4$ solution of pH 4.1 results in a mixture of pH 5.6. To this solution, 10 ml of pre-cooled 0.2 M Na_2SeSO_3 solution (pH 10.1) is added with constant stirring. Here the resulting pH is comparatively alkaline i.e., around 7.9 and the solution is light green in colour. This light colour becomes darker as reaction proceeds and finally becomes black at the end of the reaction. Here initial nucleation period is only 15 minutes while the time of deposition is around 30 minutes at 5^0C. It is to be noted that timings mentioned here are not constant, but varies with the extent of pre-cooling of the reactants and temperature of the reaction bath. In order to get sufficiently thick films of Cu_3Se_2, two

dippings are performed consecutively on the same SnO_2 substrate. For certain analyses, these films are deposited on glass substrates also. Then two or three dippings are given by reducing the time of deposition of each dip. Such films are found to be non-uniform. On attaining terminal thickness, the slides are taken out, rinsed in distilled water and then dried in flowing air.
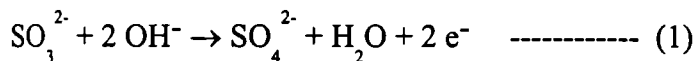
Bath 1:1 Na

Here the concentration of Cu:Se is maintained at 1:1, as in the case of Bath 1:1. With the aim of increasing the pH of the resulting mixture of 0.2 M $CuSO_4$ and 0.3 M TSC, from 4.8 to a value of 5.6, a few drops of sodium hydroxide solution is added. It is to be specifically noted that addition of NaOH solution should be done drop by drop with constant stirring.

Before adding $Na_2 SeSO_3$ solution, pH of the mixture of $CuSO_4$ and TSC is made ~5.6 by the addition of 3 M NaOH solution (~ 5 drops). Optimisation of this step has to be done very carefully, as this is the deciding stage of the final pH of the solution and thereby the composition of the deposited film. Objective of this step is to adjust the pH to approximately 7.9, when 0.2 M Na_2SeSO_3 is added. This reaction is carried out at temperatures below 10^0C and time of deposition is around 50 minutes. Here also, this time is not a fixed parameter, as rate of deposition will depend on the extent of pre-cooling of the solution and also on the temperature of deposition. Considerable thickness is obtained on two consecutive dips with constant stirring. Samples are then removed from the bath and rinsed in distilled water and dried in warm air. These samples are here after referred to as *sample No. 2*, for convenience.

## 2.3 Chemistry behind the formation of $Cu_{2-x}Se$ and Cu_3Se_2 phase

Deposition of copper selenide thin films involves controlled release of copper ions from the copper trisodium citrate complex $[Cu(TSC)^{2+}]$ and its reaction with $SeSO_3^{2-}$ ions of Na_2SeSO_3 present in the reaction bath. In Cu_2Se phase copper is in Cu^{+1} state and in Cu_3Se_2 it is in the mixed state of Cu^{+1} and Cu^{2+} state.

As mentioned in the section (2.2.3.1), excess of sodium sulfite is always used for preparing sodium selenosulfate solution. The excess sulfite ions present, converts to sulfate ions in the presence of hydroxyl ion as follows: -

$$SO_3^{2-} + 2\,OH^- \rightarrow SO_4^{2-} + H_2O + 2\,e^- \quad \text{------------} \quad (1)$$

In Bath 1:1, Bath 1:1 LT, Bath 2:1, Bath 3:1 and Bath 5:1 which results in $Cu_{2-x}Se$ phase, Cu^{2+} is reduced to Cu^{1+} by the above excess electrons [85].

$$Cu^{2+} + e^- \rightarrow Cu^{1+} \quad \text{----------------} \quad (2)$$
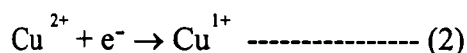
So the final reaction occurring at a neutral or slightly acidic pH is

$$2\,Cu^{1+} + Se\,SO_3^{2-} + 2\,OH^- \rightarrow Cu_2Se + SO_4^{2-} + H_2O \quad \text{-----------} \quad (3)$$
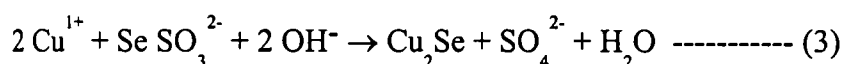
This leads to the formation of Cu (I) selenide (more precisely $Cu_{2-x}Se$ in this case).

In Bath 1:1 Na and Bath 1:2, the final pH of the reacting mixture is around 7.9, i.e. it is more basic than the earlier mentioned baths. Moreover, as the reaction proceeds the solution becomes more and more alkaline. Then the preferred reaction in the presence of e^- from eqn. (1) becomes

$$3\,Cu^{2+} + 2\,Se\,SO_3^{2-} + 4\,OH^- + 2e^- \rightarrow Cu_3Se_2 + 2\,SO_4^{2-} + 2\,H_2O \quad \text{----------}(4)$$
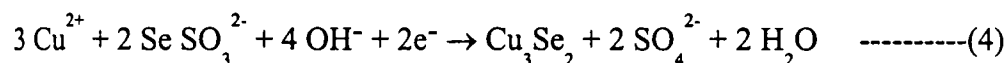
This leads to the formation of Cu_3Se_2 phase.

In Bath 1:1 Na the reaction given by eqn (4) is enhanced by the addition of NaOH solution to the reacting mixture, thereby increasing the OH^- ion concentration. While in Bath 1: 2 this reaction is enhanced by the presence of excess concentration of $SeSO_3^{2-}$ ion when compared to Cu^{2+} ions in the reaction bath.

2.4 Conclusion

In this chapter the significance of the semiconducting material copper selenide is highlighted with brief mention to various preparation techniques. Cu_2Se and $CuSe$ are the frequently deposited phases of copper selenide using CBD. In the present work, $Cu_{2-x}Se$ and Cu_3Se_2 phases were prepared from similar reaction bath. This forms the first report of preparation of Cu_3Se_2 by CBD. It was observed that pH of the final reaction mixture is the major factor deciding of the phase of the deposited film.

Bath conditions	pH (CuSO$_4$ +TSC)	pH (CuSO$_4$+TSC+ Na$_2$SeSO$_3$)	pH (after deposition)
Bath 1:1	4.8±0.1	7.1±0.1	7.7±0.1
Bath 2:1	4.3±0.1	6.4±0.1	6.7±0.1
Bath 3:1	4.2±0.1	5.8±0.1	6.1±0.1
Bath 5:1	3.9±0.1	4.6±0.1	4.6±0.1
Bath 1:2	5.6±0.1	7.9±0.1	10.1±0.1
Bath 1:1Na	4.8±0.1	(+NaOH few drops) 7.9±0.1	10.1±0.1

Table (2.2) Comparison table of various preparation conditions

The films of Cu$_{2-x}$Se and Cu$_3$Se$_2$ phases could be prepared either by varying the Cu:Se ratio in the reaction bath or by controlling the pH of the bath that contains equal amounts of Cu and Se ions. The various preparation conditions are summarised in Table (2.2) and Table (2.3).

Bath condition	Conc. of reactants	Temperature of deposition (^{0}C)	Time of deposition (min)	Resulting phase
Bath 1:1	0.2 M $CuSO_4$ 0.3 M TSC 0.2 M Na_2SeSO_3	27	70	$Cu_{2-x}Se$
Bath 1:1 LT	0.2 M $CuSO_4$ 0.3 M TSC 0.2 M Na_2SeSO_3	5	~ 4hrs	$Cu_{2-x}Se$
Bath 2:1	0.4 M $CuSO_4$ 0.5 M TSC 0.2 M Na_2SeSO_3	27	40	$Cu_{2-x}Se$
Bath 3:1	0.6M $CuSO_4$ 0.7 M TSC 0.2 M Na_2SeSO_3	27	30	$Cu_{2-x}Se$
Bath 5:1	1M $CuSO_4$ 1 M TSC 0.2 M Na_2SeSO_3	27	20	$Cu_{2-x}Se$
Bath 1:2	0.1M $CuSO_4$ 0.2 M TSC 0.2 M Na_2SeSO_3	5	30	Cu_3Se_2
Bath 1:1 Na	0.2M $CuSO_4$ 0.3 M TSC 0.2 M Na_2SeSO_3 NaOH (3 M)	5	50	Cu_3Se_2

Table (2.3)   pH during the various stages of reaction (all the reactants added in equal volume)

Reference

[1] D. R. Acosta, E. P. Zironi, E. Montoya, W. Estrada, *Thin Solid Films*, 288 (1996) 1.

[2] E. Y. Wang and I. Hsu, *J. Electrochem. Soc.*, 125 (1978) 1328.

[3] T. Feng, A. K. Ghosh and C. Fishman, *J. Appl. Phys.*, 50 (1979) 4972.

[4] G. Sasikala, P. Thilakan, C. Subramanian, *Solar Energy Mater. Solar Cells*, 62 (2000) 275.

[5] R. M. Murray and R. D. Heyding, *Can. J. Chem.*, 53 (1975) 878.

[6] R. N. O'Brien and K. S. V. Santhanam, *J. Electro Anal. Chem.*, 260 (1989) 231.

[7] R. D. Heyding, *Can. J. Chem.*, 44 (1966) 1234.

[8] S. K. Haram, K. S. V. Santhanam, M. Neumann-Spallart and C. Levy Clement, *Mater. Res. Bull.*, 27 (1992) 1185.

[9] S. K. Haram and K. S. V. Santhanam, *Thin Solid Films*, 238 (1994) 21.

[10] Z. Vucic, O. Milat, V. Horvatic and Z. Ogorelec, *Phys. Rev. B*, 24 (1981) 5398.

[11] H. Okimura, T. Matsumae and R. Makabe, *Thin Solid Films*, 71 (1980) 53.

[12] A. Tonejc, *J. Mater. Sci.*, 15 (1980) 3090.

[13] T. Saitoh, S. Matsubara and S. Minagawa, *Jpn. J. Appl. Phys.*, 16 (1977) 807.

[14] T. Takahashi, O. Yamamoto, F. Matsuyama and Y. Noda, *J. Solid State Chem.*, 16 (1976) 35.

[15] N. Frangis, C. Manolikas and S. Amelinckx, *Phys. Stat. Sol. (a)*, 126 (1991) 9.

[16] G. P. Sorokin, Hu. M. Papshev and P. T. Oush, *Sov. Phys. Solid State*, 1 (1996) 1810.

[17] A. M. Hermann and L. Fabick, *J. Crystal Growth*, 61 (1983) 658.

[18] I. Grozdanov, *Synthetic Metals*, 63 (1994) 213.

[19] M. Aven and D. A. Cusano, *J. Appl. Phys.*, 35 (1964) 606.

[20] B. Tell and J. J. Wiegand, *J. Appl. Phys.*, 48 (1977) 5321.

[21] R. Kondo, H. Okimura and Y. Sakai, *Jpn. J. Appl. Phys.*, 10 (1971) 1547.

[22] W. S. Chen, J. M. Stewart and R. A. Mickelsen, *Appl. Phys. Lett.*, 46 (1985) 1095.

[23] T. L. Chu, S. S. Chu, S. C. Lin and J. Yue, *J. Electrochem. Soc.*, 131 (1984) 2182.

[24] R. N. O' Brien and K. S. V. Santhanam, *J. Electrochem. Soc.*, 139 (1992) 434.

[25] S. C. Park, S. H. Kwon, J. S. Song and B. T. Ahn, *Sol. Energy Mater. Sol. Cells*, 50 (1998) 43.

[26] Y. Hachiuma, A. Ashida, N. Yamamoto, T. Ito and Y. Cho, *Sol. Energy Mater, Sol. Cells*, 35 (1994) 247.

[27] P. D. Fochs, W. George and P. D. Augustus, *J. Crystal Growth*, 3 (1968) 122.

[28] S. Kashida and J. Akai, *J. Phys. C: Solid State Phys.*, 21 (1988) 5329.

[29] M. A. Korzhuev, *Tech. Phys.*, 43 (1998) 1333.

[30] V. Horvatic, Z. Vucic and O. Milat, *J. Appl. Phys.*, 15 (1982) L 957.

[31] L. Thouin, S. Rouquette-Sanchez and J. Vedel, *Electrochemica Acta*, 38 (1993) 2387.

[32] S. Massaceessi, S. Sanchez and J. Vedel, *J. Electrochem. Soc.*, 140 (1993) 2540.

[33] R. N. Bhattacharya, A. M. Fernandez, M. A. Contreras, J. Keane, A. L. Tennunt, K. Ramananthan, J. R. Tuttle, R. N. Noufi and A. M. Hermann, *J. Electrochem. Soc.,* 143 (1996) 854.

[34] I. Grozdanov, *Semicond. Sci. Technol.*, 9 (1994) 1234.

[35] V. M. Garcia, P. K. Nair and M. T. S. Nair, *J. Crystal Growth*, 203 (1999) 113.

[36] G. K. Padam and S. K. Gupta, *J. Phys. D; Appl. Phys.*, 28 (1995) 783.

[37] G. K. Padam, *Thin Solid Films,* 150, (1987) L 89.

[38] C. Levy Clement, M. Neumann- Spallart, S. K. Haram and K. V. S. Santhanam, *Thin Solid Films*, 302 (1997) 12.

[39] C. Kaito, A. Nonaka, S. Kimura, N. Suzuki and Y. Saito, *J. Crystal Growth*, 186 (1998) 386.

[40] M. Shojiri, C. Kaito, Y. Saito, K. Teranishi and S. Sekimoto, *J. Crystal Growth*, 52 (1981) 883.

[41] R. J. Caveney, *J. Crystal Growth*, 2 (1968) 85.

[42] R. B. Shafizade, I. V. Ivanova and M. M. Kazinets, *Thin Solid Films*, 35 (1976) 169.

[43] O. C. Kopp and O. B. Cavin, *J. Crystal Growth*, 67 (1984) 391.

[44] A. Pajaczkowska, *J. Crystal Growth*, 7 (1970) 93.

[45] S. G. Ellis, *J. Appl. Phys.*, 38 (1967) 2906.

[46] B. Tell, J. L. Shay and H. M. Kasper, *J. Appl. Phys.*, 43 (1972) 2469.

[47]   B. Tell and H. M. Kasper, *J. Appl. Phys.*, 45 (1974) 5367.

[48]   T. Saitoh, S. Matsubara and S. Minagawa, *J. Electrochem. Soc.*, 123 (1976) 403.

[49]   O. Osawa, M. Iwase and H. Okimura, *Jpn. J. Appl. Phys.*, 19 (1980) 165.

[50]   A. Ashida, Y. Hachiuma, N. Yamamoto, T. Ito and Y. Cho,, *J. Mat. Sci. Lett.*, 13 (1994) 1181.

[51]   J. H. Schon and E. Bucher, *Appl. Phys. Lett.*, 73 (1998) 211.

[52]   L. L. Kazmerski, M. Hallerdt, P. J. Ireland, R. A. Michelsen and W.S. Chen, *J. Vac. Sci. Technol.*, 1 (1983) 395.

[53]   R. Klenk, T. Walter, H. W. Schock and D. Cahen, *Adv. Mater.*, 5 (1993) 114.

[54]   A. M. Fernandez, P. J. Sebastian, R. N. Battacharya, R. Noufi, M. Contreras, A. M. Hermann, *Semicond. Sci. Technol.*, 12 (1996) 994.

[55]   W. N. Shafarman, R. Klenk, B. E. Mc Candless, *J. Appl. Phys.* 79 (1996) 7324.

[56]   T. Yamaguchi, J. Matsufusa, H. Kabasawa and A. Yoshida, *J. Appl. Phys.*, 69 (1991) 7714.

[57]   M. Nishtani, T. Negami, M. Terauchi and T. Hirao, *Jap. J. Appl. Phys.*, 31 (1992) 192.

[58]   E. R. Don, R. Hill and G. J. Russel, *Solar Cells*, 16 (1986) 131.

[59]   L. Stolt, J. Hedstorm, J. Kessler, M. Ruckh, K. Velthaus and H. W. Schock, *Appl. Phys. Lett.*, 62 (1993) 597.

[60]   J. W. Park, G. Y. Chung, B. T. Ahn, H. B. Im and J. S. Song, *Thin Solid Films*, 245 (1994) 174.

[61]   B. M. Basol and V. K. Kapur, *IEEE Trans. Electr. Dev.*, 37 (1990) 418.

[62]   R. D. Varrin, Jr., S. Verma, R. W. Birkmire, B. E. Mc Candlers and T. W. F. Russel, *Proc. 21ˢᵗ IEEE Photovoltaic Specialists Conf.*, Kissimmee, (1990) 529.

[63]   P. K. Vidyadharan Pillai, K. P. Vijayakumar and P. S. Mukherjee, *J. Mat. Sci. Lett.*, 13 (1994) 1725.

[64]   M. Pattabi, P. J. Sebastian, X. Mathew and R. N. Battacharya, *Solar Energy Mater. Sol. Cells*, 63 (2000) 315.

[65]   J. S. Park, Z. Dong, S. Kim and J. H. Perepezko, *J. Appl. Phys.*, 87 (2000) 3683.

[66]   M. Inoue, C. Cruz- Vazquez, M. B. Inoue, K. W. Nebesny and Q. Fernando, *Synth. Met.*, 55 (1993) 3748.

[67] D. C. Trivedi and S. K. Dhawan, *Synth. Met.*, 59 (1993) 267.

[68] S. Yanagida, T. Enokida, A. Shindo, T. Shiragami, T. Ogata, T. Fukumi, T. Sagakami, H. Mori and T. Sakata, *Chem. Lett.*, (1990) 1773.

[69] D. C. Trivedi and S. Srinivasan, *J. Mat. Sci. Lett.*, 8 (1989) 709.

[70] G. Gustaffson, Y. Cao, G. M. Treacy, F. Clavetter, N. Colanen and A. J. Heeger, *Nature*, 357 (1992) 477.

[71] S. K. Dhawan and D. C. Trivedi , *J. Appl. Electrochem*, 22 (1992) 563.

[72] C. Gasgrande, S. Ponero, P. Prosperi and B. Scrosati, *J. Appl. Electrochem*, 22 (1992) 195.

[73] N. G. Cluchnikov, *J. Techn. Phys.*, 24 (1954) 833.

[74] Z. Ogorelec and D. Selinger, *J. Mat. Sci.*, 6 (1971) 136.

[75] R. B. Shafizade, I. V. Ivanova and M. M. Kazinets, *Thin Solid Films*, 55 (1978) 211.

[76] C. A. Estrada, P. K. Nair, M. T. S. Nair, R. A. Zingaro and E. A. Meyers, *J. Electrochem. Soc.*, 141 (1994) 802.

[77] A. Mandal and P. Pramanik, *J. Solid State Chem.*, 47 (1983) 81.

[78] A. Mondal and P. Pramanik, *J. Solid State Chem.*, 55 (1984) 116.

[79] D. B. Johnson and L. C. Brown, *J. Appl. Phys.*, 40 (1969) 4217.

[80] H. Morikawa, M. Shiojiri and E. Suito, *J. Appl. Phys.*, 42 (1971) 2143.

[81] N. Morimotto and K. Koto, *Science*, 152 (1966) 345.

[82] H. Morikawa, *Jap. J. Appl. Phys.*, 11 (1972) 431.

[83] A. Arias- Carbajal Readigos, V. M. Garcia, O. Gomezdaza, J. Campos, M. T. S. Nair and P. K. Nair, *Semicond. Sci. Technol.*, 15 (2000) 1022.

[84] Sunny Mathew, *Ph.D. Thesis*, Cochin University of Science and Technology, Kochi, India, (1994).

[85] G. M. Barrow, *Physical Chemistry*, 3rd ed., McGraw-Hill, Tokyo (1973) 668.

CHAPTER-3

Characterisation of copper selenide thin films

3.1 Introduction

Preparation and characterisation of any material are two equally important aspects like the two sides of a coin. In the case of thin films, appropriate characterisation often widens the scope of applications. However characterising thin films with precision is a challenging job.

This thesis work includes: -

i) Morphological characterisation by visual appearance, thickness measurement using Tolansky method and Stylus method and surface morphological studies using SEM (Scanning Electron Microscope).

ii) Structural characterisation using XRD (X-Ray Diffraction) analysis.

iii) Optical characterisation using absorption and transmission spectral studies.

iv) Compositional analysis using XPS (X-ray Photoelectron Spectroscopy), ICP (Inductively Coupled Plasma) and XRD analysis.

v) Electrical characterisation using Hall measurements

3.2 Morphological characterisation

Microstructure and thickness have profound influence on the properties of thin films. For instance, when copper selenide finds application as an absorber layer in the field of photovoltaics, two major requirements are large grain size and a film thickness around 2µm [1]. Moreover, in solar cells where $Cu_{2-x}Se$ is used as window material, the poor cell efficiency was attributed to non-uniformity and presence of pinholes in the $Cu_{2-x}Se$ film [2].

3.2.1 Visual appearance

Thin films of $Cu_{2-x}Se$ prepared from Bath 1:1, Bath 2:1, Bath 3:1 and Bath 5:1 were reddish brown in colour [2] and uniform in appearance. Bath 1:1 Na and Bath 1:2 resulted in Cu_3Se_2 films with a bluish green colour. The group of cuprosic selenides, which includes Cu_3Se_2, is known to have a similar colour [3]. When observed with naked eye the film from Bath 1:1 Na was more uniform than that from Bath 1:2. In short, $Cu_{2-x}Se$ phase has a reddish colour, while Cu_3Se_2 is bluish green. Hence preliminary differentiation of the two phases was very easy.

3.2.2 Thickness measurement

Thickness of as-prepared films was measured using Tolansky technique. For this method, it is necessary to have a sharp and well defined straight edge of the film. Usually CBD films have a curved hazy edge, as the solution bath forms a meniscus curved downwards due to capillary rise. In order to get a sharp edge, glass slides were masked with tightly wound teflon tapes before dipping in the reaction bath. After the final stage of drying the films, teflon tapes were removed carefully.

In the case of $Cu_{2-x}Se$ film, thickness of one-dip was found to be around 0.2 µm. As two-dip and three-dip films were thicker than the measurable range of this technique, they were analysed using gravimetric method. The thickness was estimated to be around 1 µm 1.2 µm. For Cu_3Se_2 film the thickness of two-dip was near 1.2 µm.

In order to counter check the accuracy of this method, Stylus profiling was also done on few of the samples and the results were found to agree with the Tolansky method. Stylus profiler makes use of a diamond probe, which moves over the film surface. When this probe encounters the step formed by the thin film edge, a corresponding electrical signal is generated from which thickness of the film can be calculated.

3.2.3 Surface morphology

Scanning electron microscope (SEM) was used for studying surface morphology and micro structural features of the as-prepared copper selenide thin films. In this technique, secondary electrons are emitted from the surface layer of the film and hence the micrograph obtained will be a faithful reproduction of the surface features.

SEM equipment of Hitachi Co. (model: S 2400) was used for the present study. As copper selinide films were low resistive, no additional conducting coating was given to the film surface. 15 K magnification was chosen as most suitable for observing grains in the as-prepared thin films. From this morphology study, it was possible to understand the effect of varying the relative concentration of copper in the reaction mixture, the effect of substrate and temperature of deposition on the grain size and also to differentiate $Cu_{2-x}Se$ phase from Cu_3Se_2 phase.

Micrographs of $Cu_{2-x}Se$ film prepared from Bath 1:1 and Bath 2:1 are shown in Fig.(3.1) and Fig.(3.2) respectively. Both have more or less same appearance and
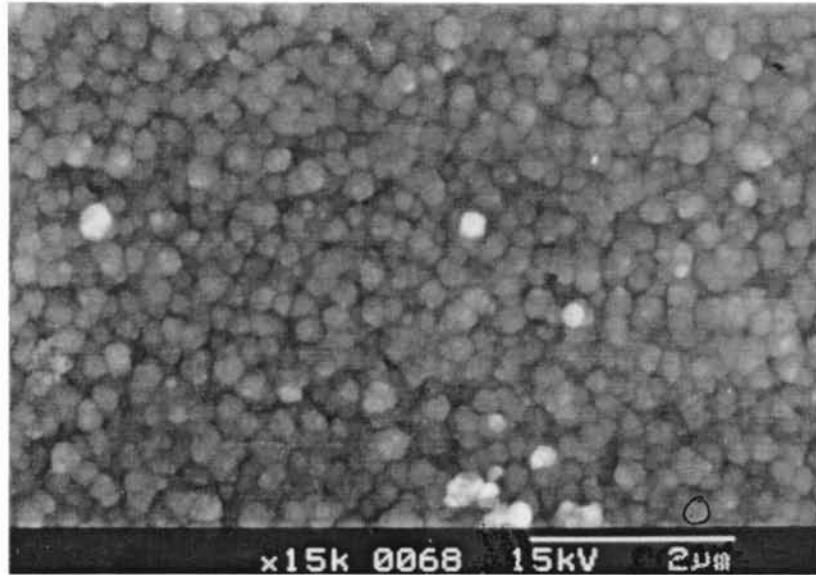
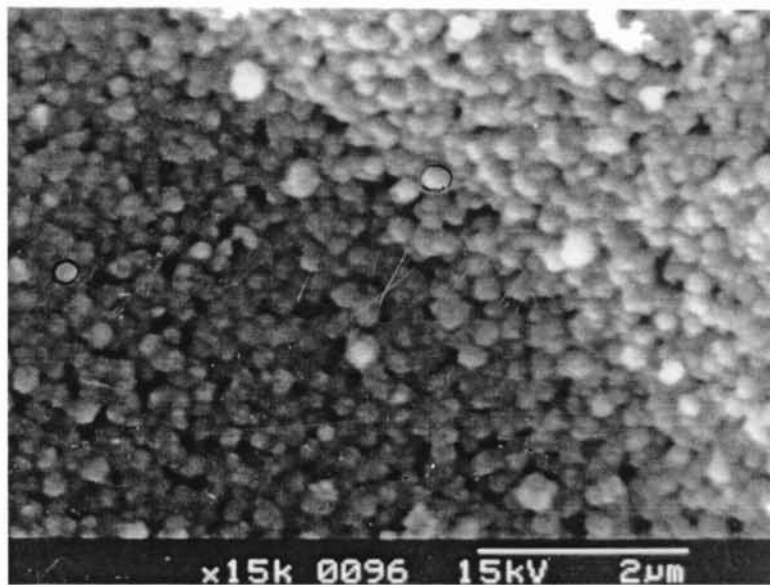Fig (3.1)   SEM micrograph of $Cu_{2-x}Se$ film from Bath 1:1

Fig .(3.2)   SEM micrograph of $Cu_{2-x}Se$ film from Bath 2:1

average grain size around 0.2 μm. Grain boundaries are well defined even in the as-prepared form. Detailed examination reveals that film from Bath 1:1 is slightly more uniform than the film from Bath 2:1. The micrographs of film prepared from Bath 3:1 and Bath 5:1 [Fig.(3.3) and Fig.(3.4)] show that the grain boundaries become more diffused when the relative concentration of copper is increased beyond a Cu:Se ratio of 2:1. In films from Bath 5:1, the granularity of the phase is almost lost. In the present work, due to the most uniform surface morphology, the films from Bath 1:1 are chosen as the representative sample of the $Cu_{2-x}Se$ phase (referred as *sample No: 1*).

All the above mentioned films were deposited on glass substrate. However Fig.(3.5) shows the film deposited from Bath 1:1 on SnO_2 substrate. Average grain size in this case is found to be 0.3 μm. This reveals the effect of substrate on grain size of $Cu_{2-x}Se$ phase, i.e. bigger grain size is obtained on SnO_2 substrates than on glass substrates.

Comparison of SEM micrograph of film from Bath 1:1 LT [Fig.(3.6)] with Fig.(3.1) reveals the effect of temperature of deposition on the surface morphology. It can be observed that surface of the film deposited at low temperature is not uniform as the grains have a tendency to grow as clusters. Moreover the grain boundaries are not well defined.

Fig.(3.7) shows the micrograph of Cu_3Se_2 phase deposited from Bath 1:1 Na. Here average grain size is around 0.4 μm. When compared with standard $Cu_{2-x}Se$ phase (Fig.(3.1)), surface of Cu_3Se_2 film shows ups and downs along with cluster formation. The grain size of Cu_3Se_2 phase is almost double that of $Cu_{2-x}Se$ phase.

Hence the general conclusions are:

i) $Cu_{2-x}Se$ film from Bath 1:1 is very uniform with distinct grains of average size 0.2 μm.

ii) The gradual increase in concentration of copper in the reaction bath leads to poor film morphology.

iii) Deposition at low temperature is found to result in grain growth in the form of clusters.

iv) When compared with $Cu_{2-x}Se$ phase, Cu_3Se_2 phase grows in clusters with less defined grain boundaries, but with a larger grain size of the range 0.4 μm.
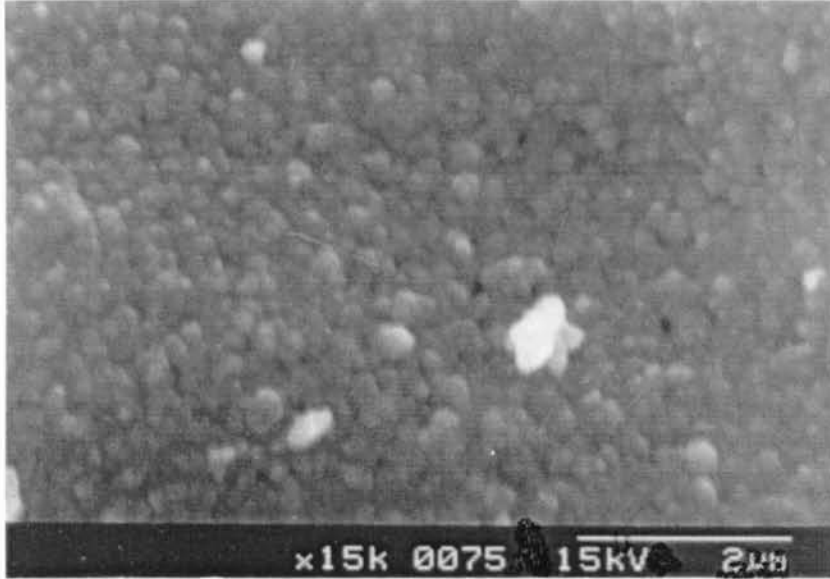
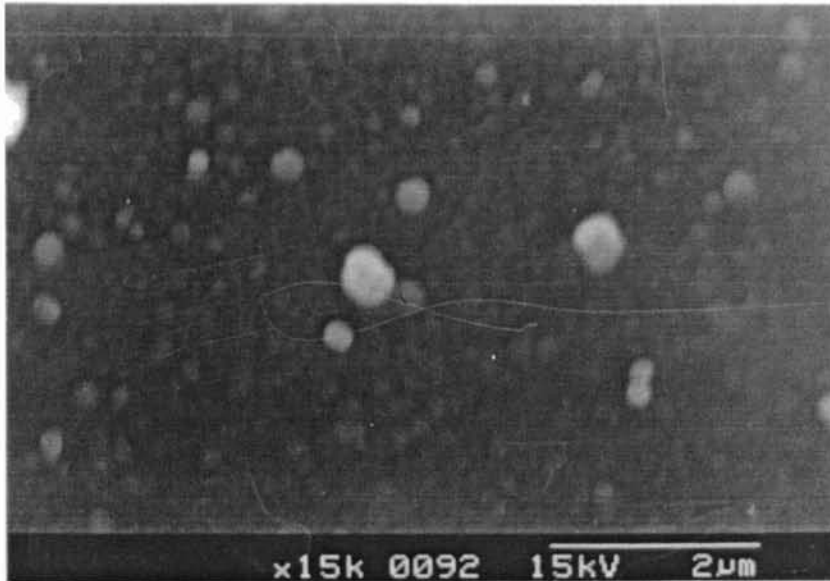Fig (3.3)   SEM micrograph of $Cu_{2-x}Se$ film from Bath 3:1

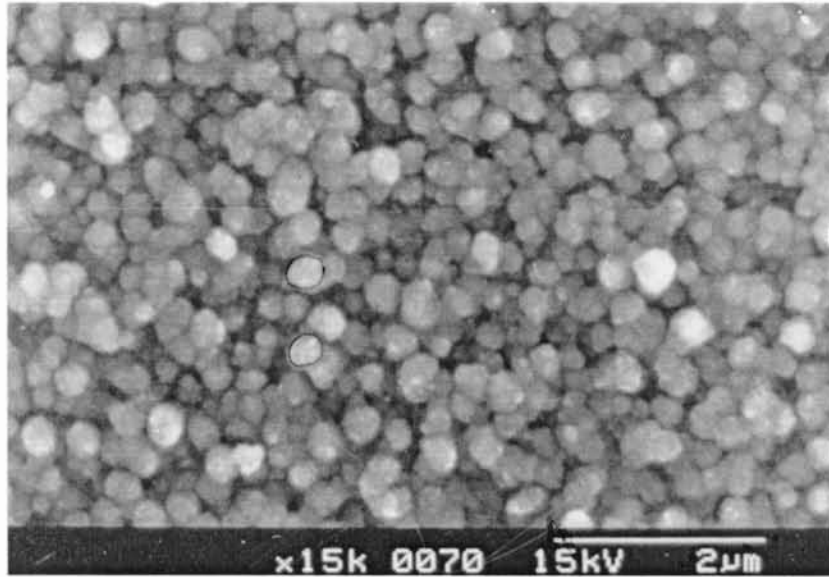Fig (3.4)   SEM micrograph of $Cu_{2-x}Se$ film from Bath 5:1

Fig (3.5)   SEM micrograph of $Cu_{2-x}Se$ film from Bath 1:1 SnO_2
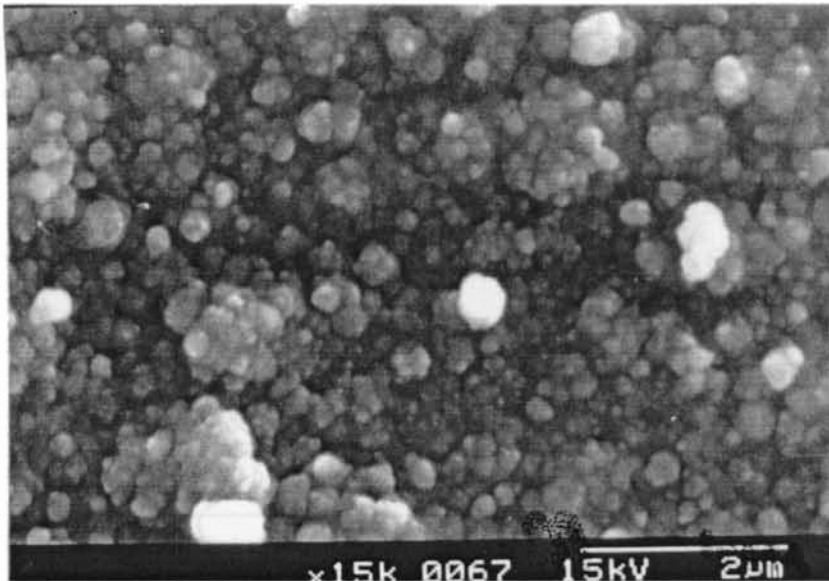

Fig (3.6)   SEM micrograph of $Cu_{2-x}Se$ film from Bath 1:1 LT

This study on grain size and surface nature is significant when these thin films find applications in optoelectronics and photovoltaics.

3.3 Structural characterisation

3.3.1 XRD analysis

X-ray diffraction is the most convenient tool for crystallographic structural analysis. In the present work this was used as a major analytical technique for differentiating various phases of the as-prepared copper selenide thin films. This analysis was done using Rigaku (D.Max.C) X-ray diffractometer, which makes use of Cu $K_{\alpha 1}$ (λ=1.5405 Å) radiation. After preliminary trials, the scan range for 2θ was fixed between 20^0 and 55^0 for these thin films.

a) $Cu_{2-x}Se$ phase

XRD pattern of the film from Bath 1:1 is shown in Fig.(3.8). On comparing the d values of this spectrum with the standard JCPDS data index 6-0680, the structure was identified as cubic phase of $Cu_{2-x}Se$. In the standard data the highest intensity is attributed to (022) plane, while in the present case peak corresponding to (111) plane has maximum intensity. Due to the amorphous nature of the glass substrate the background intensity is very high in the spectrum. The d values and the relative intensities after background correction are shown in Table (3.1).

d (Å) experimentally observed	d (Å) as per JCPDS file 6-0680	hkl	I/I_0 (Observed)	I/I_0 (Standard)
3.323	3.330	111	100	90
2.030	2.030	022	71	100
1.729	1.729	113	18	80

Table (3.1) X-ray diffraction parameters of cubic $Cu_{2-x}Se$ film

The cubic phase of $Cu_{2-x}Se$ is usually known as the high temperature phase [4-9]. However depending on the extent of non-stoichiometry in the copper selenide
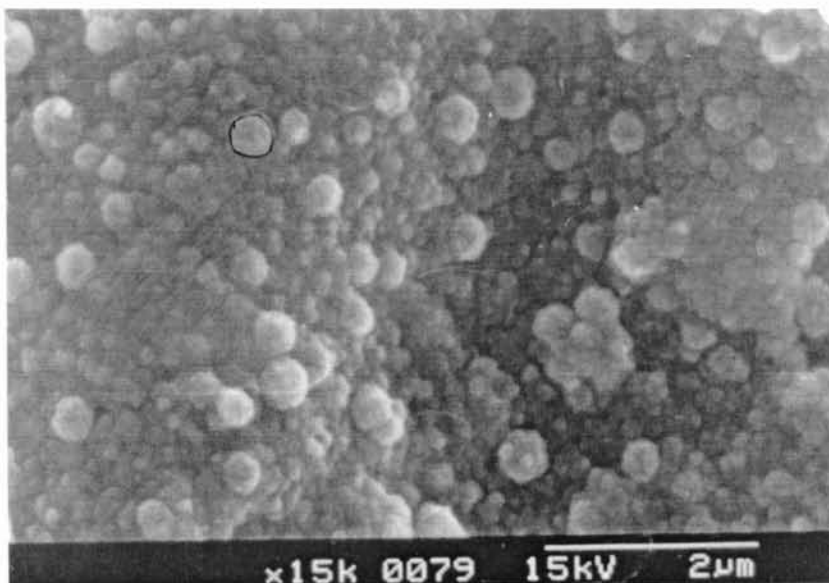
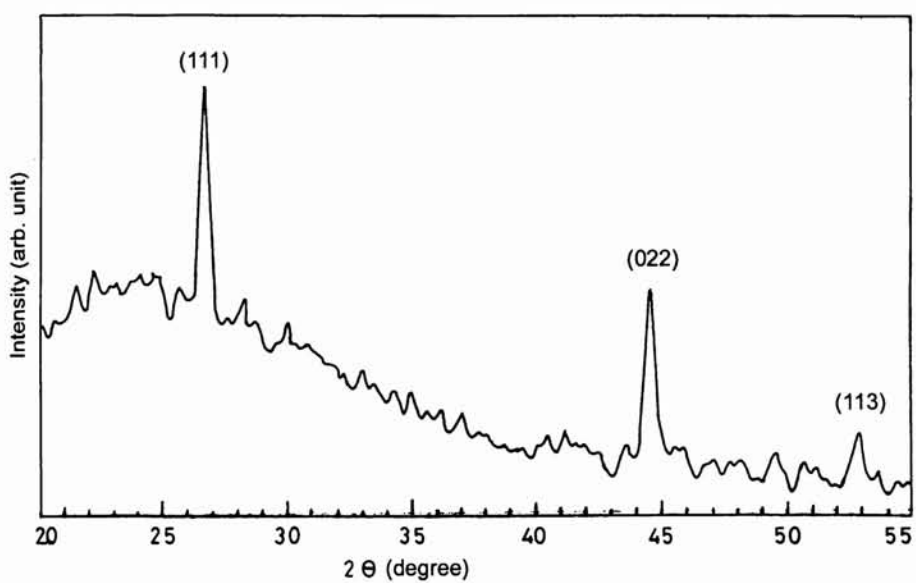Fig (3.7)   SEM micrograph of Cu_3Se_2 film from Bath 1:1 Na.

Fig (3.8)   XRD spectrum of $Cu_{2-x}Se$ film from Bath 1:1

phase, the cubic phase can occur even at room temperature. The phase diagram shown in Fig.(3.9), as reported by Tonejc *et al.* [10], depicts this situation clearly. It suggests that the low temperature phase exists as the single phase only if the composition is around $Cu_{1.997}Se$. At this composition when the temperature is increased to 130^0C, the high temperature phase begins to appear and at a temperature above 140^0C the sample completely gets converted to the high temperature phase. The low temperature to high temperature transition always occurs through a stage of mixed phase. But when $1.97 \geq (2-x) \geq 1.84$, the low temperature phase is highly unstable in air and it gets converted to high temperature phase, at temperatures lower than 130^0C. From the figure it is clear that at composition $x \geq 0.2$ the high temperature phase can occur as a single phase at temperatures above 30^0C. In the present case, the composition was analysed to be $x \geq 0.2$ (refer section 3.5) and it justifies the cubic phase at room temperature. Similar results are reported in other publications also [1,2,11-13].

b) Cu_3Se_2 phase

XRD pattern of the films deposited from Bath 1:1 Na and Bath 1:2 were similar. However as the samples from Bath 1:1 Na were more uniform, they were chosen as the standard film of Cu_3Se_2 phase (referred to as Sample No.2). The XRD spectrum of this is shown in Fig.(3.10) and the d values coincide with the JCPDS data index 47-1745 for tetragonal Cu_3Se_2 phase. All the major diffraction peaks in the standard file were repeatedly reproduced in the sample. As only a thin layer of this material could be deposited on a plane glass substrate, the intensities of the diffraction peaks were very small. Hence Cu_3Se_2 films were preferably deposited on SnO_2 coated glass. XRD spectrum of Cu_3Se_2 on glass and on SnO_2 coated glass were the same except for the difference in peak intensities, background intensities and the presence of peaks from SnO_2. Table (3.2) shows the XRD parameters of the Cu_3Se_2 film (the relative intensities being calculated after background correction).
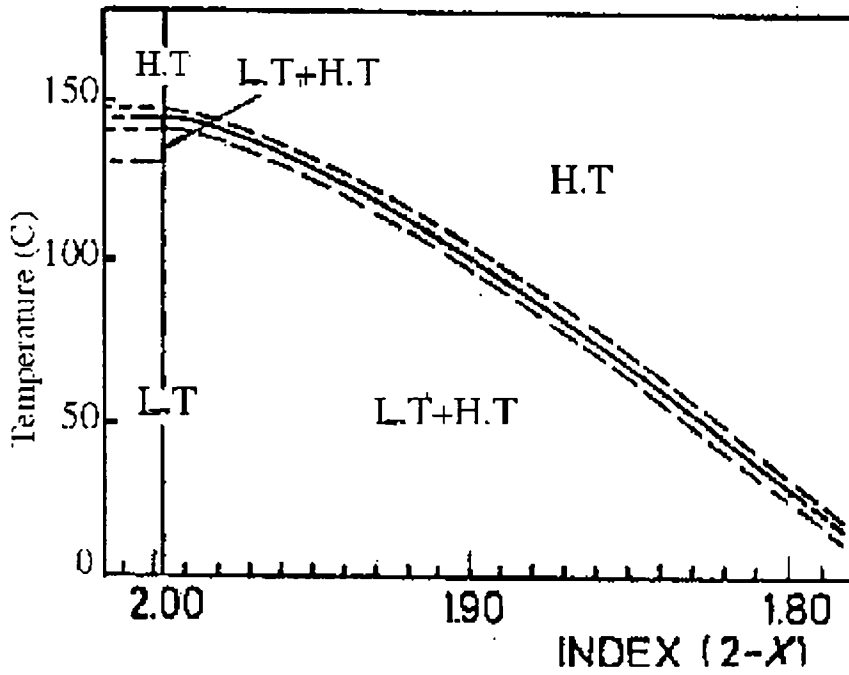
Fig. (3.9)   Phase diagram of low temperature (L.T) and high temperature (H.T)
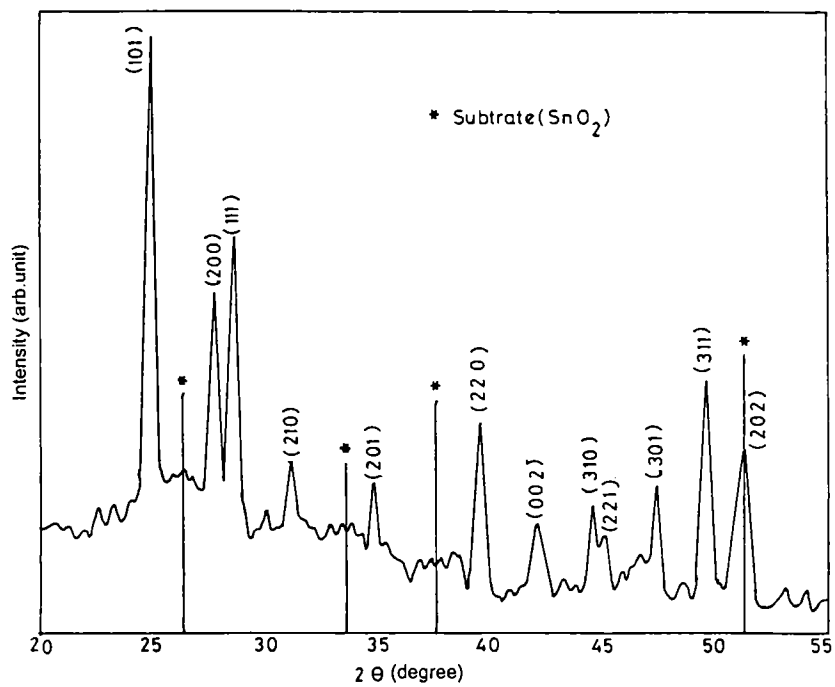phase of $Cu_{2-x}Se$ in relation to stoichiometry and temperature

Fig (3.10)   XRD spectrum of Cu_3Se_2 film from Bath 1:1 Na

d (Å) experimentally observed	d (Å) as per JCPDS file 47-1745	hkl	I/I_0 (Observed)	I/I_0 (Standard)
3.575	3.557	101	100	100
3.214	3.202	200	44	55
3.126	3.111	111	56	61
2.874	2.864	210	13	19
2.563	2.563	201	16	20
2.270	2.264	220	35	51
2.143	2.139	002	16	19
2.029	2.024	310	19	30
2.008	2.001	221	11	21
1.914	1.910	301	24	34
1.833	1.830	311	46	63
1.781	1.778	202	31	47

Table (3.2) X-ray diffraction parameters of tetragonal Cu_3Se_2 film

c) Effect of increase in film thickness of $Cu_{2-x}Se$ phase

Fig.(3.11) shows the XRD spectrum of $Cu_{2-x}Se$ films after one dip, two dip and three dip respectively. The peak heights were found to increase considerably with thickness. Values of FWHM (full width at half maximum) of the peak corresponding to the characteristic (022) plane in these three cases are tabulated in Table (3.3) along with the maximum peak intensity. Decrease in FWHM of the peak with increase in the number of dippings shows improvement in crystallinity of the $Cu_{2-x}Se$ film with increase in thickness.

No: of dippings	FWHM	Maximum intensity (counts/s)
1 dip	2.226	112
2 dip	0.949	181
3 dip	0.541	485

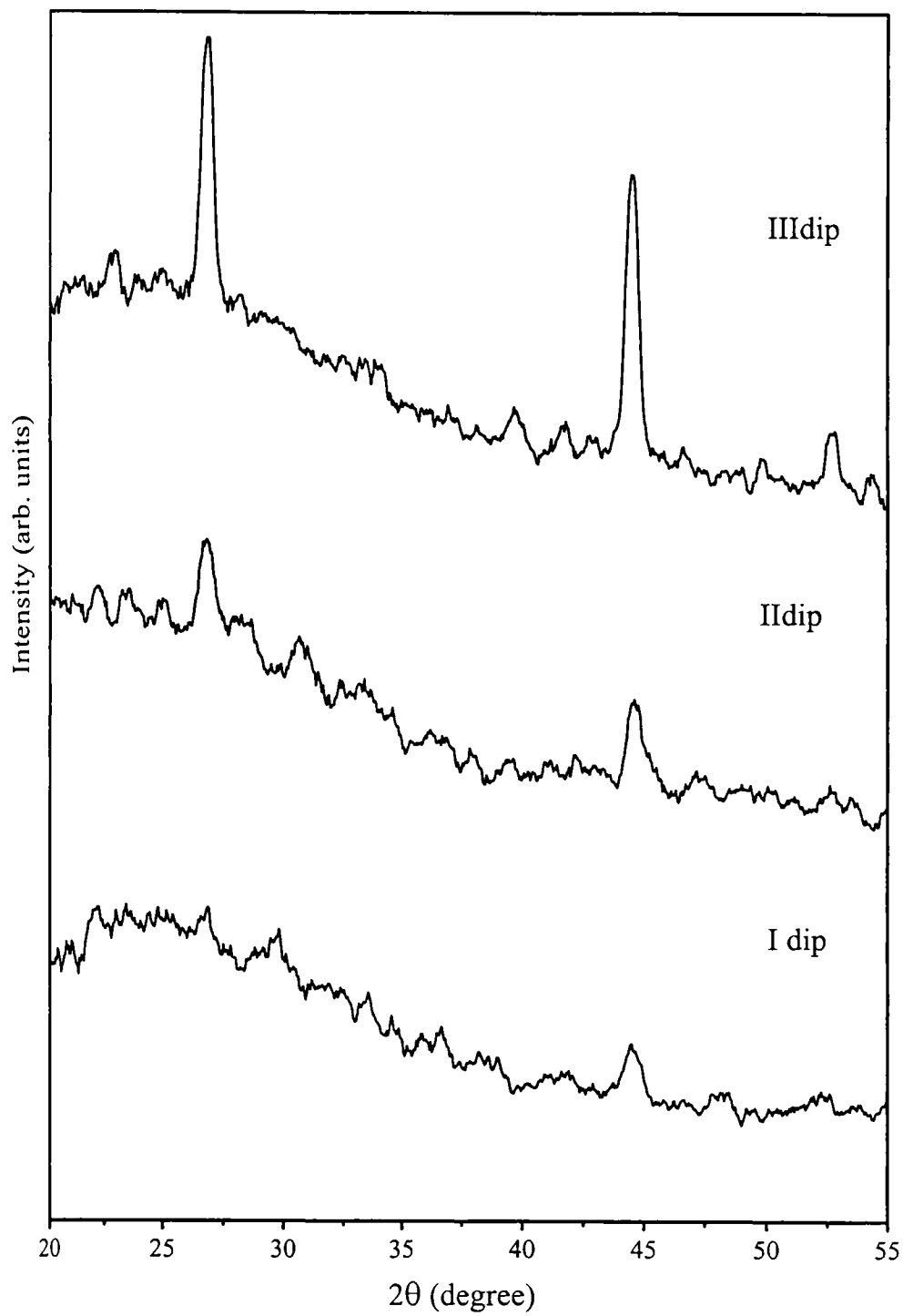Table (3.3) Variation in FWHM and maximum intensity of XRD peak with increase in film thickness

Fig.(3.11)   Variation in XRD spectrum of $Cu_{2-x}Se$ film with thickness

d) Effect of increase in the relative concentration of copper in the reaction bath

Fig.(3.12) shows the XRD spectrum of films from Bath 1:1, Bath 2:1, Bath 3:1 and Bath 5:1 in succession. This reveals the influence of gradual increase in relative concentration of copper for a fixed concentration of selenium in the reaction bath. Peak intensity and FWHM of (022) plane for this series of $Cu_{2-x}Se$ film are tabulated in Table (3.4).

Bath conditions	FWHM	Maximum intensity (c/s)
Bath 1:1	0.589	181
Bath 2:1	0.949	209
Bath 3:1	1.495	170
Bath 5:1	1.548	158

Table (3.4)   Variation in FWHM and maximum intensity of the XRD peak with increase in copper concentration in the reaction bath

The highest intensity of (022) peak is for films from Bath 2:1 and it suggests maximum thickness. Further decrease in peak intensity for films from Bath 1:3 and Bath 1:5 shows decrease in film thickness. This is obvious with naked eye also. When the relative concentration of copper in the reaction bath is increased, the rate of reaction increases, leading to faster precipitation and thereby resulting in thinner films. Here the gradual increase in FWHM hinds to the gradual decrease in grain size of the $Cu_{2-x}Se$ film. SEM micrograph also supports this result.

3.4 Optical characterisation

Optical properties are very significant as far as applications in any optoelectronic devices are concerned. Optical band gap and absorption coefficient are two important parameters of a solar cell material.

In the present study, optical characterisation was done to the determination of nature of absorption and transmission spectra and energy bandgap of copper selenide. These properties have dependence on grain size and chemical composition of the thin films. Therefore it is logical to study the optical properties in correlation with the above mentioned factors.
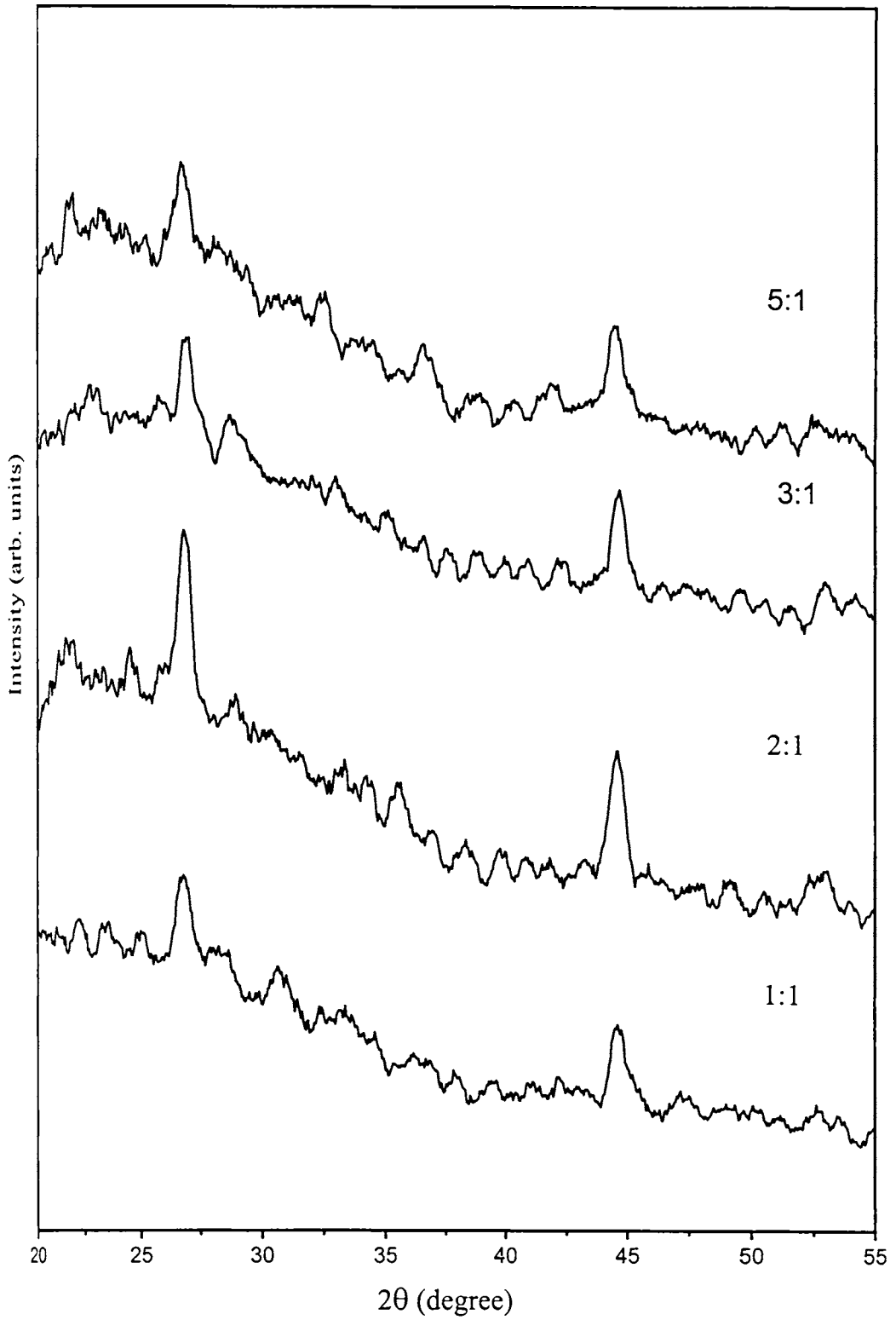
Fig.(3.12)   Variation in XRD spectrum of $Cu_{2-x}Se$ film
with relative concentration of Cu in the reaction bath

3.4.1 Optical absorption

UV-VIS-NIR spectrophotometer (U-3410 model of Hitachi group) was used for the optical studies. Studies were mainly conducted in the range 340 nm to 2000 nm. Band edge calculated from the absorption spectrum was used as a tool to differentiate the formation of the two different phases of copper selenide.

Determination of optical band gap is based on the photon induced electronic transition between conduction band and valance band. At the absorption edge, absorption coefficient α can be expressed as

$$\alpha = (h\nu - Eg)^{\gamma} \quad [14].$$

This was used to find out the nature of transition in the thin film material. Here $h\nu$ stands for photon energy, Eg for band gap and γ is a constant which is equal to $\frac{1}{2}$ for allowed direct transition, $\frac{3}{2}$ for forbidden direct transition and 2 for allowed indirect transition.

For both $Cu_{2-x}Se$ and Cu_3Se_2 thin films, the plot of $(\alpha t h\nu)^2$ versus photon energy was found to be linear as shown in Fig.(3.13) and Fig.(3.14) (t stands for the film thickness). The graphs suggest a direct bandgap for both the materials. Extrapolation of these curves to zero absorption coefficient showed the optical energy gap of the $Cu_{2-x}Se$ phase as 2.20 eV and Cu_3Se_2 phase as 2.83 eV. This band gap of $Cu_{2-x}Se$ phase is comparable with that reported earlier by Garcia *et al.* and others [1,12,15]. To the best of our knowledge this is the first report on the band gap of Cu_3Se_2 phase and hence no comparison is possible [16,17].

Band edge calculated for one dip, double dip and triple dip of the $Cu_{2-x}Se$ film showed a shift towards lower values in succession, Fig.(3.15). The results are tabulated in Table (3.5). This is due to the effect of increase in average grain size with gradual increase in the number of dips. High value of band gap for the one-dip film suggests the very small size of the crystals. This blue shift of the optical spectra is a usual phenomenon in the case of chemically deposited thin films [18,19]. In the present case, the results are also supported by XRD analysis (refer section 3.3.1.c).

No: of dippings	Band gap (eV)
I dip	2.31
II dip	2.20
III dip	2.05

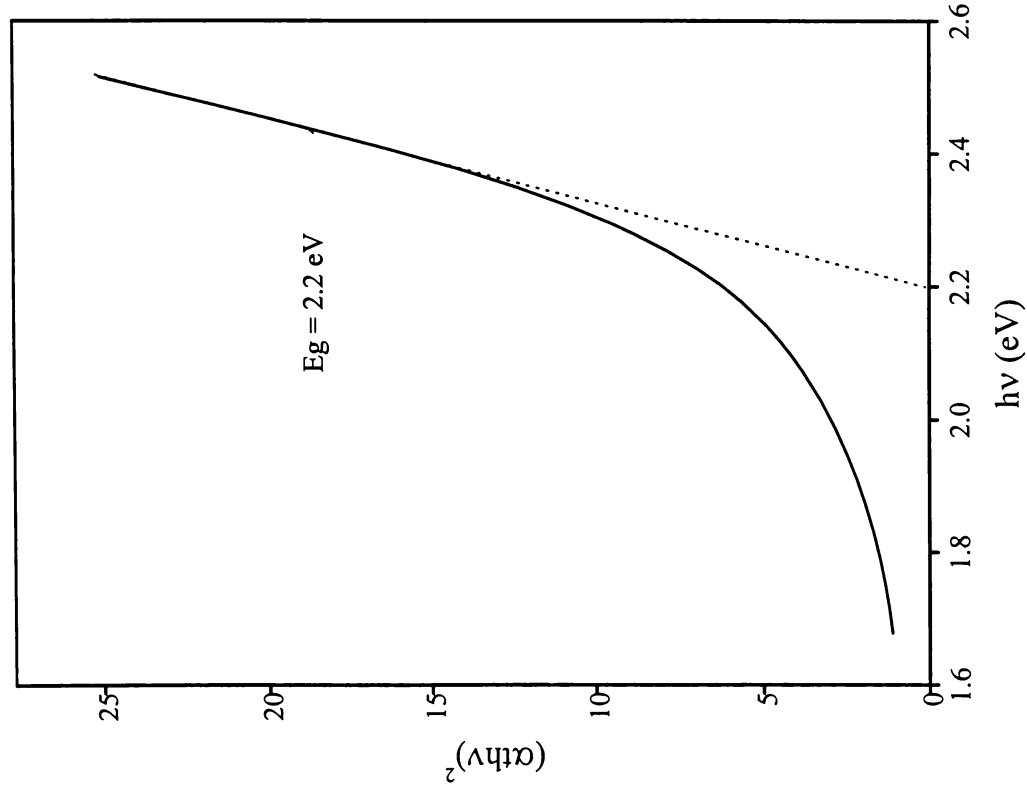Table (3.5) Variation in absorption edge of the $Cu_{2-x}Se$ film with thickness

Fig.(3.14) $(\alpha th\nu)^2$ vs. hν graph of Cu$_3$Se$_2$ film
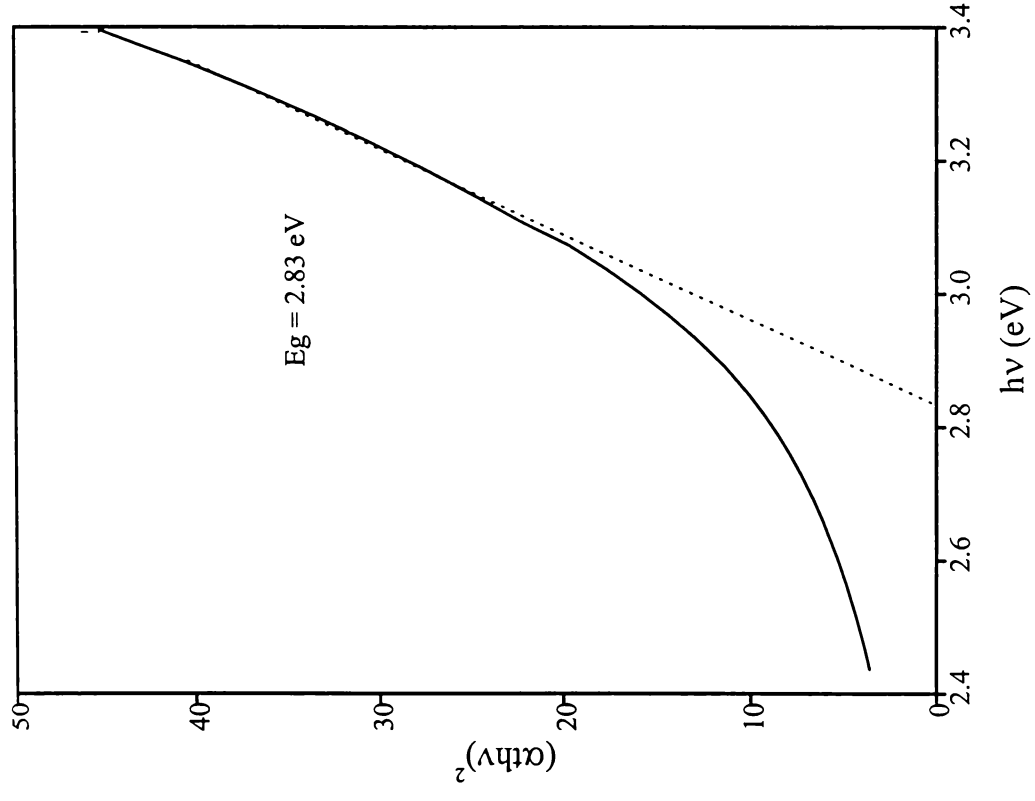

Fig.(3.13) $(\alpha th\nu)^2$ vs. hν graph of Cu$_{2-x}$Se film

Absorption spectrum is also found to vary slightly with increase in relative concentration of copper in the reaction mixture. The absorption edge calculated for films from the Bath 1:1, Bath 2:1, Bath 3:1 and Bath 5:1 (Fig (3.16)) are tabulated in Table (3.6). The slight increase in the band edge with increase in relative concentration of copper may be the result of decrease in grain size (as suggested in section 3.3.1.d), decrease in film thickness and decrease in the non-stoichiometric index (as mentioned in section 3.5.3).

Bath condition	Band gap (eV)
Bath 1:1	2.20
Bath 2:1	2.31
Bath 3:1	2.32
Bath 5:1	2.34

Table (3.6)   Variation in absorption edge with increase in relative
concentration of Cu in the reaction bath

3.4.2 Optical transmission

Fig.(3.17) shows the transmittance spectra of the $Cu_{2-x}Se$ film deposited from Bath 1:1 and the Cu_3Se_2 film deposited from Bath 1:1 Na respectively. The peak value of transmittance is around 780 nm for the $Cu_{2-x}Se$ film while it is around 580 nm for Cu_3Se_2 films. A substantial decrease in transmittance is observed through out the IR region for both the phases. This is the result of free carrier absorption in this degenerate semiconductor films [1]. This transmittance spectrum of $Cu_{2-x}Se$ suggests a potential application of these films as microwave (IR) shielding coating or selective solar control coating [12,13]. Such effects have been reported for all copper selenides in general [20].

3.5 Compositional analysis

Characterisation by optical or electrical methods can be thought of as indirect way of analyzing a material, for these properties in turn depend on the primary quality of chemical composition or stoichiometry. Often the lack of repeatability and discrepancy between the expected behaviour and experimental observation, are due to lack of proper analysis and documentation of the composition of the material.

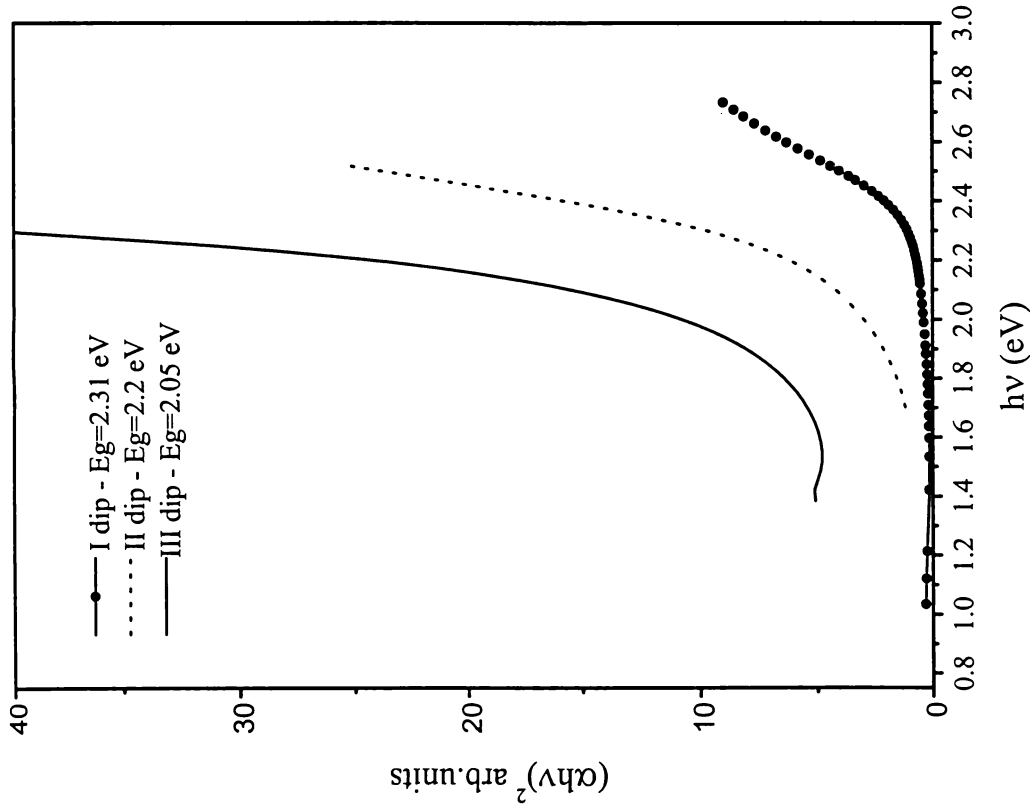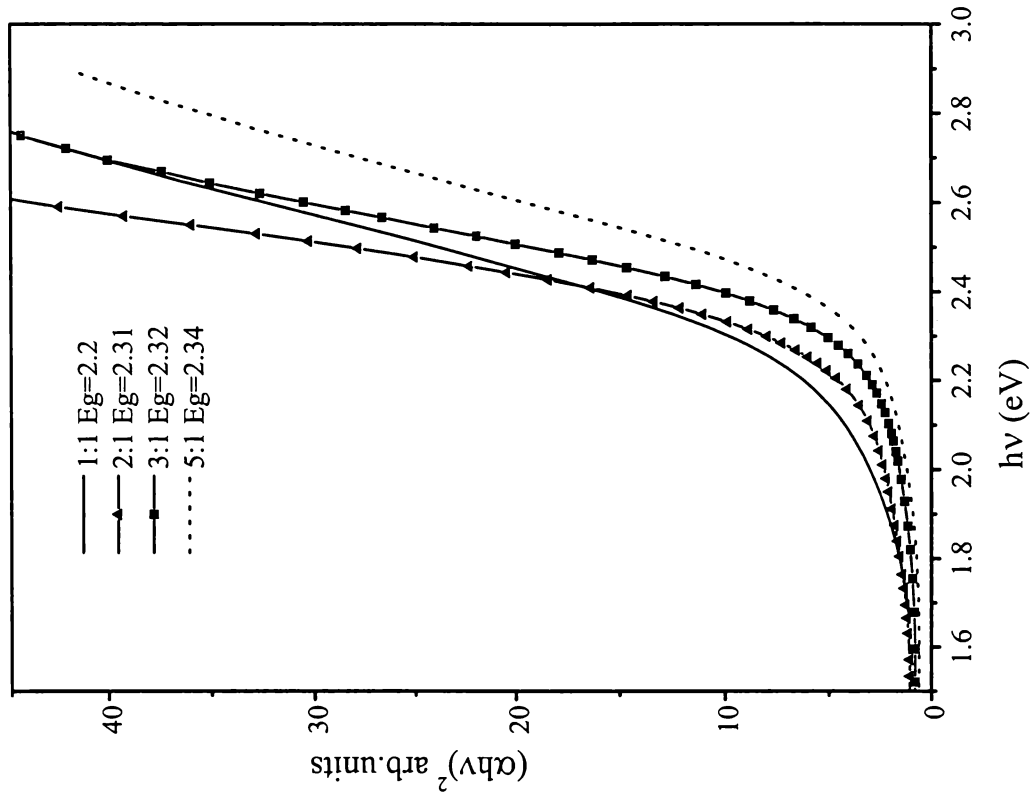Fig.(3.16) Variation in absorption edge of Cu_{2-x} Se film with relative concentration of Cu in the reaction bath

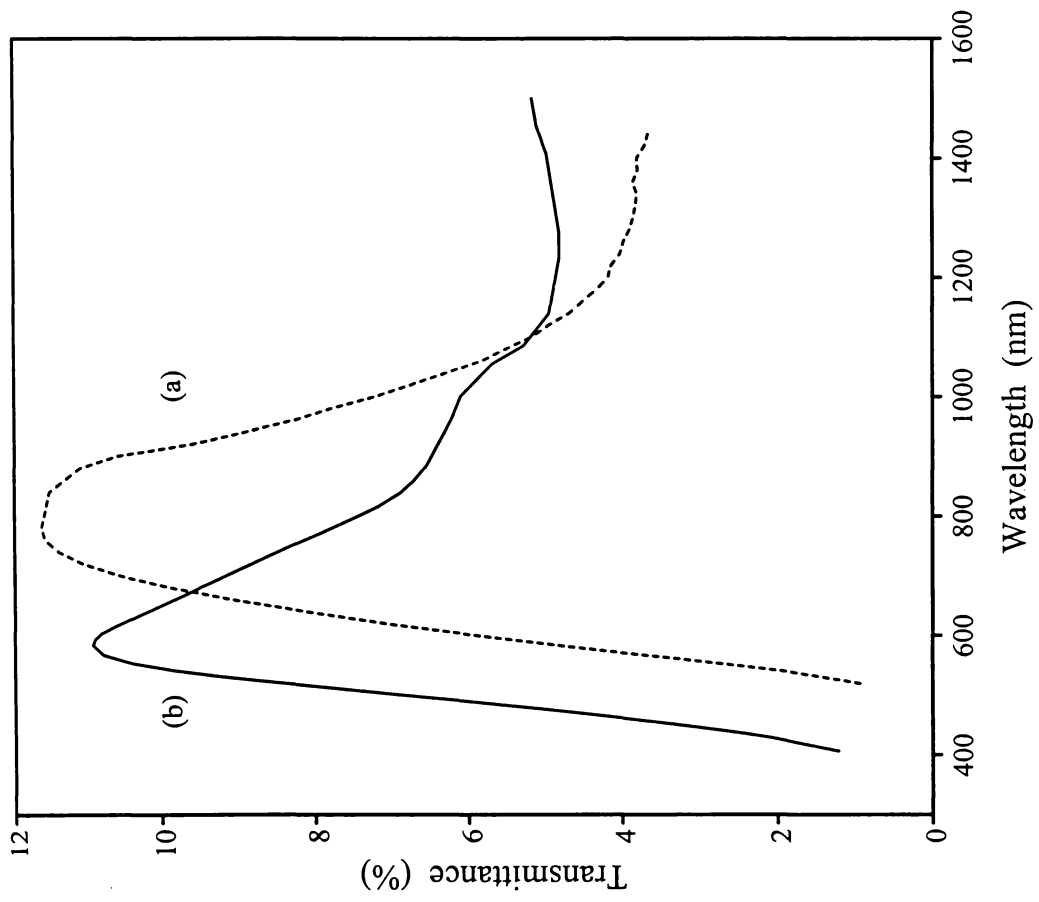Fig.(3.15) Variation in absorption edge of Cu_{2-x} Se film with thickness

Fig. (3.17) Transmission spectra of (a) $Cu_{2-x}Se$ film (b) Cu_3Se_2 film

X-ray photoelectron spectroscopy (XPS) is considered as one of the most powerful tool, for characterising the chemical composition of thin films [21]. In the present work this technique was used for elemental analysis. Inductively coupled plasma (ICP) analysis was also done as a bulk analytical technique to confirm the stoichiometry as suggested by XPS analysis. Indirect interpretation of composition from XRD analysis is also included in this section.

3.5.1 XPS analysis

In XPS analysis it is possible to predict the chemical environment of various elements and to evaluate the percentage composition. It is also possible to have depth profile of the required region by sputtering the surface layers of the sample with heavy ions. Chemical environment of each element is interpreted by comparing the calculated value of binding energy from the XPS spectrum with the standard value for high purity elements and compounds.

Here this technique was used to analyse the uniformity of composition and also the atomic concentration along the depth of the copper selenide thin film. But as little reference is available on the XPS study of various phases of copper selenide, a comparative study of this material was not possible.

A ULVAC–PHI unit (model 5600) employing argon ion sputtering was used for the present XPS analysis. Here Al K_α X-ray (1486.6 eV) with a beam diameter of 0.8 mm and a power of 400 W was used as the incident beam. An argon ion gun with 3 kV voltage was employed for etching.

Fig.(3.18) shows the XPS depth profile of the as-prepared $Cu_{2-x}Se$ thin film. This sample was deposited on SnO_2 substrate. Hence the elements analysed by this technique included tin, oxygen and silicon (Sn, O, and Si) apart from copper and selenium (Cu and Se). In this figure, the two peaks of Cu refer to $2p_{1/2}$ and $2p_{3/2}$, one peak of Se refers to $3d_{5/2}$ and one peak of O refers to 1s electronic spectrum (referred in succession from left to right in the figure). The bottom layer of this figure refers to the surface of the film while the top portion corresponds to the substrate region. The substrate region can also be identified from the presence of Sn and O signal corresponding to SnO_2. This picture reveals the slight diffusion of copper and selenium into the SnO_2 substrate. Each horizontal line of the spectrum refers to signal collected after etching the surface for 1 minute in succession. This $Cu_{2-x}Se$ sample
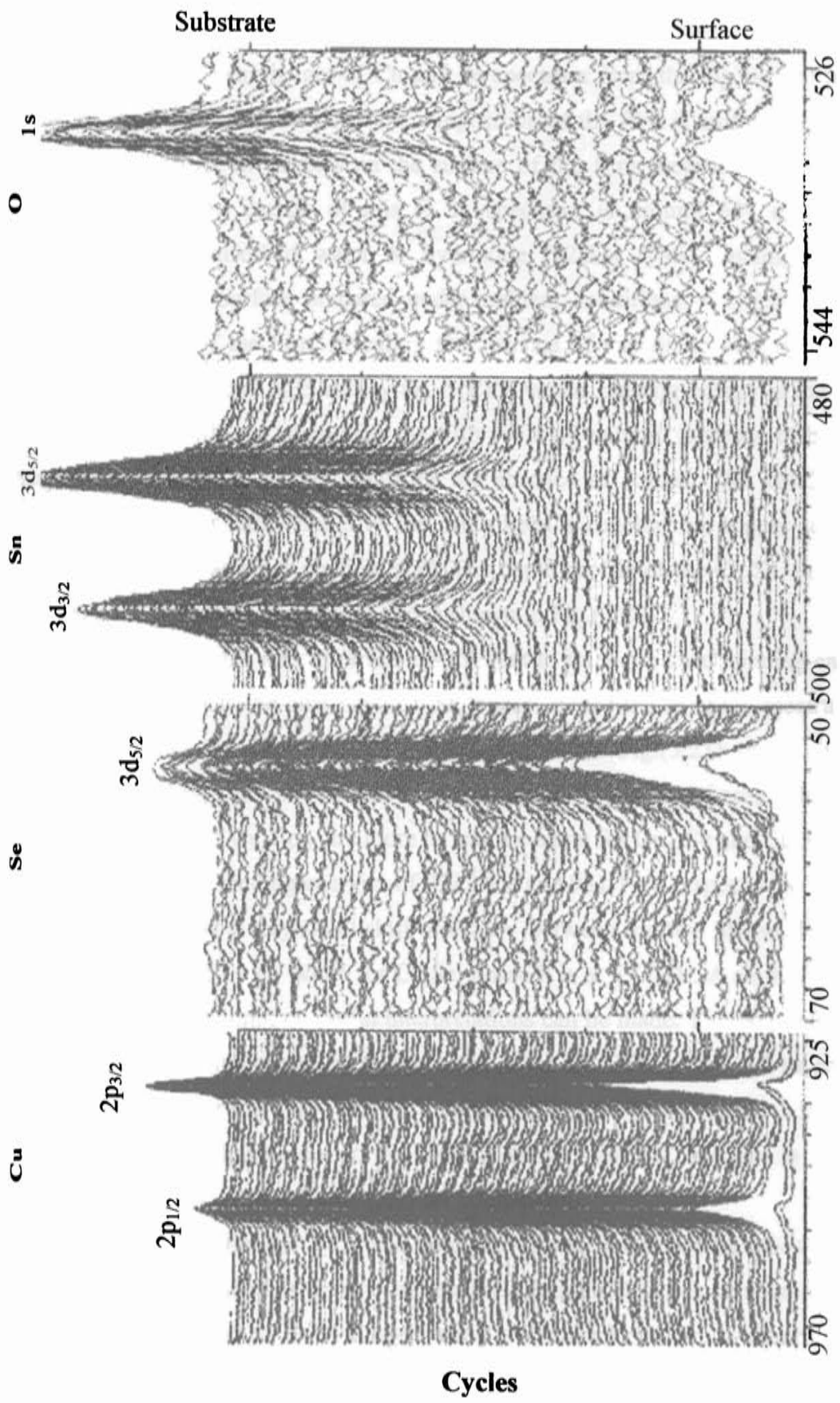
Fig. 3.18 XPS depth profile of as-prepared $Cu_{2-x}Se$ film

was etched for 100 cycles and hence there are 100 horizontal lines for each element in the spectrum.

The constant peak height of Cu and Se spectrum from the top surface to the bottom layer of the film shows that the composition of the film is uniform across its thickness. In the first two cycles on the surface of the film presence of oxygen is obvious. The binding energy of this O 1s spectrum is around 531 eV, which corresponds to chemisorbed water or hydroxide [22,23]. This contamination is unavoidable for any surface prepared under ambient conditions. Oxygen signal is absent in the bulk of the film, revealing the absence of any oxide impurity phase. Fig.(3.19) shows the total XPS survey i.e. N(E)/E versus binding energy in the wide range of 0 eV to 1400 eV taken after the fifth cycle of etching. Absence of binding energy corresponding to oxygen confirms the absence of oxides. This result is of importance as copper oxide impurity has often been a concern for copper selenide films prepared in an aqueous medium [24]. The depth profile of the Cu_3Se_2 thin film has more or less the same appearance and is shown in Fig.(3.20).

This depth profile spectrum was insufficient to trace the exact binding energy of Cu and Se in the $Cu_{2-x}Se$ phase and Cu_3Se_2 phase. Hence the enlarged spectrum of these signals, after the fifth cycle of etching was taken. Fig.(3.21) shows the Cu spectrum while Fig(3.22) shows the Se spectrum for both the phases. The peak positions of Cu 2p and Cu 2 $p_{3/2}$ are more or less the same for $Cu_{2-x}Se$ and Cu_3Se_2, and they are positioned at binding energies of 952.1 eV and 931.1 eV respectively. The Se $3d_{5/2}$ spectrum shows a very small shift of 0.2 eV between the two phases. For $Cu_{2-x}Se$ film it is seen at 53.9 eV while for Cu_3Se_2 phase it is at 53.7 eV. A shift of 0.2 eV being within the error limit, no useful interpretations can be made. The only reference available for the binding energy of this material is for the CuSe phase and its energy values are 952 eV for Cu $2p_{1/2}$, 932.5 eV for Cu $2p_{3/2}$ and 55 eV for Se $3d_{5/2}$ [20]. Kasmerski et al. [25] have reported the binding energies for Cu_xSe phase in general and the values are included in Table (3.7) for comparison.

Atomic concentration of Cu and Se could also be measured by this analysis. But as the response of the instrument was relatively less for Se when compared to Cu, a correction factor had to be evaluated using a standard sample. Standard CuSe powder (Soekawa Chemical) was analysed and the figurative results are tabulated along with the data from the atomic concentration spectra of the present $Cu_{2-x}Se$ and Cu_3Se_2 films, Table (3.8). Fig.(3.23) shows the percentage composition of $Cu_{2-x}Se$
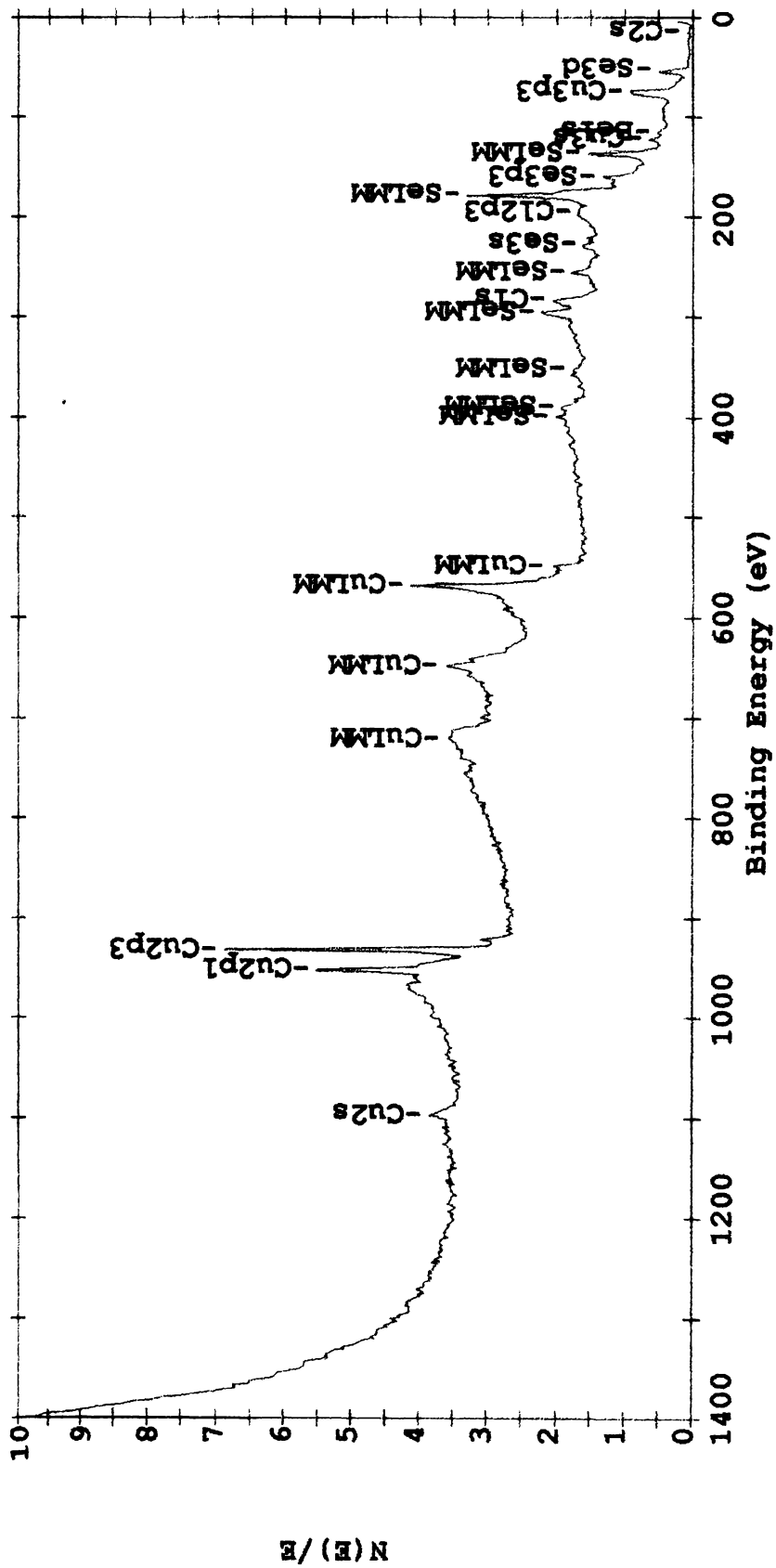
Fig.(3.19) Total XPS survey of as-prepared $Cu_{2-x}Se$ film.
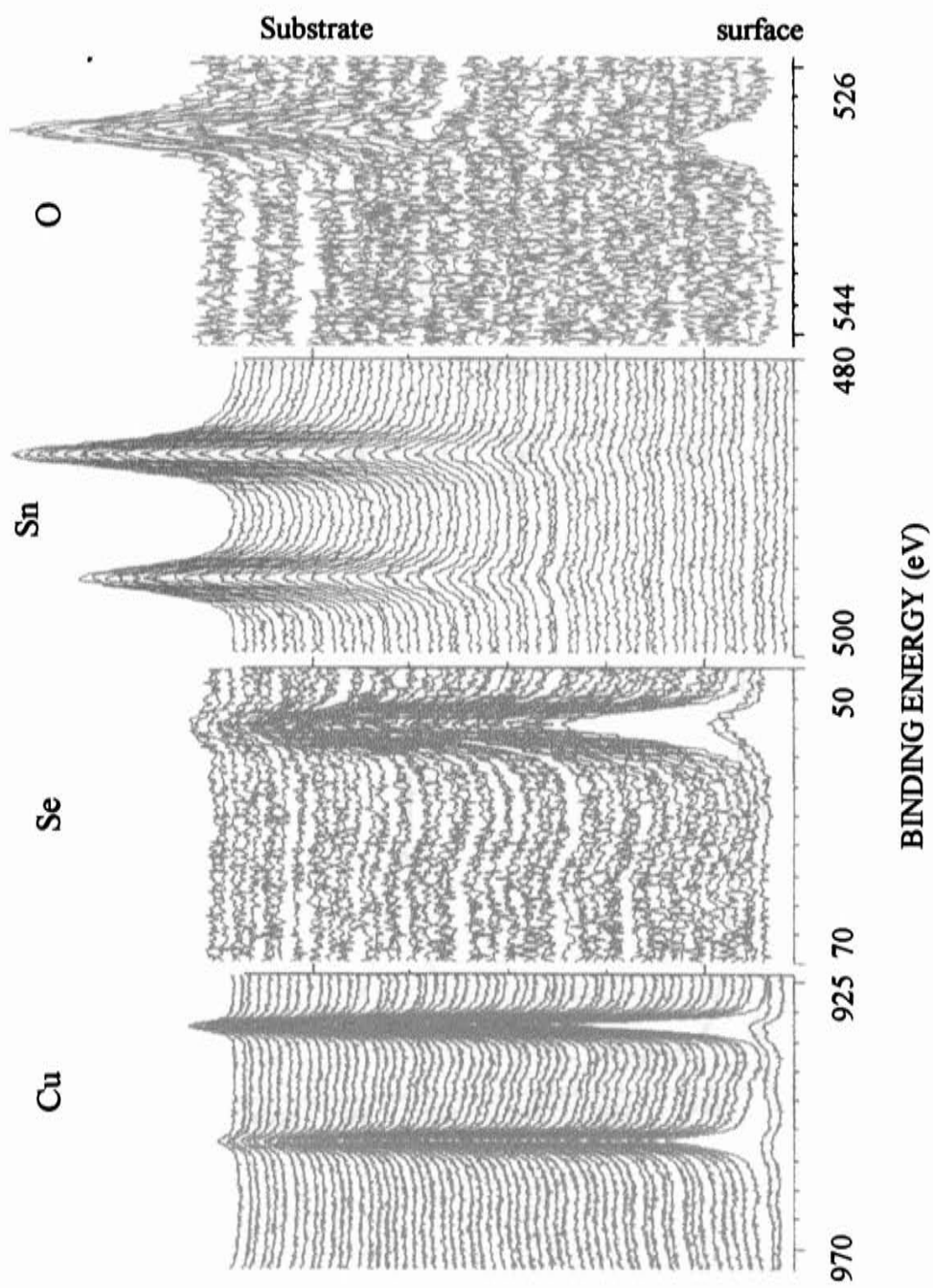
Fig. (3.20) XPS depth profile of as prepared Cu_3Se_2 film
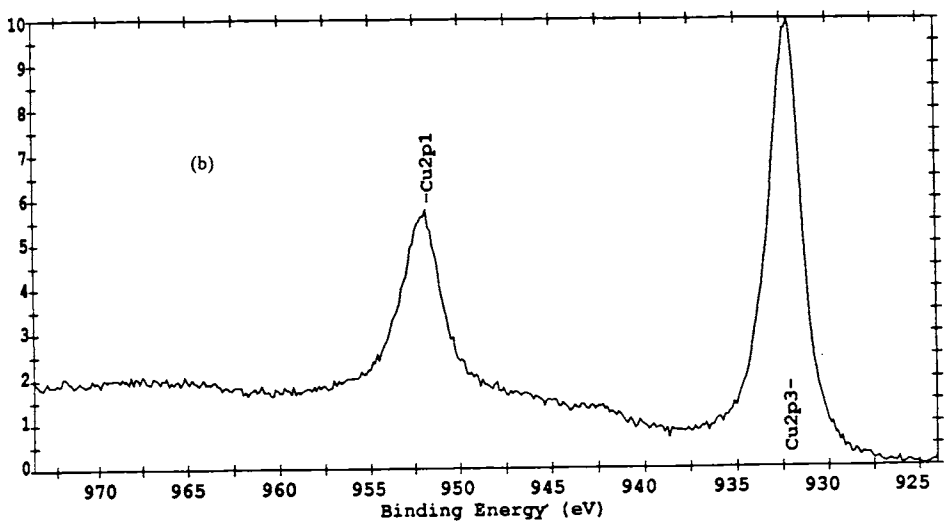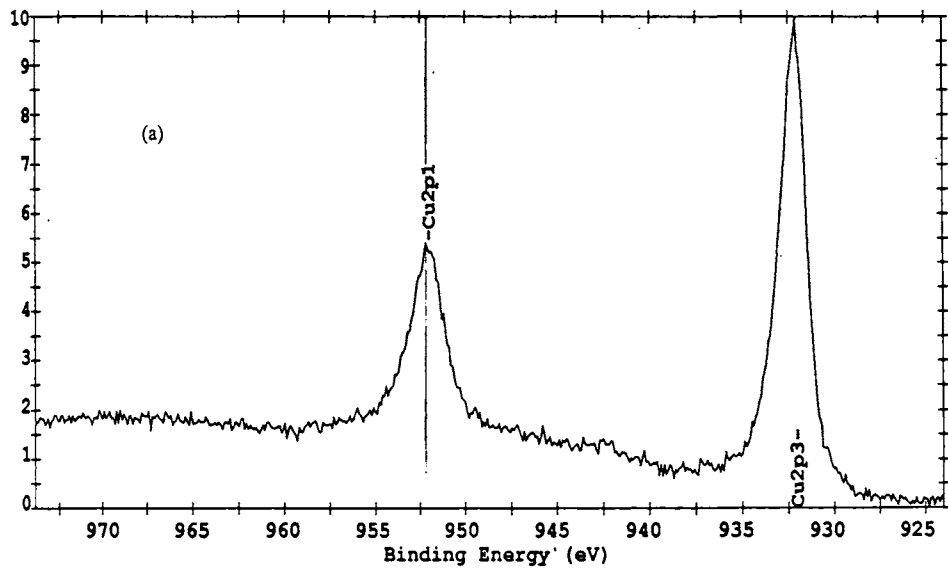
Fig (3.21)   XPS spectrum of copper after the 5th cycle of etching of
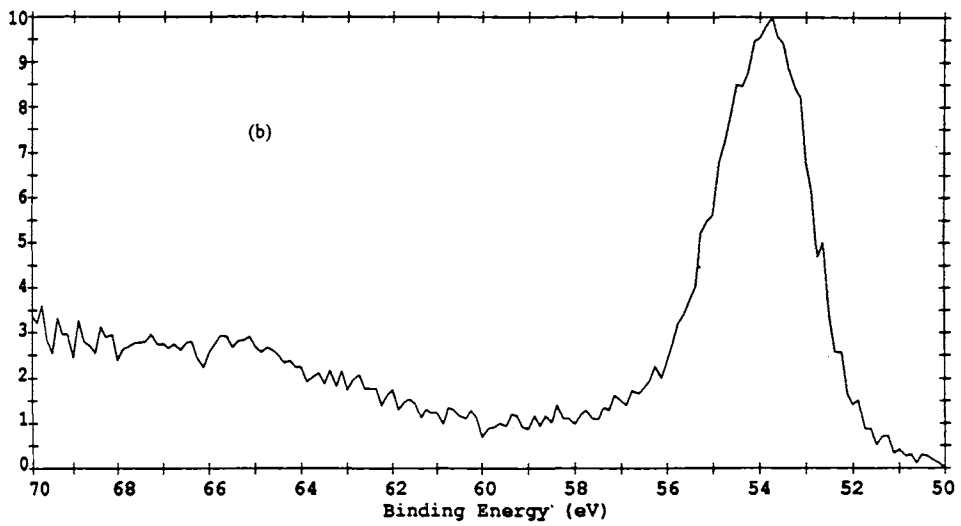
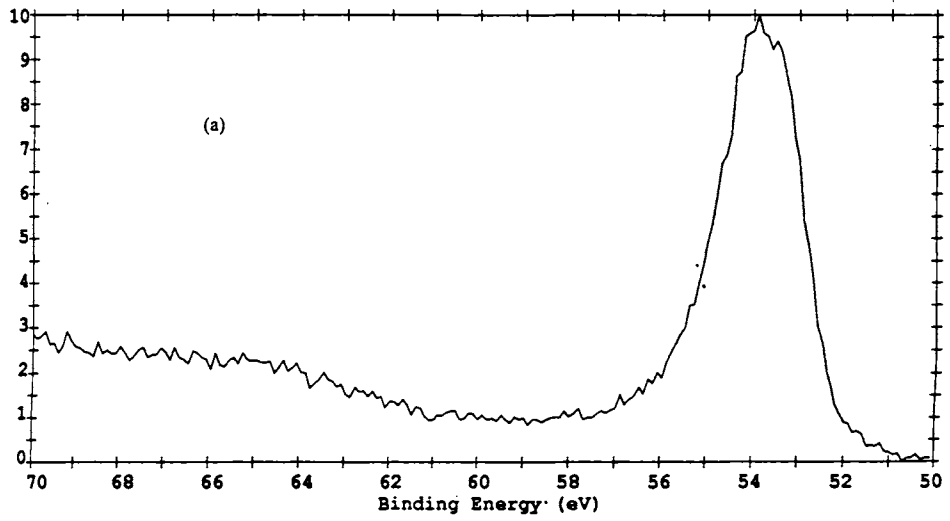(a) $Cu_{2-x}Se$ and (b)Cu_3Se_2 phases.

Fig (3.22)   XPS spectrum of selenium of (a) $Cu_{2-x}Se$ and (b) Cu_3Se_2 phases after the 5th cycle of etching
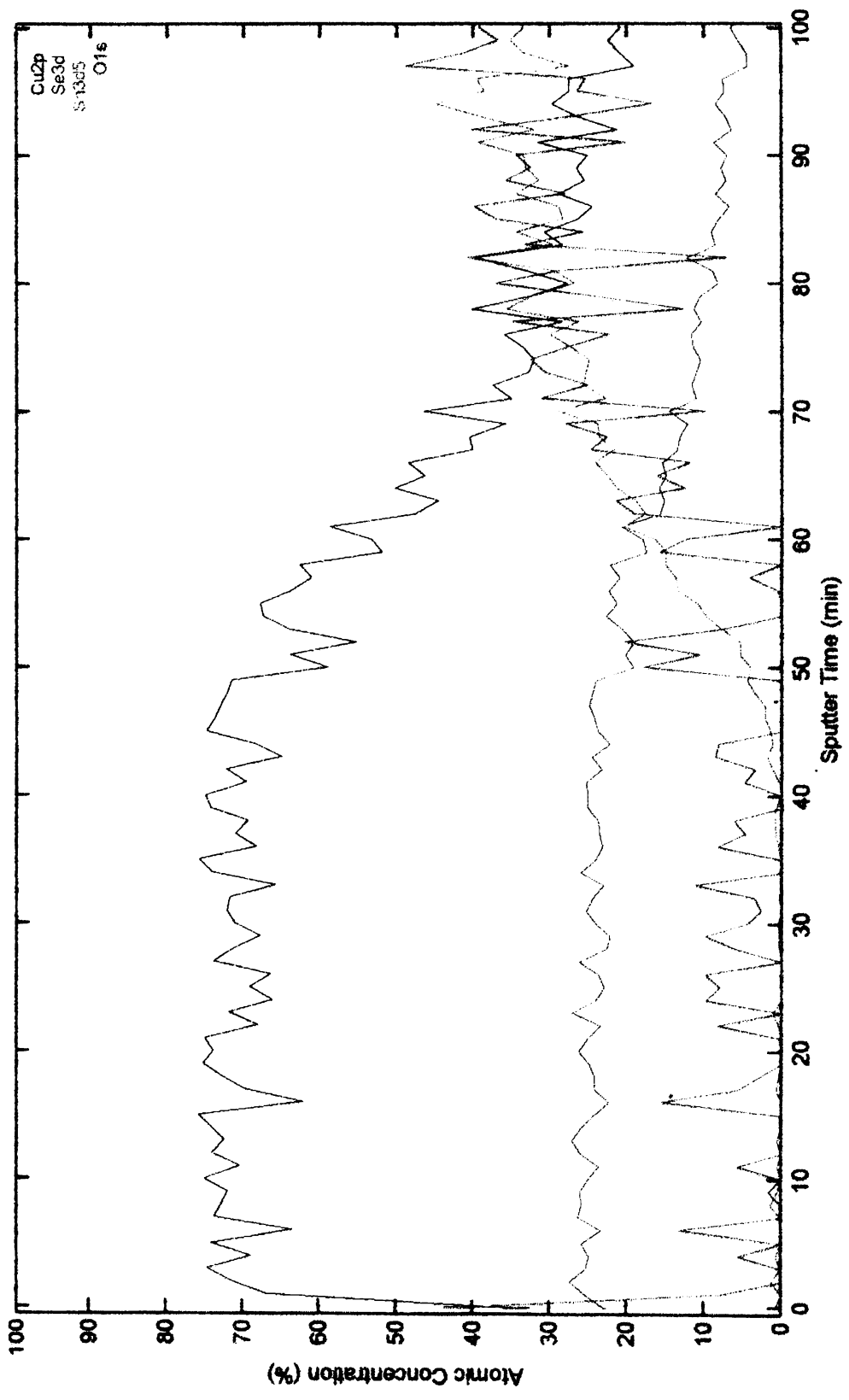
Fig. (3.23)   Percenrage composition graph of Cu₂-ₓSe thin film

phase before applying the correction. From the table it can be seen that the estimated stoichiometry of $Cu_{2-x}Se$ is $Cu_{1.82}Se$ where x = 0.18. Similarly for Cu_3Se_2 phase, the Cu:Se value is estimated to be 1.58:1. This is very close to the expected value of 1.5:1.

	Binding energy (eV)		
	Cu 2p ½	Cu 2p 3/2	Se 3d 5/2
$Cu_{2-x}Se$ (from the present work)	952.1	932.1	53.9
Cu_3Se_2 (from the present work)	952.1	932.1	53.7
Cu_xSe (reported by Kazmerski et al.)	952.1	932.3	54.5
CuSe (standard sample powder-Solekawa chemicals) studied in the same instrument	952	932	54.2

Table (3.7) Binding energy values of Cu and Se in copper selenide

Sample	Element	Area cts -eV/s	Sensitivity factor	Concentration (%)	Uncorrected Cu/Se	Corrected Cu/Se
CuSe standard	Se 3d	3386	14.570	40.62	1.46	1.00
	Cu 2p3	20432	60.150	59.38		
$Cu_{2-x}Se$ (from present work)	Se 3d	3659	14.570	27.28	2.66	1.82
	Cu 2p3	40273	60.150	72.72		
Cu_3Se_2 (from present work)	Se 3d	4053	14.570	30.24	2.31	1.58
	Cu 2p3	38603	60.150	69.76		

Table (3.8) Cu/Se ratio as calculated from XPS analysis

3.5.2 ICP analysis

Inductively coupled plasma (ICP) analysis was performed on copper selenide samples to confirm the stoichiometry. The thin film samples were completely dissolved in conc. HNO_3 for this analysis. The resulting solution was diluted to a very low concentration and it was sprayed as a fine jet into an evacuated high temperature space where it gets converted to plasma state. Then the emission line intensity of each element was quantitatively measured and was fitted on to a standard graph. The

standard graph is drawn separately for Cu and Se by measuring the emission counts of a solution containing known concentration of these elements at various dilution. In the present case standard solutions of $CuSO_4$ and Na_2SeSO_3 were used. Making use of this standard graph, copper to selenium ratio in the sample solution was calculated depending on the corresponding emission intensity.

$Cu_{2-x}Se$ thin films showed Cu:Se ratio to be around 1.80:1, while for Cu_3Se_2 film this ratio was around 1.54:1. These values support the expected proportion of Cu and Se in the two as-prepared phases. This is in agreement with the XPS results.

3.5.3 XRD analysis

The inter planar spacing (d) of the (022) plane of the cubic phase of copper selenide has a linear dependence on the stoichiometry of this compound as shown in Fig.(3.24). This inter dependence has been used by many researchers to evaluate the value of non-stoichiometric index 'x' in the $Cu_{2-x}Se$ phase [10, 26].

In the present study also, this linear dependence of d value on 'x' has been used to understand the effect of variation in the relative concentration of Cu in the thin film deposition bath. XRD spectrum of films from Bath 1:1, Bath 2:1, Bath 3:1 and Bath 5:1 were taken with special emphasis on the 2θ region 42^0 to 47^0. Corresponding to the peak position of the (022) plane, d values were noted from the spectrum. Fig.(3.25) shows the selected area view of graph in Fig.(3.24) where the experimental d values fit in.

Table (3.9) shows these experimental d values tabulated against Cu/Se ratio as obtained from Fig.(3.25). Corresponding to the slight increase in d value from Bath 1:1 to Bath 5:1 in succession, there is a slight increase in the Cu/Se value there by resulting in corresponding decrease in the 'x' value of the $Cu_{2-x}Se$ phase. The corresponding 'x' value and resulting chemical formula is also included in the table. Though these results vary slightly from the XPS and ICP analysis, the general trend shown by this indirect method of compositional analysis can be accepted.

An important inference from these results is that, it is possible to influence the stoichiometry of $Cu_{2-x}Se$ phase to a small extent by changing the relative concentration of Cu and Se in the reaction bath.

Deposition bath	d values	Cu/Se value	'x' value	Chemical formula
Bath 1:1	2.030	1.7145	0.29	$Cu_{1.71}Se$
Bath 2:1	2.0311	1.7302	0.27	$Cu_{1.73}Se$
Bath 3:1	2.0322	1.7429	0.26	$Cu_{1.74}Se$
Bath 5:1	2.0365	1.8026	0.19	$Cu_{1.81}Se$

Table (3.9)   Variation of stoichiometry of $Cu_{2-x}Se$ film with relative concentration of Cu in the reaction bath as obtained from Fig. (3.25)

To understand the influence of temperature of deposition on stoichiometry, the d values of the film from Bath 1:1 and Bath 1:1 LT were compared by fitting into the standard graph of Fig (3.24) as in the above case. Fig.(3.26) shows the experimental d values fitted on to the standard graph. The results are tabulated in Table (3.10).

Deposition bath	d values	Cu/Se value	'x' value	Chemical formula
Bath 1:1	2.0300	0.7145	0.29	$Cu_{1.71}Se$
Bath 1:1 LT	2.0257	0.6534	0.35	$Cu_{1.65}Se$

Table (3.10) Variation of stoichiometry of $Cu_{2-x}Se$ film with temperature of deposition as obtained from Fig. (3.26)

From this observation it can be inferred that if the copper selenide deposition is carried out at low temperature, the incorporation of selenium into the deposited thin film can be enhanced. In the present case, the deposited phase shifts from the chemical formula $Cu_{1.71}Se$ to $Cu_{1.65}Se$. This forms the first report of a novel and simple method to improve the selenium content in selenide films deposited using CBD technique.

3.6 Electrical characterisation

3.6.1 Hall measurements

Hall measurements along with resistivity measurements were done on $Cu_{2-x}Se$ and Cu_3Se_2 films and the present work forms the first detailed report of the kind. This study helped to understand the conduction mechanism of copper selenides to a great extent. Variation in resistivity with temperature could be understood in terms of carrier density and mobility. The influence of variation in copper concentration in the
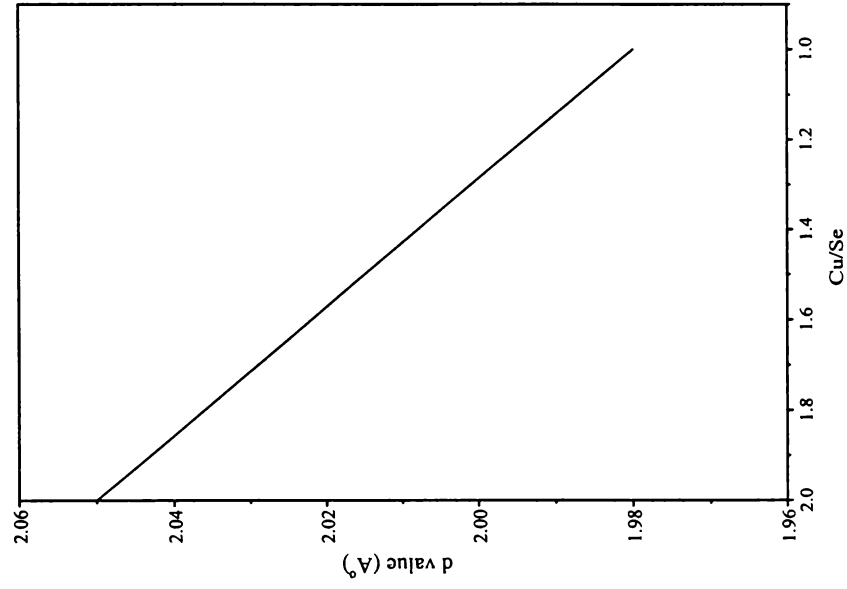
Fig.(3.24) Linear dependence of interplanar spacing (d) of the XRD peak of (022) plane on the stoichiometry of Cu₂₋ₓSe phase
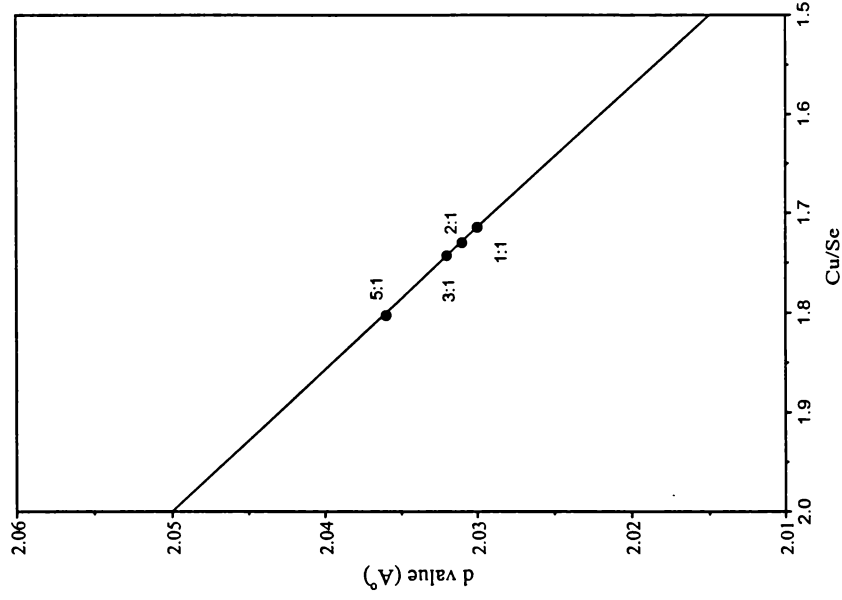
Fig.(3.25) Variation in the stoichiometry of Cu₂₋ₓSe phase with relative Cu to thiosulphate bath
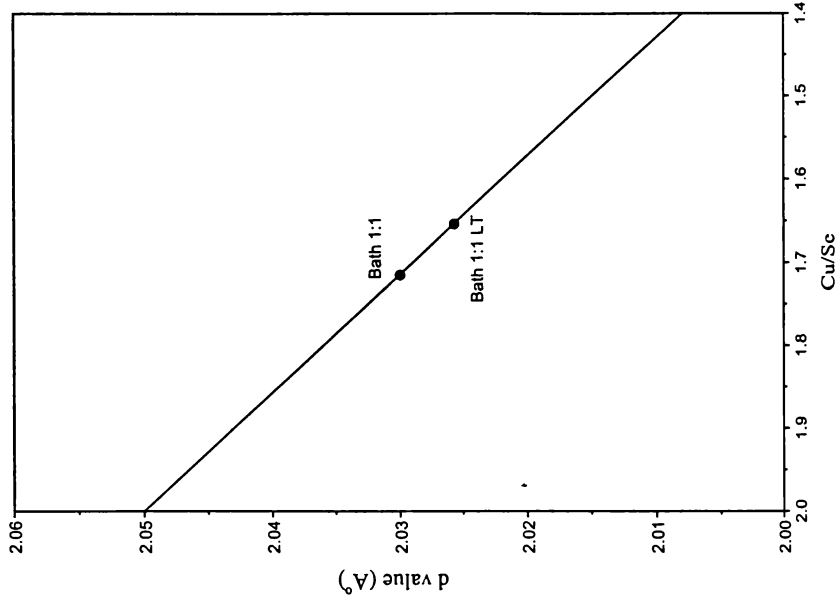
Fig.(3.26) Variation in the stoichiometry of Cu₂₋ₓSe phase with temp of deposition

reaction bath on the resistivity of the as-prepared films was noted from this study. The effect of temperature of deposition on the carrier density and mobility was also studied.

After loading the sample of 1sq.cm area on the sample holder with thermal grease and then evacuating the enclosure, linearity check was done to confirm the uniformity and ohmic behaviour of the contact. Resistivity of the sample was measured by Vander Pauw method. Hall effect measurements were carried out to determine the mobility, density of carriers, Hall coefficient and type of carriers.

For analysing the Hall measurement data in detail, here the following points are considered:

1. Copper selenide is a defect semiconductor showing extrinsic behaviour in the temperature range -192^{0}C to 700^{0}C depending on the extent of non-stoichiometry [27]. Here copper vacancies act as acceptors [28]. Hence all forms of copper selenide have p-type conductivity where the concentration of holes depends on the copper deficiency [29].

2. Effect of copper vacancy should be understood in relation to superlattice crystal structure of cubic $Cu_{2-x}Se$ phase [30]. A model of this is shown in Fig.(3.28). This consists of an immobile sublattice of cubic cage structure (constituted by four Se ions and four Cu ions) and a disordered mobile cation subsystem formed by the remaining Cu ions statistically distributed over the cage interstitial sites.

3. Copper vacancy scattering is the major factor that determines the mobility and hence resistivity of the material.

4. Carrier scattering by grain boundaries in the film will only cause relatively little reduction in mobility when compared to the decrease in mobility due to copper vacancy scattering [28].

5. The carrier concentration of copper selenide phase is always in the order of 10^{20}-10^{22}cm^{-3}. Such high values make this material a degenerate semiconductor, or in other words this is equivalent to a highly doped semiconductor. Hence mobility is generally found to have inverse proportionality with carrier concentration.

```
d a c b  d a c b  d a c b  d a c b  d a
```
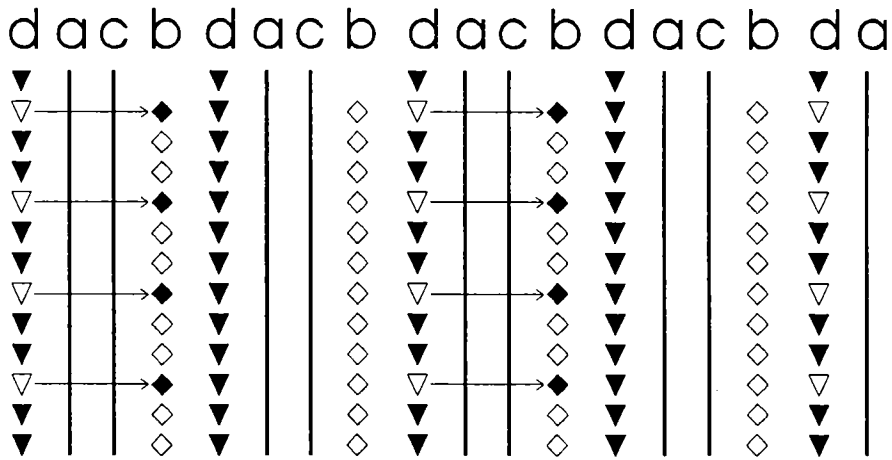
Fig.(3.27)   Structure of $Cu_{2-x}Se$

Stacking sequence of the planes along the b super lattice axis ($[111]_{fcc}$ direction). Immobile planes are a and c (a – Se cage plane and c – Cu cage plane). Mobile planes of Cu are b and d (b – terahedrally coordinated d – octahedrally coordinated). Here the arrows indicate pairing between tetrahedral vacancy and octahedral ions.

a) Comparison of as-prepared $Cu_{2-x}Se$ and Cu_3Se_2 phases: [Table (3.11)]

Holes are the majority carriers in both $Cu_{2-x}Se$ and Cu_3Se_2 phases. As-prepared $Cu_{2-x}Se$ film is found to be low resistive. Resistivity is around $8\times10^{-4}\ \Omega$cm and it agrees with the earlier reported values [4, 31]. Cubic phase of $Cu_{2-x}Se$ is usually reported as a superionic conductor where ionic conductivity varies with the non-stoichiometry index 'x', Fig (3.28) [32]. In the present case as the 'x' value is evaluated to be around 0.18 [section 3.5.1], the contribution from ionic conductivity will be very low. According to the above reference, for x ~ 0.18 the contribution of ionic conductivity at room temperature will be only around $1\times10^{-2}\ \Omega^{-1}cm^{-1}$, while the net observed conductivity in the present case is in the order of $1\times10^{3}\ \Omega^{-1}cm^{-1}$. This indicates that the ionic contribution to the conductivity of the as-prepared phase is negligible [27].

The resistivity of the as-prepared $Cu_{2-x}Se$ film is found to be less by an order when compared to that of Cu_3Se_2 film which is around $6\times10^{-3}\ \Omega$cm. The carrier concentration is found to be ~ $5\times10^{20}\ cm^{-3}$ in both the phases at room temperature but there is difference in resistivity. The increase in resistivity of Cu_3Se_2 is the result of

very low carrier mobility. Hall coefficient of both phases is in the order of $1 \times 10^{-2} \, cm^3 C^{-1}$.

	$Cu_{2-x}Se$	Cu_3Se_2
Resistivity (Ω-cm)	8.0×10^{-4}	6.6×10^{-3}
Mobility (cm^2/Vs)	1.5×10^1	1.7
Carrier density (cm^{-3})	5.2×10^{20}	5.6×10^{20}
Hall coefficient (cm^3/C)	1.2×10^{-2}	1.1×10^{-2}
Sheet resistance (Ω/cm^2)	8	6.6×10^1
Type of carriers	Hole	Hole

Table (3.11)   Comparison of Hall parameters of $Cu_{2-x}Se$ and Cu_3Se phases

b) *Effect of variation in copper concentration in the reaction bath*: [Table (3.12)]

In order to understand the role of relative concentration of Cu and Se in the reaction bath, Hall measurements were done on films prepared at various concentrations of Cu for a fixed concentration of 0.2 M Se. The results of films from Bath 1:1, Bath 2:1, Bath 3:1 and Bath 5:1 are tabulated in Table (3.12).

Bath 1:1 film is found to have very low resistance when compared to the rest. This may be due to the fact that there can be large deviation for this film from the stoichiometric form Cu_2Se. The decrease in resistivity with increase in the value of x has been reported by other researchers also, Fig.(3.29) [28, 33]. In films from Bath 2:1, Bath 3:1 and Bath 5:1, it is seen that the resistivity is higher by an order when compared with Bath 1:1 films. But the order of resistivity of films from Bath 2:1, Bath 3:1 and Bath 5:1 is almost same. This depicts the saturation of 'x' at a stable value with the increase in concentration of the copper in reaction mixture.

XRD studies of section (3.3.1) and SEM studies of section (3.2.3) have revealed the decrease in grain size of the $Cu_{2-x}Se$ film with the increase in copper concentration in the reaction bath. Diffused grain boundaries and smaller grain size increases the grain boundary scattering of the majority carriers. This may also contribute to the decrease in the mobility and increase in resistivity with increase in copper ion concentration in the reaction bath of $Cu_{2-x}Se$ film.
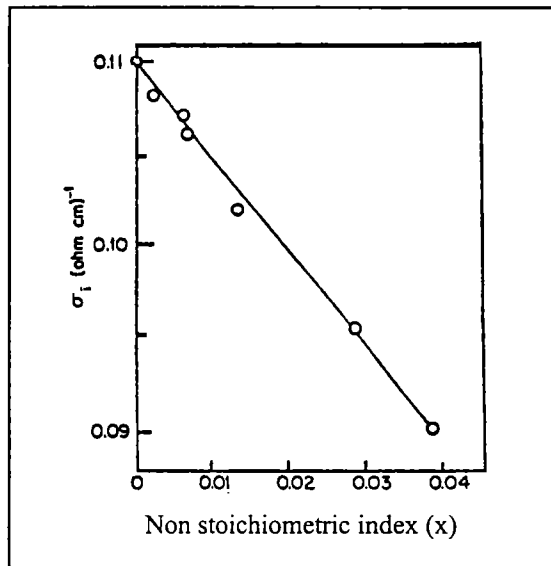
Fig.(3.28)   Ionic conductivity of $Cu_{2-x}Se$ phase at 150^0C
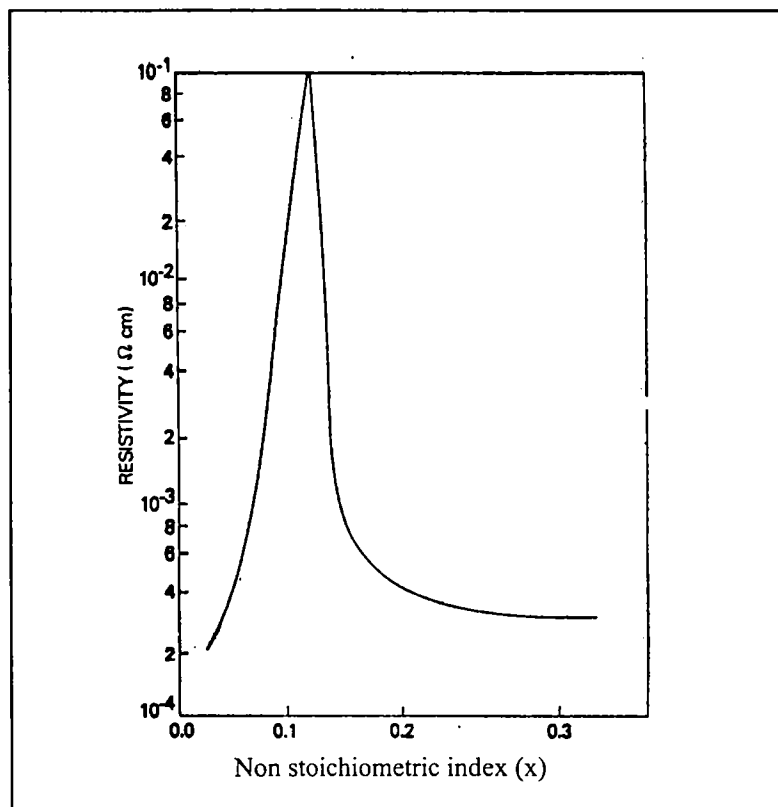as a function of non-stoichiometric index 'x'

Fig.(3.29)   Graph showing decrease in resistivity of $Cu_{2-x}Se$ phase
with increase in the non-stoichiometric index 'x'.

	Bath 1:1	Bath 2:1	Bath 3:1	Bath 5:1
Resistivity (Ω-cm)	8×10^{-4}	1.6×10^{-3}	1.7×10^{-3}	2.4×10^{-3}
Mobility (cm²/ Vs)	1.5×10^{1}	6.1	5	3.5
Carrier density (cm⁻³)	5.2×10^{20}	6.4×10^{20}	7.2×10^{20}	7.3×10^{20}
Hall coefficient (cm³/ C)	1.2×10^{-2}	9.7×10^{-3}	8.7×10^{-3}	8.5×10^{-3}
Sheet resistance (Ω/ cm²)	8	1.6×10^{1}	1.7×10^{1}	2.4×10^{1}
Type of carriers	Holes	Holes	Holes	Holes

Table (3.12)   Effect of variation of copper concentration in the reaction
mixture on the Hall parameters of $Cu_{2-x}Se$ film

c) Effect of temperature (300 K- 400 K) on $Cu_{2-x}Se$ film: [Table (3.13)]

In order to understand the effect of temperature on electrical properties of $Cu_{2-x}Se$ phase, Hall measurements were conducted in the temperature range 300 K- 400 K. To confirm the results, this study was carried out in films from Bath 1:1, Bath 2:1 and Bath 3:1. All of them showed the same trend with regard to resistivity and related parameters. Resistivity is found to increase slightly with temperature, unexpected of ordinary semiconductors. This is due to the decrease in mobility, which predominates the effect of increase in carrier density as observed from the table. This effect is more pronounced in films prepared from Bath 1:1. This may be due to the large deviation from the stoichiometric form of Cu_2Se.

This metallic behaviour of decrease in mobility with increase in temperature can be explained as follows: When temperature increases more and more copper ions diffuse from the immobile cage structure into the mobile sublattice. The resulting increase in copper vacancy in the immobile subsystem leads to the decrease in mobility of holes.

For the same range of temperature, Hall coefficient is found to vary from 10^{-2} to 10^{-4} cm³C⁻¹ in Bath 1:1 films and from 10^{-2} to 10^{-3} cm³C⁻¹ in Bath 2:1 films. In the case of Bath 5:1 films, this variation is less pronounced. From these observations, it can be inferred that the influence of temperature on carrier density is less pronounced in film having better stoichiometry. All these films invariably show p- type conduction in this temperature range.

Bath 1:1			
	300 K	350 K	400 K
Resistivity (Ω-cm)	8×10^{-4}	9.1×10^{-4}	9.9×10^{-4}
Mobility (cm^2/ Vs)	1.5×10^{1}	1.3	9.7×10^{-1}
Carrier density (cm^{-3})	5.2×10^{20}	5.3×10^{21}	6.5×10^{21}
Hall coefficient (cm^3/ C)	1.2×10^{-2}	1.2×10^{-3}	9.6×10^{-4}
Sheet resistance (Ω/ cm^2)	8	9.1	9.9
Type of carriers	Hole	Hole	Hole

Bath 2:1			
	300 K	350 K	400 K
Resistivity (Ω-cm)	1.6×10^{-3}	2.1×10^{-3}	2.3×10^{-3}
Mobility (cm^2/ Vs)	6.1	2.7	2.3
Carrier density (cm^{-3})	6.4×10^{20}	1.1×10^{21}	1.2×10^{21}
Hall coefficient (cm^3/ C)	9.7×10^{-3}	5.6×10^{-3}	5.2×10^{-3}
Sheet resistance (Ω/ cm^2)	1.6×10^{1}	2.1×10^{1}	2.3×10^{1}
Type of carriers	Hole	Hole	Hole

Bath 3:1			
	300 K	350 K	400 K
Resistivity (Ω-cm)	1.7×10^{-3}	1.8×10^{-3}	1.9×10^{-3}
Mobility (cm^2/ Vs)	5	3.9	1.4
Carrier density (cm^{-3})	7.2×10^{20}	8.8×10^{20}	2.3×10^{21}
Hall coefficient (cm^3/ C)	8.7×10^{-3}	7.1×10^{-3}	2.7×10^{-3}
Sheet resistance (Ω/ cm^2)	1.7×10^{1}	1.8×10^{1}	1.9×10^{1}
Type of carriers	Hole	Hole	Hole

Table (3.13) Effect of temperature on Hall parameters of $Cu_{2-x}Se$ films

d) Effect of temperature on the deposition of Cu$_{2-x}$ Se film: [Table (3.14)]

Hall parameters of film deposited at low temperature (Bath 1:1 LT) was compared with the film deposited at room temperature (Bath 1:1). This revealed the

influence of deposition temperature on electrical properties of the film. It is found that resistivity becomes almost half when deposition is carried out at low temperature. This is due to the fact that at low temperature, film deposition proceeds in a more ordered manner resulting in better crystallinity and improved mobility. Hence due to increase in mobility, sheet resistance is seen to decrease from 8 Ωcm^{-2} to 4.5 Ωcm^{-2}.

	Room temperature	Low temperature
Resistivity (Ω-cm)	8.0×10^{-4}	4.5×10^{-4}
Mobility (cm^2/ Vs)	1.5×10^{1}	4.3×10^{1}
Carrier density (cm^{-3})	5.2×10^{20}	3.2×10^{20}
Hall coefficient (cm^3/ C)	1.2×10^{-2}	1.9×10^{-2}
Sheet resistance (Ω/ cm^2)	8	4.5
Type of carriers	Hole	Hole

Table: (3.14) Effect of temperature of deposition on the Hall parameters of $Cu_{2-x}Se$ film

e) Effect of temperature (300 K- 400 K) on Cu_3Se_2 films: - [Table (3.15)]

In the range of temperature 300 K to 400 K Cu_3Se_2 films are found to behave in a different manner when compared to $Cu_{2-x}Se$ films. Resistivity of Cu_3Se_2 phase is found to decrease with temperature, similar to the general behaviour of semiconductors.

On heating Cu_3Se_2 phase disproportionates into $Cu_{2-x}Se$ and Se (refer section 4.2.2.2). A cation vacancy or an anion presence can contribute to hole concentration and so the presence of Se is equivalent to two holes [27]. Hence carrier concentration increases as observed in Table (3.15). Here inspite of increase in carrier concentration an increase in mobility is observed. The sheet resistance is found to decrease from 66 Ω cm^{-2} to 9.5 Ωcm^{-2} in the temperature range 300 K to 400 K. Corresponding to the increase in carrier density the Hall coefficient is found to decrease from 10^{-2} to 10^{-3} order.

	300 K	350 K	400 K
Resistivity (Ω-cm)	6.6×10^{-3}	1.5×10^{-3}	9.5×10^{-4}
Mobility (cm^2/Vs)	1.7	5.5	6
Carrier density (cm^{-3})	5.6×10^{20}	7.4×10^{20}	1.1×10^{21}
Hall coefficient (cm^3/C)	1.1×10^{-2}	8.4×10^{-3}	5.6×10^{-3}
Sheet resistance (Ω/cm^2)	6.6×10^1	1.5×10^1	9.5
Type of carriers	Hole	Hole	Hole

Table (3.15)   Effect of temperature on Hall parameters of Cu_3Se_2 film

3.7 Conclusion

$Cu_{2-x}Se$ films deposited from Bath 1:1 were found to be most uniform and it was considered as the representative sample of this phase. Cu_3Se_2 films deposited from Bath 1:1 Na were chosen as the representative sample of this phase. $Cu_{2-x}Se$ phase had a reddish brown colour while Cu_3Se_2 had a bluish green colour.

SEM analysis helped to understand the film morphology of these films. XRD analysis confirmed the formation of the two different phases of copper selenide. Optical absorption studies showed the band gap of $Cu_{2-x}Se$ phase and Cu_3Se_2 phase to be 2.2 eV and 2.8 eV respectively. Variation in band edge with the increase in thickness of the film was also studied.

XPS analysis helped to evaluate the percentage composition. The chemical formula suggested for the two phases was $Cu_{1.8}Se$ and $Cu_{3.1}Se_2$. ICP analysis supported these results. Hall measurement studies showed both the phases to be of low resistance. Cu_3Se_2 phase was found to be comparatively more resistive than $Cu_{2-x}Se$ phase. The carrier density was generally high and the carrier mobility low for both the phases. With increase in copper ion concentration in the reaction bath of $Cu_{2-x}Se$ phase, decrease in mobility of the carriers and hence increase in resistivity was observed. In the case of $Cu_{2-x}Se$, resistivity increased with temperature while in the case of Cu_3Se_2 resistivity decreased with temperature. Carrier mobility was found to increase in the $Cu_{2-x}Se$ film when the deposition was carried out at low temperatures.

Reference

[1]   V. M. Garcia, P. K. Nair and M. T. S. Nair, *J. Crystal Growth*, 203 (1999) 113.

[2]   H. Okimura, T. Matsumae and R. Makabe, *Thin Solid Films*, 71 (1980) 53.

[3]   J. W. Mellor, *A Comprehensive Treatise on Inorganic and Theoretical Chemistry*, Vol. X, Longmans.

[4]   S. K. Haram and K. S. V. Santhanam, *Thin Solid Films*, 238 (1994) 21.

[5]   A. Tonejc and A. M. Tonejc, *J. Solid State Chem.*, 39 (1981) 259.

[6]   R. M. Murray and R. D. Heyding, *Can. J. Chem.*, 53 (1975) 878.

[7]   V. Horvatic, Z. Vucic and O. Milat, *J. Phys. C: Solid State Phys.*, 15 (1982) L 957.

[8]   Z. Vucic, V. Horvatic and O. Milat, *Solid State Ionics*, 13 (1984) 127.

[9]   J. Gladic, O. Mitat, Z. Vucic and V. Horvatic, *J. Solid State Chem.*, 91 (1991) 213.

[10]   A. Tonejc, *J. Mater. Sci.*, 15 (1980) 3090.

[11]   G. K. Padam and S. K. Gupta, *J. Phys. D; Appl. Phys.*, 28 (1995) 783.

[12]   I. Grozdanov, *Semicond. Sci. Technol.*, 9 (1994) 1234.

[13]   I. Grozdanov, *Synthetic Metals*, 63 (1994) 213.

[14]   R. A. Smith, *Semiconductors*, 2nd Edition, Academic Publishers (1989).

[15]   A. M. Hermann and L. Fabick, *J. Crystal Growth*, 61 (1983) 658.

[16]   M. Lakshmi, K. Bindu, S. Bini, K. P. Vijayakumar, K. C. Sudha, T. Abe and Y. Kashiwaba, *Thin Solid Films*, 370 (2000) 89.

[17]   M. Lakshmi, K. Bindu, S. Bini, K. P. Vijayakumar, K. C. Sudha, T. Abe and Y. Kashiwaba, *Thin Solid Films*, 386 (2001) 127.

[18]   S. Gorer and G. Hodes, *J. Phys. Chem.*, 98 (1994) 5338.

[19]   M. A. Malik, P. O' Brien and N. Revaprasadu, *Adv. Mater.*, 11 (1999) 1441.

[20]   C. A. Estrada, P. K. Nair, M. T. S. Nair, R. A. Zingaro and E. A. Meyers, *J. Electrochem. Soc.*, 141 (1994) 802.

[21]   A. Levasseur, P. Vinatier and D. Gonbeau, *Bull. Mater. Sci.*, 22 (1999) 607.

[22]   C. Liu, C. Pettenkofer and H. Tributsch, *Surface Sci.*, 204 (1988) 537.

[23]   A. N. Buckley and R. Woods, *Appl. Surface Sci.*, 27 (1987) 437.

[24]   S. K. Haram, K. S. V. Santhanam, M. Neumann-Spallart and C. Levy Clement, *Mater. Res. Bull.*, 27 (1992) 1185.

[25]   L. L. Kazmerski, O. Jamjoum, P. J. Ireland and S. K. Ded, *J. Vac. Sci. Technol.*, 19 (1981) 467.

[26] R. B. Shafizade, I. V. Ivanova and M. M. Kazinets, *Thin Solid Films*, 55 (1978) 211.

[27] Z. Ogorelec and B. Celustka, *J. Phys. Chem. Solids*, 30 (1969) 149.

[28] S. G. Ellis, *J. Appl. Phys.*, 38 (1967) 2906.

[29] B. Celustka and Z. Ogorelec, *J. Phys. Chem. Solids*, 27 (1966) 957.

[30] Z. Vucic, O. Milat, V. Horvatic and Z. Ogorelec, *Phys. Rev. B*, 24 (1981) 5398.

[31] T. Saitoh, S. Matsubara and S. Minagawa, *Jpn. J. Appl. Phys.*, 16 (1977) 807.

[32] T. Takahashi, O. Yamamoto, F. Matsuyama and Y. Noda, *J. Solid State Chem.*, 16 (1976) 35.

[33] W. S. Chen, J. M. Stewart and R. A. Mickelsen, *Appl. Phys. Lett.*, 46 (1985) 1095.

CHAPTER 4

Interphase conversion of $Cu_{2-x}Se$ and Cu_3Se_2 thin films

4.1 Introduction to phase conversions in copper selenide

4.2 Interphase transformation of as-prepared $Cu_{2-x}Se$ and Cu_3Se_2 phases

    4.2.1 Transformation of $Cu_{2-x}Se$ phase to Cu_3Se_2 phase

        4.2.1.1 Characterisation

            i) SEM analysis

            ii) XRD analysis

            iii) Optical studies

            iv) XPS analysis

            v) Hall measurements

        4.2.1.2 Theory behind the transformation

    4.2.2 Transformation of Cu_3Se_2 phase to $Cu_{2-x}Se$ phase

        4.2.2.1 Characterisation

            i) SEM analysis

            ii) XRD analysis

            iii) Optical studies

            iv) Hall measurements

        4.2.2.2 Theory behind the transformation

    4.2.3 Cyclic nature of the interphase transformation

    4.2.4 Prevention of interphase transformation

4.3 Growth of excrescence in $Cu_{2-x}Se$ phase

4.4 Effect of annealing on $Cu_{2-x}Se$ phase

4.5 Conclusion

Reference

4.1 Introduction to phase conversions in copper selenide

a) $Cu_{2-x}Se$ phase

Phase transition in $Cu_{2-x}Se$ is very complicated. Controversy regarding this starts from its nomenclature of "high temperature phase" and "low temperature phase". While many call the high temperature phase as α and the low temperature phase as β [1-4], others have used the same notation in opposite meaning [5-8]. In order to avoid this confusion, this notation has been avoided in the present work as far as possible.

Two main points of disagreement regarding $Cu_{2-x}Se$ are (i) structure of its low temperature phase and (ii) temperature of transition of low temperature phase to high temperature phase. It is interesting to note that, while majority of the reports assign monoclinic structure for the low temperature phase [9-10] proposal of orthorhombic structure [11], tetrahedral structure and hexagonal structure [2, 10, 12] are not uncommon. Santosh *et al.* [13] attributed these crystallographic structural variations of low temperature phase to the method of preparation of the compound. Whatever be the low temperature phase, it is well accepted that the high temperature phase is always cubic.
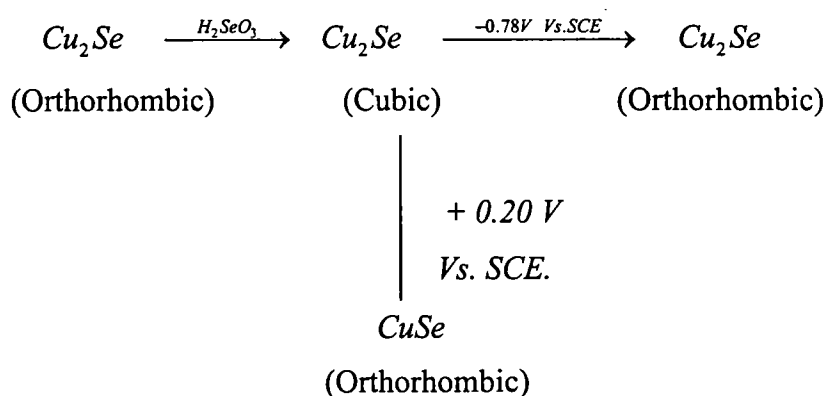
The perfect stoichiometric form of $Cu_{2-x}Se$ (viz. Cu_2Se were $x = 0$) rarely exists [1]. Hence in most of the reports, though the phase is mentioned as Cu_2Se they deal with $Cu_{2-x}Se$. In the present work also $Cu_{2-x}Se$ phase is considered and Cu_2Se is thought of as a special case of $x = 0$. The cubic $Cu_{2-x}Se$ has a very narrow range of homogeneity at room temperature centered at $Cu_{1.8}Se$ [5]. It is stated that low temperature phase exists as a single phase, only if the constitution is about $Cu_{1.997}Se$ [7]. So also, when $x > 0.2$, the cubic phase co-exists with Cu_3Se_2 and when $x < 0.15$ the cubic phase co-exists with the $Cu_{2-x}Se$ orthorhombic form [14].

Transition of the low temperature phase of $Cu_{2-x}Se$ to its high temperature phase is very confusing. While some reports state that the transition occurs over a 30^0C interval centered at 123^0C [9], few others expect this to vary from 110^0C to room temperature [3, 15]. Dependence of temperature of transition on non-stoichiometric index 'x' is well accepted. It is found that transition temperature decreases with increasing value of 'x' [Fig.(3.9)] [7,16] and also with increasing value of pressure [Fig.(4.1)] [9].

Transition of low temperature phase to the high temperature one is found to be reversible. The high temperature cubic phase on cooling undergoes phase transition back to the low temperature phase [16,17]. This cyclic transition is reported to be faster than the fastest temperature change attainable in the X-ray camera [7,8]. This phase transformation is a first order transformation. It shows a sharp increase in electronic conductivity and a sudden symmetrical change in linear expansion coefficient at the transition temperature. A second order phase transition, which leaves the crystal structure undisturbed, is also reported for $Cu_{2-x}Se$. [10]

Dialatometric investigations have been carried out in detail to clearly understand these phase transitions [2,18]. A volume contraction of 1.4% is reported during the first order transition from low temperature phase to high temperature phase [17]. The low temperature phase is anisotropic due to the specific ordering of the cation subsystem along monoclinic axis. But in the high temperature phase the cation subsystem is completely disordered and this leads to isotropy. In Vucic's view [10] this transition corresponds to an order-disorder transition of the mobile cation subsystem, along with rhombohedral to cubic symmetry transformation of the immobile cage formed by Cu and Se atoms.

Low temperature to high temperature phase transition is usually achieved either by heating the material [3,8,18] or by electrochemical polarization [6,14]. Various transformations are reported in liquid bath deposition procedures that include electrodeposition as well as electroless depositions. Santhanam et $al.$ reported a series of phase transitions of copper selenide at room temperature [13]. This can be schematically represented as

$$Cu_2Se \xrightarrow{\quad H_2SeO_3 \quad} Cu_2Se \xrightarrow{\quad -0.78V \quad Vs.SCE \quad} Cu_2Se$$

(Orthorhombic)   (Cubic)   (Orthorhombic)

$$\Big|\ +\ 0.20\ V$$
$$Vs.\ SCE.$$
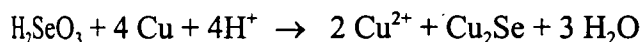
$CuSe$

(Orthorhombic)

$Cu_{2-x}Se$ phase (cubic) deposited using CBD technique was electrochemically polarized to the low temperature phase (orthorhombic) in another report also [14].
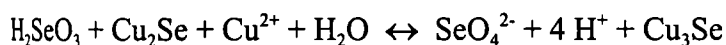
This transition was found to occur when the copper vacancies reach a critical value of $x < 0.15$ and was induced by the impurity phase of Cu_3Se_2 present in the cubic $Cu_{2-x}Se$ phase.

Tonejc *et al.* [8] studied the low temperature to high temperature phase transition with respect to the disappearance of an X-ray diffraction peak of the low temperature phase at $2\theta = 13^0$. This transition was found to be cyclic and repeatable with no hysterisis effect. It is a temperature dependent and time independent phenomenon. A similar transition of $Cu_{2-x}Se$ at room temperature from its tetragonal structure to its cubic structure was reported by S. G. Ellis [1].

Apart from the usual low temperature and high temperature phases, a new phase called γ phase is also reported [4]. This is obtained when the high temperature phase is quenched rapidly to liquid nitrogen temperature. There are also rare reports of formation of phases like Cu_3Se from Cu_2Se [19]. During the reaction of H_2SeO_3 with Cu plate, Cu_2Se results according to the reaction

$$H_2SeO_3 + 4\ Cu + 4H^+\ \rightarrow\ 2\ Cu^{2+} + Cu_2Se + 3\ H_2O$$

As Cu^{2+} concentration increases, another reaction

$$H_2SeO_3 + Cu_2Se + Cu^{2+} + H_2O\ \leftrightarrow\ SeO_4^{2-} + 4\ H^+ + Cu_3Se$$

takes place giving Cu_3Se phase.

b) Cu_3Se_2 phase

Cu_3Se_2 disproportionates at 135^0C to $Cu_{2-x}Se$ and β-CuSe [5]. Reverse reaction of these products back to Cu_3Se_2 is very slow. Cu_3Se_2 is stable at 25^0C to at least 35 k bar of pressure. But at a temperature around 140^0C and at pressure of 5 K bar, it disproportionates to $Cu_{2-x}Se$ and $CuSe_2$ (Pyrite). Here the reverse reaction is found to be very fast [9].

In solid-state reaction between Cu and Se films [20], it is found that Cu_3Se_2 can transform to $Cu_{2-x}Se$ phase with the topoaxial relation (100) Cu_3Se_2 // (100) $Cu_{1.8}Se$ and (011) Cu_3Se_2 // (011) $Cu_{1.8}Se$. During this transformation an intermediate phase with a super lattice structure is formed.

c) CuSe phase

The low temperature and atmospheric pressure modification of CuSe is called the α CuSe. This transforms abruptly to β CuSe (orthorhombic) at 51^0C. At 120^0C

this transforms completely to γ CuSe. Both these transformations are rapidly reversible. The decomposition of this monoselenide occurs at 382°C to $Cu_{2-x}Se$ and Se at atmospheric pressure [5]. In a high pressure study the same author observed the disproportionation of α CuSe to Cu_3Se_2 and $CuSe_2$ occurring at pressure above 5 k bar at room temperature [9].

A more recent report on electron diffraction study on phase transition of CuSe to Cu_2Se in vacuum shows that the rate of transition is different depending on the primary temperature [21].

$$CuSe \xrightarrow{100-300°C} Cu_{2-x}Se \xrightarrow{300°C} Cu_2Se \xrightarrow{\text{Cooling to room temperature}} Cu_2Se$$

$$\text{(fcc)} \qquad \qquad \cdot \text{(fcc)} \qquad \qquad \text{(low temperature}$$
$$\text{modification)}$$

$$CuSe \xrightarrow{>350°C} Cu_2Se \xrightarrow{\text{Cooling to room temperature}} Cu_2Se$$

$$\text{(fcc)} \qquad \qquad \text{(low temperature}$$
$$\text{modification)}$$

In solid-solid reaction between Cu and Se film, Shiojiri et al. [20] observed that CuSe crystals appear immediately when Cu is in contact with Se film. Slowly with time, this changes to Cu_3Se_2 and later to $Cu_{1.8}Se$.

d) $CuSe_2$ phase

This diselenide phase has two modifications viz. pyrite and marcasite. Of these, the pyrite modification is remarkably stable at atmospheric pressure. Marcasite $CuSe_2$ decomposes to form CuSe and Se at 342°C [5]. At room temperature under a pressure less than 5 k bar, marcasite $CuSe_2$ transforms to pyrite phase. This modification melts at 545°C and 20 k bar [9].

4.2 Interphase transformation of as-prepared $Cu_{2-x}Se$ and Cu_3Se_2 phases

In the present work, the $Cu_{2-x}Se$ phase is found to convert to Cu_3Se_2 phase under specific conditions. Reverse transformation of Cu_3Se_2 to $Cu_{2-x}Se$ phase is also found to be possible by annealing. These two conversions are dealt separately in the following sections.

"Sample No.1" refers to the standard as-prepared $Cu_{2-x}Se$ film from Bath 1:1. These films are uniform and reddish brown in colour. *"Sample No. 2"* refers to the standard as-prepared Cu_3Se_2 film prepared from Bath 1:1 Na. These films are also uniform and are bluish green in colour.

4.2.1 Transformation of $Cu_{2-x}Se$ phase to Cu_3Se_2 phase.

On exposure to ambient conditions, reddish brown colour of as-prepared $Cu_{2-x}Se$ thin film (sample No.1) is found to change slowly to bluish green (typical of Cu_3Se_2 phase)[22]. This conversion does not occur throughout the film in the initial stage, but begins at some arbitrary location and progresses radially with time. There is no definite incubation period for this conversion to begin. This period is found to vary from hours to months. Reason for this indefiniteness is discussed in the section pertaining to the theory behind the conversion. Such Cu_3Se_2 films, resulting from the slow aging of the $Cu_{2-x}Se$ phase, are referred to as *"sample No.3"*.

When as-prepared $Cu_{2-x}Se$ film (sample No.1) is given a final dipping in Bath 1:1 Na or in dilute Na_2SeSO_3 solution for a few minutes, $Cu_{2-x}Se$ phase gets converted to Cu_3Se_2 phase with bluish green colour. The Cu_3Se_2 phase obtained by this procedure is referred to as *"sample No.4"*.

4.2.1.1 Characterisation
i) SEM analysis

Fig.(4.2) shows the micrograph of sample No.3. This micrograph, when compared with that of the as-prepared $Cu_{2-x}Se$ phase (Fig.(3.1)) reveals the formation of few round beads (drops) of considerable size on the film surface. The bright appearance of these drops in this electron analytical technique is due to accumulation of charge as a result of electron bombardment. This suggests the formation of some low resistive material on which charge accumulation is possible. In the present case, it is expected to be Cu drops that are formed on the copper selenide surface with age [31]. This is quite possible as the conversion of $Cu_{2-x}Se$ to Cu_3Se_2 results in free copper (as explained in section 4.2.1.2).

Fig.(4.3) shows the micrograph of sample No.4. On comparing this with sample No.1, it can be inferred that Cu has diffused in the form of small discrete
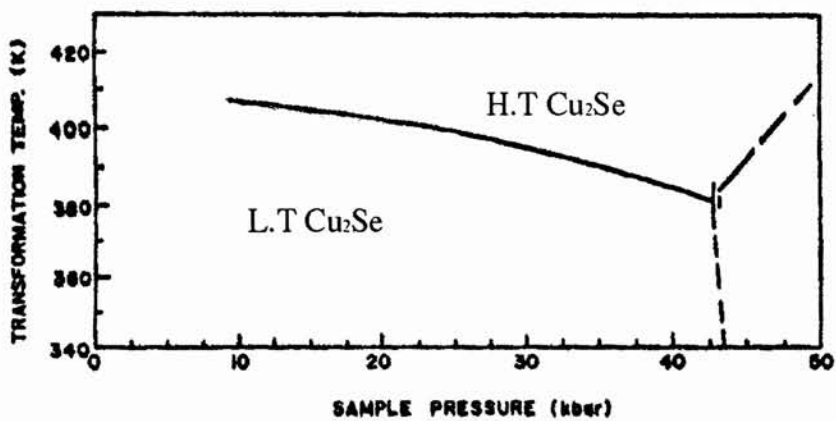
Fig.(4.1)   Pressure dependence of
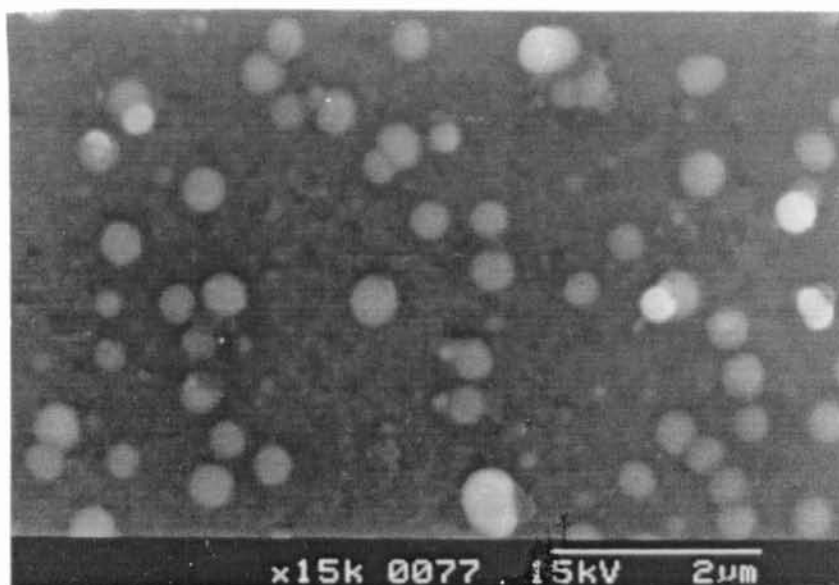   transition temperature of Cu_2Se.

Fig (4.2)   SEM micrograph of sample No.3 (Cu_3Se_2 phase resulting
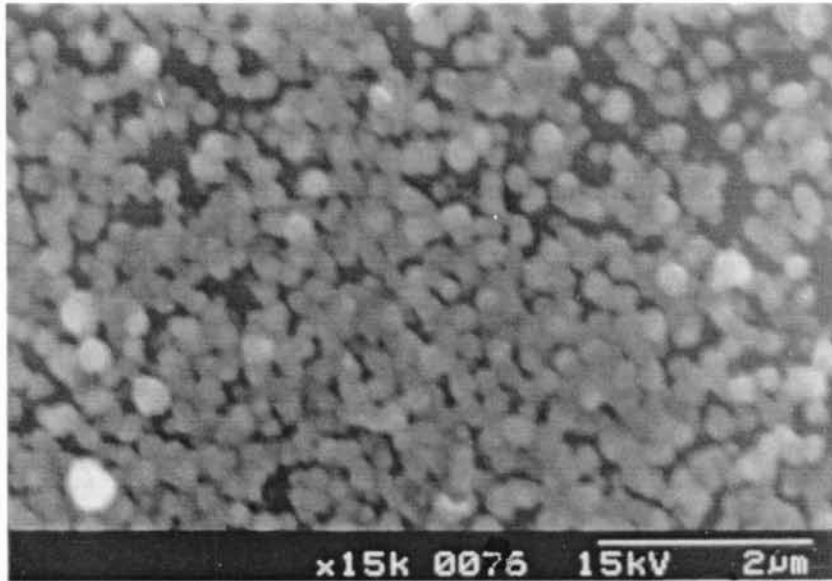   from the aging of $Cu_{2-x}Se$ phase)

Fig (4.3)   SEM micrograph of sample No.4 (Cu_3Se_2 phase resulting
from dipping of $Cu_{2-x}Se$ film in selenium solution)

grains on to the film surface. This may be due to the phase conversion of $Cu_{2-x}Se$ to Cu_3Se_2 when dipped in Na_2SeSO_3 solution.

ii) XRD analysis

Morphological observations formed the preliminary stage of identification of phase transformation, while XRD analysis formed the confirmatory stage.

Figures (4.4.a) and (4.4.b) show the XRD pattern of as-prepared $Cu_{2-x}Se$ film before and after the phase conversion due to aging (i.e. sample No.1 and sample No.3). A series of X-ray diffractograms taken at a regular interval of two weeks, revealed intermediate stages of conversion from Fig.(4.4.a) to Fig.(4.4.b). They depicted a gradual decrease of peak intensities of $Cu_{2-x}Se$ phase and a slow development of peaks corresponding to Cu_3Se_2. The final transformed phase as represented by Fig.(4.4.b) appears to be less crystalline with low peak intensities when compared with the as-prepared Cu_3Se_2 phase (sample No.2). But it should be specially mentioned that each of these small peaks corresponds to the standard JCPDS data file 47-1745 for the tetragonal Cu_3Se_2 phase. The d values of these XRD spectra are listed in Table (4.1). This transformation is obvious from the disappearance of the typical peaks of $Cu_{2-x}Se$ phase (reference JCPDS file 6-0680).

The X-ray diffractogram of sample No.4 is shown in Fig.(4.4.c). The crystallinity of Cu_3Se_2 phase of this sample is better than sample No.3. This suggests a simpler method to prepare Cu_3Se_2 phase. Original preparation condition of Cu_3Se_2 required low temperature as described in Chapter 2. Moreover, the film surface was not so uniform. Another drawback was the difficulty to obtain thicker films of Cu_3Se_2 phase on bare glass substrate. But in the present method, i.e. dipping of $Cu_{2-x}Se$ thin film in Na_2SeSO_3 solution, required thickness can be obtained for the Cu_3Se_2 film at room temperature. Such film surfaces are found to be comparatively more uniform, though presence of diffused Cu was observed in SEM micrograph in Fig.(4.3). But this Cu was not revealed in XRD analysis. This may be due to the fact that, the copper grains are not crystalline or its quantity is too less to be identified in a bulk analytical technique like XRD.
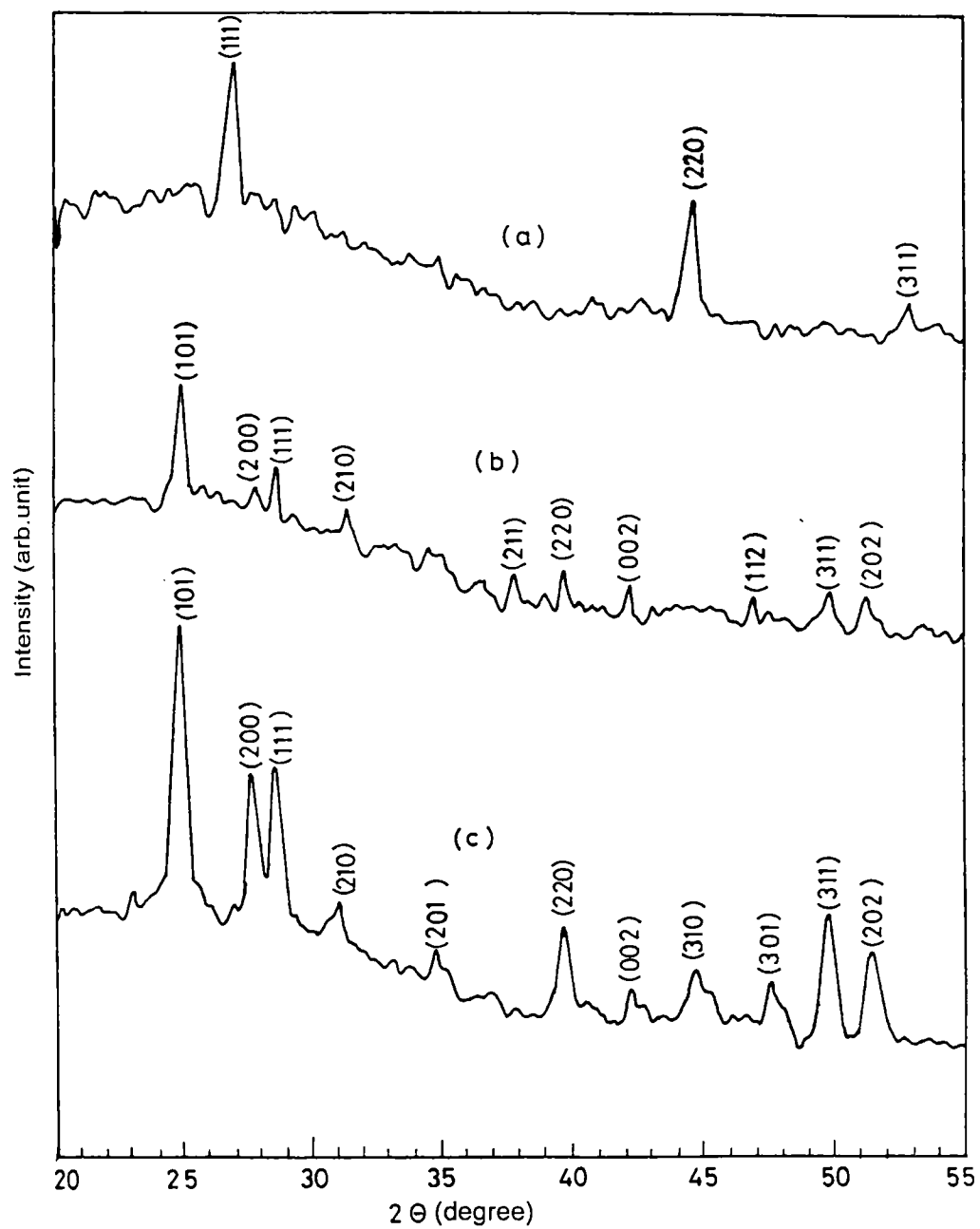
Fig (4.4)   XRD spectrum of (a) sample No.1 (b) sample No.3 and (c) sample No.4

Experimentally observed d values (Å)					Standard JCPDS values			
sample No. 1 Cu$_{2-x}$Se	sample No.2 Cu$_3$Se$_2$	sample No.3 Cu$_3$Se$_2$	sample No.4 Cu$_3$Se$_2$	sample No. 5 Cu$_{2-x}$Se	File 47-1745 Cu$_3$Se$_2$ d(Å)	hkl	File6-0680 Cu$_{2-x}$Se d(Å)	hkl
3.323	3.575	3.566	3.573	3.311	3.557	101	3.330	111
2.030	3.214	3.212	3.212	2.023	3.202	200	2.030	220
1.729	3.126	3.118	3.118	1.726	3.111	111	1.729	311
	2.874	2.859	2.882		2.864	210		
	2.563	-	2.575		2.563	201		
	-	2.380	-		2.380	211		
	2.270	2.265	2.265		2.264	220		
	2.143	2.139	2.139		2.139	002		
	2.029	-	2.027		2.024	310		
	2.008	-	-		2.001	221		
	-	1.933	-		1.934	112		
	1.914	-	1.912		1.910	301		
	1.833	1.831	1.831		1.830	311		
	1.781	1.781	1.779		1.778	202		

Table (4.1)   Comparison of XRD parameters of samples with the standard data of Cu$_{2-x}$Se and Cu$_3$Se$_2$ phases.

iii) *Optical studies*

Figure (4.5) shows the optical percentage transmittance of the Cu$_{2-x}$Se film before and after phase conversion (sample No.1 and sample No.3). Transmission peak shows a shift from 780 nm to around 540 nm. This value was around 580 nm for the as-prepared Cu$_3$Se$_2$ phase [Fig.(3.17)]. Moreover, due to this conversion to Cu$_3$Se$_2$ phase, the percentage transmittance has reduced considerably from 12% to less than 4%. For the as-prepared Cu$_3$Se$_2$ phase this was almost in the same range of Cu$_{2-x}$Se.

This difference in transmittance spectra of the Cu_3Se_2 phase converted from $Cu_{2-x}Se$ and the as-prepared Cu_3Se_2 (sample No.3 and sample No.2) may be due to the incorporation of impurity phase of copper oxide [23].

Direct band gap energy of these samples was calculated from the absorption spectrum by plotting $(\alpha t h\nu)^2$ against photon energy [Fig.(4.6)] (α being the absorption coefficient, t the film thickness and hν the photon energy). Formation of Cu_3Se_2 phase could be confirmed from shift of the absorption edge from 2.20 eV to 2.73 eV. The slight variation of band gap of this Cu_3Se_2 phase from the earlier observed value of 2.83 eV in section [3.4.1] may be due to the formation of copper oxide resulting from oxygen incorporation. Absorption edge of copper oxide is comparatively towards the lower range, i.e. around 2 eV [24].

iv) XPS analysis

XPS analysis of sample No.3 was done to get a better insight to the process of phase conversion. This particular sample No. 3 was obtained from $Cu_{2-x}Se$ phase as a result of aging for a period of 4 months. No appreciable binding energy shift for Cu and Se signals was observed between this transformed phase and the original phase. Fig.(4.7) shows the depth profile of the sample. The presence of a slight peak for the O 1s signal throughout the sample thickness is obvious along with the strong signals of Cu and Se. This suggests the formation of small quantities of oxide impurity in the copper selenide phase as a result of aging. Binding energy of this oxygen is found to be around 530 eV, which corresponds to metal oxide. This value is different from that of the surface oxygen species having binding energy 532 eV. This value corresponds to hydroxide or chemisorbed water [25] and it appears only as a surface contaminant. Fig.(4.8) shows the percentage concentration of each element in the sample and it reveals the concentration of oxygen to be around 9%. The total XPS survey, i.e. N(E)/E versus binding energy graph, recorded after the 5th cycle of etching also shows the presence of oxygen [Fig (4.9)]. This oxidation accounts for decrease in crystallinity of sample No.3 as shown by Fig.(4.4.b) and also for the slight discrepancies in the optical studies as already mentioned.

Another important point that was understood from the XPS studies is that aging need not necessarily lead to phase conversion or oxide phase formation. To prove this, an as-prepared $Cu_{2-x}Se$ phase stored in dry atmosphere for 4 months time
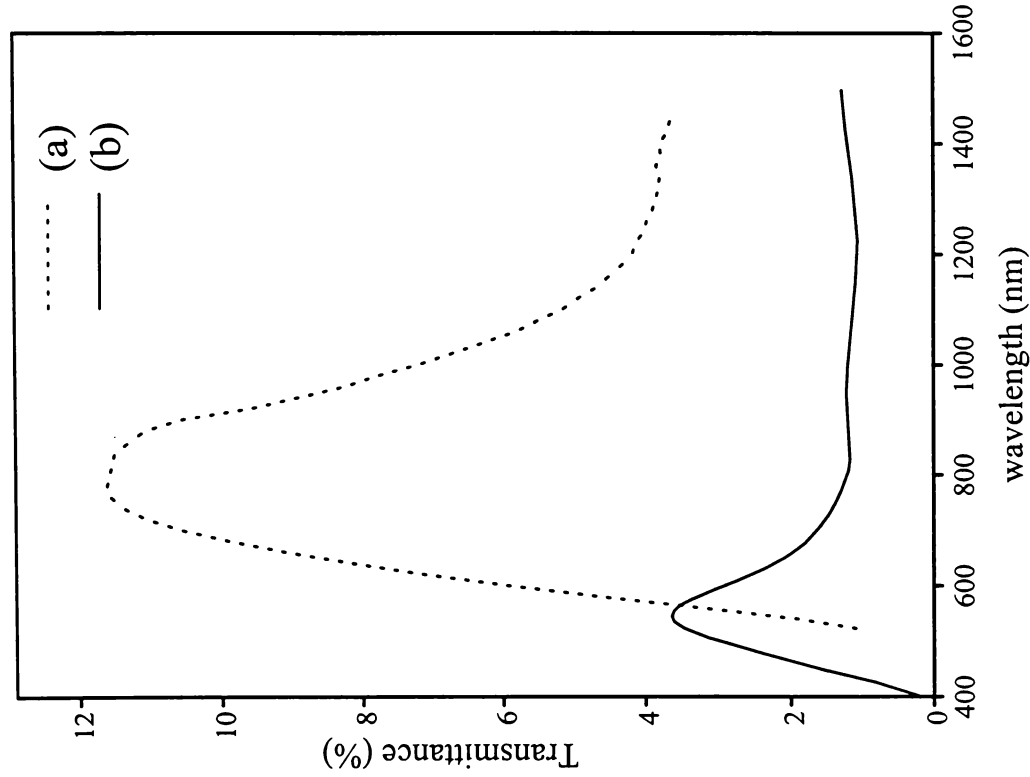
Fig.(4.6) $(\alpha h\nu)^2$ vs. photon energy plot of
(a) sample No.1 (b) sample No.3

Fig. (4.5) Optical percentage transmission spectra of
(a) sample No.1 and (b) sample No.3.
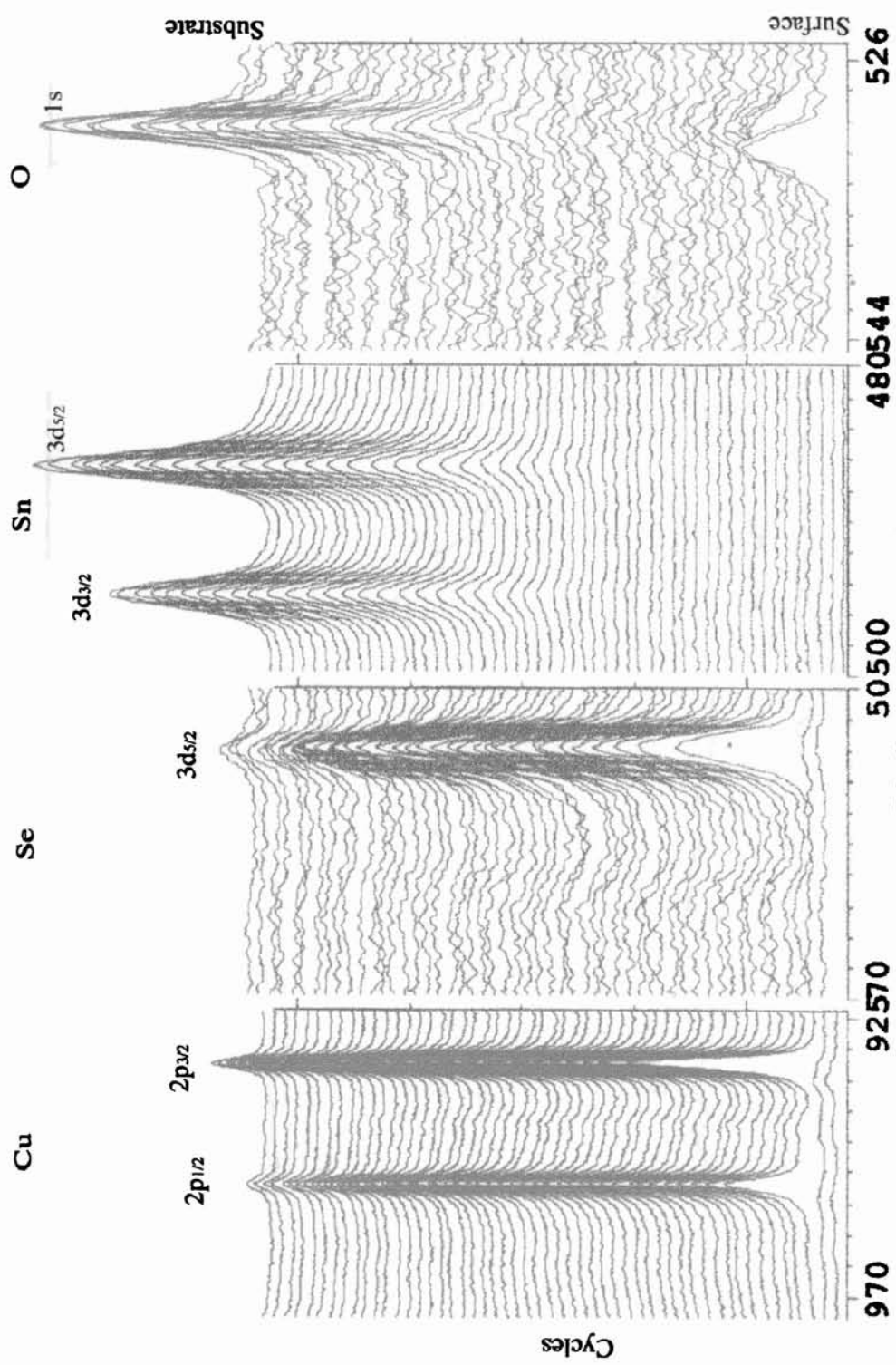
Fig.(4.7) XPS depth profile of sample No.3
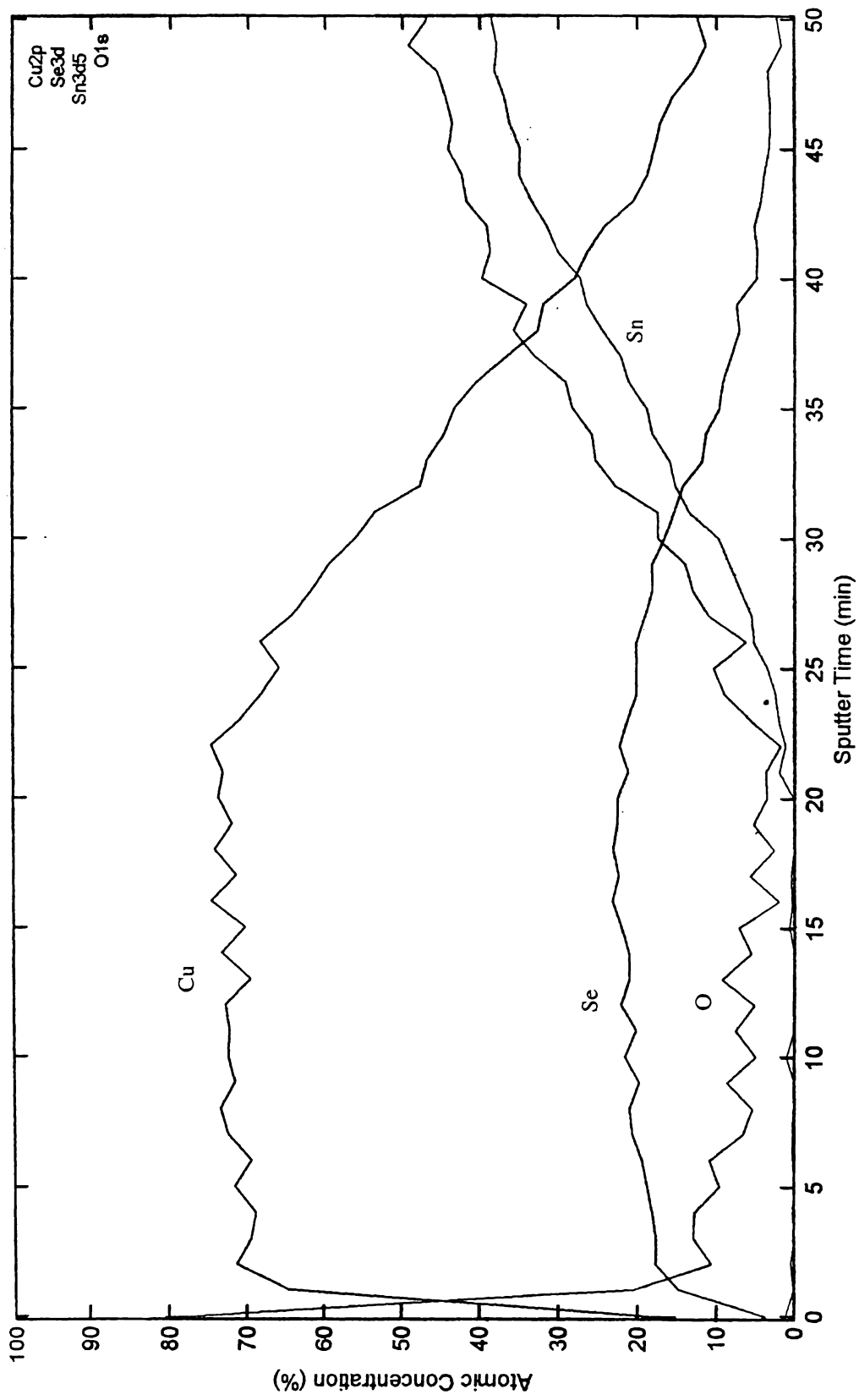
Fig.(4.8)   Percentage composition of sample No.3 as obtained from XPS analysis.

Fig. (4.9) Total XPS survey of sample No.3 after the 5th cycle of etching.

without any phase conversion was analysed using XPS depth-profiling, Fig.(4.10). In the figure, it is clear that presence of oxygen is limited only to the surface in the case of this sample. There is no oxygen trace remaining after 1 minute of etching. This study revealed that if stored in a dry atmosphere the phase conversion of $Cu_{2-x}Se$ can be prevented to a great extent.

v) Hall measurements

Hall measurements were used as one of the major techniques to understand the mechanism of interphase conversion. All the basic ideas regarding the conduction process in copper selenide, as mentioned in section (3.6.2), holds good as a background for explaining the interphase conversion.

Table (4.2) summarises the results on Cu_3Se_2 phase converted from $Cu_{2-x}Se$ by aging (sample No.3) and by dipping in Na_2SeSO_3 solution (sample No.4). In the case of sample No.3, carrier concentration has increased and mobility has significantly decreased by an order. This supports the possible disproportionation of Cu (I) as:

$2Cu (I) \rightarrow Cu (II) + Cu (s)$ [Refer section 4.2.1.2]

leading to the phase conversion. When Cu (I) is converted to Cu (II) and Cu (s), the Cu (s) diffuses out from the grain boundaries, while the Cu (II) contributes to the Cu_3Se_2 phase formation. This diffusing out of Cu atoms increases the Cu ion vacancy in the crystal structure leading to increase in hole density. This in turn reduces the mobility. The fact that the crystallinity of the aged samples are less than the as-prepared samples may also be contributing to the decrease in mobility.

When compared with the as-prepared Cu_3Se_2 phase, the copper vacancy density is high. Formation of small amount of copper oxide, as shown by XPS analysis of the aged sample, may also contribute to increase in Cu vacancy. Diffusion of copper out of the grain boundaries aids in conduction, leading to slightly lower resistance than the as-prepared Cu_3Se_2 phase. For the same reason of higher carrier concentration in the aged film, the Hall coefficient is found to be as low as $6.2\times10^{-3} cm^3/C$, while the as-prepared film has a value of $1.1\times10^{-2} cm^3/C$.
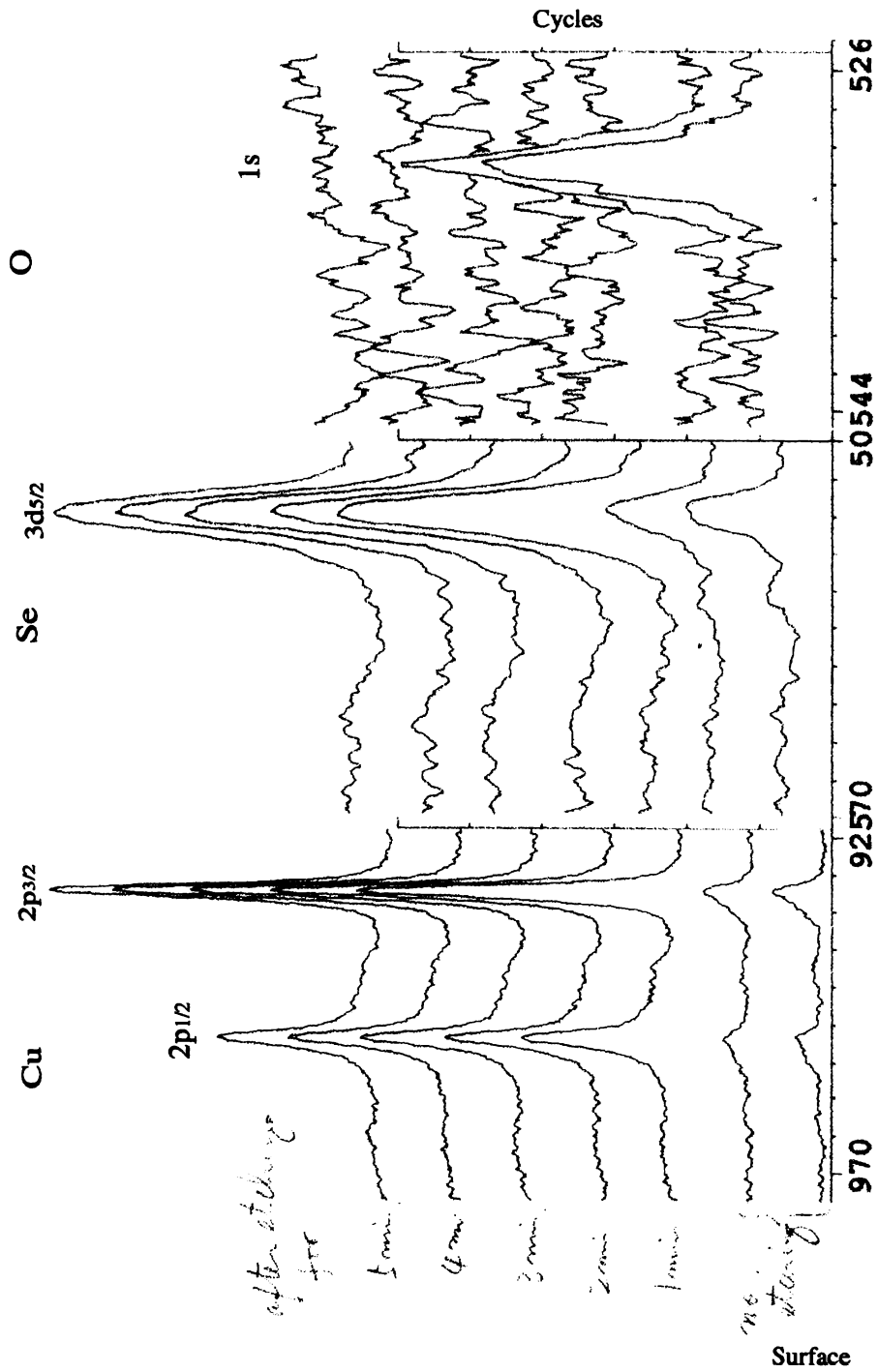
Fig.(4.10) XPS depth profile of sample No.1 stored for 4 months without phase conversion.

	$Cu_{2-x}Se$ as-prepared (sample No.1)	$Cu_{2-x}Se \rightarrow$ Cu_3Se_2 (aged) (sample No.3)	$Cu_{2-x}Se \rightarrow Cu_3Se_2$ (dipped) (sample No.4)	Cu_3Se_2 as-prepared (sample No.2)
Resistivity (Ω-cm)	8.0×10^{-4}	4.8×10^{-3}	9.2×10^{-4}	6.6×10^{-3}
Mobility ($cm^2/$ Vs)	1.5×10^1	1.3	2.5	1.7
Carrier density (cm^{-3})	5.2×10^{20}	1.0×10^{21}	2.7×10^{21}	5.6×10^{20}
Hall co-efficient (cm^3/C)	1.2×10^{-2}	6.2×10^{-3}	2.3×10^{-3}	1.1×10^{-2}
Sheet resistance (Ω/cm^2)	8	4.8×10^1	9.2	6.6×10^1
Type of carriers	Hole	Hole	Hole	Hole

Table (4.2)   Hall measurements of sample No.3 and sample No.4 in comparison with sample No.1 and sample No.2.

In sample No.4 the expected process of disproportionation is same as above. Here also the increase in carrier concentration must be due to the significant diffusing out of Cu to the film surface as seen in SEM micrograph in Fig.(4.3), leading to the increase in Cu vacancies. This in turn reduces the mobility from 15 to 2.5 cm^2/Vs. Due to the presence of Cu(s) on the film surface, the resistance is found to remain in 10^{-4} order, though the phase gets converted to Cu_3Se_2.

4.2.1.2 Theory behind the transformation

When $Cu_{2-x}Se$ thin film is left to itself in the ambient conditions, it slowly gets converted to Cu_3Se_2. This happens due to two reasons: - i) instability of Cu (I) in $Cu_{2-x}Se$ phase and (ii) high diffusion coefficient of mobile copper atoms.

In $Cu_{2-x}Se$ copper is in Cu (I) state while in Cu_3Se_2 it is in a mixed state of Cu (I) and Cu (II) [26]. It is generally observed that Cu (II) is more stable than Cu (I) and hence preferred [27]. So when initiated by suitable stimulating factor, the Cu (I) disproportionates according to the reaction.
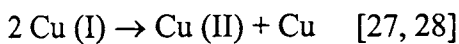
2 Cu (I) $\rightarrow$ Cu (II) + Cu   [27, 28]

This process only involves internal transfer of an electron from one of the Cu (I) to another Cu (I), so that more stable forms of Cu (II) and Cu exists [29].

This would mean intermediate stages of

$$Cu_{2-x}Se \rightarrow Cu_{2-x^1}Se + Cu$$
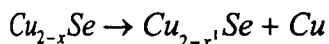
where $x^1 > x$. i.e. the copper selenide slowly shifts towards the selenium rich phase. When this disproportionation proceeds, it results in a stable situation where $x^1 \sim 0.5$. Thus $Cu_{2-x}Se$ phase gets converted to Cu_3Se_2.

$$2\,Cu_{2-x}Se \quad \rightarrow \quad Cu_3Se_2 + Cu$$
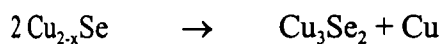
Formation of small amounts of copper oxide as observed in XPS study may also contribute to the lowering of the Cu concentration in $Cu_{2-x}Se$ phase, leading to Cu_3Se_2 phase formation.

Structure of $Cu_{2-x}Se$ consists of a sublattice of immobile cage structure of Cu and Se ions and another sublattice of mobile copper ions [10]. The mobile Cu forming a superionic sublattice has high diffusion mobility [30]. It is known that mobile Cu ions are in a more disordered state in the $Cu_{2-x}Se$ sublattice than in the liquid phase [31]. Hence in the solid state itself, when stimulated by a suitable external factor, the mobile Cu ions diffuse out after the disproportionation as elemental Cu. This makes the remaining phase Se rich. Or in other words this leads to the conversion of $Cu_{2-x}Se$ to Cu_3Se_2. There are few reports [14, 21] that mention Cu_3Se_2 as an impurity phase appearing in $Cu_{2-x}Se$. This supports the above mentioned transformation.

The high diffusion coefficient of copper has been emphasised by Shirojiri *et al.* [20] while explaining the solid-solid reaction between Cu and Se films kept in contact with each other at room temperature. The immediate formation of CuSe crystals at the interphase and the slow formation of Cu_3Se_2 and further $Cu_{2-x}Se$ phase, due to the high diffusion rate of copper atoms into the selenium film was documented by the high-resolution electron microscopic studies.

Hiroshi Morikawa [32] reported a similar effect in terms of crystal defects in Cu_3Se_2. In electron microscopic studies he observed fine structures in the Cu_3Se_2 crystal. The extra stripes on the diffraction pattern were interpreted as due to narrow Cu crystal precipitates on the (111) and (021) defect planes. In spite of this defect formation Se ions (due to its very large size when compared to Cu atoms) will frame up the unit cell in the same manner as a perfect Cu_3Se_2 crystal. Ionic radius of Se^{2-} is 191 pm while that of Cu is 128 pm.

In the present case the external factor that stimulates the phase conversion was traced out to be ions in the presence of humidity. These ions in ambient conditions

can induce electron transfer process required for the disproportionation of Cu (I). As it is not easy to quantify this stimulating factor, the incubation period for this phase transformation cannot be predicted.

In order to confirm the role of external ions and humidity, the $Cu_{2-x}Se$ film was stored in different conditions like (i) diffusion vacuum (ii) in deionised water (iii) at low temperature (iv) in desiccator and (v) in open atmosphere susceptible to metal ions and alkaline or acidic pH along with the ambient humidity. After two weeks it was observed that films stored in vacuum, deionised water, at low temperature and in desiccator remained intact. This ruled out the direct role of oxygen, water, temperature and humidity in the transformation of $Cu_{2-x}Se$ phase to Cu_3Se_2 phase. But the films exposed to ambient conditions got converted to Cu_3Se_2 phase within a period of 2 to 3 days. Hence it was concluded that the stimulant for conversion was some factor present in the atmosphere, which is active in the presence of humidity. According to the chemistry of Cu (I) [27], in the presence of electrostatic interaction with the surroundings Cu (I) has the tendency to convert to Cu (II). In the present case, this electrostatic interaction may be due to the presence of ions like H^+, Na^+ or OH^- in the presence of atmospheric humidity. But no definite incubation period was observed for this solid solution decomposition as was reported in earlier works [31].

Influence of this stimulant was observed in an adverse manner when the $Cu_{2-x}Se$ film was exposed directly to fuming hydrochloric acid vapour. Within few minutes time it was observed that the reddish brown phase of $Cu_{2-x}Se$ phase got converted to greenish colour of Cu_3Se_2. On further exposure all the copper diffused out forming CuCl. This white precipitate soluble in HCl was partly carried away by the acid fumes. The remaining film had the brick red colour of amorphous selenium. Similarly when dipped in dilute acetic acid, $Cu_{2-x}Se$ phase converted to uniform Cu_3Se_2 phase in 48 hrs.

As mentioned earlier when $Cu_{2-x}Se$ phase is dipped in Bath 1:1 Na solution or in 0.1 M Na_2SeSO_3 solution, then also this phase conversion occurs. This may be brought out by the presence of excess Na^+ in both the cases.

From the above observations it is concluded that variation in pH of the external surrounding or the presence of any ionic species forms the stimulant for the conversion of $Cu_{2-x}Se$ phase to Cu_3Se_2 phase. Or in other words, Cu (I) state of copper in $Cu_{2-x}Se$ phase is stable only around neutral pH where the concentration of charged species is minimum.

4.2.2 Transformation of Cu_3Se_2 phase to $Cu_{2-x}Se$ phase

As-prepared Cu_3Se_2 thin film (sample No.2) has a bluish green colour, as mentioned in chapter 3. When this film is annealed in air at 140^0C for 1hr, it gets converted to the reddish brown phase of $Cu_{2-x}Se$. This annealing need not be slow and hence it is usually done by keeping the Cu_3Se_2 thin film for 1 hr in a hot air oven maintained at 140^0C. Such $Cu_{2-x}Se$ sample converted from as–prepared Cu_3Se_2 film are hereafter referred as *"sample No.5"*.

4.2.2.1 Characterisation

i) SEM analysis

Fig.(4.11) shows the SEM micrograph of sample No.5. The average grain size is found to be higher than that of the as-prepared $Cu_{2-x}Se$ film (sample No.1). Presence of irregular shaped large islets on surface of the film could not be interpreted with certainity. It is assumed to be due to segregations of Se or oxides of selenium.

ii) XRD analysis

Fig.4.12 (a) and 4.12(b) give the XRD patterns of sample No.2 and sample No.5 resulting from the annealing of sample No.2. High intensity of the diffraction peaks reveals good crystallinity for both the phases. Table (4.1) includes the d values of these two samples in comparison with as-prepared $Cu_{2-x}Se$ phase. It can be seen that all the d values of sample No.5 coincide with that of sample No.1.

Based on the variation in the d value of the (022) plane of the cubic phase of sample No.5 and sample No.1, stoichiometry was graphically predicted as depicted in Fig.(4.13). The results tabulated in Table (4.3) suggest that sample No.5 has a composition of $Cu_{1.62}Se$ while sample No.1 is $Cu_{1.71}Se$. Increased selenium content in sample No.5 is justifiable as this is derived from a comparatively selenium rich phase (i.e. Cu_3Se_2).
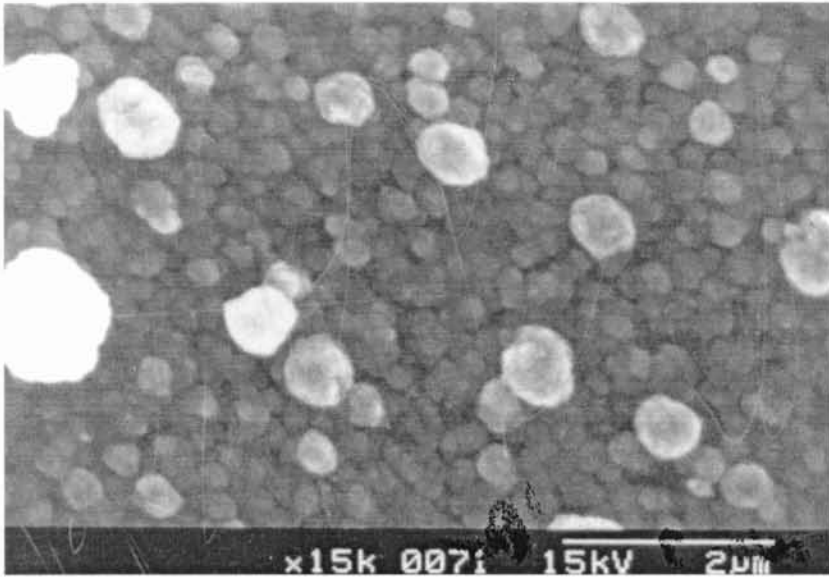
Fig. (4.11)   SEM micrograph of sample No.5 ($Cu_{2-x}Se$ phase resulting from annealing of Cu_3Se_2 phase).
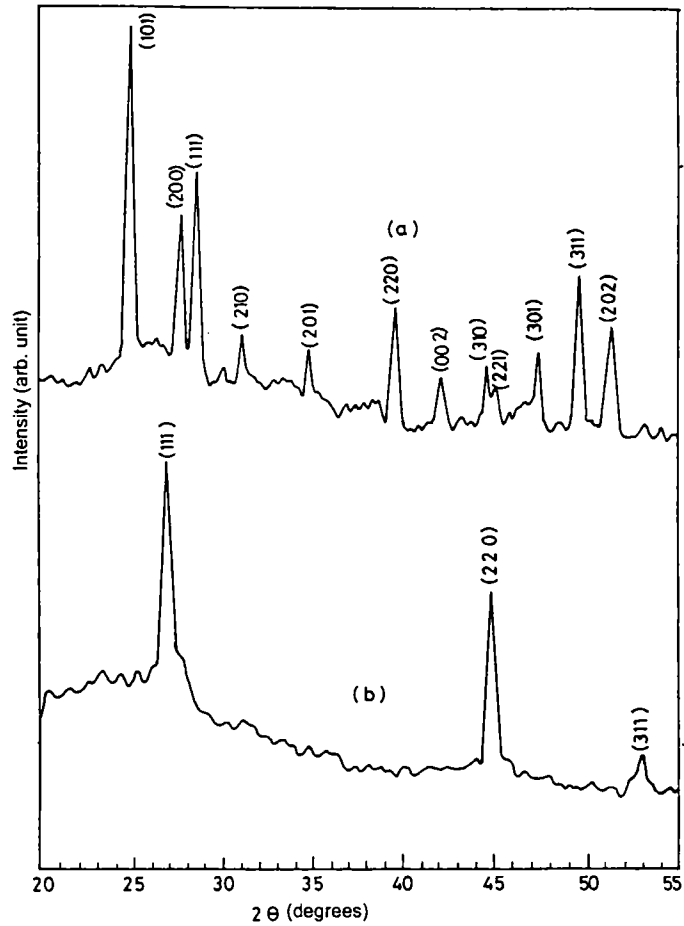
Fig.(4.12)   XRD spectrum of (a) sample No.2 and (b) sample No.5
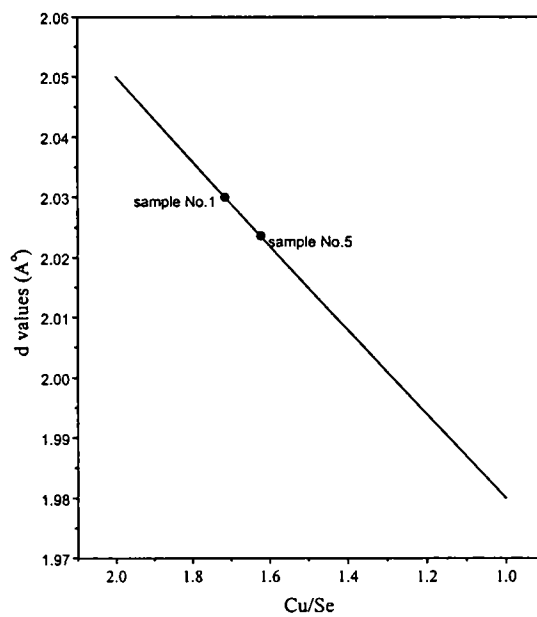
Fig.(4.13)   Evaluation of stoichiometry of sample No.1 and

sample No.(5) from the XRD data

Sample code	d value	Cu/Se	x value	Chemical formula
Sample No.1	2.0303	1.7145	0.29	$Cu_{1.71}Se$
Sample No.5	2.0236	1.6214	0.38	$Cu_{1.62}Se$

Table (4.3)   Evaluation of stoichiometry of sample No.1 and sample No.5
from the d values of (022) plane of the XRD spectrum.

iii) Optical studies

Just as Fig.(4.5) refers to the transmittance spectra of $Cu_{2-x}Se$ phase converted to Cu_3Se_2 phase, Fig(4.14) refers to the transformation of Cu_3Se_2 to $Cu_{2-x}Se$ phase. Both these figures are similar except for an increase in transmittance exhibited by sample No.5, Fig.(4.14). This may be due to the annealing effect on crystal defects. Same effect can be clearly observed in Fig.(4.15) where $Cu_{2-x}Se$ phase (sample No.1) is annealed under same conditions for reference. Band gaps calculated for sample No.2 and sample No.5 (i.e. before and after this phase conversion) are 2.84 eV and 2.27 eV respectively [Fig.(4.16)].

iv) Hall measurements

Table (4.4) shows the Hall measurement data of $Cu_{2-x}Se$ phase converted from Cu_3Se_2. The solid reaction behind this conversion leads to Se rich Cu(I)selenide (refer section 4.2.2.2). The presence of excess Se anions increases carrier density in a similar way as absence of Cu cations does. But presence of anions aids the mobility of holes. Hence mobility is found to increase from 1.7cm /Vs to 8 cm²/Vs. The slightly low resistivity of the film when compared to as-prepared $Cu_{2-x}Se$ phase must be due to the large extend of non stoichiometry existing in such films when it is derived from the Se rich phase of Cu_3Se_2.
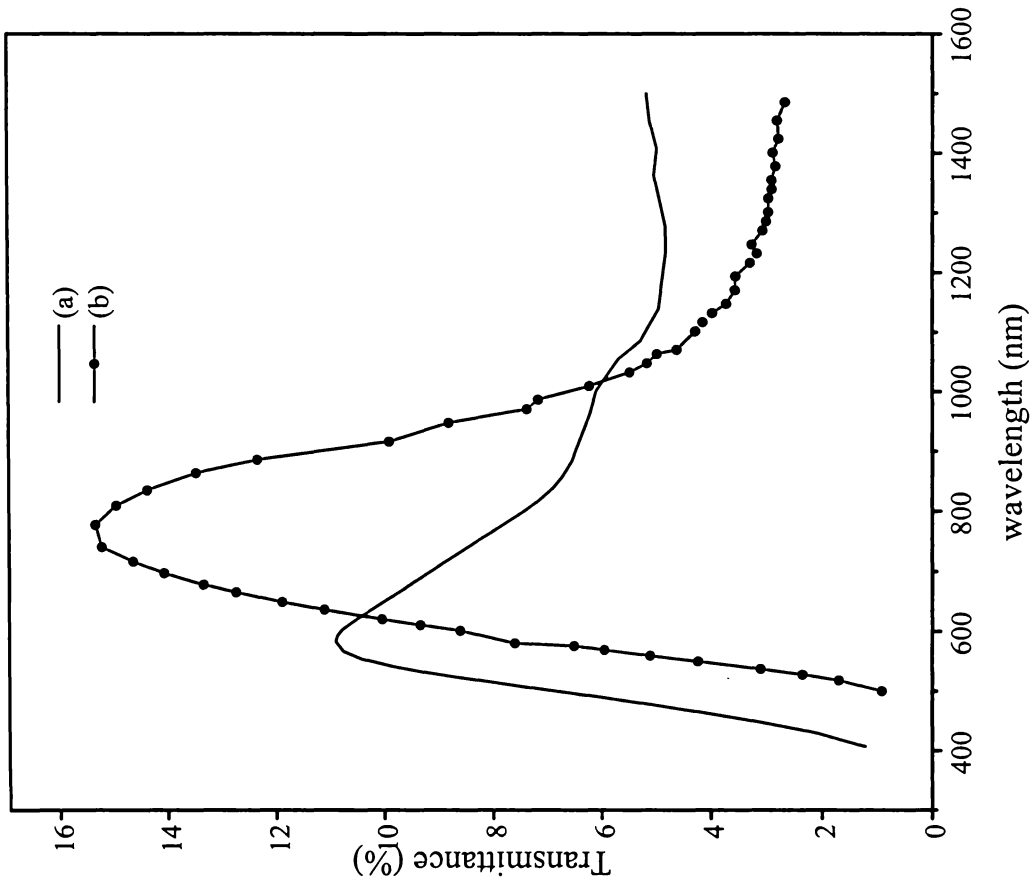
Fig.(4.14) Optical transmission spectra of
(a) sample No.2 and (b) Sample No. 5

Fig. (4.16) $(\alpha th\nu)^2$ plots of (a) sample No.2
and (b) sample No.5
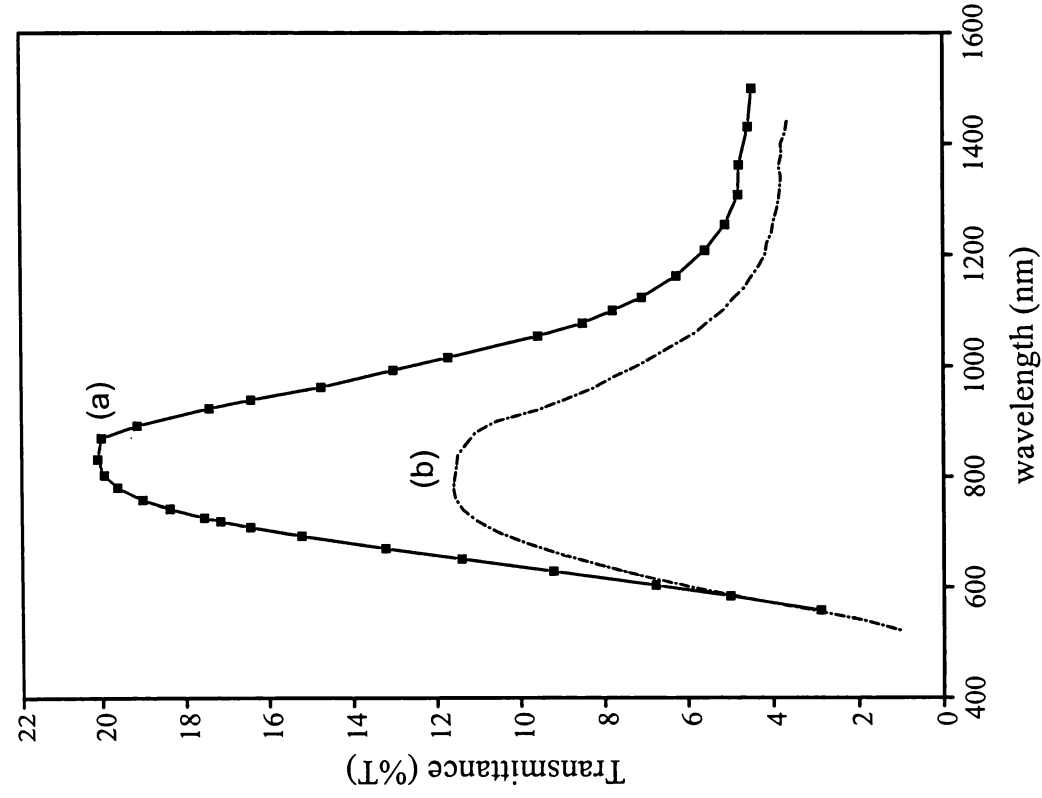
Fig. (4.15) optical transmission spectra of Cu_{2-x} Se phase
(a) before annealing (b) after annealing.
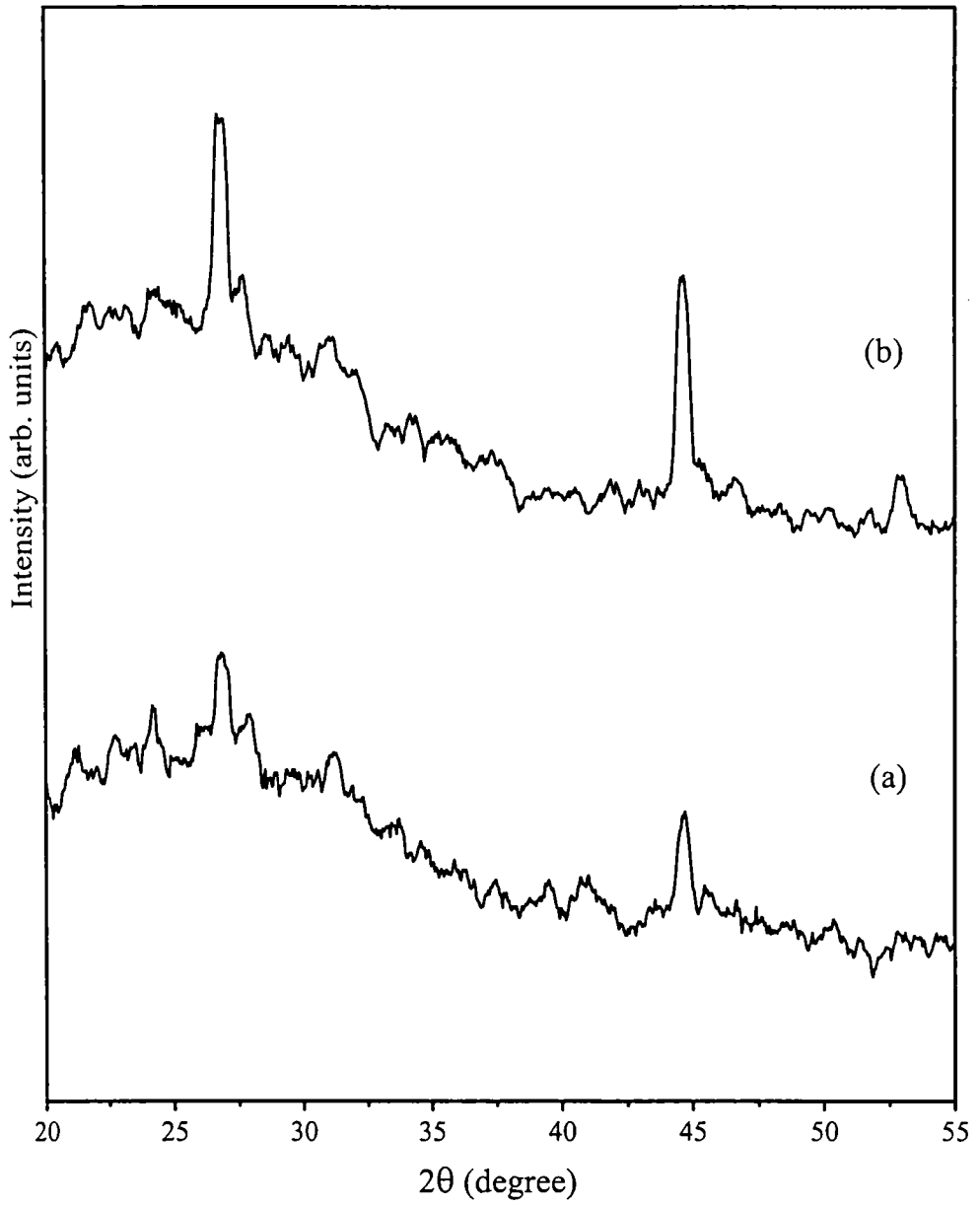
Fig.(4.17)   XRD spectrum revealing low crystallinity of
(a) as-prepared $Cu_{2-x}Se$-> Cu3Se2 -> $Cu_{2-x}Se$ sample
(b) when compared with as-prepared Cu_3Se_2 -> $Cu_{2-x}Se$ sample

	Cu_3Se_2 as-prepared (sample No.2)	$Cu_3Se_2 \rightarrow Cu_{2-x}Se$ (annealed at $140^{\circ}C$) (sample No.5)	$Cu_{2-x}Se$ as-prepared (sample No.1)
Resistivity (Ω-cm)	6.6×10^{-3}	4.5×10^{-4}	8.0×10^{-4}
Mobility (cm^2/Vs)	1.7	8.0	1.5×10^1
Carrier density (cm^{-3})	5.6×10^{20}	1.7×10^{21}	5.2×10^{20}
Hall coefficient (cm^3/C)	1.1×10^{-2}	3.6×10^{-3}	1.2×10^{-2}
Sheet resistance(Ω/cm^2)	6.6×10^1	4.5	8
Type of carriers	Hole	Hole	Hole

Table (4.4) Hall measurements of sample No.5 in comparison with sample No.1 and sample No.2

4.2.2.2 Theory behind the transformation

When Cu_3Se_2 phase is annealed at $140^{\circ}C$ for 1 hour, it gets converted to $Cu_{2-x}Se$. This happens due to the dissociation of Cu_3Se_2 into $Cu_{2-x}Se$ and elemental selenium according to the reaction.

$$2\,Cu_3Se_2 \rightarrow 3\,Cu_{2-x}Se + Se$$
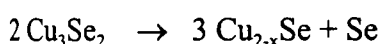
This $Cu_{2-x}Se$ can be thought of as Cu deficient or Se rich Cu(I)selenide phase. XRD analysis of this transformation has shown that slow sublimation of Se can occur with prolonged annealing even at low temperature [refer section (4.4)]. A similar decomposition was reported for CuSe by Heyding [5].

4.2.3 Cyclic nature of the interphase transformation

Conversions of $Cu_{2-x}Se$ to Cu_3Se_2 and Cu_3Se_2 to $Cu_{2-x}Se$ are found to be cyclic. When $Cu_{2-x}Se$ is aged in ambient conditions or dipped in Na_2SeSO_3 solution, stability of Cu^{+1} decreases and it partly converts to Cu^{2+}. This also leads to diffusing out of Cu to the film surface making the remaining phase selenium rich and there by getting converted to Cu_3Se_2. When this is annealed at $140^{\circ}C$ it converts back to $Cu_{2-x}Se$. But in the reverse direction of the cycle it is found that the crystallinity decreases. XRD spectrum in Fig.(4.17) shows this effect. The SEM in Fig.(4.18) reveals the diffused grain boundaries at this stage. It is expected that this reverse cycle of conversion is based on decomposition of Cu_3Se_2 to $Cu_{2-x}Se$ with heating. When such a film is again left for aging (i.e. forward process of 2nd cycle), it is observed that the rate of
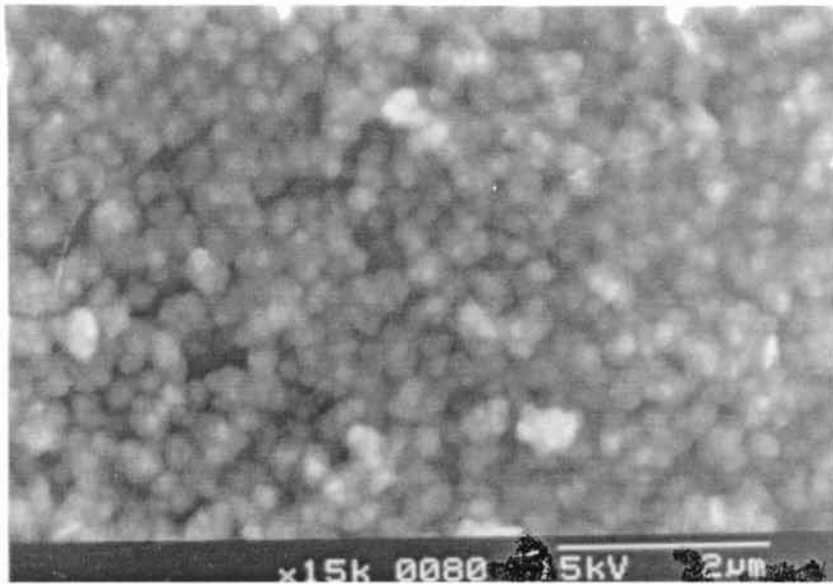
Fig. (4.18)   SEM micrograph of $Cu_{2-x}Se \rightarrow Cu_3Se_2 \rightarrow Cu_{2-x}Se$ sample

conversion is significantly reduced. This may be the effect of annealing cycle by which stability of Cu^{1+} is improved. Then the diffusion of copper to form drops on the surface is reduced considerably. In short, it is observed that this conversion has a cyclic nature though the quality of the film degrades after every cycle.

Same is the case with as-prepared Cu_3Se_2 film. When annealed it dissociates into $Cu_{2-x}Se$ and Se. When this $Cu_{2-x}Se$ phase is left for aging it converts back to Cu_3Se_2 phase. But this happens at a very slow rate. So to conclude, the phase conversion observed in $Cu_{2-x}Se$ and Cu_3Se_2 phases is cyclic but the rate of conversion is considerably reduced after each heating cycle.

4.2.4 Prevention of interphase transformation

Interphase conversion can be avoided by simple methods. When the as-prepared $Cu_{2-x}Se$ phase is annealed at 150^0C for 2hrs, the Cu (I) state is found to gain stability. This will prevent the conversion to Cu_3Se_2 phase to a great extend. Such samples when stored in dry atmosphere are found to remain intact even after one or two years. Similarly, as-prepared Cu_3Se_2 phase can be kept intact by avoiding any sort of heat treatment. Heat treatment stabilises $Cu_{2-x}Se$ phase while avoiding heat leads to the stability of Cu_3Se_2 phase.

4.3 Growth of excrescence in $Cu_{2-x}Se$ phase

Superionic conductors like $Cu_{2-x}Se$ with mixed electronic and ionic conductivity are known to exhibit growth of excrescences. Excrescences include growth of new formations like 'whiskers', 'moustaches', 'drops' or 'fractal growths' [33]. This is based on the development of the metallic sublattice of copper as a result of disproportionation of $Cu_{2-x}Se$.

The series of SEM micrographs included in Fig.(4.19) show the growth of excrescences in the $Cu_{2-x}Se$ phase. The first micrograph (a) shows the as-prepared $Cu_{2-x}Se$ film where there is no excrescence. Micrographs (b), (c) and (d) show the stages of gradual growth of excrescences (all these being taken under a magnification of 800 times). The last micrograph (e) shows the well-grown excrescence in the form of fractal growth (under 20 times magnification). This can be observed even with naked eyes. The time of aging of the as-prepared films as mentioned in the Fig.(4.19)
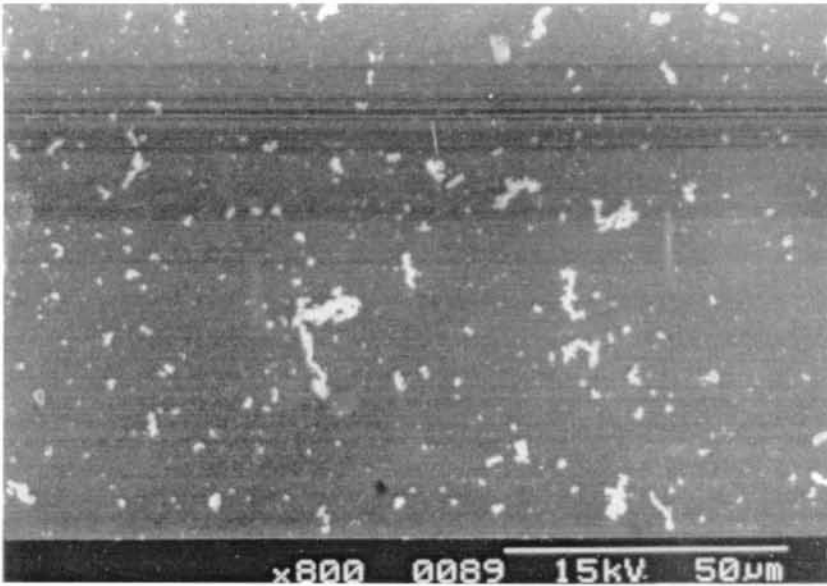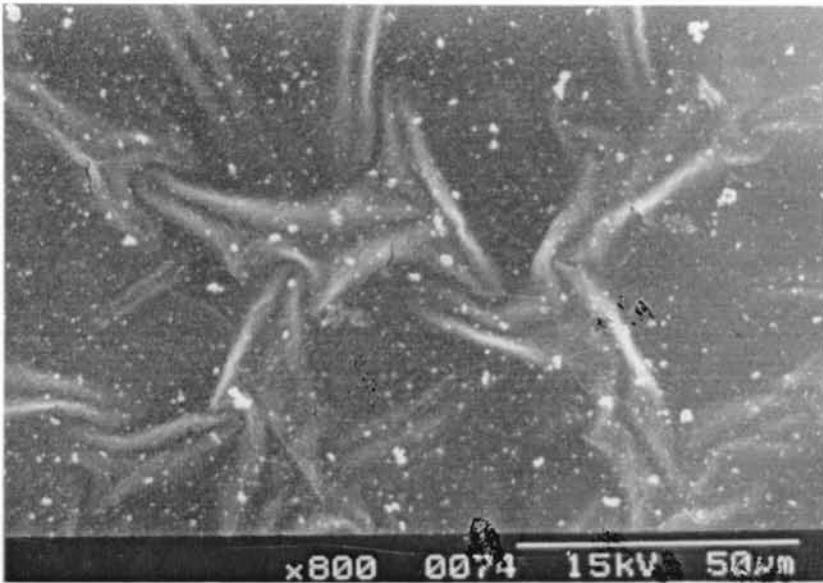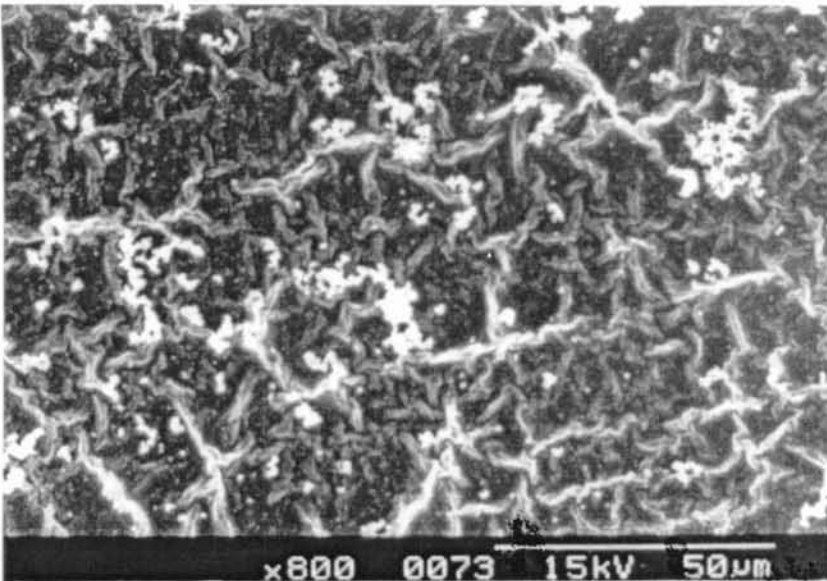
(a) Fresh sample
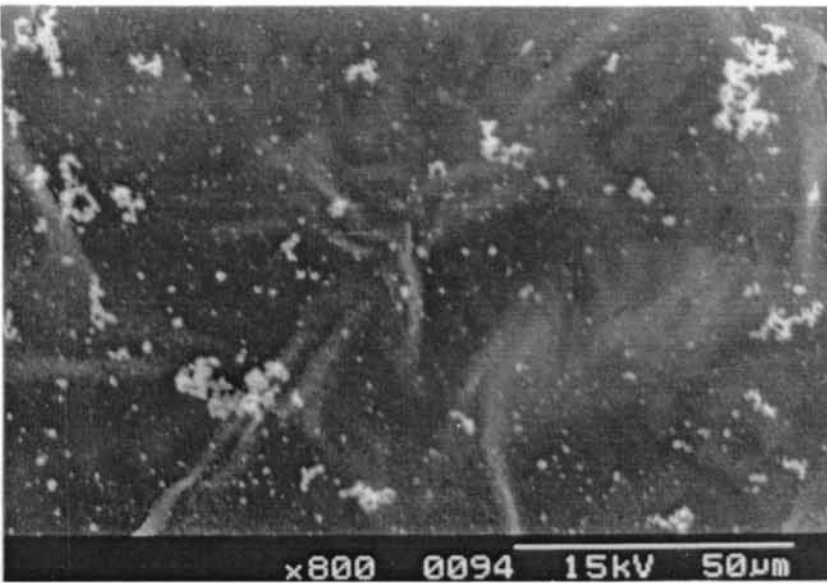
(b) After 3 days

Fig. (4.19)   SEM micrographs that reveals the gradual growth of Cu excrescence in
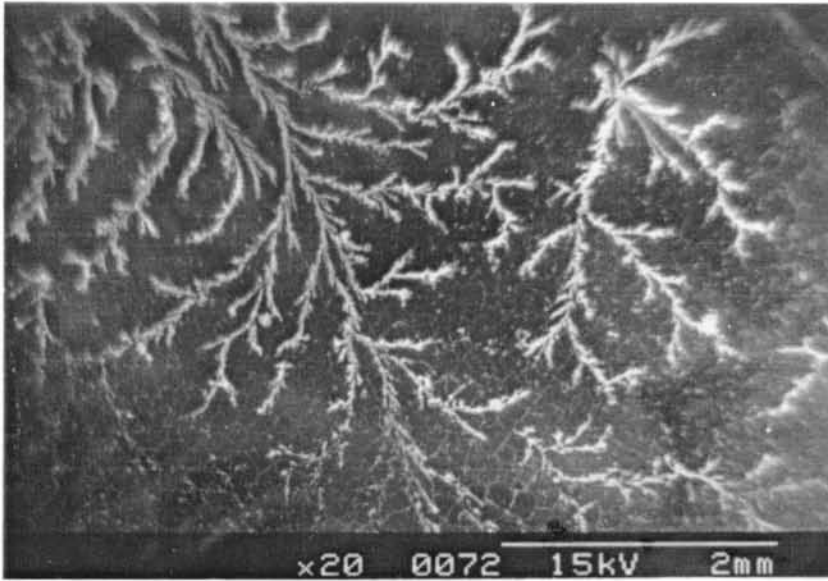Cu$_{2-x}$Se film in the form of fractal growth.

© After 1 week

(d) After 1 month

Fig. (4.19)   SEM micrographs that reveals the gradual growth of Cu excrescence in Cu$_{2-x}$Se film in the form of fractal growth.
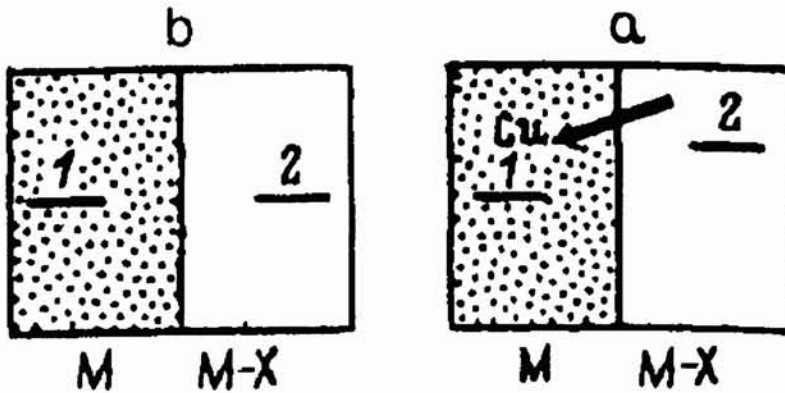
(e) After few months

Fig. (4.19)   SEM micrographs that reveals the gradual growth of
Cu excrescence in $Cu_{2-x}Se$ film in the form of fractal growth.

Fig. (4.20)   Arrangement of chemical potential level of Cu in metallic phase M and in
a M-X compound phase (a) before Cu diffusion (b) after Cu diffusion.

is arbitrary. This is because depending on ambient conditions the growth rate of excrescences can vary.

Growth of excrescences is usually reported as stimulated by factors like concentration, temperature, pressure differentials, ionizing radiations, electromagnetic fields and plastic deformation of the samples. But in the present work the stimulant for the growth was traced out to be the variation in pH of the surrounding atmosphere, or generally the presence of any charged atomic species in the presence of humidity [as explained in section (4.2.1.2)]. Here the observed excrescence is some time in the form of fractal growth as in Fig.(4.19), or in the form of drops as in Fig.(4.2). The condition under which these two cases results could not be differentiated in the present study. But in both cases the presence of copper excrescence could be clearly observed in the micrograph as bright regions. This is a result of charge accumulation in Cu due to the incidence of electron beam during image recording.

Since the chemical potential of Cu in elemental state (μ_M) is less than the chemical potential of Cu in $Cu_{2-x}Se$ (μ_{M-x}) [Fig.4.20.a], copper exists in a supersaturated state in $Cu_{2-x}Se$ [31]. In the presence of a suitable external stimulant, this supersaturated solid solution in copper selenide could attain equilibrium state by undergoing the decomposition reaction

$Cu_{2-1}Se \rightarrow Cu_{2-x^1}Se + Cu$ (where x^1 is greater than x)
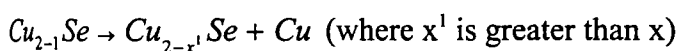
with the formation of interstitial and surface microdeposits of Cu. As explained in section (4.2.1.2), this happens due to the disproportionation of Cu (I) to Cu (II) and Cu. Diffusion coefficient of this mobile Cu is in the order of 1-100 μm [30]. Moreover, in non-stoichiometric $Cu_{2-x}Se$ the high concentration of Cu vacancies permits the very rapid diffusion of copper [34].

These micro deposits of copper formed by the diffusion mechanism forms the primary excrescence. In other words, the primary excrescence results due to the instability of the condition $\mu_M > \mu_{M-x}$. But once the system stabilizes by the formation of micro deposits of Cu, an equilibrium state is established in the system ($\mu_M \sim \mu_{M-x}$) Fig.(4.20.b). Migration of Cu in these primary excrescences to the film surface leads to the growth of secondary excrescences in the form of fractal growth or drops. The nucleation center for primary excrescence can be the defect centers of the sample [30, 32, 35], while the primary excrescences form the nucleation center for secondary excrescences.

It is reported that when the local increase in the Cu concentration is around $\Delta Cu \geq 10^8$ cm^{-3}, it results in excrescence [31]. This ΔCu can be attained by a pressure difference $\Delta P \sim 0.3\text{-}0.6$ GPa [36], an electric current density $J \sim 0.1$ A/mm^2 [37] or similar factors. In the present case, ions in the ambient atmosphere in the presence of humidity are found to stimulate the growth of excrescence. To summarise, Cu (I) in as-prepared $Cu_{2-x}Se$ phase is unstable. When stimulated by external ions in the presence of atmospheric humidity $Cu_{2-x}Se$ phase disproportionates into elemental copper and a relatively selenium rich copper selenide phase. This Cu diffuses out to form excrescence. When this process leads to a situation where x $\sim$ 0.5, the $Cu_{2-x}Se$ phase converts to Cu_3Se_2 phase.

In the present study, in order to avoid the growth of copper excrescences and the phase transformation that follows, it is suggested to store the film in a neutral dry atmosphere. Another method is to anneal the as-prepared $Cu_{2-x}Se$ film in air at 150^{0}C for 2hrs., so that the copper ions in Cu (I) state attain better stability. By this procedure it is observed that the copper ion migration and the consequent phase conversion can be reduced considerably.

Another interesting observation is that this sort of migration or growth is not observed in the as-prepared Cu_3Se_2 phase. This stability can be accounted by assuming the Cu_3Se_2 phase as a special case of $Cu_{2-x}Se$, where x $\sim$ 0.5. In a detailed study of formation of excrescences in $Cu_{2-x}Se$ phase, M. A. Korzhev [31] has suggested the shifting of the solid state stoichiometry into a safe range of large x value as a method to prevent the growth of both primary and secondary excrescences. This justifies the stability of Cu_3Se_2 phase.

4.4 Effect of annealing on $Cu_{2-x}Se$ phase

The interesting observation of phase change when Cu_3Se_2 film was annealed, prompted to study the effect of annealing the $Cu_{2-x}Se$ film. $Cu_{2-x}Se$ film from Bath 1:1 was considered for this study. In order to avoid influence of atmospheric oxygen at high temperatures, annealing at a pressure of 10^{-5}m bar was preferred at temperatures 100^{0}C, 200^{0}C, 300^{0}C and 400^{0}C.

Substrate of $Cu_{2-x}Se$ film was found to influence the stability of the phase during annealing. Samples deposited on glass and on SnO$_2$ coated glass, when annealed to a temperature of 300^{0}C were found to be stable. But at 400^{0}C samples on

glass substrate suffered a discoloration to bluish-ash along with the development of pinholes. This is attributed to significant evaporation of selenium at high temperatures [7, 9].

$Cu_{2-x}Se$ film on SnO_2 substrate could withstand a temperature of $400^\circ C$ without decomposing. This suggests an extra stability for the sample on SnO_2 substrate. But as SnO_2 is a crystalline and conducting substrate, samples prepared on it could not be used for X-ray diffraction studies and electrical studies. Hence samples prepared on glass were preferred for such analysis.

i) SEM analysis

SEM micrograph of $Cu_{2-x}Se$ film annealed at four different temperatures at an interval of $100^\circ C$ was taken. Fig.(4.21.a) and Fig.(4.21.b) show the morphology of films annealed at $200^\circ C$ and $300^\circ C$ respectively. Micrographs of the samples annealed at temperatures of $100^\circ C$ and $400^\circ C$ are not included here, as they showed the same trend as the samples annealed at $200^\circ C$ and $400^\circ C$ respectively.

It is found that grain size improves up to an annealing temperature of $200^\circ C$. But annealing at $300^\circ C$ and $400^\circ C$ leads to diffused grain boundaries and smaller grain size. Apart from this many bright islets of selenium appear on the film surface at these high temperatures. This leads to the conclusion that degradation of the film becomes significant at $300^\circ C$ and at higher temperatures.

ii) XRD analysis

Effect of annealing on crystallinity and stoichiometry of the $Cu_{2-x}Se$ phase was studied in detail using XRD analysis. It is found that crystallinity of the as-prepared films improves due to annealing for 1 hr at $100^\circ C$, Fig.(4.22.b). Further improvement in crystallinity was observed in the case of film annealed at $200^\circ C$, Fig.(4.22.c). This is reflected in the decrease of FWHM value of the (022) peak. But further increase in temperature [Fig.4.22. d and e] resulted in deterioration in crystallinity as observed from the peak heights and FWHM values tabulated in Table (4.5). This may be due to the considerable escape of selenium at temperatures above $200^\circ C$ and this supports the observations seen in SEM analysis, Fig.(4.21.b).

Using the extrapolated standard relation of the d values of (022) plane of cubic copper selenide on the composition of the material [Fig.(3.24)], the effect of annealing on stoichiometry could be interpreted. Table (4.6) shows the d values,
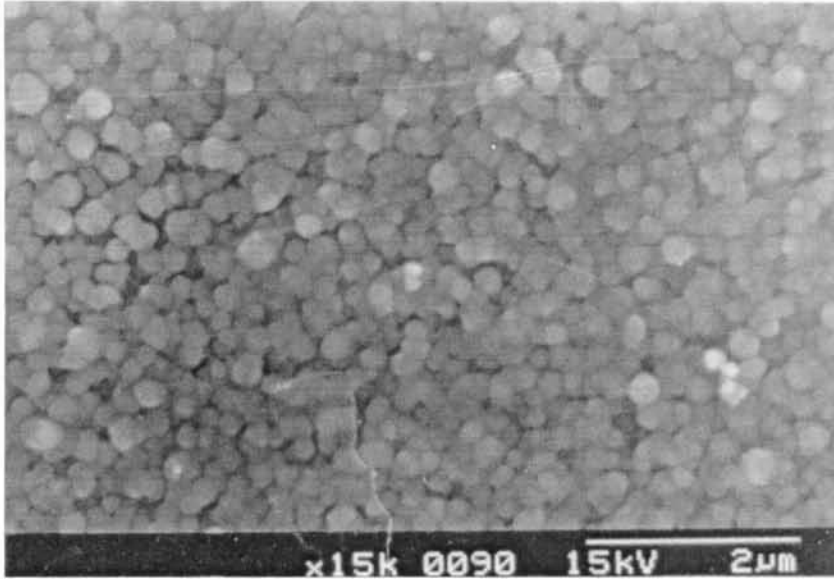
(a)
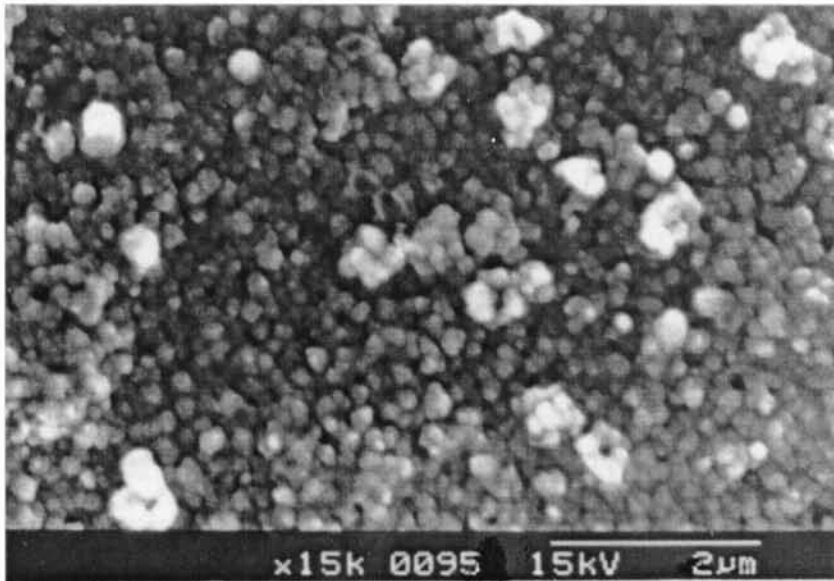
(b)

Fig. (4.21)   SEM micrographs of $Cu_{2-x}Se$ film

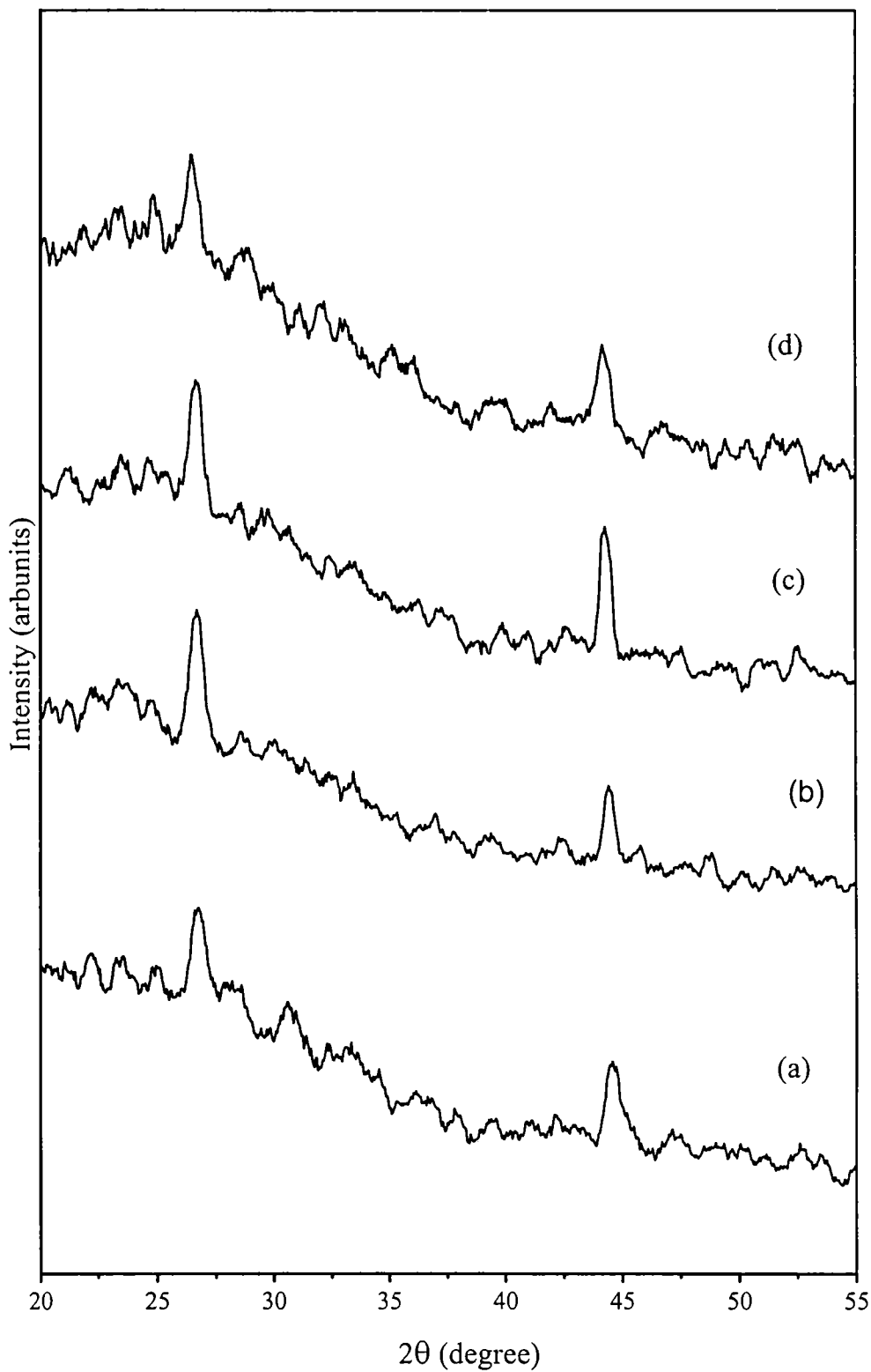(a) annealed at 200^0C (b) annealed at 300^0C.

Fig.(4.22) XRD spectrum showing the effect of annealing $Cu_{2-x}Se$ film.
(a) unannealed (b) annealed at 100^0C (c) annealed at 200^0C
(d) annealed at 300^0C (e) annealed at 400^0C.

Cu/Se ratio and x values, as derived by fitting the experimental d values on standard graph, Fig.(4.22). This suggests that there is a significant improvement in stoichiometry as a result of annealing. But annealing above 200°C is found to lead to significant deterioration of the film due to formation of pinholes and loss of crystallinity. Hence the best method to improve the film quality is to anneal at 200°C for longer duration.

Annealing conditions	Intensity (cps)	FWHM
Un annealed	181	0.590
100°C	200	0.588
200°C	312	0.476
300°C	235	1.249
400°C	178	1.070

Table (4.5) Effect of annealing on intensity and FWHM value of the XRD peak corresponding to (022) plane of $Cu_{2-x}Se$.

Annealing conditions	d values	Cu/Se	x values	Chemical formula
Un annealed	2.0300	1.7145	0.29	$Cu_{1.71}Se$
100°C	2.0365	1.8095	0.19	$Cu_{1.81}Se$
200°C	2.0409	1.8697	0.13	$Cu_{1.87}Se$
300°C	2.0431	1.9010	0.1	$Cu_{1.9}Se$
400°C	2.0585	2.1172	-0.12	$Cu_{2.12}Se$

Table (4.6) Evaluation of stoichiometry of $Cu_{2-x}Se$ thin film as a result of annealing at various temperatures.

(iii) *Optical studies*

Fig.(4.23) shows shift in band edge of the $Cu_{2-x}Se$ samples as a result of annealing. The band gap of 2.20 eV of the as-prepared film reduces to 2.16 eV on annealing at 200°C. Gradual shift of band edge at various annealing temperatures is tabulated in Table (4.7). This decrease in band gap may be due to increase in grain
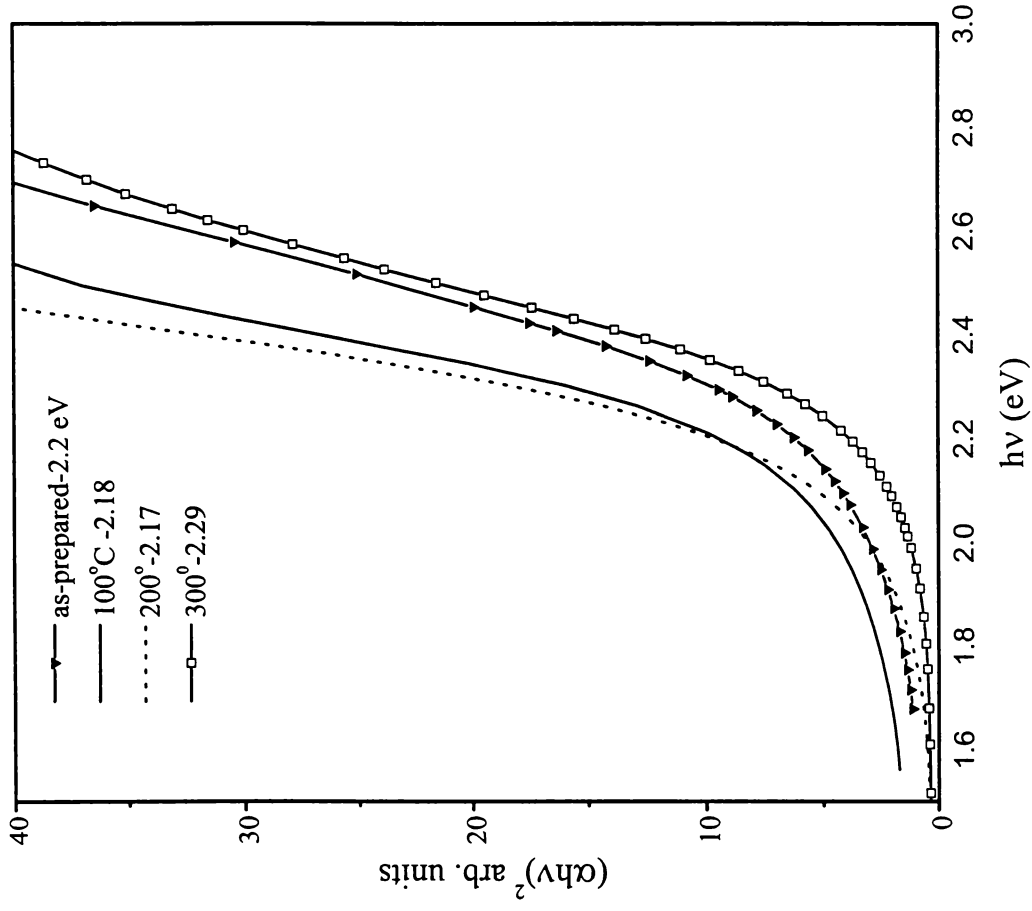
Fig.(4.23) Shift of optical band edge of Cu_{2-x} Se film as a result of annealing
(a) unannealed (b) annealed at 100°C (c) annealed at 200°C (d) annealed at 300°C

size. Higher annealing temperatures are found to increase the absorption edge further. This may be due to considerable escape of Se leading to poor crystallinity.

Fig.(4.24) shows the percentage transmittance graph of the annealed samples. It can be observed that all these samples show free carrier absorption leading to peak like nature for the transmittance graph. Annealing is found to increase the percentage of transmittance considerably. Increase in transmittance value of this sample annealed at $300^{0}C$ when compared to the sample annealed at $200^{0}C$ is a result of considerable escape of Se. But this situation arises only at a temperature of $400^{0}C$ if the thin film is deposited on SnO_2 substrate. Fig.(4.25) shows this result. This suggests an extra stability for the films on SnO_2 substrate as mentioned earlier.

Annealing temperature	Band gap (eV)
un annealed	2.20
$100^{0}C$	2.16
$200^{0}C$	2.14
$300^{0}C$	2.07

Table (4.7)   Shift of optical band gap of $Cu_{2-x}Se$ film as a result of annealing.

For the films deposited on glass, the peak value of transmittance shifts from the as-prepared value of 780 nm to 785 nm and 840 nm on annealing at $100^{0}C$ and $200^{0}C$ respectively. But annealing at $300^{0}C$ leads to the retrace of the peak position to 750 nm. Difference in the behaviour of the sample annealed at $300^{0}C$ is attributed to considerable escape of Se at $300^{0}C$. The results are tabulated in Table (4.8).

Annealing temperature	Maximum % transmittance	Wavelength of maximum transmittance
un annealed	11%	780
$100^{0}C$	45%	785
$200^{0}C$	38%	840
$300^{0}C$	41%	750

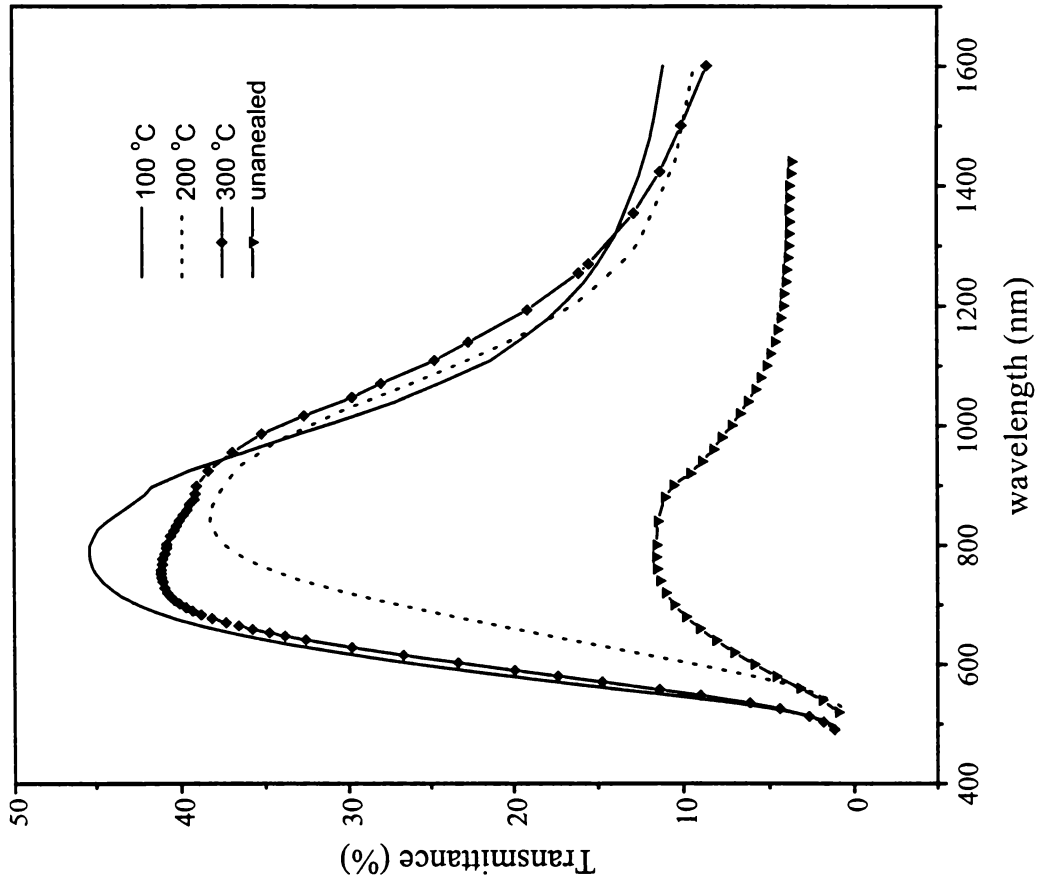Table (4.8)   Effect of annealing on the transmission spectra of $Cu_{2-x}Se$ film.

Fig. (4.24) Effect of annealing on the optical transmission spectra of Cu_{2-x} Se film deposited on glass substrate.
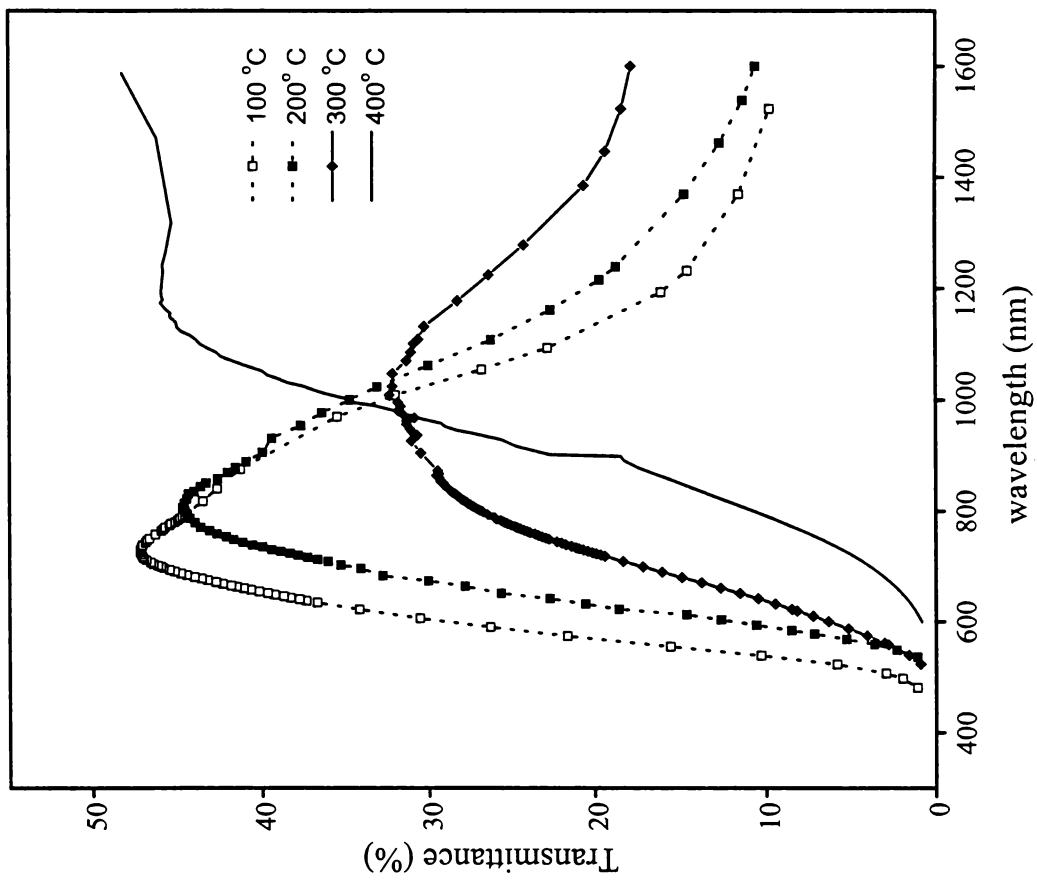
Fig. (4.25) Effect of annealing on the optical transmission spectra of Cu_{2-x} Se film deposited on SnO_2 substrate.

iv) *Hall measurements*

Table (4.9) shows the effect of annealing on the Hall parameters of $Cu_{2-x}Se$ phase. As mentioned earlier, the film deposited on glass when annealed at 400^0C was found to get damaged and hence could not be used for this analysis. Hence the samples used for the Hall measurements were those annealed at temperatures of 100^0C, 200^0C and 300^0C for duration of 1 hr.

Resistivity is found to increase as a result of annealing. This is possibly due to slight evaporation of selenium, which leads to improved stoichiometry, i.e. $Cu_{2-x}Se$ becomes $Cu_{2-x'}Se$ (where $x' < x$). With the decrease in carrier density the Hall coefficient is found to increase slightly.

	As-prepared	100^{0}C	200^{0}C	300^{0}C
Resistivity (Ω-cm)	8.0×10^{-4}	1.7×10^{-3}	1.9×10^{-3}	2.2×10^{-3}
Mobility (cm^2/ Vs)	1.5×10^1	9.7	9	8.3
Carrier density (cm^{-3})	5.2×10^{20}	3.8×10^{20}	3.5×10^{20}	3.3×10^{20}
Hall coefficient (cm^3/ C)	1.2×10^{-2}	1.6×10^{-2}	1.7×10^{-2}	1.8×10^{-2}
Sheet resistance (Ω/ cm^2)	8	1.7×10^1	1.9×10^1	2.2×10^1
Type of carriers	Hole	Hole	Hole	Hole

Table (4.9)   Effect of annealing on the Hall parameters of $Cu_{2-x}Se$ film.

4.5 Conclusion

The $Cu_{2-x}Se$ and Cu_3Se_2 thin films prepared using the CBD technique are found to undergo cyclic interphase conversion. When exposed to ambient conditions, the $Cu_{2-x}Se$ phase gets converted to Cu_3Se_2 phase along with the formation of Cu excrescences and some copper oxide. Attempts to trace out the stimulant behind this transformation are also included in this chapter. The Cu_3Se_2 phase converts to $Cu_{2-x}Se$ phase when annealed in air at a temperature above $140^{\circ}C$.

From these studies, it can be concluded that the tetragonal Cu_3Se_2 phase is stable in ambient conditions while the cubic $Cu_{2-x}Se$ phase is stable at temperatures above 140° C. Measures to prevent these phase transitions are also discussed. This phase conversion is of much relevance when these copper selenide phases find its various applications.

Reference

[1] S. G. Ellis, *J. Appl. Phys.*, 38 (1967) 2906.

[2] V. Horvatic, Z. Vucic and O. Milat, *J. Phys. C: Solid State Phys.*, 15 (1982) L 957.

[3] T. Takahashi, O. Yamamoto, F. Matsuyama and Y. Noda, *J. Solid State Chem.*, 16 (1976) 35.

[4] N. Frangis, C. Manolikas and S. Amelinckx, *Phys. Stat. Sol. (a)*, 126 (1991) 9.

[5] R. D. Heyding, *Can. J. Chem.*, 44 (1966) 1234.

[6] Z. Ogorelec and B. Celustka, *J. Phys. Chem. Solids*, 30 (1969) 149.

[7] A. Tonejc, *J. Mater. Sci.*, 15 (1980) 3090.

[8] A. Tonejc and A. M. Tonejc, *J. Solid State Chem.*, 39 (1981) 259.

[9] R. M. Murray and R. D. Heyding, *Can. J. Chem.*, 53 (1975) 878.

[10] Z. Vucic, O. Milat, V. Horvatic and Z. Ogorelec, *Phys. Rev. B*, 24 (1981) 5398.

[11] S. K. Haram, K. S. V. Santhanam, M. Neumann-Spallart and C.Levy-Clement, *Met. Res. Bull.*, 27 (1992) 1185.

[12] R. B. Shafizade, I. V. Ivanova and M. M. Kazinets, *Thin Solid Films*, 35 (1976) 169.

[13] S. K. Haram and K. S. V. Santhanam, *Thin Solid Films*, 238 (1994) 21.

[14] C. Levy Clement, N. Neumann- Spallart, S. K. Haram and K.V.S. Santhanam, *Thin Solid Films*, 302 (1997) 12.

[15] M. Hansen, *Constitution of Binary Alloys*, Mc Graw-Hill Book. Co. Inc., NewYork, 1958.

[16] S. Kashida and J. Akai, *J. Phys. C: Solid State Phys.*, 21 (1988) 5329.

[17] J. Gladic, O. Milat, Z. Vucic and V. Horvatic, *J. Solid State Chem.*, 91 (1991) 213.

[18] Z. Vucic, V. Horvatic and O. Milat, *Solid State Ionics*, 13 (1984) 127.

[19] R. N. O'Brien and K. S. V. Santhanam, *J. Electro Anal. Chem.*, 260 (1989) 231.

[20] M. Shojiri, C. Kaito, Y. Saito, K. Teranishi and S. Sekimoto, *J. Crystal Growth*, 52 (1981) 883.

[21] R. B. Shafizade, I. V. Ivanova and M. M. Kazinets, *Thin Solid Films*, 55 (1978) 211.

[22] J. W. Mellor, *A Comprehensive Treatise on Inorganic and Theoretical Chemistry*, Vol. X, Longmans.

[23] M. Lakshmi, K. Bindu, S. Bini, K. P. Vijayakumar, K. C. Sudha, T. Abe and Y. Kashiwaba, *Thin Solid Films*, 370 (2000) 89.

[24] M. Ristov and G. J. Sinadinovski, *Thin Solid Films*, 123 (1985) 63.

[25] G. Smestad, A. Ennaoui, S. Fiechter, H. Tributsch, W. K. Hofmann and M. Birkholz, *Solar Energy Materials*, 20 (1990) 149.

[26] H. Morikawa, *Jap. J. Appl. Phys.*, 11 (1972) 431.

[27] A. F. Trotman-Dickenson (Executive Ed.), *Comprehensive Inorganic Chemistry*, Vol. 3, Pergamon Press, Oxford (1973), 16.

[28] N. N. Green Wood, A. Earnshaw, *Chemistry of Elements*, Maxwell Macmillan International Edition, p. 1386.

[29] A. F. Trotman-Dickenson (Executive Ed.), *Comprehensive Inorganic Chemistry,* Vol. 3, Pergamon Press, Oxford (1973), 17.

[30] M. A. Korzhuev, N. K. Abrikosov and V. F. Bankina, *Sov. Tech. Phys. Lett.*, 10 (1984) 627.

[31] M. A. Korzhuev, *Tech. Phys.*, 43 (1998) 1333.

[32] H. Morikawa, *Jap. J. Appl. Phys.*, 11 (1972) 431.

[33] M. A. Korzhuev, B. A. Efimova, E. A. Obraztsova and O. P. Fedorova, *Phys. Status Solidi A*, 124 (1991) 115.

[34] K. Hauffe, *Oxidation of Metals*, Plenum Press, New York (1965) p-336, 118.

[35] M. A. Korzhuev, N. K. Abrikosov and I.V. Kuznetsov, *Sov. Phys. Tech. Phys.*, 31 (1986) 484.

[36] M. A. Korzhuev and A. V. Laptev, *Sov. Phys. Tech. Phys.*, 29 (1987) 1524.

[37] M. A. Korzhuev and A. V. Laptev, *Sov. Phys. Tech. Phys.*, 34 (1989) 419.

CHAPTER – 5

Iron pyrite thin films

5.1 Introduction

High production cost of solar cell materials is the major factor that limits the commercial applications of photovoltaic cells. In such a context, much attention has been given on highly absorbing photoactive semiconductors that are abundant and nontoxic. Today the widely used material is crystalline silicon. This material poses no direct problems for the environment, but has the disadvantage of high material consumption and high-tech material processing. It is said that for 1 GW photovoltaic instillation, approximately 8000 tons of high quality silicon is required. The other leading materials of this field viz. GaAs, CdTe or $CuInSe_2$ have the disadvantage of containing toxic substances such as Cd, Te, Ga, In or Se which makes them less attractive for mass production.

Iron pyrite is an eco-friendly material that is abundant in nature. It is a promising candidate with a minority carrier diffusion length much larger than its absorption length (200 Å at 2 eV) [1] and higher carrier mobility even in thin film form (200-300 cm^2/Vs) [2]. In the visible range this material has a high absorption coefficient (α) of 6×10^5 cm^{-1} [3-5]. Table (5.1) gives the comparison of this material with the other known absorbers. Fig.(5.1) shows the absorption length ($1/\alpha$) of FeS_2 in comparison with other semiconductor materials [6]. With such a high absorption coefficient this material is projected as the most suitable material for sensitisation type solar cells [7].

	C-Si	a-si :H	$CuInSe_2$	$CuInS_2$	FeS_2
Energy gap (eV)	1.1	1.5-1.8	0.95	1.53	0.95
Absorption co-efficient α $(cm)^{-1}$ at 2 eV	5×10^3	3×10^4	2×10^5	2×10^5	6×10^5
Absorption length α^{-1} (Å)	2×10^4	3.3×10^3	5×10^2	5×10^2	1.7×10^2
Quantum efficiency %	25	-	25-30	20	80-90

Table (5.1)   Comparative data of FeS_2 related to few well known absorber materials

5.2 Properties of iron pyrite

Unless specially mentioned, the term 'pyrite' refers to iron pyrite (FeS_2), even though the term actually refers to a particular structure. FeS_2 generally crystallises in a pyrite structure, which can be visualised by replacing the Na atoms in the NaCl structure with Fe atoms and Cl atoms by sulfur dimmers. It also crystallises in marcasite structure, an orthorhombic modification present in nature. Marcasite phase often appears during preparation of pyrite, but it can be converted to pyrite by annealing the sample under sulfur atmosphere at high temperature. Fig.(5.2) shows the phase relation of Fe-S system [6].

Optical band edge reported for this material has a very wide range [5,8,9]. I. J. Ferrer et al. [5] has summarised the values in the form of a table, Table (5.2). This unusual behaviour is due to the fact that the general expression to determine the band gap nature and the value of E_g (given below) is not applicable for this semiconductor.

$$(\alpha h v)^n = A \ (hv - E_0),$$

E_0 being the transition energy (E_0 is E_g for direct transitions, $E_0 = E_g \pm E_p$ for indirect transitions, where E_p is the energy of the associated phonon) and n depending on the transition type, n = ½, ⅓, 2 or ⅔ for allowed indirect, forbidden indirect, allowed direct and forbidden direct transitions respectively. This equation is defined to describe electronic transitions in semiconductors between parabolic bands [10-12]. But this is not the case with pyrite. From band structure calculations carried out by Bullett [13], it is known that the top of the conduction band is rather flat. Hence as the pyrite band edges are different from those of ordinary semiconductors, it might be necessary to modify the simple equations used to investigate direct or indirect transitions.
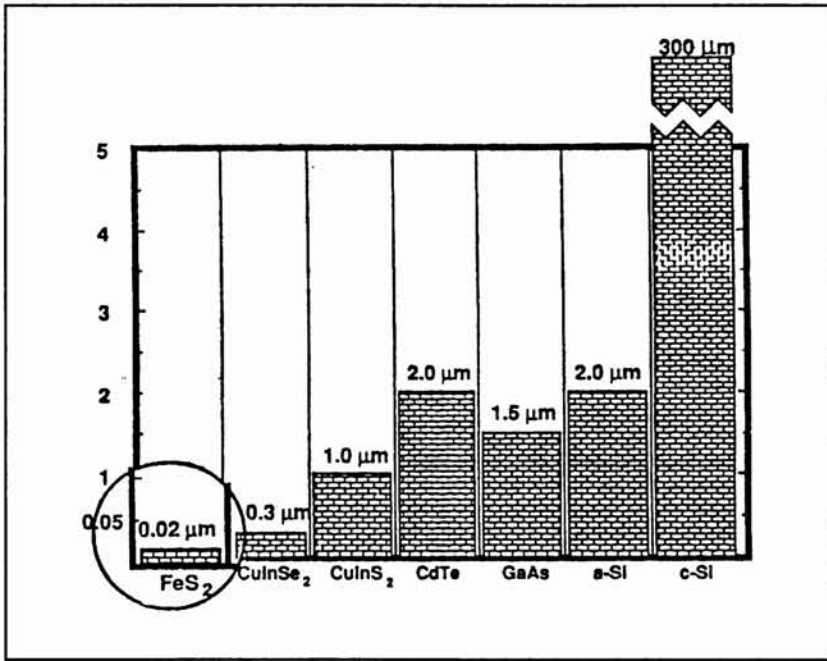
Fig.(5.1)   Comparison of the absorption length for different semiconductor
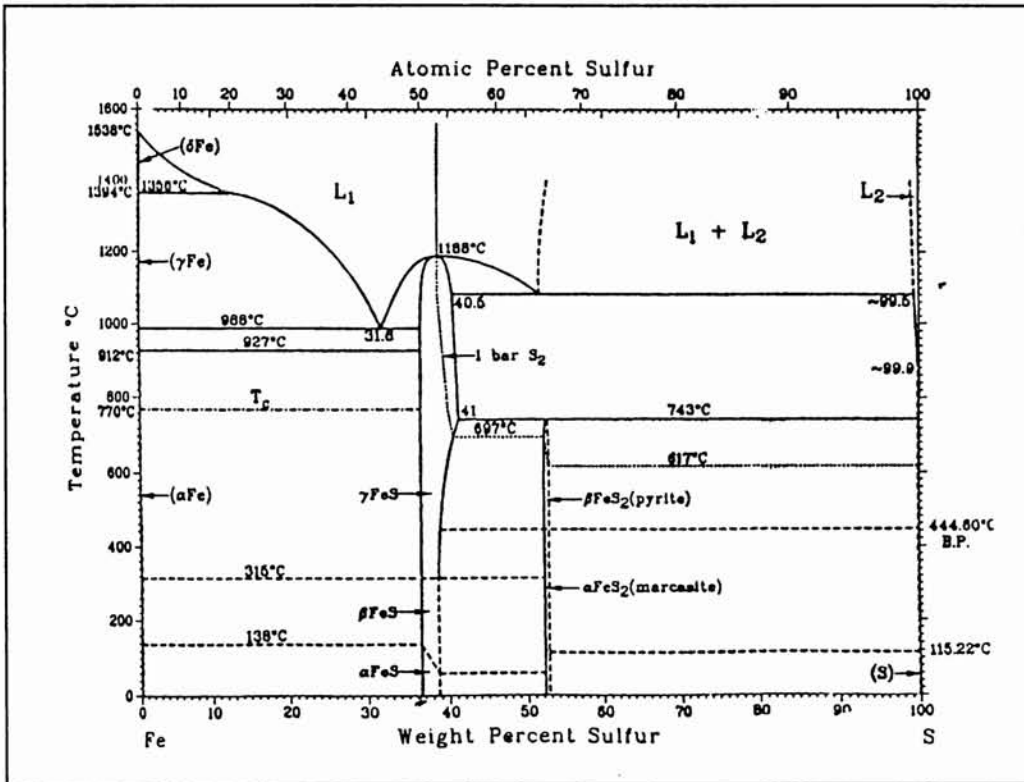   materials.


Fig (5.2)   Phase relations in the Fe-S system

E_a (eV)	Transition type	Experimental Technique	Sample nature
0.9		photocurrent	natural and synth. single crystal
0.95	indirect	quantum efficiency	natural and synth. single crystal
0.9		reflectance	natural and synth. single crystal
0.95		reflectance	natural single crystal
0.96	allowed indirect	optical absorption	natural single crystal
1.6	indirect	reflectance	natural single crystal
0.9	direct	reflectance	synthetic samples
0.84 1.03	indirect direct	quantum efficiency	synthetic samples
0.9 0.84		quantum efficiency	single and polycrystal
0.95	indirect	quantum efficiency	thin films
2.62 1.45 1.05	direct indirect	transmittance	thin films
1.95 1.12	forb. direct forb. indirect	transmittance	thin films
1.82	indirect	absorption coefficient	thin films
1.5 0.6	direct indirect	absorption coefficient	thin films

Table(5.2)   Reported values of Eg and corresponding transition type of pyrite (FeS$_2$)

In a chemical vapour transport (CVT) sample, typical Hall mobility of electrons was in the range of 230-366 cm^2/Vs and carrier concentration in the order of 10^{16}cm^{-3}. A very high electron mobility of 1000 cm^2/Vs was observed at a low temperature of 150 K. Though n-type conduction is usually reported [14-15], there are

also reports of p-type conduction [16-19] in pyrite. The electrical resistivity of this material is reported as a few Ωcm [20].

Pyrite when acting as an electrode in electrochemical cell [6] reacts with water to produce Fe^{3+}, SO_4^{2-}, H^+ and electrons according to the reaction

$$FeS_2 + 8 H_2O \rightarrow Fe^{3+} + 2 SO_4^{2-} + 16 H^+ + 15 e^-$$
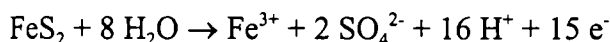
Under illumination and in the absence of electron donors such as Br^- or I^-, the material photo corrodes via. holes. The reaction is

$$FeS_2 + 8 H_2O + 15 h^+ \rightarrow Fe^{3+} + 2 SO^{4-} + 16 H^+$$
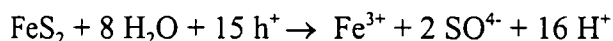
In the presence of electron donor species, the system will have kinetic stability. Pyrite has only a very narrow stability domain. This is obvious from Fig.(5.3) which represents the potential-pH diagram for iron-sulfur-water system. Solid lines enclose the areas of stability for the solid phase and the dashed lines define the equilibrium between solution species.

Electrochemical treatment of atomic hydrogen based on the proton reduction was found to be effective in increasing the photo effect. Hydrogen interaction with both the pyrite surface and the bulk plays a significant role. Electrochemical treatment is an etching process by which impurities such as FeS can be eliminated (by H_2S formation) or oxygen can be removed from the surface. In addition, neutralization of bulk defects by insertion of hydrogen also occurs.

5.3 Iron pyrite based solar cells

Pyrite is comparatively a new material in the field of photovoltaics and for the same reason cells based on this are still on trial basis. Few of the reports that have appeared on this material in this field are summarised below.

5.3.1 Photo electrochemical solar cells

Generally in photo electrochemical solar cells (PEC) based on semiconductors like Si, GaAs, etc., there are severe thermodynamic restrictions for stability. However in FeS_2 these restrictions are minimized to a great extend due to the fact that photo excitation in this material involves a non-bonding electronic transition that avoids breaking of bonds.

A PEC based on n-type FeS_2 with high quantum efficiency and high stability in presence of I^-/I^{3-} redox couple has been reported [20-22]. Fig.(5.4) shows the photocurrent action spectrum across an n-FeS_2/electrolyte (5M KI) interface. The measured quantum efficiency at the maximum of spectral sensitivity exceeds 90%. This indicates the possibility of using this material for solar energy conversion.

Figure (5.5) shows the output characteristics of a similar cell at 100 mWcm^{-2} illuminations. The electrolyte used was 4 M HI, 0.05 M I_2 along with 2 M CaI_2. This cell reported a conversion efficiency of 2.8% [6].

A correlation between photovoltage and S/Fe ratio is shown in Table (5.3). Here I_{ph} and I_d are photocurrent and dark current respectively. The best results were obtained for a S/Fe ratio close to 2 (in these cases Zn was used as the dopant).

S:Fe	Zn Conc. ($\mu g/g$)	Voc (mV)	I_{ph}/I_d
1.98	2300	208	74
1.96	2000	193	165
1.94	3400	176	70
1.88	4500	160	15

Table (5.3)   Correlation between photo voltage and S/Fe ratio.

In all these cells the limiting factor for high efficiency is the high dark current, which leads to a small photovoltage.

5.3.2 n- pyrite/ metal Schottky barriers

Different n-FeS_2/metal schottky barriers (metals like Pt, Au or Nb) were fabricated by depositing transparent metal films (50-120 A^0) on top of an electrochemically etched pyrite surface [6-23]. This was performed in vacuum by electron beam evaporation or chemical vapour transport. A schematic cross section of a pyrite diode prepared in this manner is given in Fig.(5.6).

In spite of considerable reverse current (15 mA/cm^2 at 0.7V) and poor rectifying behaviour at room temperature (j $_{forward}$/j $_{reverse}$ = 25 at 0.7 V), the n-FeS_2/Pt-barrier shows high short circuit photocurrents reaching values of 30 mA/cm^2 and saturation photo currents of 100 mA/cm^2 under illumination of 200 mW/cm^2, Fig.(5.7). The spectral response of this diode showed quantum yields of 40% and
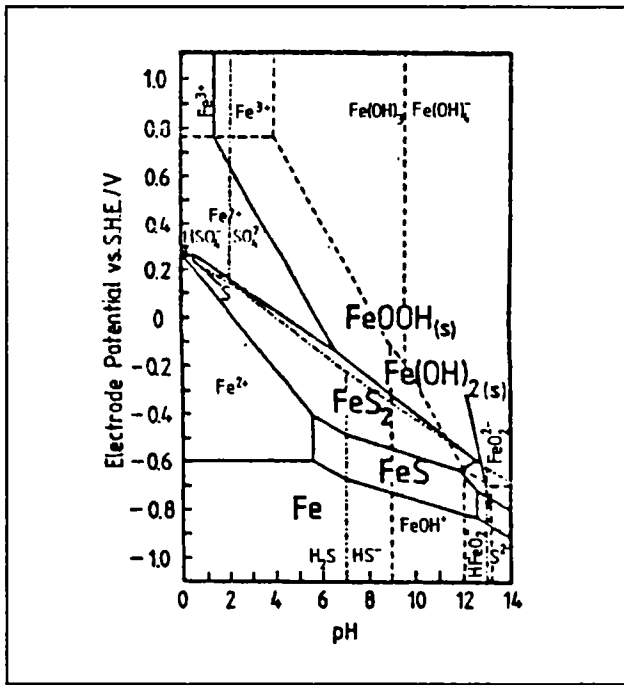
Fig.(5.3)   Potential – pH diagram for the iron-sulfur-water system at 25⁰C
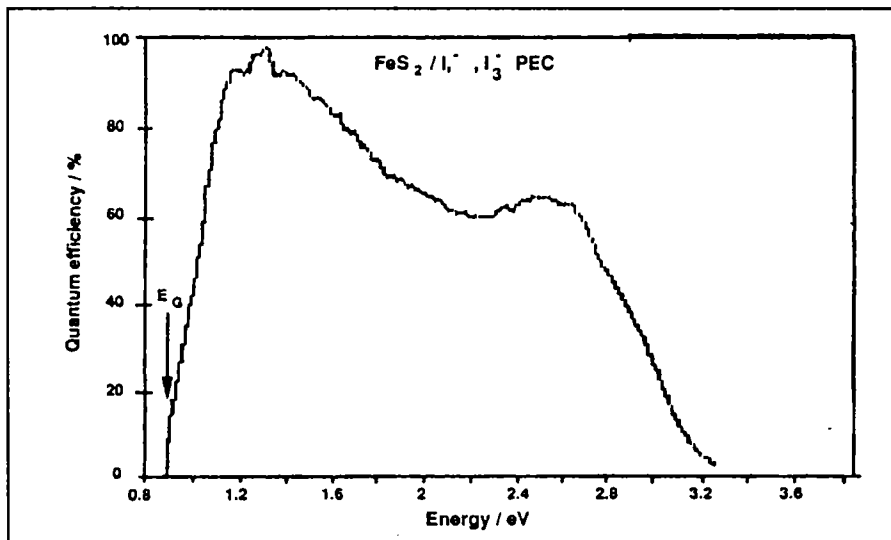

Fig.(5.4)   Quantum yield and spectral dependence of
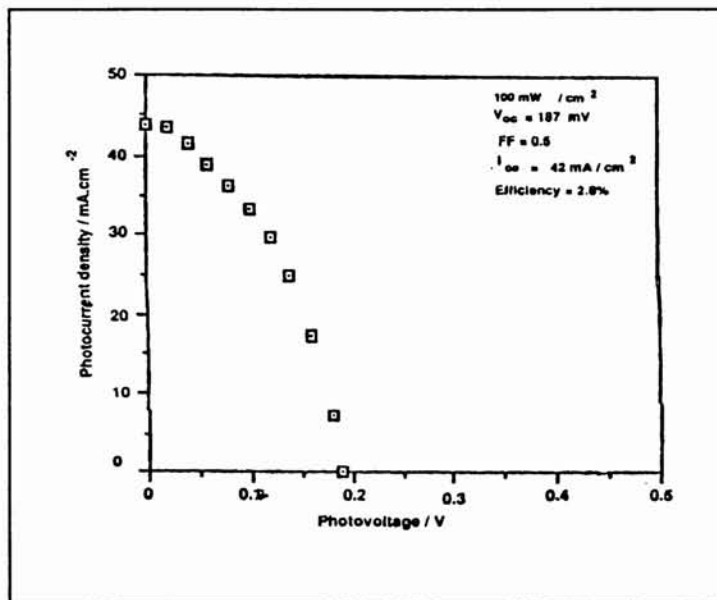photoelectrochemical cell using iodine/iodide   electrolyte

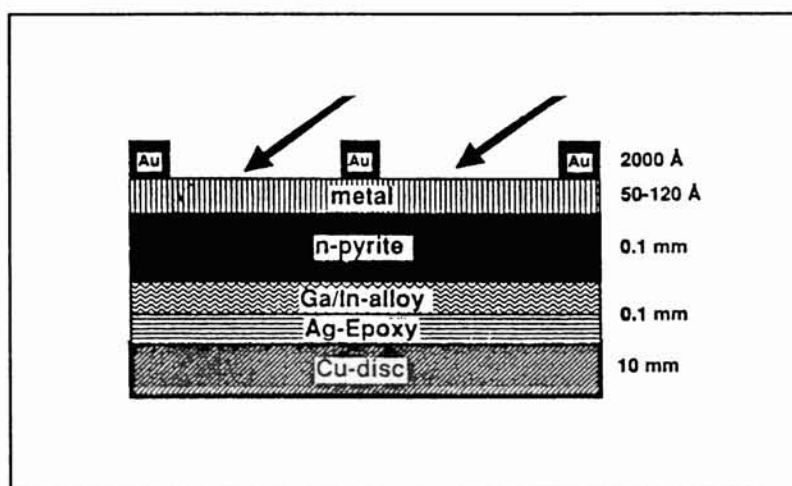Fig.(5.5)   Power output of a photo electro chemical cell using iodine/iodide electrolyte

Fig.(5.6)   A schematic cross section of a pyrite/metal diode

70%, at 1.3 eV photon energy under short -circuit and bias condition (0.7 V) respectively. A high density of bulk defects (viz. sulfur deficiency) and surface states were the factor that limited the junction performance [24].

5.3.3 Thin layer solar cell

Improvements in FeS_2 films have lead to development of thin film based solar cells with a p-i-n structure [6]. Here an ultra thin film (10-15nm) of pyrite is deposited on large band gap materials like TiO_2 WO_3, ZnO, etc. so that the visible and near infrared light is absorbed in the pyrite film. The strategy adopted is to develop a solar cell where the absorber layer of FeS_2 absorbs the visible light and injects the electrons into the conduction band of large band gap material. Thus generating a photovoltage. The reaction of holes occurs with an electron donating electrolyte. Or in other words, an appropriate redox electrolyte reacts with the holes like a p-type contact. Such a p-i-n device, where a very thin layer of intrinsic pyrite is sandwiched between suitable p and n-type window material, is capable of converting light into electrical energy. Fig.(5.8) shows such a $TiO_2/FeS_2/electrolyte$ interface. In contrast to a conventional p-n junction where the device absorbs light as well as transport the charge carrier, the pyrite-sensitised device separates the function of light absorption and carrier transport. This type of cell was tried by Ennaoui et al.[7] and Fig.(5.9)] shows its reported photoresponse. In that study it was found that FeS_2 layers thicker than $150A^0$ decreases the photo effect drastically.

5.4 Methods of preparation of iron pyrite

The various methods of preparation of FeS_2 as reported in literature are summarized in the form of a table, with mention to references.
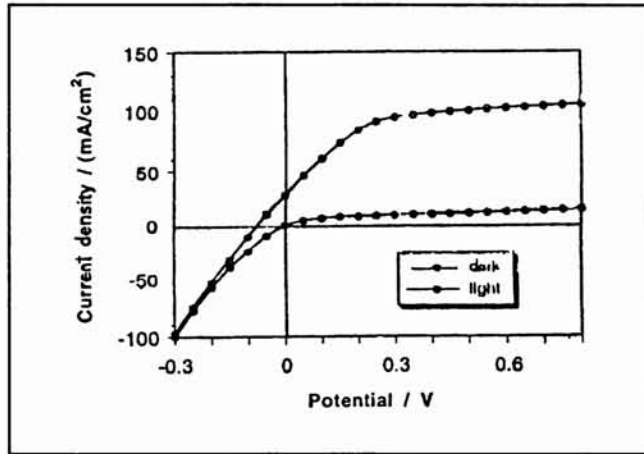
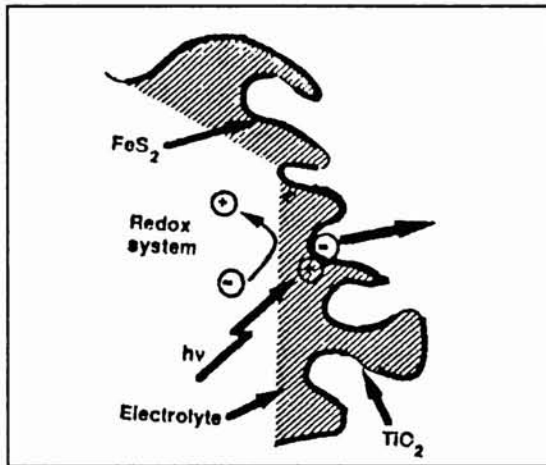Fig.(5.7)   Current–voltage characteristics of a pyrite/Pt diode

Fig.(5.8)   Schematic morphology of the TiO_2/FeS_2 contact
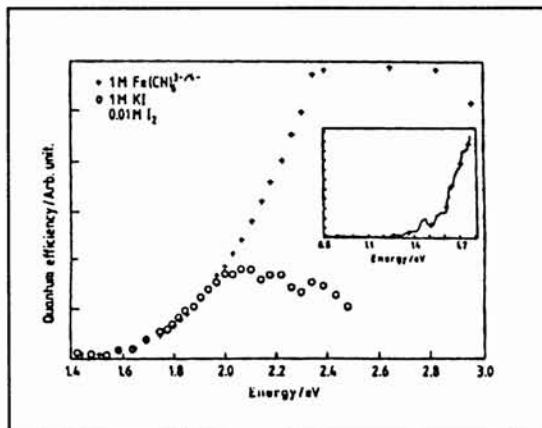showing electron injection

Fig.(5.9)   Photo voltage vs. time for an electrode in the
presence of an iodine/iodide electrolyte

Method of preparation	Properties/Studies/Observations
A. Sulfurisation of iron film [17,25-30] Ref.[17], thermal evaporation of iron powder on glass substrate at 200^0C; sulfurisation under nitrogen flux for 30 min.; Fe film kept at 280^0C and sulfur source at 180^0C.	Resistivity – $10^{-2}\Omega$ cm; p-type conduction; band gap of 1.45 eV (direct) and 1.31 eV indirect.
B. Sputtering [18,31-32] Ref.[18], magnetron sputtering; FeS_2 target of 99.9% purity; sputtering gas of sulfur plasma and small quantities of Ar.	Conductivity - $4\Omega^{-1}cm^{-1}$; Carrier density -$5x10^{18}$ cm^{-3}; Mobility - 5 $cm^2V^{-1}s^{-1}$ p- type conduction Sulfur content - 60 to 65%
C. Vapour phase epitaxial growth (VPE) [33] Substrate-natural pyrite at 595^0C; transport agent–bromine; source-mixture of FeS_2 and ZnS powder; source temperature 590^0C; duration of deposition-1 week.	MPSM (Microwave photoconductivity scanning microscope) studies.
D. Flash evaporation [30,34] Ref.[34], source- natural pyrite powder of size 50-75 μm; pressure-10^{-5}Torr; source temperature-1400^0C; substrate-glass or SnO_2 coated glass; substrate temperature ~120^0C.	Annealing in an inert atmospheric leads to loss of sulfur; $Fe_{1-x}S$ phase transfers to FeS_2 by annealing in sulfur atmosphere; sulfur pressure-500 torr, time of sulfurisation-120 min., temperature 350^0C; as-prepared resistivity-$2x10^{-2}\Omega$cm sulfurised resistivity-$2x10^{-1}\Omega$cm; optical absorption-$2x10^5$ cm^{-1} at hv > 1.5 eV.

E. MOCVD [7,35-37] Ref[35], deposition of iron by decomposing iron pentacarbonyl onto a hot substrate, in the presence of hydrogen sulfide gas; source temperature 25^0C; reaction pressure 1000 mbar; growth temperature ~ 140^0C.	For substrate temperature greater than 170^0C, conductivity greater than 10^3 $(\Omega cm)^{-1}$; TRMC (Time Resolved Microwave Conductivity) measurements.
F. Electrodeposition [38] Direct electrodeposition of Fe and S in an aqueous solution of $FeSO_4$ and $Na_2S_2O_3$ on titanium sheets for 60 min; pH adjusted using H_2SO_4; post annealing in sulfur atmosphere in 40 min. around 500^0 in nitrogen atmosphere.	EPMA analysis showed Fe/S ratio to be around 1; XPS analysis revealed the formation of FeS; stoichiometric poly crystalline pyrite thin films were obtained after post annealing in sulfur atmosphere.
G. CVT (Chemical Vapour Transport) [3,39] Ref.[3], FeS_2 powder prepared by ampule synthesis; 2 g FeS_2 powder and 5 mg As dopant taken in quartz ampule: pressure 10^{-5} mbar along with 0.5 mg/cm^3 bromine; FeS_2 powder heated to 800^0C and the powder free end to 550^0C for 10 days, the next 10 days the temperature gradient is reversed to get pyrite.	Absorption co-efficient at 632nm-6.4x10^5 cm^{-1}; Eg-0.95 eV (indirect); complex refractive index n = 4.032-3.245i at 632.8 nm. It was found that light is absorbed within a layer of $160A^0$ of FeS_2.
H. Spray pyrolysis [40-42] Ref.[40], spray solution-0.03 M, x ml $FeCl_3$ and 2.24 x ml thiourea; carrier gas nitrogen; temperature of substrate-350^0C, vacuum- 28 inch Hg; duration of spray-30 min; evaporation of free sulfur was also done to reduce the oxygen partial pressure.	Resistivity- 0.16 Ωcm; presence of impurity phase of $Fe_{1-x}S$; band gap 0.82 eV (indirect), absorption coefficient-1.6x10^5 cm^{-1} at 850 nm; doping with ruthenium found to be good; photoconductivity studies.

I. CBD (Chemical Bath Deposition) [43] Ref.[43], prepared in organic medium; 0.02 M iron pentacarbonyl mixed with 0.04 M sulfur dissolved in 250 ml xylene under argon atmosphere; temperature of deposition-140^{0}C; time of deposition-few minutes.	X-ray fluorescence study reveled Fe-33.45%, S-66.55%; TRMC, ICP-MS and SEM studies; in a photo electrochemical setup with an electrolyte of HI, CaI$_2$ and I$_2$, they showed good photoelectric behaviour with high quantum efficiency.
J. Sulfurisation of iron oxide film [44] Ref.[44], reaction of Fe$_3$O$_4$ or Fe$_2$O$_3$ with elemental sulfur vapour in open or closed ampoules; temperature of sulfurisation-350^{0}C; duration of sulfurisation 0.5-2hrs.	p-type conduction; band gap-1.3eV (direct), 0.93 eV (indirect); conversion of Fe$_3$O$_4$ to pyrite found easier.

5.5 Preparation of iron pyrite thin film using CBD technique

In the present work preparation of iron pyrite (FeS$_2$) thin films was tried using chemical bath deposition technique in aqueous medium. This chapter summarises the various attempts made to prepare stoichiometric pyrite films. The complete work done on this material is presented, highlighting various stage of development.

Glass slides were first washed in soap solution and then in freshly prepared chromic acid solution, so as to remove the oil particles. It was then washed in running water and later ultrasonic cleaning was done. Once again it was washed in double distilled water and dried in an oven. This formed the substrate for thin film deposition. On few instances SnO$_2$ coated glass substrates were also tried and the details regarding preparation of SnO$_2$ layer is already included in section (2.2.2).

5.5.1 Stage :1

Ferric chloride (FeCl$_2$) was chosen as the Fe source and thiourea [CS(NH$_2$)$_2$] as the sulfur source. In order to control the rate of reaction between these two reagents, it was necessary to complex the Fe ions. Triethanol ammine (TEA) was

selected as the suitable complexing agent. The complex was then dissolved in ammonium hydroxide solution before addition of thiourea under constant mechanical stirring. Cleaned glass substrates were introduced into the beaker in vertical position. The reaction mixture was maintained at a constant high temperature. The expected reaction was

$$2[Fe(TEA)]^{3+} + 4\ CS(NH_2)_2 + 8\ OH^- \rightarrow 2\ FeS_2 + 2\ TEA + 4\ CO(NH_2)_2 + 4\ H_2O$$
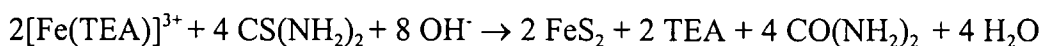
After trying a large number of permutations and combinations of deposition parameters like concentration of reactants, temperature of deposition, duration of deposition, etc., the final procedure adopted was as follows: To 10 ml of 1 M $FeCl_3$ solution, 5 ml of TEA was added and stirred well. 20 ml of NH_4OH solution was added to this in order to dissolve the iron complex. Later 10 ml of 1M Thiourea was mixed with stirring. The duration of deposition was about 80 minutes at 70^0C. After deposition the samples were washed in water and dried in hot air. The resulting film had a brown colour. Thickness measured by gravimetric method was around 0.4 μm for single dip.

Optical absorption studies conducted on these samples showed a direct band gap of 3.1 eV and indirect band gap of 1.84 eV. Though iron pyrite has a very wide range of reported band gaps as shown in Table (5.2), these values were found to be higher than all the reported values. The resistivity of this material was found to be higher than the expected value by a few orders of magnitude (Ry~$10^7\Omega$ cm). XRD analysis done on this thin film revealed the amorphous nature. These samples were annealed at various temperatures ($100-350^0C$) in air as well as in vacuum, inorder to improve the crystallinity. But this yielded no results, except for the fact that the films got completely cracked at high temperature. Fig.(5.10) shows the SEM micrograph of such a sample under 1K magnification when annealed at 350^0C in vacuum.

The elemental analysis of this as-prepared phase was also done. Figure (5.11) shows the XPS depth profile done using X-rays from Al anode operated at 3 kV. The bottom layer of the figure corresponds to the surface layer of the film while the top region refers to the SiO_2/glass substrate. The X-axis gives the binding energy in eV, while each horizontal line corresponds to the signal collected after each etching cycle. The binding energies of 2p $_{3/2}$ of Fe at 710 eV, $2p_{1/2}$ of Fe at 72.5 eV and 1s of O at 530 eV, along with the absence of any sulfur signal reveals the formation iron oxide [45] and not iron sulfide. Binding energy of surface oxygen at 532 eV corresponds to
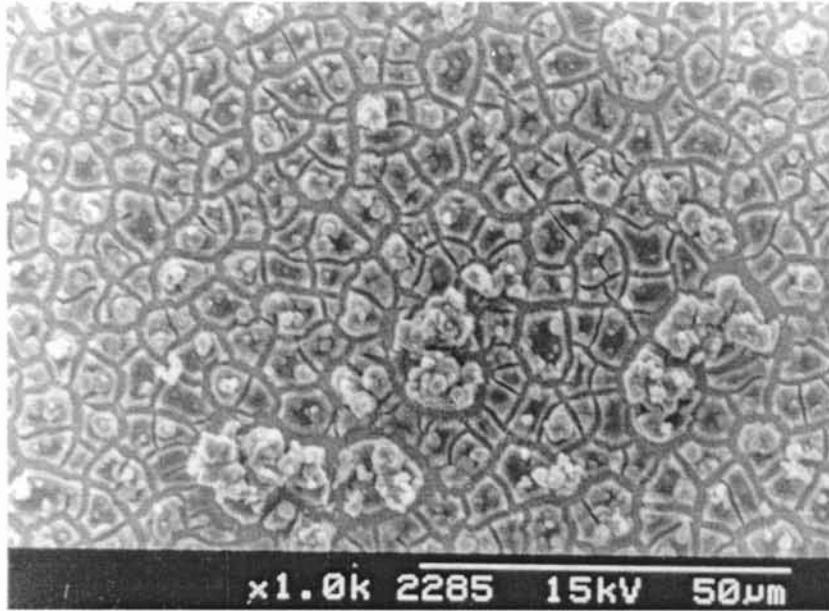
Fig (5.10)   SEM micrograph of as-prepared film annealed at
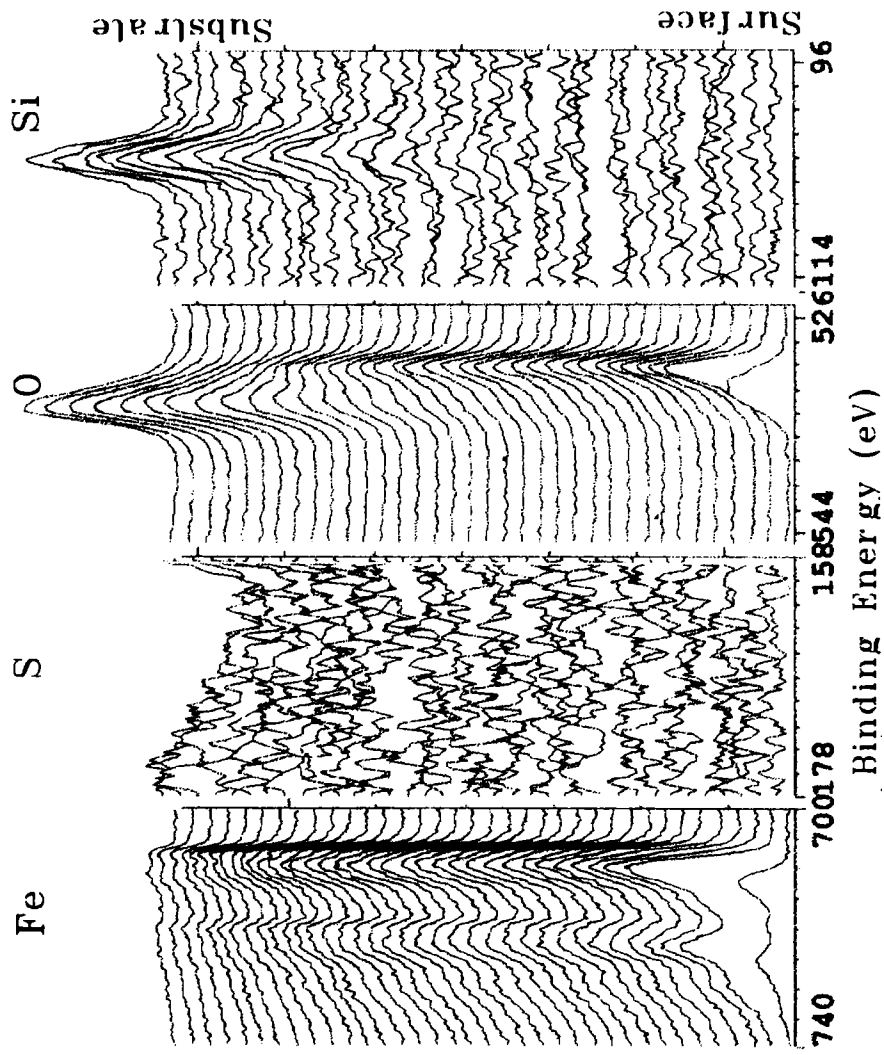350^0C in vacuum

Fig.(5.11)   XPS depth profile of as-prepared film of stage:1

physisorbed oxygen [46]. Figure (5.12) shows the atomic concentration of this depth profile. It is obvious that this oxide phase of iron contains iron double than of oxygen.

The as-prepared films from 1 M $FeCl_3$ and 1M Thiourea were thus found to be uniform film of iron oxide rather than iron sulfide.

5.5.2 *Stage: 2*

As a next stage of trial, the relative concentration of iron in the CBD reaction mixture was reduced to half. Here 10 ml of 0.5 M $FeCl_3$ was made to react with 10 ml of IM Thiourea. 3 ml and 5 ml of TEA and NH_4OH respectively were used for controlling this reaction. Here the time of deposition was 1 hr. at 70^0C. The as-prepared films had a yellowish brown colour, unlike the earlier case. The thickness of these films was very less and gravimetric measurements proved this to be around 0.2 μm for first dip, 0.4 μm for second dip and 0.5 μm for third dip. The optical absorption studies showed a slight shift of band gap towards the earlier reported values. The plot of $(\alpha thv)^2$ versus hv plot revealed an indirect gap of 2.94 eV while the plot of $(\alpha thv)^{1/2}$ versus hv plot revealed an indirect gap of 1.67 eV (α stands for absorption coefficient, t the thickness of the film and hv the incident photon energy). This is shown in Fig.(5.13) and Fig.(5.14). From XRD analysis Stage:2 samples were also found to be amorphous.

As-prepared fresh samples were then analysed by XPS, after removing the surface layer by argon ion sputtering for 2 minutes. Strong signals of iron and sulfur with binding energies around 707 eV and 161 eV respectively was observed as in Fig.(5.15). This analysis of fresh sample was done at RSIC, Madras. Though the exact percentage composition of the material could not be evaluated, the stoichiometry was found to be poor. The same sample was analysed in Japan, after a period of two months. The XPS depth profile in Fig.(5.16) revealed interesting results. It was observed that sulfur signal was present only on the bottom layers. Iron sulfide was found to get converted to oxides of iron from the top surface towards the depth of the film. In the converted region Fe signal showed a B.E of 709.3 eV corresponding to iron oxide. In the inner layers of the film, Fe signal showed a slight kink 706.7 eV corresponding to FeS_2. The corresponding sulfur peak was at 160.4 eV.

The above results can be justified as follows: As the film preparation is carried out in an aqueous alkaline medium, there is chance of formation of small quantities of
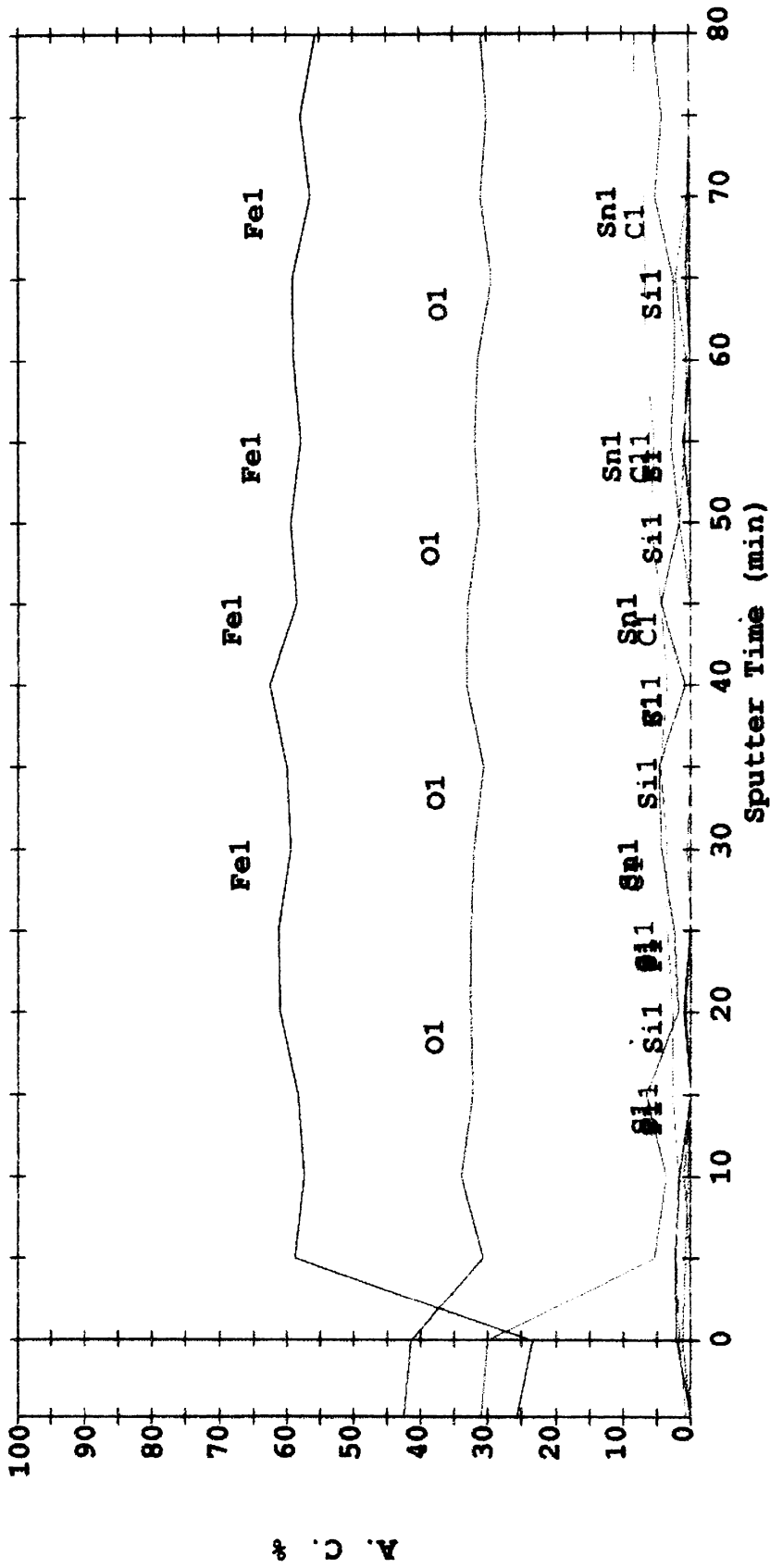
Fig.(5.12) Percentage composition of as-prepared film of stage: 1
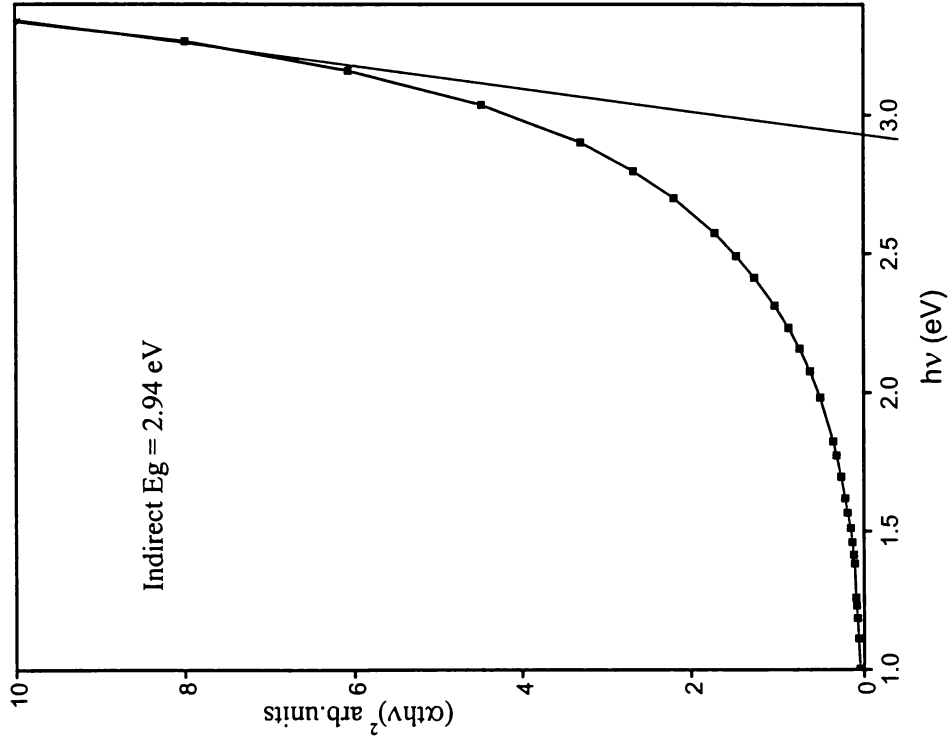
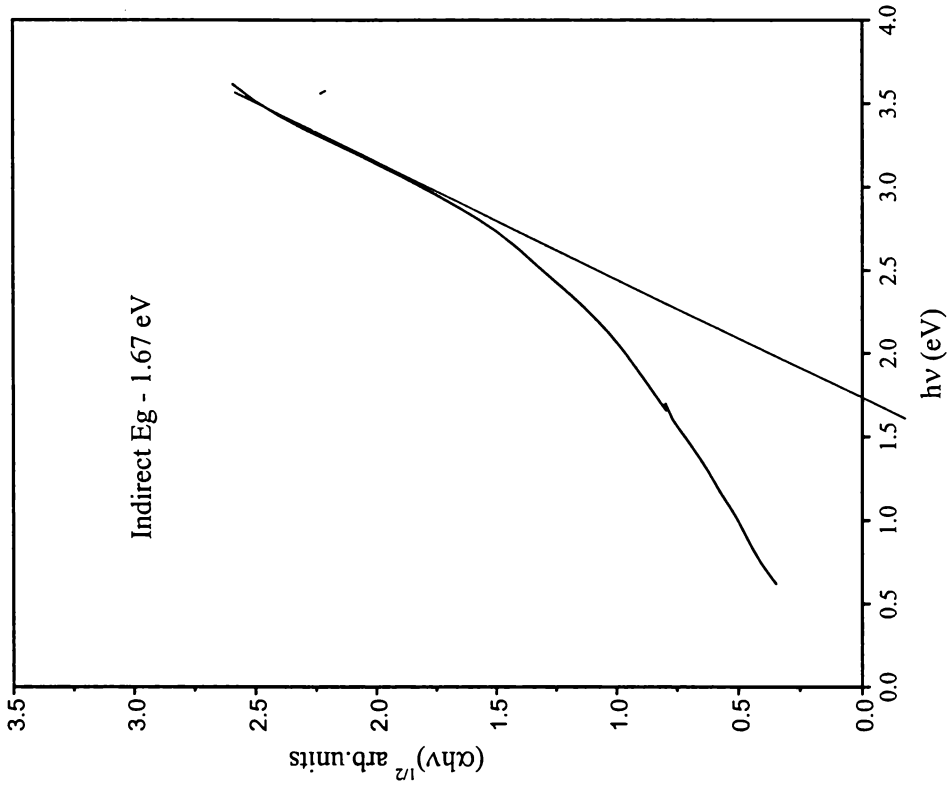Fig. (5.14) $(\alpha h\nu)^{1/2}$ vs. hν plot of as-prepared film of stage :2

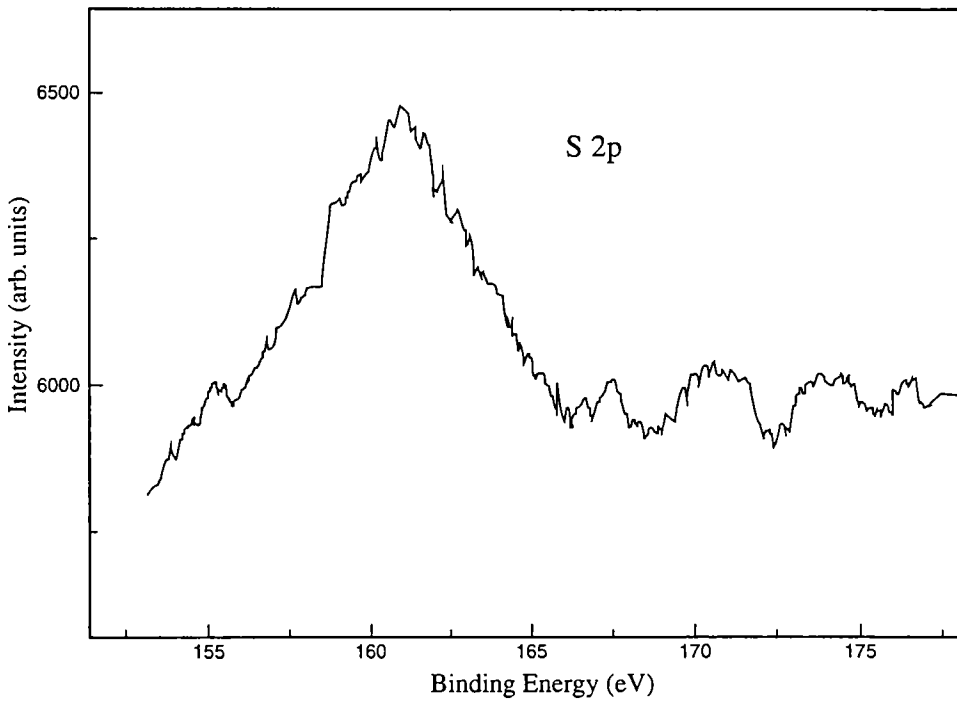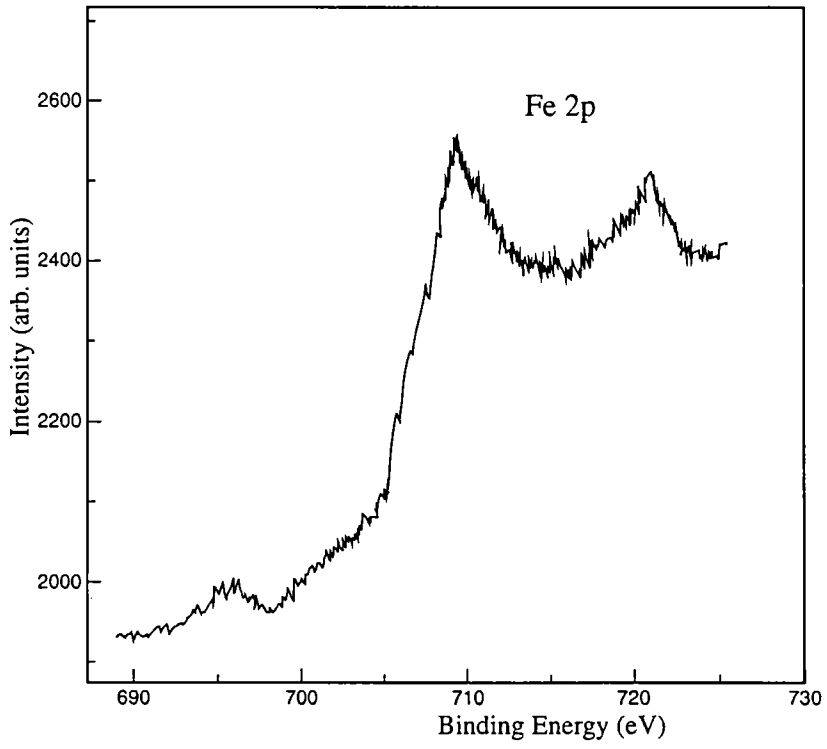Fig. (5.13) $(\alpha h\nu)^2$ vs. hν plot of as-prepared film of stage :2

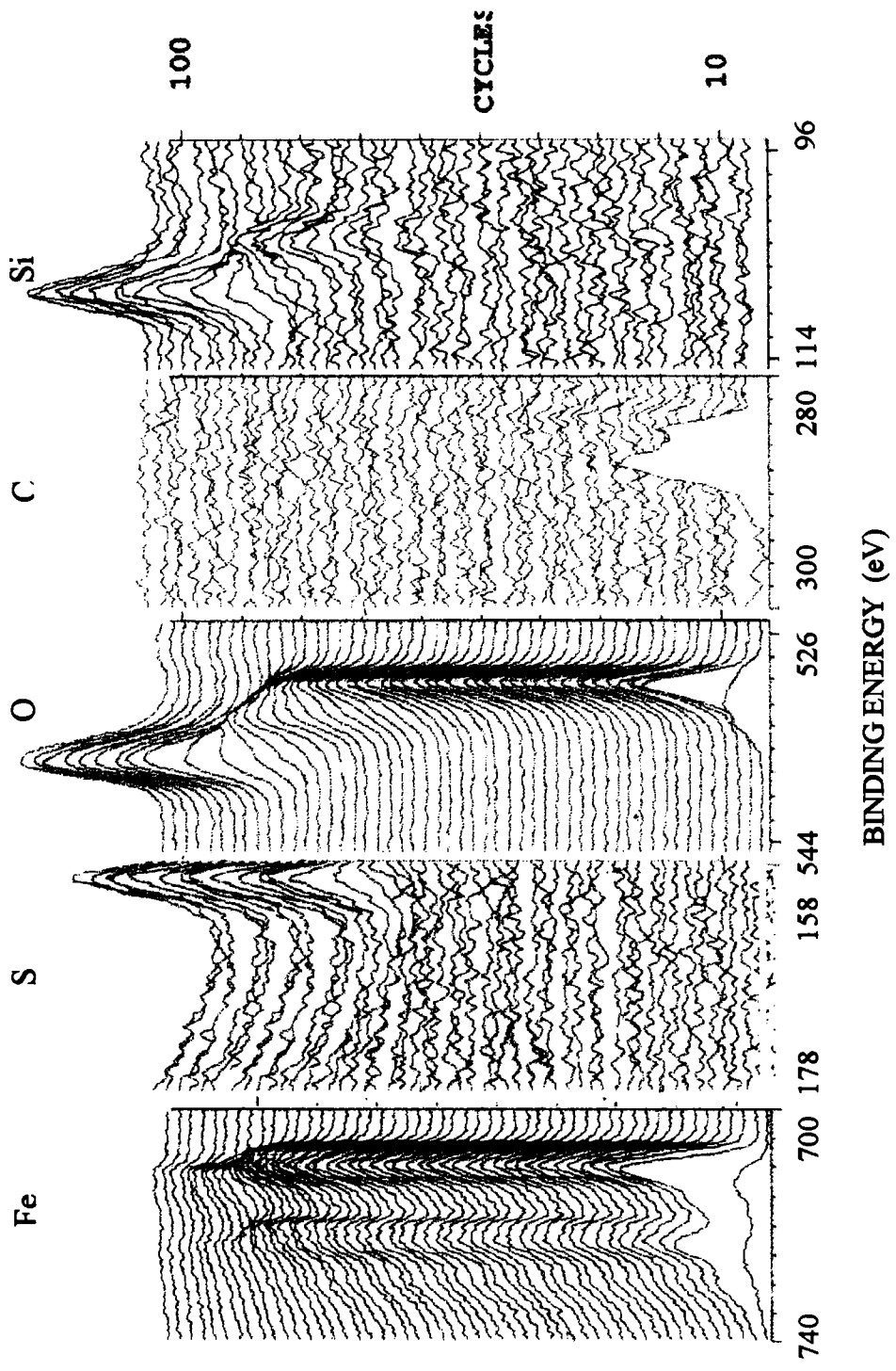Fig.(5.15)   XPS signals of stage : 2 thin films

Fig.(5.16) XPS depth profile the sample of stage: 2 after a period of 2 months

iron oxide impurity phase. This is possible as pyrite has a very narrow stability domain as shown in Fig.(5.3) [6]. This metal oxide impurity imparts hydrophilicity to the pyrite film [46]. This lead to the slow corrosion of the already sulfur deficient phase of iron sulfide into oxides of iron. This hydrophilicity is obvious in the as prepared film, in the form of reduction of resistance by two orders of magnitude, when the film is kept in humid atmosphere.

Thus in Stage:2, with higher relative concentration of sulfur in the reaction mixture, it was possible to incorporate small quantities of sulfur to the as- deposited films. But disproportionate increase in sulfur resulted in no film formation. Stage:2 could only lead to a sulfur deficient pyrite phase which was found to be unstable in ambient conditions.

5.5.3 *Stage: 3*

Trials were done to substitute thiourea with more active sulfur releasing reagents like sodium sulfite and thioacetamide. Sodium sulfite was found to be highly reactive with iron and hence it was difficult to control the precipitation to get film formation.

With thioacetamide the reaction could be controlled after many trials. 10 ml of 0.25 M $FeCl_3$ was mixed with 2 ml TEA and 5 ml NH_4OH solution and stirred well. To this mixture 20 ml of 0.5 M thioacetamide was added. The reaction was complete within 20 minutes at a temperature of 70^0C. For considerable thickness, two or three successive dipping was required.

This sample when analysed by XPS (7 months after preparation), showed strong signals of iron and sulfur [Fig.(5.17)]. The 3p signal of Fe at 54.2 eV and the $2p_{3/2}$ signal of S at 161.7 eV supported the formation of iron sulfide [47]. But the atomic concentration (%) graph as shown in Fig.(5.18) revealed another major draw back. Here though 10% of sulfur was present on the surface, the concentration of oxygen through out the sample was found to be higher than the concentration of Fe. In all the other cases though oxygen was present, its concentration was always less than half the concentration of Fe.

In Sage:3, though the stoichiometry and stability of the as-prepared iron sulfide film is found to improve by choosing thioacetamide as sulfur source, this lead to increase in the concentration of oxygen impurity.
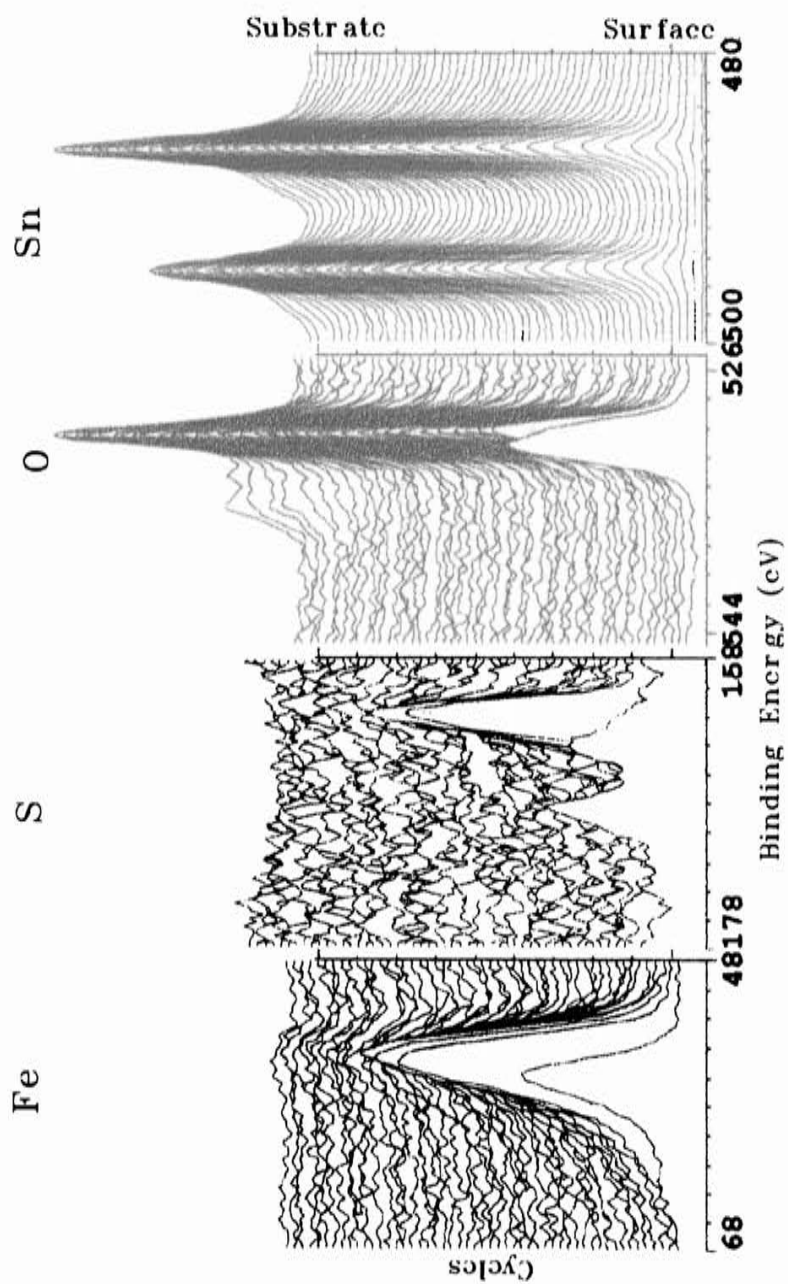
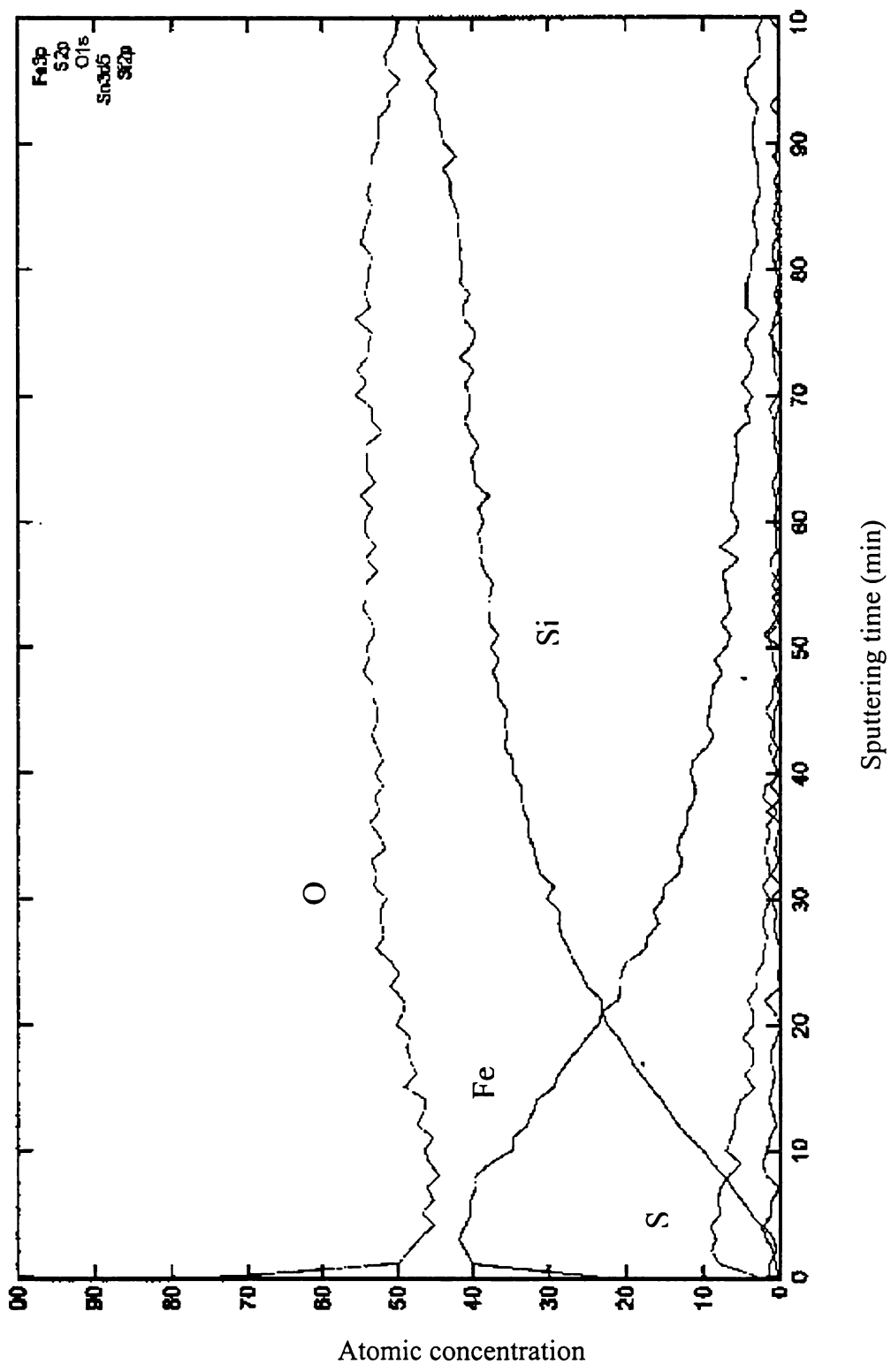Fig.(5.17)   XPS depth profile of thin film sample from stage:3

Fig. (5.18) Percentage composition from XPS analysis of sample from stage : 3

5.5.4 *Stage: 4*

In this stage, trial was done to improve the stoichiometry of the pyrite by applying a small potential to the substrate at the time of deposition. Sample were prepared from solution bath containing ferric chloride and thiourea as explained in Stage:2. SnO_2 coated glass was used as substrate, in order to apply a potential at the time of deposition. For the sake of comparison, samples were prepared with $-1.5V$, $+1.5V$ and $0V$ applied to the substrate. Thin film prepared under $+1.5V$ had a pale yellow colour, while sample under

$-1.5V$ had a deep brown colour. These samples were analysed using Secondary Ion Mass Spectroscopy (SIMS). Fig.(5.19) shows the comparative results of these samples. One general point noted in this analysis was the significant diffusion of SnO_2 in to the thin film surface. On comparing the figures in Fig.(5.19) it can be seen that the intensity or counts/sec of the sulfur increased from $2x10^3$ to $5.5x10^3$ on application of a positive potential, while a negative potential reduced the counts to $1x10^3$. The influence of potential on the iron concentration was found to be less and it remained in the range of 1×10^5 c/s

Hence in Stage:4 it was concluded that, though a positive potential could influence the sulfur concentration, it was not appreciable enough to be considered for preparation of stoichiometric iron sulfide.

5.5.5 *Stage: 5*

This stage involves the sulfurisation of iron oxide films from Stage:2. Sulfurisation of thin films is a very frequently used technique adopted for attaining the required stoichiometry of sulfides [48-51]. In the case of iron sulfide, it is already established that the path way to FeS_2 by the action of sulfur vapour on Fe_3O_4 or Fe_2O_3 is preferred to the path $Fe \rightarrow FeS \rightarrow FeS_2$ [44]. The Gibbs phase triangle of Fe-O-S system in Fig.(5.20), demonstrate equilibrium among oxide, sulfide and sulfate phase. When sulfur acts on any iron oxide, reaction similar to the following may happen.

$$2\,Fe_2O_2^{(s)} + 11\,S \rightarrow 4\,FeS_2^{\,(s)} + 3SO_2(g)$$

$$Fe_3O_4^{(s)} + 8\,S \rightarrow 3\,FeS_2^{\,(s)} + 3SO_2(g)$$
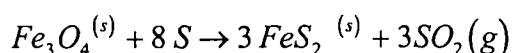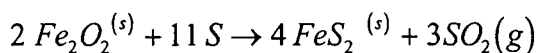
With these information in mind, a sulfur annealing chamber was fabricated, Fig.(5.21). It consists of two horizontal tubular sections, one the sample chamber and the other the sulfur powder chamber. Resistive heating could be given to both the
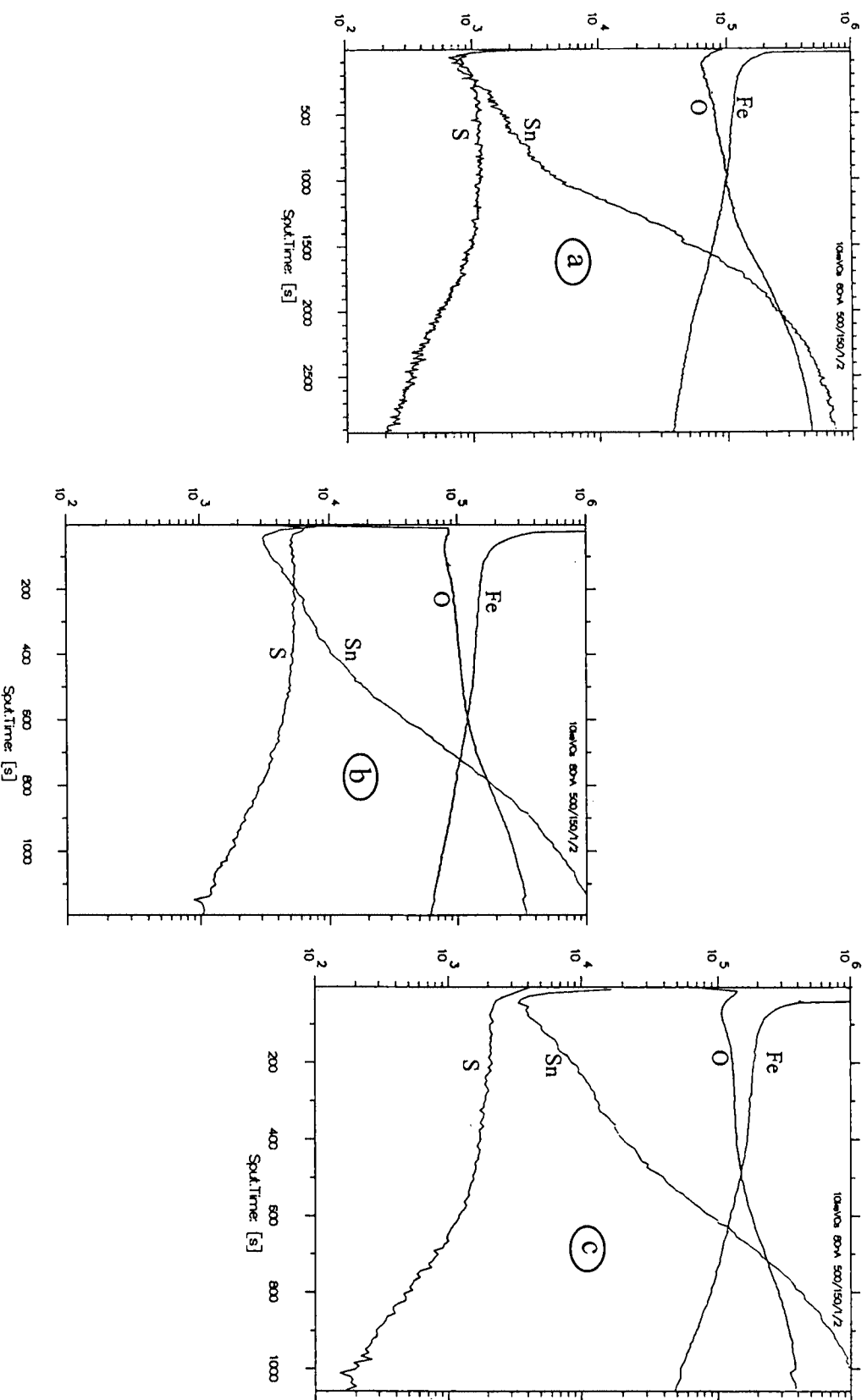
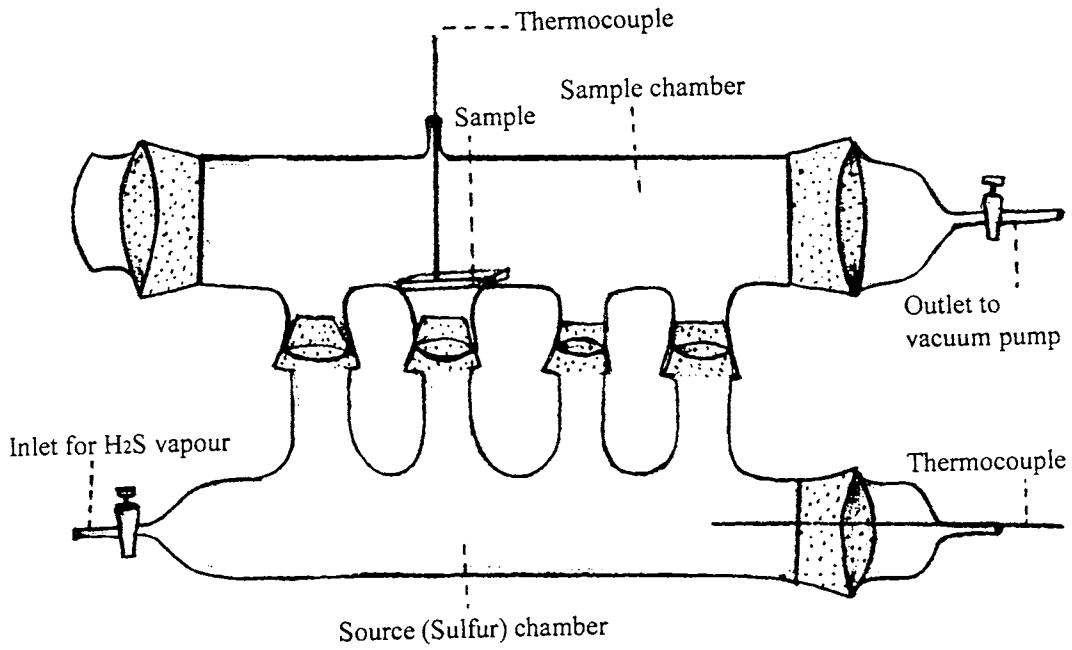Fig (5.19)   SIMS spectra (a) with −1.5V (b) with +1.5V (c) with 0V

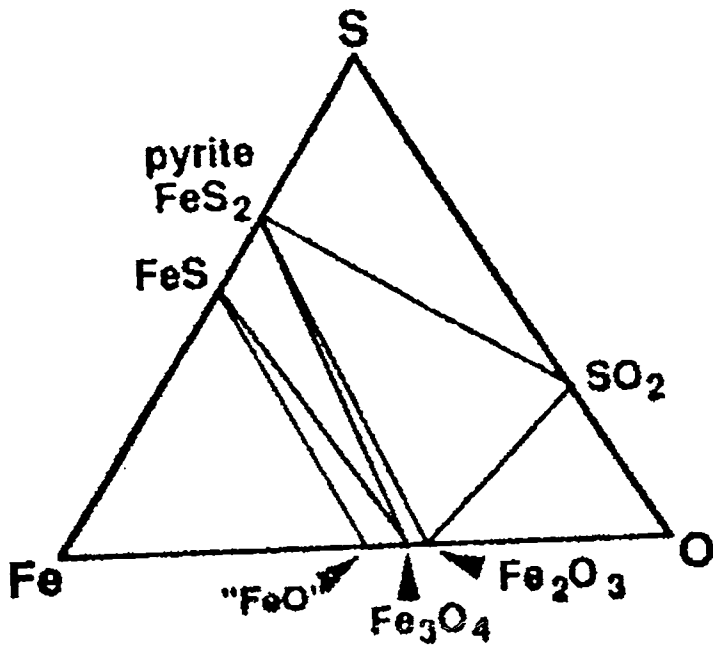Fig (5.21)   Schematic representation of sulfur annealing chamber

Fig (5.20)   Gibbs phase triangle of Fe-O-S system

sections separately. The sample chamber could be heated to 300^0C while the sulfur chamber to 200^0C. ,

Sample prepared in Stage:2 was the precursor for Stage:5. Sulfur powder was introduced into the sulfur chamber and heated prior to heating of the sample chamber. This helped to reduce the partial pressure of oxygen in the sample chamber. Initially, samples were placed in the sample chamber in such a way that hot sulfur vapour from the sulfur chamber could directly hit the sample surface(as shown in figure). But this arrangement was found to damage the film, when the duration of annealing was extended to few hours. Hence the samples were kept at the intermediate space in the sample chamber, where direct hit of hot sulfur vapour could be avoided. The sample chamber was heated in a slow manner and a thermocouple kept in contact with the sample was used to sense the temperature. Annealing was done at various temperatures like 110^0C, 150^0C, 190^0C, 200^0C, 220^0C, 230^0C and 270^0C. Duration of annealing was initially fixed at 1hr. The effect of this sulfur annealing process was monitored by optical absorption studies. From the initial studies it was decided to extend the duration of annealing to 2 hr, in order to make the effect of annealing more pronounced. It was observed that the direct band gap slowly shifted from the as-prepared value of 2.94 eV to 2.67 eV when annealed in sulfur atmosphere for 2 hrs at 200^0C. But further increase in temperature lead to an increase in the band gap. Fig.(5.22) shows a few of the selected graphs. Similarly, the indirect band gap shifted from the as prepared value of 1.67 eV to 0.97 eV when annealed at 200^0C for 2 hrs. As in the above case, further increase in annealing temperature in found to have reverse effect on indirect band gap. Figure (5.23) shows the $(\alpha thv)^{\frac{1}{2}}$ vs hv graph and the figurative results are given as the inset. From this study it was inferred that annealing at a temperature of 200^0C lead to the conversion of iron oxide to iron sulfide. But annealing above 200^0C in the presence of air leads to the formation of iron oxide once again. Figure (5.24) shows the scanning electron micrograph of a sulfur-annealed film.

The XPS depth profile of such a sample annealed at 200^0C for 2 hr is shown in Fig.(5.25). The presence of Fe and S signals is obvious throughout the sample. The binding energies around 709.6 eV and 161.9 eV for the Fe and S peaks respectively, is found to be near the expected value of 708.6 eV and 161.7 eV [47] for pure FeS_2.
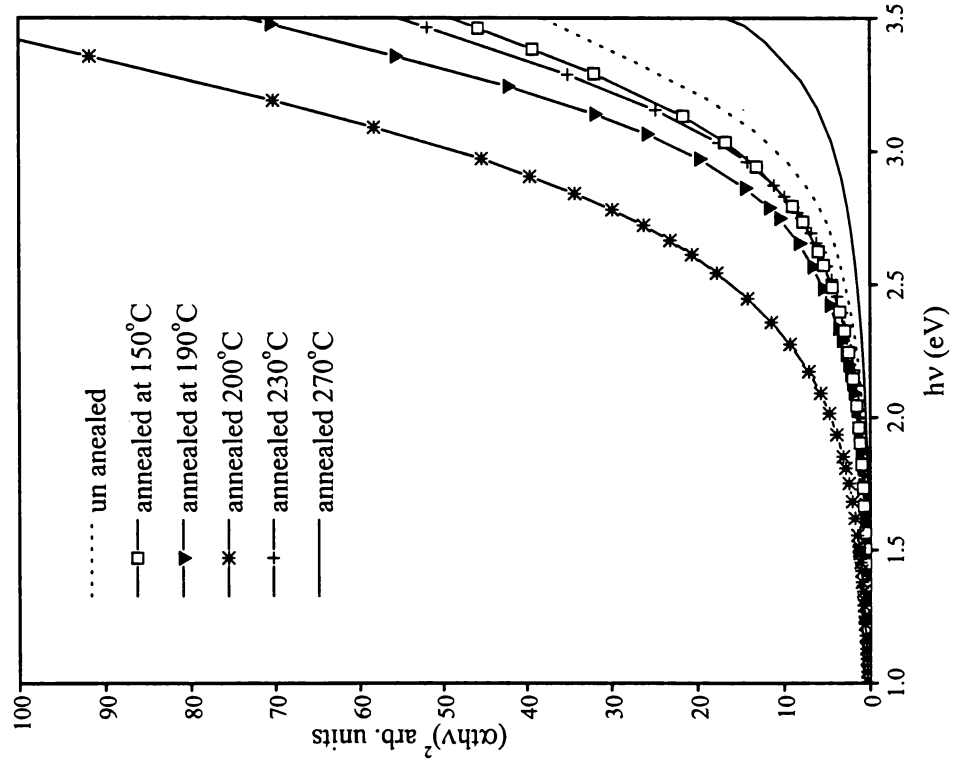
Fig. (5.23) Variation in $(\alpha h\nu)^{1/2}$ vs. $h\nu$ plot as a
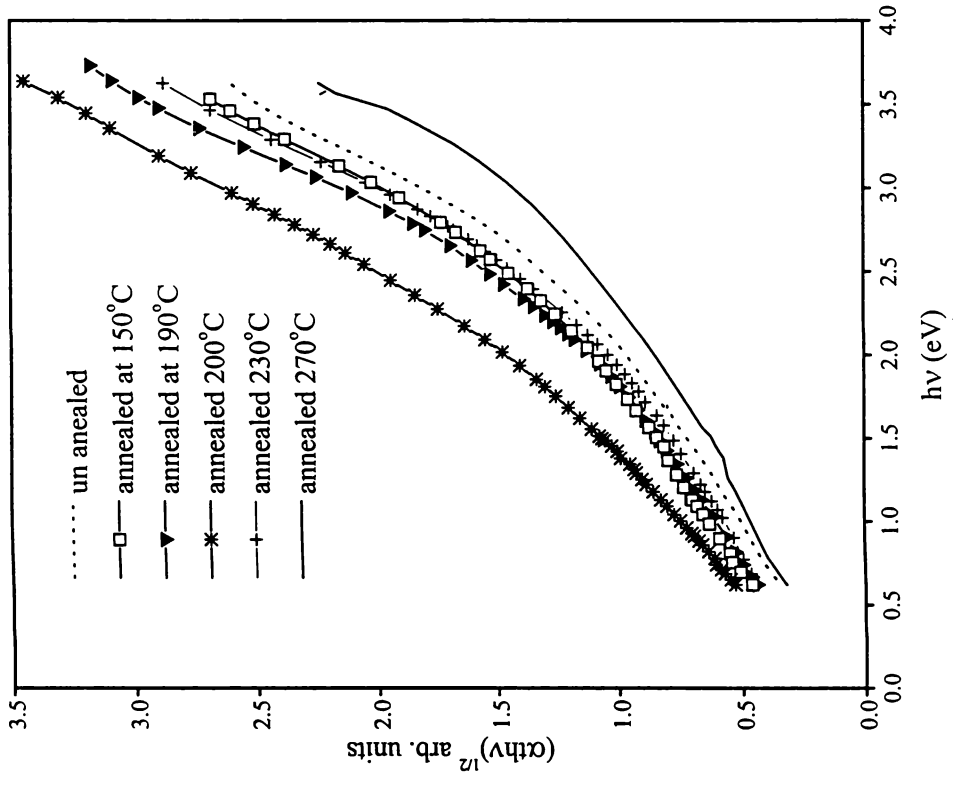result of annealing in sulfur atmosphere

Fig. (5.22) Variation in $(\alpha h\nu)^2$ vs. $h\nu$ plot as a result of
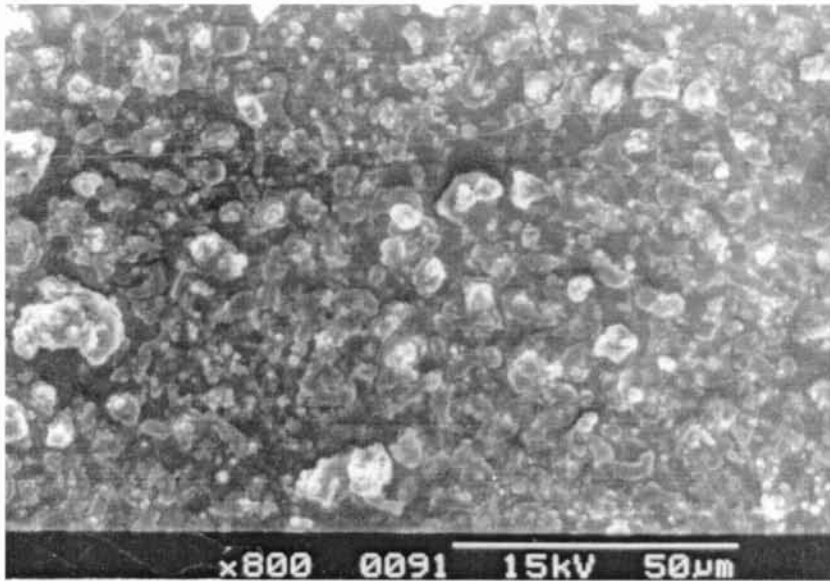annealing in sulfur atmosphere.

Fig (5.24)   SEM micrograph of sample annealed at 200^0C
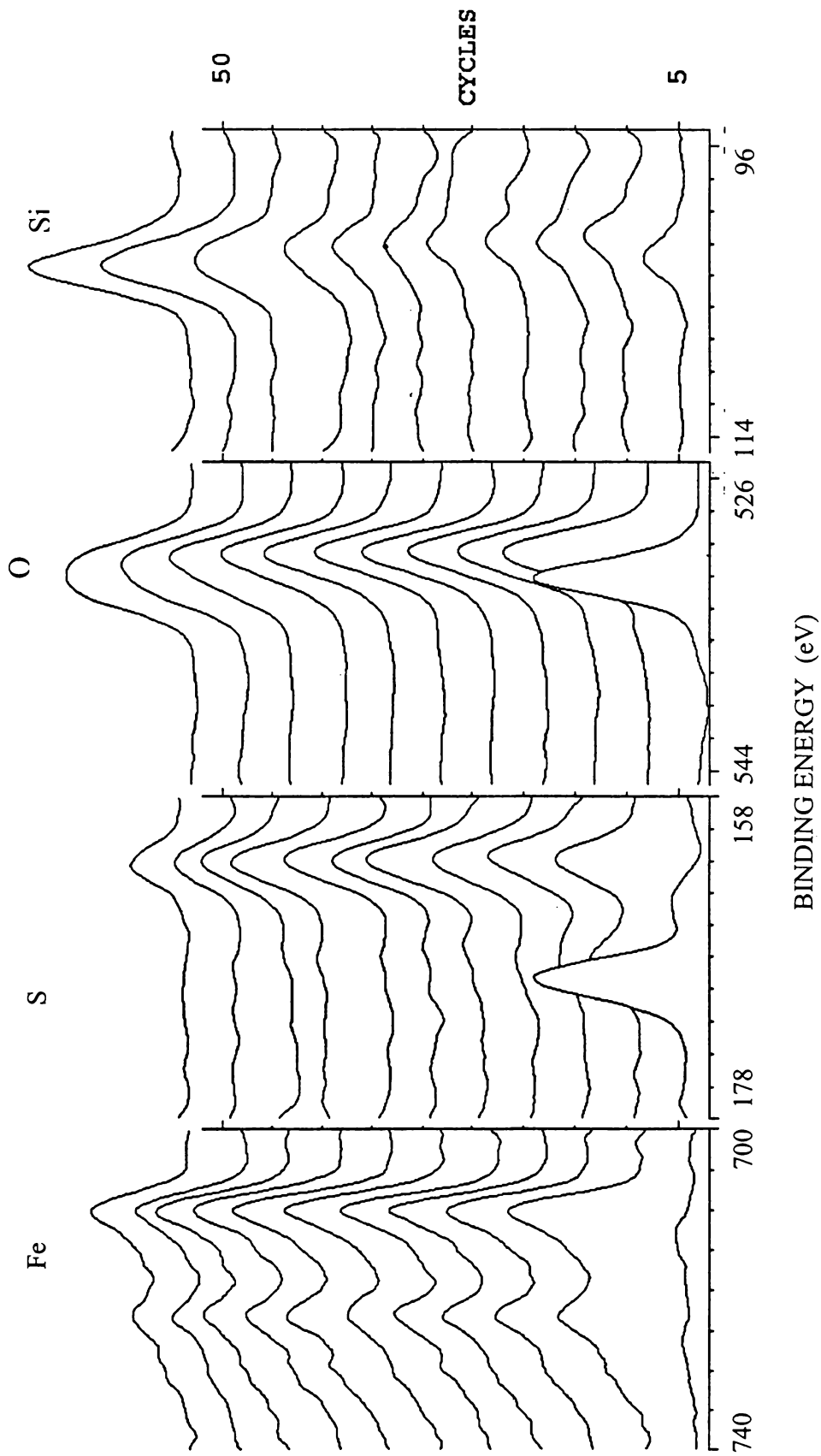in sulfur atmosphere

Fig. (5.25) XPS depth profile of sample annealed at 200^0 C in sulfur atmosphere

But here also presence of oxygen was not negligible. This leads to the conclusion that conversion of iron oxide to iron sulfide was not complete.

5.6 Conclusion

Iron pyrite with its high absorption coefficient, suitable band gap and eco-friendly nature is a suitable material for photovoltaic applications. In the present work efforts were made for the first time to prepare this material by CBD technique in aqueous medium. Analysis of freshly prepared samples showed the sulfur concentration in the as-prepared films to be considerably less than concentration of iron. Moreover, it was observed that these sulfur deficient samples were unstable in ambient conditions and it slowly gets converted to iron oxide. Hence it was concluded that it is impossible to deposit iron sulfide by using CBD technique. By the process of sulfurisation, the sulfur content could be increased to some extent. However, as annealing was tried in the presence of oxygen the formation of iron oxide could not be avoided at higher temperatures. The possible suggestion for improvement of stoichiometry is to anneal the sample for longer durations and at higher temperatures in the absence of air. This may lead to the replacement of oxygen by sulfur, thuse resulting in pyrite.

Reference

[1]   A. Ennaoui and H. Tributsh, *Solar Cells*, 13 (1984) 197.

[2]   T. A. Bither, R. J Bouchard, W. H. Cloud, P. C. Donohue and W. J. Siemons, *Inorg. Chem.*, 7 (1968) 2208.

[3]   A. Ennaoui, S. Fiechter, H. Goslowsky and H. Tributsch, *J. Electrochem. Soc.*, 132 (1985) 1580.

[4]   S. Bausch, B. Sailer, H. Keppner, G. Willeke, E. Bucher and G. Frommeyer, *Appl. Phys. Lett.*, 57 (1990) 25.

[5]   I. J. Ferrer, D. M. Nevskaia, C. de las Heras and C. Sanchez, *Solid State Commun.*, 74 (1990) 913.

[6]   A. Ennaoui, S. Fiechter, Ch. Pettenkofer, N. Alonso-Vante, K. Buker, M. Bronold, Ch. Hoptner and H. Tributsch, *Sol. Energy Mater. Sol. Cells*, 29 (1993) 289.

[7]   A. Ennaoui, S. Fiechter and H. Tributsch, M. Giersig, R. Vogel and H. Weller, *J. Electrochem. Soc.*, 139 (1992) 2514.

[8]   W. W. Kou and M. S. Seehra, *Phys. Rev. B*, 18 (1978) 7062.

[9]   C. de las Heras, I. J. Ferrer and C. Sanchez, *J. Appl. Phys*, 74 (1993) 4551.

[10]   J. Pankove, *Optical Process in Semiconductors*, Ch. 3 (1971) 34.

[11]   F. Basani and G. Pastoriu, *Electronic States and Optical Transmissions in solids*, Ch.5 (1975) 149.

[12]   K. Seegar, *Semiconductor Physics- An Introduction*, Ch.11 (1985) 302.

[13]   D. W. Bullett, *J. Phys. C: Solid State Phys.*, 15 (1982) 6163.

[14]   A. L. Echarri and C. Sanchez, *Solid State Commu.*, 15 (1974) 827.

[15]   R. Schieck, A. Hartmann, S. Fiechter, R. Konenkamp and H. Wetzel, *J. Mater. Res.*, 5 (1990) 1567.

[16]   J. R. Ares, M. Leon, N. M. Arozamena, J. Sanchez- Paramo, P. Celis, I. J. Ferrer and C. Sanchez, *J. Phys. Condens. Mater.*, 10 (1998) 4281.

[17]   B. Rezig, H. Dahman and M. Kenzari, *Renewable Energy*, 2 (1992) 125.

[18]   G. Willeke, R. Dasbach, B. Sailer and E. Bucher, *Thin Solid Films*, 213 (1992) 271.

[19]   O. Blenk, E. Bucher and G. Willeke, *Appl. Phys. Lett.*, 62 (1993) 2093.

[20] A. Emaoui, S. Fiechter, W. Jargermann and H. Tributsh, *J. Electrochem. Soc.*, 133 (1986) 97.

[21] A. Ennaoui and H. Tributsch, *Sol. Energy Mater.*, 14 (1986) 461.

[22] A. Ennaoui and H. Tributsch, *J. Electroannal. Chem.*, 204 (1986) 185.

[23] K. Buker, N. Alonso – Vante and H. Tributsch, *J. Appl. Phys.*, 72 (1992) 5721.

[24] N. Bronold, C. Pettenkofer and W. Jargermann, *J. Appl. Phys*, 76 (1994) 5800.

[25] J. R. Ares, I. J. Ferrer, F. Cuevas and C. R Sanches, *Thin Solid Films*, 387(2001) 97.

[26] C. de las Heras, J. L. Martin de Vidales, I. J. Ferrer and C. R Sanches, *J. Meter. Res.*, 11 (1995) 211.

[27] G. Pimenta, W. Sehroder and W. Kantek Ber. Bunsenges, *Phys-Chem.*, 95 (1991) 1470.

[28] G. Pimenta and W. Kautek, *Thin Solid Films*, 219 (1992) 37.

[29] S. Bausch, B. Sailer, H. Keppner, G. Willeke and E. Bucher, *Appl. Phy. Lett.*, 57 (1990) 25.

[30] I. J. Ferrer and C. Sanchez, *J. Appl. Phys.*, 70 (1991) 2641.

[31] D. Lichtenberger, K. Ellmer, R. Schieck and S. Fiechter, *Appl. Surface Sci.*, 70 (1993) 583.

[32] M. Birkholz, D. Lichtenberger, C. Hopfner and S. Fiechter, *Sol. Energy Mater. Sol. Cells*, 27 (1992) 243.

[33] A. Ennaoui, G. Schlichthorl, S. Fiechter and H. Tributsh, *Sol. Energy Mater. Sol. Cells*, 25 (1992) 169.

[34] C. de las Heras and C. Sanchez, *Thin Solid Films*, 199 (1991) 259.

[35] G. Chatzitheodorus, S. Fiechter, R. Konenkamp, M. Kunst, W. Jaegermann and H. Tributsch, *Met. Res. Bull.*, 21(1986)1481.

[36] B. Thomas, K. Ellmer, M. Muller, C. Hopfner, S. Fiechter and H. Tributsch, *J. Crystal Growth,* 170 (1997) 808.

[37] A. Ennaoui, S. Schroetter, S. Fiechter and H. Tributsch, *J. Mater. Sci. Lett.*, 11 (1992) 1131.

[38] Sigeyuki Nakamura and Akio Yamamoto, Sol.Energy Materials & Sol. Cells, 65 (2001) 79.

[39] S. Fiechter, J. Mai and A. Ennaoui, *J. Crystal Growth*, 78 (1986) 438.

[40] G. Smestad, *Sol. Energy Mat.*, 18 (1989) 299.

[41]   A. K. Abass, Z. A. Ahmed and R. E. Tahir, *Phys. Stat. Sol. (a)*, 97 (1986) 243.

[42]   A. K. Abass, Z. A. Ahmed and R. E. Tahir, *J. Appl. Phys.*, 61(1987) 2339.

[43]   Chatzitheodorou, S. Fiechter, M. Kunst, J. Luck and H. Tributsch, *Mat. Res. Bull.*, 23 (1988) 1261.

[44]   G. Smestad, A. Ennaoui, S. Fiechter, H. Tributsch, W. K. Hofmann and M. Birkholz, *Sol. Energy. Mat.*, 20 (1990) 149.

[45]   Liu Chongyang, C. Pettenkofer and H .Tributsch, Surface Sci., 204 (1988) 537.

[46]   A. N. Buckley and R. Woods, *Appl. Surface Sci.*, 27 (1987) 437.

[47]   G. Panzner and B. Egert, *Surface Sci.*, 144 (1984) 651.

[48]   T. Ohashi, K. Inakoshi, Y. Hashimoto and K. Ito, *Sol. Energy Mater. Sol. Cells*, 50 (1998) 37.

[49]   R. P Wijesundara, L. D. R. D. Pereram K. D. Jayasuriya, W. Siripala, K. T. L. De Silva, A. P. Samantilleke and I. M Dharmadasa, *Sol. Energy Mater. Sol. Cells*, 61 (2000) 277.

[50]   F. O. Adurodija, J. Song, S. D Kim, S. K. Kim and K. H. Yoon, *Jpn. J. Appl Phys.*, 37 (1988) 4248.

[51]   M. Abaab, M. Kanzari, B. Rezig and M. Brunel, *Sol. Energy Mater. Sol. Cells*, 59 (1999) 299.

CHAPTER 6

Conclusion

Chemical bath deposition (CBD)

CBD is one of the simplest, very convenient and probably the cheapest method for thin film preparation. Review of this technique projects its scope for tomorrow. Semiconducting thin films prepared by chemical deposition find applications as photo detectors, solar control coatings and solar cells. It is only 10 years since chemically deposited thin films have found their active role in thin film solar cells. In the present scenario where cost effectiveness is the major limiting factor that prevents the day-to-day use of solar cells, CBD is looked upon with much expectation.

Attraction of this technique in photovoltaics is based on the direct use of thin films prepared by this method and also on the fact that films prepared by this technique can form precursors for preparing other leading ternary materials of this field such as $CuInS_2$ and $CuInSe_2$.

Factors influencing the deposition process includes (a) nature and concentration of reactants and complexing agent (b) temperature, pH and duration of deposition and (c) nature and spacing of the substrates. In the first chapter a comparative study of the photoresponse of thin films prepared using this method are included. Apart from this, the advantages and disadvantages of CBD are also elaborated.

Solar cells using CBD-CdS of the configuration glass/SnO_2:F/CdS/CdTe/In and MgF_2/ITO/ZnO/CdS/CIGS/Mo/glass have reported efficiency of 14.5% and 17% respectively. These efficiencies are appreciable when compared with the maximum efficiency of 24.5% reported for Si solar cells prepared with the most sophisticated technique. 'All-CBD Cell' is an idea of great scope. The initial trial of a photovoltaic junction of CBD-CdS/CBD-$CuInSe_2$ with an efficiency of 3.1% was reported from the Thin Film Photovoltaic Divison of Cochin University of Science & Technology. CdS is one of the materials that has seen day light in the field of CBD, but other materials such as CdSe, Cu_xS, ZnSe, $CuInSe_2$, $CuInS_2$ and Cu_2Se are on their way to success. These materials are reviewed in the first chapter with emphasis on preparation using this simple technique.

Copper selenide

Copper selenide is a p-type semiconductor that finds application in photovoltaics. Several heterojunction systems such as $Cu_{2-x}Se/ZnSe$ (for injection electro luminescence), $Cu_2Se/AgInSe_2$ and Cu_2Se/Si (for photodiodes), $Cu_{2-x}Se/CdS$, $Cu_{2-x}Se/CdSe$, Cu_xSe/InP and $Cu_{2-x}Se/Si$ for solar cells are reported. A maximum efficiency of 8.3% was achieved for the $Cu_{2-x}Se/Si$ cell. There are various preparation techniques for copper selenide like vacuum evaporation, direct reaction, electrodeposition and CBD.

Cu_2Se and $CuSe$ are the frequently deposited phases of copper selenide, using this chemical method. In the present work, $Cu_{2-x}Se$ and Cu_3Se_2 phases were prepared from similar reaction bath. This forms the first report of preparation of Cu_3Se_2 by CBD. It was observed that pH of the final reaction mixture is the major factor deciding the composition of the deposited film. Films of $Cu_{2-x}Se$ and Cu_3Se_2 phases could be prepared either by varying the Cu:Se ratio in the reaction bath or by controlling the pH of the bath that contains equal amounts of Cu and Se ions.

At a pH around 6.8, the preferred reaction leads to $Cu_{2-x}Se$ phase while at a pH of around 7.8, the preferred reaction leads to the formation of Cu_3Se_2 phase. The fact that rate of reaction increases in alkaline pH makes it necessary to slow down the reaction rate by controlling the temperature in the case of Bath 1: 1 Na and Bath 1: 2.

Thin films of $Cu_{2-x}Se$ prepared from Bath 1:1, Bath 2:1, Bath 3:1 and Bath 5:1 were reddish brown in colour and uniform in appearance. Bath 1:1 Na and Bath 1:2 resulted in Cu_3Se_2 films with a bluish green colour. Film from Bath 1:1 Na was more uniform than that from Bath 1:2. Thickness of two dip $Cu_{2-x}Se$ films and Cu_3Se_2 films were around 1 μm and 1.2 μm respectively.

SEM analysis showed the $Cu_{2-x}Se$ films from Bath 1:1 to be very uniform with distinct grains of average size 0.2 μm. Cu_3Se_2 phase grew in clusters with less defined grain boundaries, but with a larger grain size of the range 0.4 μm. The gradual increase in the concentration of copper in the reaction bath leads to poor film morphology.

XRD analysis confirmed the formation of the two phases of copper selenide. It also revealed the increase in grain size of $Cu_{2-x}Se$ phase with the increase in thickness of the film and also the decrease in grain size with the increase in concentration of Cu in the reaction mixture. Stoichiometric interpretations from XRD analysis showed that it was possible to slightly influence the composition of the $Cu_{2-x}Se$ film by varying the relative concentration of reactants in the reaction bath. Similarly, low temperature deposition was found to increase the Se content in the deposited thin film. It was also inferred that if $Cu_{2-x}Se$ deposition is carried out at low temperature, the incorporation of selenium into the thin film could be increased. In the present case, the deposited phase shifts from the chemical formula $Cu_{1.71}Se$ to $Cu_{1.65}Se$. This forms the first report of a novel and simple method to improve the selenium content in selenide films deposited using CBD technique.

Optical absorption studies showed the band gap of $Cu_{2-x}Se$ phase and Cu_3Se_2 phase to be 2.2 eV and 2.8 eV respectively. Variation in band edge ~ 0.2 eV with the increase in thickness of the film suggested a small improvement in grain size. Peak value of transmittance is around 780 nm for the $Cu_{2-x}Se$ film while it is around 580 nm for Cu_3Se_2 films. A substantial decrease in transmittance is observed through out the IR region for both the phases due to free carrier absorption.

XPS analysis showed that the composition of $Cu_{2-x}Se$ film and Cu_3Se_2 film to be uniform through out the thickness. But there was no detectable binding energy shift between the phases. The percentage composition as calculated from this analysis, suggested the chemical formula for the two phases as $Cu_{1.8}Se$ and $Cu_{3.1}Se_2$. ICP analysis showed Cu:Se ratio of $Cu_{2-x}Se$ films and Cu_3Se_2 films to be around 1.80:1 and 1.54:1 respectively.

Electrical measurements revealed $Cu_{2-x}Se$ phase to be low resistive than Cu_3Se_2 phase. Hall mobilities were comparatively low in both these p-type copper selenide phases due to the high carrier concentration of the order of $10^{20}/cm^{-3}$. With the increase in copper ion concentration in the reaction bath of $Cu_{2-x}Se$ phase, decrease in mobility of the carriers and hence increase in resistivity was observed. In the case of $Cu_{2-x}Se$, resistivity increased with temperature while in the case of Cu_3Se_2 resistivity decreased with temperature. Carrier mobility was found to increase when the deposition was carried out at low temperatures.

On exposure to ambient conditions, the as-prepared $Cu_{2-x}Se$ thin films converts to Cu_3Se_2 phase. There is no definite incubation period for this conversion. The factor that initiates the conversion was traced to be the presence of charged particles (ions) in the ambient atmosphere. When as-prepared $Cu_{2-x}Se$ film is given a final dipping in Bath 1:1 Na or in dilute Na_2SeSO_3 solution for a few minutes, then also the $Cu_{2-x}Se$ phase gets converted to Cu_3Se_2 phase.

SEM studies revealed the formation of copper drops or fractal growths during the process of conversion. This is quite possible as the process behind the conversion is a disproportionation reaction leading to elemental copper formation.

XRD spectrum showed the slow disappearance of the characteristic peak of $Cu_{2-x}Se$ phase and the appearance of the peaks corresponding to Cu_3Se_2 phase during conversion. The X-ray diffractogram of Cu_3Se_2 sample prepared by dipping as-prepared $Cu_{2-x}Se$ in Na_2SeSO_4 had better crystallinity than the Cu_3Se_2 sample resulting through the aging of $Cu_{2-x}Se$.

Formation of Cu_3Se_2 phase from $Cu_{2-x}Se$ was confirmed from the shift of the absorption edge from 2.20 eV to 2.73 eV. The slight variation of band gap of this Cu_3Se_2 phase from the earlier observed value of 2.83 eV may be due to the formation of copper oxide resulting from oxygen incorporation.

XPS depth profile of the sample transformed due to aging showed the presence of oxygen trace throughout the sample thickness along with the strong signals of Cu and Se. This suggests the formation of small quantities of oxide impurity in the copper selenide phase as a result of aging. Presence of oxygen was confirmed from the total XPS survey spectrum taken after the 5th cycle of etching. At the same time the XPS analysis of the $Cu_{2-x}Se$ phase that was preserved in a dry atmosphere showed absence of oxygen along the film depth. This suggested that phase conversion can be avoided if stored in dry atmosphere.

Hall measurement studies showed an increase in carrier concentration in the converted samples. This must be due to the significant diffusion of Cu to the film surface as seen in SEM micrograph in Fig.(4.3), leading to the increase in Cu vacancies. This in turn reduces the mobility. The fact that the crystallinity of the aged samples are less than the as-prepared samples may also be contributing to the decrease in mobility in such samples.

It is generally observed that Cu (II) is more stable than Cu (I) and hence preferred. So when initiated by suitable stimulating factor, some Cu (I) in $Cu_{2-x}Se$ disproportionates according to the reaction.
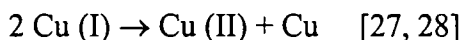
$$2\,Cu\,(I) \rightarrow Cu\,(II) + Cu \quad [27, 28]$$

This process only involves internal transfer of an electron from one of the Cu (I) to another Cu (I), so that more stable forms of Cu (II) and Cu exists. When this disproportionation proceeds, it results in a stable situation where $x^1 \sim 0.5$. Thus $Cu_{2-x}Se$ phase gets converted to Cu_3Se_2.

When Cu_3Se_2 film is annealed in air at 140^0C for 1hr, it gets converted to the reddish brown phase of $Cu_{2-x}Se$. In such films the average grain size is found to be higher than that of the as-prepared $Cu_{2-x}Se$ film. Presence of irregular shaped large islets on surface of the film as observed in SEM could be due to segregations of Se or oxides of selenium. This conversion of $Cu_{2-x}Se$ to Cu_3Se_2 was confirmed by absorption and XRD studies.

It is expected that the dissociation of Cu_3Se_2 occur according to the reaction

$$2\,Cu_3Se_2 \rightarrow 3\,Cu_{2-x}Se + Se$$
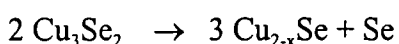
The solid reaction behind this conversion leads to Se rich Cu(I)selenide. The presence of excess Se anions increases the carrier density as well as mobility. The slightly low resistivity of the film when compared to as-prepared $Cu_{2-x}Se$ phase must be due to the large extend of non-stoichiometry existing in such films when it is derived from the Se rich phase of Cu_3Se_2.

Apart from this, the effect of annealing the $Cu_{2-x}Se$ phase was also studied. Substrate of $Cu_{2-x}Se$ film was found to influence the stability of the phase during annealing. Samples deposited on glass were found to be stable up to 300^0C while samples were stable till 400^0C on SnO_2 coated glass.

It was found that grain size improves up to an annealing temperature of 200^0C. But annealing at 300^0C and 400^0C leads to diffused grain boundaries and smaller grain size. From the SEM observations it was concluded that degradation of the film becomes significant at temperatures equal to or greater than 300^0C. XRD analysis supported this inference. The indirect evaluation of stoichiometry of the annealed samples showed that the best method to improve film quality is to anneal at 200^0C for a longer duration. Effect of annealing on the band edge was also studied.

Conversions of $Cu_{2-x}Se$ to Cu_3Se_2 and Cu_3Se_2 to $Cu_{2-x}Se$ are found to be cyclic. When $Cu_{2-x}Se$ is aged in ambient conditions or dipped in Na_2SeSO_3 solution it leads to diffusion of Cu to the film surface, making the remaining phase selenium rich and there by getting converted to Cu_3Se_2. When this is annealed at 140^0C it converts back to $Cu_{2-x}Se$. But in the reverse direction of the cycle it is found that the crystallinity decreases. Same is the case with as-prepared Cu_3Se_2 film. When annealed it dissociates into $Cu_{2-x}Se$ and Se. When this $Cu_{2-x}Se$ phase is left for aging it converts back to Cu_3Se_2 phase. But this happens at a very slow rate. To conclude, the phase conversion observed in $Cu_{2-x}Se$ and Cu_3Se_2 phases is cyclic but the rate of conversion is considerably reduced after each heating cycle.

Inter phase conversion can be avoided by simple methods. When the as-prepared $Cu_{2-x}Se$ phase is annealed at 150^0C for 2hrs, the Cu (I) state is found to gain stability. This will prevent the conversion to Cu_3Se_2 phase. Such samples when stored in dry atmosphere are found to remain intact even after one or two years. Similarly, as-prepared Cu_3Se_2 phase can be kept intact by avoiding any sort of heat treatment. Heat treatment stabilises $Cu_{2-x}Se$ phase while avoiding heat leads to the stability of Cu_3Se_2 phase.

Iron pyrite

Iron pyrite is a comparatively new material in the field of photovoltaics. In the present work attempts were made to prepare this material by CBD technique. Analysis of freshly prepared samples showed the sulfur concentration in the as-prepared films to be considerably less than concentration of iron. Moreover it was observed that these sulfur deficient samples were unstable in ambient atmosphere and it slowly gets converted to iron oxide. Hence it was concluded that it is impossible to deposit iron sulfide by using CBD technique.

Trials to deposit this material by applying a small voltage during deposition also resulted in failure. Later, with the idea of sulfurisation of these iron oxide films a sulfur annealing chamber was fabricated and sulfurisation was tried. This gave some hopes of improvement. As a result of sulfur annealing at 200^0C for 2 hrs., the direct band gap is found to shift from 2.94 eV to 2.67 eV (nearest reported value being 2.62 eV). Indirect band gap shifts from 1.67 eV to 0.97 eV (reported value being 0.97 eV).

XPS analysis shows presence of Fe and S through out the sample, though oxygen could not be avoided.

Future scope of work

Now that morphology, crystallinity, optical band gap and phase conversions in the two phases of copper selenide is clear , work can be extended to the next phase of photoresponse characterisation. Initial trials have shown poor photoresponse for this material. This may be due to the large extent of non-stoichiometry existing in these films. Hence as a measure to improve the stoichiometry, diffusion of elemental copper (deposited by vacuum evaporation) can be tried. Moreover, even if the photo response is not as high as materials like CdS, this material can act as good window layer with its high absorption coefficient and wide band gap. As cited in some of the references, in the case of junctions with this material, barrier layer always lie more or less in the absorber material used in the formation of junction.

Further work possible in the material of iron pyrite includes sulfur annealing of the non- stoichiometric iron pyrite CBD thin films in the absence of atmospheric oxygen. Improvements in the stoichiometry have been observed during the process of sulfur annealing even in the presence of oxygen. But as higher temperatures increased the chances of oxide formation. Hence the possible suggestion for improving the stoichiometry is to anneal the samples for longer durations and at higher temperatures in the absence of air. This may lead to the replacement of oxygen by sulfur and there by resulting in pyrite.